

# APPLIED MATHEMATICS FOR RESTRUCTURED ELECTRIC POWER SYSTEMS

Optimization, Control, and  
Computational Intelligence

---

*Edited by*

Joe H. Chow

Felix F. Wu

James A. Momoh

Springer's Power Electronics and Power Systems Series  
Series Editors: M.A. Pai and Alex M. Stankovic

---

# APPLIED MATHEMATICS FOR RESTRUCTURED ELECTRIC POWER SYSTEMS

---

# POWER ELECTRONICS AND POWER SYSTEMS

*Series Editors*

**M. A. Pai and Alex Stankovic**

***Other books in the series:***

HVDC and FACTS Controllers: *Applications of Static Converters in Power Systems*  
Vijay K. Sood, 1-4020-7890-0

POWER QUALITY ENHANCEMENT USING CUSTOM POWER DEVICES  
Arindam Ghosh, Gerard Ledwich, 1-4020-7180-9

COMPUTATIONAL METHODS FOR LARGE SPARSE POWER SYSTEMS ANALYSIS:  
*An Object Oriented Approach*,

S. A. Soman, S. A. Khaparde, and Shubha Pandit, ISBN 0-7923-7591-2

OPERATION OF RESTRUCTURED POWER SYSTEMS

Kankar Bhattacharya, Math H.J. Bollen and Jaap E. Daalder, ISBN 0-7923-7397-9

TRANSIENT STABILITY OF POWER SYSTEMS: *A Unified Approach to Assessment and Control*

Mania Pavella, Damien Ernst and Daniel Ruiz-Vega, ISBN 0-7923-7963-2

MAINTENANCE SCHEDULING IN RESTRUCTURED POWER SYSTEMS

M. Shahidehpour and M. Marwali, ISBN: 0-7923-7872-5

POWER SYSTEM OSCILLATIONS

Graham Rogers, ISBN: 0-7923-7712-5

STATE ESTIMATION IN ELECTRIC POWER SYSTEMS: *A Generalized Approach*

A. Monticelli, ISBN: 0-7923-8519-5

COMPUTATIONAL AUCTION MECHANISMS FOR RESTRUCTURED POWER INDUSTRY OPERATIONS

Gerald B. Sheblé, ISBN: 0-7923-8475-X

ANALYSIS OF SUBSYNCHROUS RESONANCE IN POWER SYSTEMS

K.R. Padiyar, ISBN: 0-7923-8319-2

POWER SYSTEMS RESTRUCTURING: *Engineering and Economics*

Marija Ilic, Francisco Galiana, and Lester Fink, ISBN: 0-7923-8163-7

CRYOGENIC OPERATION OF SILICON POWER DEVICES

Ranbir Singh and B. Jayant Baliga, ISBN: 0-7923-8157-2

VOLTAGE STABILITY OF ELECTRIC POWER SYSTEMS

Thierry Van Cutsem and Costas Vournas, ISBN: 0-7923-8139-4

AUTOMATIC LEARNING TECHNIQUES IN POWER SYSTEMS,

Louis A. Wehenkel, ISBN: 0-7923-8068-1

ENERGY FUNCTION ANALYSIS FOR POWER SYSTEM STABILITY

M. A. Pai, ISBN: 0-7923-9035-0

ELECTROMAGNETIC MODELLING OF POWER ELECTRONIC CONVERTERS

J. A. Ferreira, ISBN: 0-7923-9034-2

SPOT PRICING OF ELECTRICITY

F. C. Schweppe, M. C. Caramanis, R. D. Tabors, R. E. Bohn, ISBN: 0-89838-260-2

THE FIELD ORIENTATION PRINCIPLE IN CONTROL OF INDUCTION MOTORS

Andrzej M. Trzynadlowski, ISBN: 0-7923-9420-8

FINITE ELEMENT ANALYSIS OF ELECTRICAL MACHINES

S. J. Salom, ISBN: 0-7923-9594-8

# APPLIED MATHEMATICS FOR RESTRUCTURED ELECTRIC POWER SYSTEMS

## Optimization, Control, and Computational Intelligence

Edited by  
**JOE H. CHOW**  
Rensselaer Polytechnic Institute

**FELIX F. WU**  
Hong Kong University and University of California, Berkeley

**JAMES A. MOMOH**  
Howard University and National Science Foundation



*Editors:*

Joe H. Chow  
Dept. of Electrical, Computer,  
& Systems Engineering  
Rensselaer Polytechnic Institute  
110 8<sup>th</sup> Street  
Troy, NY 12180

Felix F. Wu  
Dept. of Electrical and Electronic Engineering  
Hong Kong University  
Pokfulam Road  
Hong Kong

James Momoh  
Center for Energy Systems and Control  
Howard University  
2300 Sixth Street NW  
Washington, DC 20059

**Applied Mathematics for Restructured Electric Power Systems: *Optimization, Control, and Computational Intelligence***

Library of Congress Cataloging-in-Publication Data

A C.I.P. Catalogue record for this book is available  
from the Library of Congress.

ISBN 0-387-23470-5      e-ISBN 0-387-23471-3      Printed on acid-free paper.

© 2005 Springer Science+Business Media, Inc.

All rights reserved. This work may not be translated or copied in whole or in part without the written permission of the publisher (Springer Science+Business Media, Inc., 233 Spring Street, New York, NY 10013, USA), except for brief excerpts in connection with reviews or scholarly analysis. Use in connection with any form of information storage and retrieval, electronic adaptation, computer software, or by similar or dissimilar methodology now known or hereafter developed is forbidden.

The use in this publication of trade names, trademarks, service marks and similar terms, even if they are not identified as such, is not to be taken as an expression of opinion as to whether or not they are subject to proprietary rights.

Printed in the United States of America.

9 8 7 6 5 4 3 2 1

SPIN 11054054

[springeronline.com](http://springeronline.com)

This book is dedicated  
to Mr. Lester Fink,  
whose vision in the  
1970's on merging  
rigorous analysis  
techniques to power  
system problems is still  
relevant today, and to  
the memory of my  
father, Mr. Er-Zhi  
Zhou, a superb cable  
engineer. *JHC*

# Contents

List of Figures	xiii
List of Tables	xix
Preface	xxi
Contributing Authors	xxv
<b>1</b>	
Applied Mathematics for Restructured Electric Power Systems	1
<i>Joe H. Chow, Felix F. Wu and James A. Momoh</i>	
1    Introduction	1
2    Workshop Presentations	3
3    Synopses of the Articles in this Compilation	6
4    Conclusions	8
<b>2</b>	
Reactive Power and Voltage Control Issues in Electric Power Systems	11
<i>Peter W. Sauer</i>	
1    Introduction	11
2    Reactive Power	12
3    Reactive Power in Operations	13
4    A Fundamental Illustration	17
5    Challenges in Voltage Control and Related Security	22
6    Conclusions	23
<b>3</b>	
Identification of Weak Locations using Voltage Stability Margin Index	25
<i>Tao He, Sharma Kolluri, Sujit Mandal, Floyd Galvan and Parviz Rastgoufard</i>	
1    Introduction	26
2    Basic Mathematical Model	27
3    Application of the New Method to Large Scale Power Systems	30
4    Simulation Results	31
5    Conclusions	33

6	Future Work	35	
<hr/>			
4	Bifurcation and Manifold Based Approach for Voltage and Oscillatory Stability Assessment and Control		39
<i>Venkataramana Ajjarapu</i>			
1	Introduction	39	
2	Identification of Saddle Node, Hopf Bifurcation, and Damping Margins	43	
2.1	Identification of critical eigenvalue	45	
2.2	Damping margin identification	47	
2.3	Example	48	
3	Tracing Margin Boundaries	51	
3.1	Boundary predictor	51	
3.2	Boundary corrector	52	
3.3	Computation result	53	
4	Further Extensions	54	
4.1	Optimal margin boundary: cost based security	54	
4.2	Fast and slow time scales	55	
4.3	Impact on power system security	55	
5	Research Needs	56	
<hr/>			
5	On-Line ATC Evaluation for Large-Scale Power Systems: Framework and Tool		63
<i>Hsiao-Dong Chiang and Hua Li</i>			
1	Introduction	63	
2	Transfer Capability	68	
3	Transaction-Dependent ATC	69	
4	System Modeling	71	
5	Identify Critical Contingencies for Static Security	74	
6	Estimating Load Margins to Nose Points	80	
7	Estimating Load Margins to Static Security Violations	86	
8	Identify Critical Contingencies for Dynamic Security	87	
9	Solution Algorithm	89	
10	Numerical Studies	91	
11	Conclusions	97	
<hr/>			
6	Automating Operation of Large Electric Power Systems Over Broad Ranges of Supply/Demand and Equipment Status		105
<i>Marija Ilic</i>			
1	Introduction	106	
2	Electric Power Grids as Complex Network Systems	108	
2.1	Assumptions underlying today's operation of hierarchical systems	109	
2.2	Implications of violating monotone response	111	
2.3	The major challenge: monitoring and control outside monotone response system conditions	111	
3	Current Operating Practice: Problems and Open Questions	112	

	3.1	Historic problems of operating under stress	113
	3.2	Some possible solutions and their shortcomings	114
4	Multi-Layered Modeling, Estimation and Control Approach to Managing Electric Power Networks Over Broad Ranges of Operating Conditions	115	
	4.1	Full non-linear dynamics of electric power systems	116
	4.2	Disturbance- and control-driven multi-layered models	117
	4.3	A large-scale quasi-stationary model	118
	4.4	Multi-layered system constraints	119
5	Multi-Layered Estimation and Control	120	
	5.1	Quasi-stationary state estimators	123
	5.1.1	New quasi-stationary state estimator as the observability problem in hybrid systems	125
	5.2	Multi-layered control approach	125
	5.2.1	Adaptive control for stabilizing fast system dynamics	126
	5.2.2	Adaptive scheduling of discrete mechanical controllers	127
	5.3	Automated short-term dispatch and unit commitment over broad ranges of conditions and equipment status	128
	5.4	Particular case: Today's hierarchical control	129
6	Structural Spatial Aggregation: Managing Large Network Complexity by Means of Systematic Estimation and Control	130	
	6.1	Quasi-stationary state estimators	130
	6.1.1	Particular case: Today's hierarchical control in multi-control area interconnections	132
	6.1.2	Open questions in today's multi-control area interconnections	132
7	Conclusions and Open Questions	133	
7	Robust Control of Large Power Systems via Convex Optimization	139	
	<i>A. I. Zečević and D. D. Šiljak</i>		
1	Introduction	139	
2	Exciter Control Design using Linear Matrix Inequalities	141	
3	Some Simulation Results	145	
4	New Research Directions	147	
	4.1	Design of decentralized output control	147
	4.2	Coordinated design of power system stabilizers and robust feedback	149
	4.3	Control design with information exchange between subsystems	153
5	Conclusions	154	
8	Instability Monitoring and Control of Power Systems	159	
	<i>Eyad H. Abed, Munther A. Hassouneh and Mohamed S. Saad</i>		
1	Introduction	160	
2	Participation Factors	160	
	2.1	Modal participation factors	161
	2.2	Input-to-state participation factors	162
3	Precursor-Based Monitoring	162	
4	Case Studies	166	

4.1	Single-generator system with dynamic load	167
4.2	Single generator connected to an infinite bus	168
4.3	Three-generator nine-bus power system	171
5	Conclusions and Suggested Future Research	173
Appendix: Parameter Values for the Generators in Sections 4.1 and 4.2		176
9		
Dynamic Embedded Optimization and Shooting Methods for Power System Performance Assessment		179
<i>Ian A. Hiskens, Jung-Wook Park and Vaibhav Donde</i>		
1	Introduction	180
2	Model	181
2.1	Hybrid systems	181
2.2	Trajectory sensitivities	183
3	Dynamic Embedded Optimization	184
4	Shooting Methods	186
4.1	Limit cycles	188
4.2	Grazing phenomena	192
5	Challenges in Dynamic Performance Enhancement	195
6	Conclusions	195
10		
Computational Intelligence Techniques For Control of FACTS Devices		201
<i>Ganesh K. Venayagamoorthy and Ronald G. Harley</i>		
1	Introduction	201
2	FACTS Devices and Conventional Control	203
2.1	Static Compensators (STATCOM)	204
2.2	Static Synchronous Series Compensator (SSSC)	205
2.2.1	Modeling of SSSC	206
2.2.2	Conventional control strategy	207
2.3	Unified Power Flow Controller (UPFC)	208
2.3.1	Series branch control	210
2.3.2	Shunt branch control	211
3	Adaptive Neurocontrol of FACTS Devices	212
3.1	Neuroidentifier	213
3.2	Neurocontroller	213
3.3	Desired response predictor	214
3.4	Adaptive neurocontrol of a STATCOM based power system	215
3.4.1	Neuroidentifier	215
3.4.2	Neurocontroller	216
3.4.3	Simulation results	218
3.5	Adaptive neurocontrol of a UPFC based power system	219
3.5.1	Pre-control training phase	219
3.5.2	Post-control training phase	221
3.5.3	Simulation results	222
4	Optimal Neurocontrol with Adaptive Critic Designs	226
4.1	Optimal DHP neurocontrol of a Static Synchronous Series Compensator (SSSC)	227
4.1.1	Critic network	227

11	4.1.2 Action network	230
	4.1.3 Model network	231
	4.1.4 Simulation results	233
5	Conclusions	233
6	Future Research	235
Placement and Coordinated Tuning of Control Devices for Capacity and Security Enhancement Using Metaheuristics		239
<i>Djalma M. Falcão and Glauco N. Taranto</i>		
1	Introduction	240
2	Problem Formulation	241
	2.1 The placement problem	241
	2.2 The coordinated tuning problem	242
	2.3 The combined placement and tuning problem	242
3	The Metaheuristics Approach	243
4	Optimal Protection Devices Placement in Distribution Networks	244
	4.1 Proposed approach	245
	4.2 Genetic algorithm formulation	246
	4.3 Computational results	247
	4.3.1 Example 1	248
	4.3.2 Example 2	250
5	Coordinated Tuning of Power System Controls	253
	5.1 Problem formulation	254
	5.2 Robust tuning using GAs	255
	5.2.1 Formulation as an optimization problem	255
	5.2.2 Modified GA elements	255
	5.3 Test results	257
	5.4 Feedback signal selection	258
	5.5 Robust decentralized control	259
	5.6 Time simulation results	261
6	Conclusions and Further Developments	262
Appendix: Genetic Algorithms		264
12		
Load Forecasting		269
<i>Eugene A. Feinberg and Dora Genethliou</i>		
1	Introduction	269
2	Important Factors for Forecasts	271
3	Forecasting Methods	272
	3.1 Medium- and long-term load forecasting methods	273
	3.2 Short-term load forecasting methods	277
4	Future Research Directions	281
5	Conclusions	282
13		
Independent Component Analysis Techniques for Power System Load Estimation		287
<i>Dagmar Niebur, Ekrem Gursoy and Huawei Liao</i>		
1	Introduction	288

2	Independent Component Analysis	289
2.1	ICA source estimation model	290
2.2	ICA source assumptions	290
2.3	Objective functions for the maximization of source independence	291
2.4	FastICA source estimation algorithm	292
3	Application of ICA for Load Profile Estimation	293
3.1	Linear mixing models for load profile estimation	293
3.1.1	Power flow equations	293
3.1.2	Active power load profile model	294
3.1.3	Reactive power load profile model	295
3.1.4	Harmonic load profile model	296
3.2	Preprocessing of load profile data	297
3.3	Eliminating indeterminacy of ICs	299
3.4	FastICA based load profile estimation algorithm	299
4	Case Studies	300
4.1	Data generation	300
4.2	Error measures	301
4.3	Results for active load profile estimation	302
4.4	Results for reactive load profile estimation	305
4.5	Results for harmonic load profile estimation	307
5	Conclusions	311
6	Future Research	313
	Index	319

# List of Figures

2.1	Voltage and current waveforms.	12
2.2	Instantaneous power.	13
2.3	Decomposition of instantaneous power.	13
2.4	Illustration Case 1 (all lines in).	17
2.5	Illustration Case 2 (one line out).	18
2.6	Illustration Case 3 (two lines out).	18
2.7	Illustration Case 4 (three lines out).	19
2.8	Illustration Case 5 (four lines out).	19
2.9	Illustration Case 6 (five lines out).	20
2.10	Illustration Case 7 (two lines out - unlimited Vars).	20
2.11	Illustration Case 8 (three lines out - unlimited Vars).	21
2.12	Illustration Case 9 (four lines out - unlimited Vars).	21
2.13	Illustration Case 10 (five lines out - unlimited Vars).	21
2.14	Illustration Case 11 (five lines out - unlimited Vars - maximum power transfer).	22
3.1	A simple two-bus system.	27
3.2	Process to develop <i>PV</i> curve from Voltage-Angle and Power-Angle curves.	29
3.3	Simplify large scale power system to equivalent two-bus system.	30
4.1	Illustration of three types of boundaries.	43
4.2	Eigenvalue real part vs. parameter $\alpha$ .	46
4.3	Tangent information is used in searching for damping margin.	48
4.4	All complex eigenvalues in complex plane at base case.	49
4.5	Integrated eigenvalue with total load increase.	50
4.6	Damping ratio vs. entire system load increase.	50
4.7	Hopf and SNB detection in <i>PV</i> curve tracing for base case control.	53
4.8	Margin boundary tracing (MBT) vs. load shedding.	54

4.9	Continuation-based time domain simulation using locally parameterized time trajectory tracing.	55
5.1	The nose point load margin $\lambda_{C_0}^{np}$ for the base case power system $C_0$ .	76
5.2	The nose point load margin $\lambda_{C_k}^{np}$ for the power system under contingency $C_k$ .	76
5.3	The voltage-limit load margin $\lambda_{C_0}^v$ for the base case power system $C_0$ .	78
5.4	The voltage-limit load margin $\lambda_{C_k}^v$ for the power system under contingency $C_k$ .	78
5.5	The thermal-limit load margin $\lambda_{C_0}^{th}$ for the base case power system $C_0$ .	79
5.6	The thermal-limit load margin $\lambda_{C_k}^{th}$ for the power system under contingency $C_k$ .	80
5.7	The limit-induced bifurcation point is far away from the saddle-node bifurcation point.	84
5.8	The limit-induced bifurcation point is close to the saddle-node bifurcation point.	84
5.9	The transient-stability-limit load margin $\lambda_{C_k}^{ts}$ for the power system subject to contingency $C_k$ .	88
5.10	The overall architecture of the proposed tool for accurate evaluation of ATC.	93
6.1	Basic IT infrastructure flow for multi-layered automated estimation and control	122
7.1	Rotor angle of Generator 8.	146
7.2	Terminal voltage $V_t$ of Generator 8.	146
7.3	Matrix K with a nested BBD structure.	154
8.1	Precursor-based instability monitor with external probe signal.	164
8.2	Power spectral densities of the states of the model given in (8.16)-(8.19). The bifurcation parameter was set to $Q_1 = 2.9$ .	169
8.3	Variation of the peak value of the power spectral density of $\omega$ as a function of the bifurcation parameter $Q_1$ .	169
8.4	Power spectral densities of the states of the single generator connected to an infinite bus system. The bifurcation parameter was set to $K_A = 185$ .	171

8.5	Power spectral densities of the states of the single generator connected to an infinite bus system. The bifurcation parameter was set to $K_A = 185$ .	172
8.6	Variation of the peak value of the power spectral density of $V_R$ as a function of the bifurcation parameter $K_A$ .	172
8.7	Power spectral densities of the states $E_{fd_1}$ , $E_{fd_2}$ , and $E_{fd_3}$ . The load on Bus 5 was used as a bifurcation parameter. The load value is 4.0 p.u.	174
8.8	Power spectral densities of the states $E_{fd_1}$ , $E_{fd_2}$ , and $E_{fd_3}$ . The load on Bus 5 was used as a bifurcation parameter. The load value is 4.4 p.u.	175
8.9	Power spectral density of $E_{fd_1}$ for three values of $P_{L_5}$ (the load on Bus 5): $P_{L_5} = 4.0$ p.u. (dash-dotted line), $P_{L_5} = 4.25$ p.u. (dashed line), and $P_{L_5} = 4.4$ p.u. (solid line).	175
9.1	Jump conditions.	184
9.2	AVR/PSS block representation.	186
9.3	Damping improvement from optimally tuning PSS limits.	187
9.4	Poincaré map.	188
9.5	Non-smooth limit cycle.	191
9.6	Grazing phenomenon.	192
9.7	Impedance plane trajectories.	194
10.1	STATCOM connected to SMIB system (plant).	204
10.2	STATCOM controller.	205
10.3	Plant: 160 MVA, 15 kV (L-L) SMIB test system.	206
10.4	$P-Q$ automatic power flow control diagram for the internal control of the SSSC.	208
10.5	Single machine infinite bus power system with a UPFC (dashed lines show the “plant”).	209
10.6	Series inverter control with conventional PI controllers, with neurocontroller and the inputs to the neurocontroller including two previous time delayed values of the signals.	211
10.7	Shunt inverter control with conventional PI controllers and neurocontroller.	212
10.8	Indirect adaptive neurocontroller design structure for a nonlinear plant consisting of a neuroidentifier and a desired response predictor.	213

10.9	Neuroidentifier structure for a STATCOM neurocontroller design.	216
10.10	Neuroidentifier training for a STATCOM neurocontroller design.	216
10.11	Neurocontroller structure for a STATCOM.	217
10.12	Line voltage during a 100 ms three-phase short circuit at the midline.	218
10.13	Generator terminal voltage during a 100 ms short circuit at the midline.	218
10.14	Training of SENC to update its weights by backpropagating the error signals at L.	219
10.15	Training of SHNC to update its weights by backpropagating the error signals at L.	220
10.16	Single machine infinite bus power system with a single transmission line and a UPFC.	222
10.17	Actual signal $P_{err}(t)$ of the plant and estimated signal $\hat{P}_{err}(t)$ by the SENI.	222
10.18	Actual signal $Q_{err}(t)$ of the plant and estimated signal $\hat{Q}_{err}(t)$ by the SENI.	223
10.19	Actual signal $V_{dcerr}(t)$ of the plant and estimated signal $\hat{V}_{dcerr}(t)$ by the SHNI.	223
10.20	Actual signal $V_{err}(t)$ of the plant and estimated signal $\hat{V}_{err}(t)$ by the SHNI.	223
10.21	Terminal voltage response of the synchronous generator operating ( $P = 0.65$ p.u. and $Q = 0.12$ p.u.) for a 180 ms three phase short circuit at Bus 2.	224
10.22	Load angle response of the synchronous generator operating ( $P = 0.65$ p.u. and $Q = 0.12$ p.u.) for a 180 ms three phase short circuit at Bus 2.	225
10.23	Load angle response of the synchronous generator operating ( $P = 0.8$ p.u. and $Q = 0.15$ p.u.) for a 180 ms three phase short circuit at Bus 2.	225
10.24	Critic network adaptation in DHP showing the implementation of (10.21).	228
10.25	Input-output mapping of the model network at $t$ used in the critic network adaptation in Figure 10.24.	228
10.26	Input-output mapping of the action network at $t$ used in the critic network adaptation in Figure 10.24. $A(t)$ in Figure 10.24 is $v_{cq}(t)$ and $v_{cd}(t)$ .	229
10.27	Action network adaptation in DHP.	231

10.28	NARMAX model for on-line training of the model network.	232
10.29	A 100 ms three phase short circuit test: $\delta$ .	233
10.30	A 100 ms three phase short circuit test: $V_t$ .	234
10.31	A 120 ms three phase short circuit test: $\delta$ .	234
10.32	A 120 ms three phase short circuit test: $V_t$ .	235
11.1	Decomposed approach for the simultaneous placement and tuning problem.	243
11.2	Representation of a potential solution for the combined placement and tuning problem for the Meta-heuristics approach.	244
11.3	Illustrative solution of a control design problem using Genetic Algorithms.	245
11.4	System used in Example 1.	248
11.5	Maximum and average fitness in Example 1.	249
11.6	Comparison of $B/C$ for the expert's and GA solutions.	250
11.7	Comparison of the SAIDI index for the expert's and GA solutions.	250
11.8	System used in Example 2.	251
11.9	Closed-loop setup.	255
11.10	Three-area six-machine power system	257
11.11	GA convergence performance.	260
11.12	Frequency response of the nominal SVC POD controller (dashed line) and the GA-designed SVC POD controller (solid line).	261
11.13	Frequency response of the nominal TCSC POD controller (dashed line) and the GA-designed TCSC POD controller (solid line).	262
11.14	Rotor speeds for the load-switching simulation using the nominal SVC and TCSD POD controllers.	263
11.15	Rotor speeds for the load-switching simulation using the GA-designed SVC and TCSD POD controllers.	263
12.1	Scatter plot of the actual load vs the model.	275
12.2	Correlation between the actual load and the model.	276
12.3	Convergence of the $R^2$ for the actual load vs the model.	276
13.1	Rescaling and filtering of harmonic voltage measurements.	298
13.2	The one-line diagram of the IEEE 14-bus system.	301

13.3	Original source signals: Active power drawn by load buses.	303
13.4	Mixed signals: Active power flow through branches.	304
13.5	Comparison of smoothed original signals and estimated signals.	305
13.6	Original source signals: Reactive load profiles.	306
13.7	Mixed signals: Voltage magnitude measurements at load buses.	307
13.8	Comparisons between smoothed original and estimated reactive load profiles.	308
13.9	Modified IEEE 14-bus test system.	309
13.10	Comparison of smoothed harmonic components of current injection at Bus 5.	310
13.11	Comparison of smoothed harmonic components of current injection at Bus 10.	311
13.12	Comparison of smoothed harmonic components of current injection at Bus 12.	312
13.13	Imaginary part of the 11 <sup>th</sup> harmonic source current at Bus 12 at scale $10^{-3}$ and scale $10^{-5}$ .	313

# List of Tables

1.1	Presentations on power systems.	4
1.2	Presentations on control systems.	5
1.3	Presentations on computational intelligence.	6
2.1	Approximate values of 1.0 SIL.	15
3.1	VSMI at the nose of the <i>PV</i> curve for Amite South Region.	32
3.2	VSMI for the Gypsy - South Norco 230 kV line.	33
4.1	Index of all complex eigenvalues in Figure 4.4.	49
5.1	The five most serious contingencies ranked by load margin to system collapse.	94
5.2	The five most serious contingencies ranked by load margin to thermal limit.	94
5.3	The five most serious contingencies ranked by load margin to voltage violation.	94
5.4	Output analysis of ATC evaluation.	95
5.5	Summary of corrective-mode ATC of 600-bus system.	97
8.1	Input-to-state participation factors and spectral peaks at $\omega_c$ .	168
8.2	Input-to-state participation factors and spectral peaks at $\omega_c$ for the single generator connected to an infinite bus.	171
8.3	Input-to-state participation factors for the 3-machine nine-bus system (partial listing). The load at Bus 5 is 4.4 p.u.	174
8.A.1	Parameter values for the single generator connected to an infinite bus model.	177
11.1	Reliability indices and benefit-cost ratio for the expert's solution in Example 1.	249
11.2	Reliability indices and benefit-cost ratios for the GA solutions in Example 1.	250

11.3	Reliability indices and benefit-cost ratio for the expert's solutions in Example 2 (F4) (F: fuse, S: sectionalizing switch).	252
11.4	Reliability indices and benefit-cost ratio for the GA solutions in Example 2 (F4).	252
11.5	Reliability indices and benefit-cost ratio for the GA solutions in Example 2 (F1).	253
11.6	Open-loop operating conditions.	258
11.7	Damping ratio (in %) for closed-loop eigenvalues.	260
13.1	Errors between estimated and actual smoothed reactive load profiles.	304
13.2	Errors between estimated and actual smoothed reactive load profiles.	306
13.3	Errors between estimated and actual smoothed harmonic current profiles.	313

# Preface

This edited volume is an outgrowth of a workshop entitled “Applied Mathematics for Deregulated Electric Power Systems: Optimization, Control, and Computational Intelligence,” held in Arlington, Virginia, on November 3-4, 2003, and sponsored by the National Science Foundation. It followed several previous NSF sponsored workshops on power systems, including:

- 1 “Urgent Opportunities for Transmission System Enhancement,” organized by Professor Chen-Ching Liu from the University of Washington, held in Palo Alto, California, on October 10-12, 2001, and co-sponsored by the Electrical Power Research Institute.
- 2 “Economics, Electric Power and Adaptive Systems,” organized by Professor Bruce Wollenberg from the University of Minnesota, held in Arlington, Virginia, on March 28-29, 2002, and co-sponsored by EPRI.
- 3 “Workshop on Global Dynamic Optimization of the Electric Power Grid,” organized by Professor Ronald Harley from Georgia Institute of Technology, held in Playacar, Mexico, April 11-13, 2002, and co-sponsored by EPRI.
- 4 “Modernizing the National Electric Power Grid,” organized by Professor Mladen Kezunovic from Texas A&M University, held in New Orleans, November 18-19, 2002, and co-sponsored by Entergy, the US Department of Energy, and EPRI.

Given that the earlier workshops had focused more on identifying and prioritizing power system problems, the purpose of this Applied Mathematics Workshop was to discuss the use of new mathematical tools, such as those developed in control, optimization, and computational intelligence, for applications to power system problems. It aimed at bridging the gap between applied mathematics and electric power engineering. A draft of Chapter 1 in this book was used as a guide for workshop speakers to prepare their presentations.

Although some people feel that many ideas from applied mathematicians and power academics are simply too blue sky to be applicable, the biggest power grid blackout event in US on the afternoon of August 14, 2003, has provided added urgency to our research activities and to the workshop. As long as the US and other nations continue to operate large interconnected power systems with ever expanding complexities, new ideas are needed to ensure their reliable operation.

The details on the Applied Mathematics Workshop are available at the web site [www.ecse.rpi/homepages/chowj](http://www.ecse.rpi/homepages/chowj). The power point presentations of all the speakers can be found from the web site, including a talk on the preliminary investigation of the August 14 blackout by Professor Robert Thomas of Cornell University.

The organizers of the workshop, who are also the editors of this volume, had planned to publish the proceedings of this workshop. All the speakers were invited to submit their articles to this edited volume. It was suggested to them that the articles should follow a three-part format: (1) a description of an important power system problem or problems, (2) the current practice and/or particular research approaches, and (3) future research directions. Our intent is to use these articles to motivate further research in these challenging areas. We are grateful to receive 12 articles, all written by renowned experts in their fields. Their dedication to scientific research and scholarly work is greatly appreciated.

Dr. James Momoh, director of the Control, Networks, and Computation Intelligence Program at NSF, on leave from Howard University, was instrumental in promoting and overseeing these workshops. The first and second editors (JHC and FFW) are grateful for his leadership. His counter part at EPRI, Dr. Massoud Amin, now at University of Minnesota, deserved credits for promoting these activities in EPRI. We would also thank Drs. Vasundara Varadan, Paul Werbos, and Kishan Behati at NSF, Directorate of Engineering for providing encouragements and support to this workshop. The financial support of NSF is gratefully acknowledged.

The completion of this edited volume would not be possible without the help of Ms. Xia Jiang, a PhD student at Rensselaer Polytechnic Institute. She learned to use Latex in one-minute flat and converted all the manuscripts to a common Latex format to ensure consistencies. Ms. Xuan Wei, who just completed her PhD at Rensselaer, helped with the workshop registration. My secretary, Ms. Audrey Hayner, took care of some of the conference finances. I am grateful for their help.

At Springer, Professor M. A. Pai and Mr. Alex Greene were very supportive of this project, and Ms. Melissa Sullivan helped with the manuscript preparation. Their collaboration is appreciated.

Finally, we would also like to acknowledge the support and understanding of our families during this endeavor, for organizing the workshop and for publishing this compilation.

JOE H. CHOW, TROY, NEW YORK  
JAMES A. MOMOH, WASHINGTON, DC  
FELIX F. WU, HONG KONG  
AUGUST 2004

## Contributing Authors

**Eyad H. Abed** has been with the University of Maryland since 1983, where he is presently a Professor in the Department of Electrical and Computer Engineering and the Director of the Institute for Systems Research. He has interests in control and monitoring of uncertain nonlinear systems, especially related to problems of bifurcation control. He is currently pursuing applications in several areas, including power systems, computer networks, and supercavitating bodies.

**Venkatramana Ajjarapu** received the PhD degree in electrical engineering from the University of Waterloo, Waterloo, ON, Canada in 1986. Currently he is an Associate Professor in the Department of Electrical and Computer Engineering at Iowa State University, Ames, IA, USA. His main area of interest is in power system security. He is applying recent advances in bifurcation methods for power system applications.

**Hsiao-Dong Chiang** received the BS and MS degrees in Electrical Engineering from the National Taiwan University, Taipei, Taiwan, and the PhD degree in electrical engineering and computer sciences from the University of California at Berkeley in 1986. He is currently a Professor of Electrical and Computer Engineering at Cornell University, Ithaca, NY. His research interests include the development of theoretical foundations and analytical tools for the analysis and control of physical systems, such as power and control systems, and the use of this work to achieve valuable and practical results. He is also interested in nonlinear systems theory, computation, and application to electrical circuits, signals, and systems and in global optimization techniques and applications. Dr. Chiang received the Presidential Young Investigator Award in 1989 from the National Science Foundation.

**Joe H. Chow** is a Professor of the Electrical, Computer, and Systems Engineering Department, Rensselaer Polytechnic Institute, Troy, New York. Before joining Rensselaer in 1987, he was an application engineer in the Power System Business of General Electric, Schenectady, New York. He received his PhD degree from the University of Illinois at Urbana-Champaign.

**Vaibhav Donde** received the BE (Electrical) degree from Veermata Jijabai Technological Institute (V.J.T.I.), University of Mumbai, India in 1998. He worked with Tata Consulting Engineers, Mumbai in 1998-1999, where he was involved in power systems study and relay coordination. He received the MS and PhD degrees in electrical engineering from the University of Illinois at Urbana-Champaign in 2000 and 2004, respectively. His research interests include power systems analysis, nonlinear and hybrid dynamic systems, and control systems and applications.

**Djalma M. Falcao** received the BS degree in 1971 and MS degree in 1974 from the Federal Universities of Parana and Rio de Janeiro, Brazil, respectively, and the PhD degree (1981) from the University of Manchester Institute of Science and Technology (UMIST), UK. He is currently a Professor of Electrical Engineering at the Federal University of Rio de Janeiro, Brazil. From 1991 to 1993, he was a visiting scholar at the University of California at Berkeley, USA. His research interest is in the area of computer methods for power system simulation, optimization, and control. Prof. Falcao is a Fellow of the IEEE.

**Eugene A. Feinberg** received his MS in Applied Mathematics from Moscow University of Transportation in 1976 and PhD in Probability and Statistics from Vilnius University, Lithuania, in 1979. He immigrated to the United States in 1988 and, after holding a faculty position at Yale University, he joined the State University of New York at Stony Brook, where he is currently a Professor at the Department of Applied Mathematics and Statistics. His research interests include stochastic models of operations research, Markov Decision Processes, and industrial applications of Operations Research and Statistics. He has published more than 60 papers and edited the Handbook on Markov Decision Processes.

**Dora Genethliou** was born in Cyprus and received her bachelor degree from the University of Cyprus, in 1999 and her Master degree from Stony

Brook University, in 2001. She is currently working towards her Ph.D on electric load forecasting.

**Floyd Galvan** received his BSEE degree from Texas A&M University-Kingsville in 1986, and a Master degree in Liberal Arts from Southern Methodist University, Dallas, TX, in 1998. Floyd has been a Registered Professional Engineer in the State of Texas since 1993. Floyd has worked as an engineer for Central Power & Light Company, Central & South West Corporation, Entergy Wholesale Organization, and currently for Entergy Transmission. Floyd currently is an industrial advisor to the National Science Foundation, and is actively involved in the Nations grid modernization efforts through industry and government councils.

**Ekrem Gursoy** is currently a PhD student in electrical engineering at Drexel University. He received his BS and MS degrees in Electrical Engineering from Istanbul Technical University, Turkey, in 1998 and 2000, respectively. His main research interests are in the application of statistical techniques in power system and power quality analysis.

**Ronald G. Harley** obtained his B.Sc.Eng degree (cum laude) and M.Sc.Eng degree (cum laude) from the University of Pretoria in 1960 and 1965, respectively, and the PhD degree from London University in 1969. He is currently the Duke Power Company Distinguished Professor at the Georgia Institute of Technology, Atlanta, USA. He is a Fellow of SAIEE, IEE, IEEE, the Royal Society of South Africa, and the University of Natal, and a Founder Member of the Academy of Science of South Africa formed in 1994. His research interests are in the dynamic and transient behavior of electric machines and power systems, and controlling them by the use of power electronics and intelligent control algorithms.

**Munther A. Hassouneh** received the BS degree from Birzeit University, West Bank, in 1997, and the MS and PhD degrees in 1999 and 2003, respectively, from the University of Maryland at College Park, all in Electrical Engineering. He is currently a post-doctoral research associate at the Institute for Systems Research, University of Maryland, working on projects in nonlinear control and applications.

**Tao He** is with Technical System Planning, Entergy Services, Inc., New Orleans, LA. He received his BS degree in Electric Power Engineering from Tsinghua University, Beijing, China, in 1994 and MS degree in

Electric Power Engineering from Rensselaer Polytechnic Institute, Troy, NY, in 2000. He worked as an engineer in Power System Analysis Group for Chinese Electric Power Research Institute in Beijing from 1994 to 1998.

**Ian A. Hiskens** is an Associate Professor of Electrical and Computer Engineering at the University of Wisconsin-Madison. He received the BEng (Electrical) and BAppSc (Mathematics) degrees from the Capricornia Institute of Advanced Education, Rockhampton, Australia in 1980 and 1983, respectively, and the PhD degree from the University of Newcastle, Australia in 1991. He has held prior appointments with the Queensland Electricity Supply Industry from 1980 to 1992, the University of Newcastle from 1992 to 1999, and the University of Illinois at Urbana-Champaign from 1999 to 2002. His major research interests lie in the area of power system analysis, in particular system dynamics, security, and numerical techniques. Other research interests include nonlinear systems and control.

**Marija Ilic** received the MS and DSc degrees in systems science and mathematics from Washington University, St. Louis, MO. She is a Professor of Electrical and Computer Engineering and Engineering and Public Policy at Carnegie Mellon University, Pittsburgh, PA. She was a Senior Research Scientist in the Department of Electrical Engineering and Computer Science at the Massachusetts Institute of Technology, Cambridge (1987-2002), a tenured Associate Professor at the University of Illinois, Urbana-Champaign, and an Assistant Professor at Cornell University, Ithaca, NY. Her interests include systems aspects of operations, planning, and economics of electric power.

**Sharma Kolluri** joined Entergy Services Inc., New Orleans, LA, in 1984, and is the Supervisor of Technical Studies Group. He received his BSEE degree from Vikram University, India, in 1973, MSEE degree from West Virginia University, Morgantown, in 1978, and the MBA degree from University of Dayton in 1984. He worked for AEP Service Corporation in Columbus, Ohio from 1977 through 1984 in the Bulk Transmission Planning Group. His areas of interest are Power System Planning, Reliability, and Insulation Coordination.

**Huawei Liao** is currently a PhD student in electrical engineering at Carnegie Mellon University. He received his BS and MS from Depart-

ment of Electrical Engineering, Chongqing University in China, in 1994 and 1997, respectively. From 1997 to 2001, he taught in Dept of Electrical Engineering at Huazhong University of Science and Technology in Wuhan, China. His current work focuses on statistical signal processing for power system analysis and operation.

**Sujit Mandal** is with Technical System Planning, Entergy Services, Inc., New Orleans, LA. He received the BTech degree in electrical engineering from the Indian Institute of Technology (IIT), Kanpur, India, and the MS degree in electrical engineering from Kansas State University, Manhattan, KS, in 1997 and 1999, respectively. He worked as a consultant at Power Technologies, Inc., Schenectady, NY, from 1999 to 2000.

**James A. Momoh** received the BSEE degree (1975) from Howard University, the MSEE degree (1976) from Carnegie Mellon University, the MS degree (1980) in Systems Engineering from the University of Pennsylvania, and the PhD degree (1983) in Electrical Engineering from Howard University. Professor Momoh was the Chair of the Electrical Engineering Department at Howard University and also the Director of the Center for Energy System and Controls. He was the Program Director of the power system program at National Science Foundation from 2001-2004. His current research activities are concentrated in stability analysis, system security and expert systems design for utility firms and government agencies. In 1987, he received a National Science Foundation Presidential Young Investigator Award. Dr. Momoh is a Fellow of IEEE and a Distinguished Fellow of Nigerian Society of Engineers. He was inducted as a Member of Nigerian Academy of Engineering in 2004.

**Dagmar Niebur** is an associate professor at Drexel University's Department of Electrical and Computer Engineering. Prior to her appointment at Drexel she held research positions at the Jet Propulsion Laboratory and the Swiss Federal Institute of Technology (EPFL), Lausanne, and a computer engineering position at the University of Lausanne. She received her Diploma in Mathematics and Physics from the University of Dortmund, Germany in 1984, the Diploma in Computer Science (1987) and the PhD degree in Electrical Engineering (1994) from EPFL. Her research focuses on intelligent information processing techniques for power system monitoring and control. In 2000, she received the NSF Career Award for work in this area.

**Jung-Wook Park** received the PhD degree from the Georgia Institute of Technology in August 2003. During the period of August 2003 to August 2004, Dr. Park was a Post-Doctoral Research Associate in the Department of Electrical and Computer Engineering, University of Wisconsin-Madison, USA. He is now a Senior Researcher in the Core Technology Group of LG Electronics, Seoul, Korea.

**Parviz Rastgoufard** is Professor and Chair of the Department of Electrical Engineering and Computer Science, Tulane University, New Orleans, LA, and holds the Entergy Chair in Electric Power Engineering. He received his BSEE degree from State University of New York at Buffalo in 1976, and MS and PhD degrees in Systems Science from Michigan State University in 1978 and 1983, respectively. He was a faculty in the Department of Electrical and Computer Engineering, North Carolina State University from 1983 to 1987. His current interests include on-line security and stability assessment and control, on-line monitoring and diagnosis of transmission systems and components pattern analysis, and teaching and research on application of computational intelligence in power systems.

**Mohamed S. Saad** received the BS and MS degrees in electrical engineering from Cairo University, Egypt, in 1997 and 2000, respectively. He is currently pursuing a PhD degree in electrical engineering at the University of Maryland, College Park where he is also a graduate research assistant. He has done research on fault detection and diagnosis of electrical motors, and stability analysis and control of power systems.

**Peter W. Sauer** obtained his BS in Electrical Engineering from the University of Missouri at Rolla in 1969, and the MS and PhD degrees in Electrical Engineering from Purdue University in 1974 and 1977, respectively. His main work is in modeling and simulation of power system dynamics with applications to steady-state and transient stability analysis. He is a registered Professional Engineer in Virginia and Illinois, a Fellow of the IEEE, and a member of the U. S. National Academy of Engineering.

**Dragoslav D. Siljak** is the B & M Swig University Professor in the School of Engineering, Santa Clara University, and teaches courses in system theory and applications. His research interests are in the theory of large-scale systems and its applications to problems in control engi-

neering, power systems, economics, aerospace, and model ecosystems. He is the author of the monographs Nonlinear Systems (Wiley, 1969), Large-Scale Dynamic Systems (North Holland, 1978), and Decentralized Control of Complex Systems (Academic Press, 1991). He is an honorary member of the Serbian Academy of Sciences, and is a Life Fellow of IEEE.

**Glauco N. Taranto** is an Associate Professor of the Electrical Engineering Department of COPPE/Federal University of Rio de Janeiro, Brazil since 1995. He received his BS degree in electrical engineering from the State University of Rio de Janeiro, in 1988, MS degree in electrical engineering from the Catholic University of Rio de Janeiro, in 1991, and PhD degree in electric power engineering from Rensselaer Polytechnic Institute, Troy, NY, in 1994. His research interests include power system stability and control design, and optimization methods such as genetic algorithms.

**Ganesh Kumar Venayagamoorthy** received his BEng degree with First Class Honors in Electrical and Electronics Engineering from the Abubakar Tafawa Balewa University, Bauchi, Nigeria, and his MScEng and PhD degrees in electrical engineering from the University of Natal, Durban, South Africa, in 1994, 1999 and 2002, respectively. He is currently an Assistant Professor at the University of Missouri-Rolla, USA. His research interests are in computational intelligence, power systems, control systems, and evolving hardware. He is a 2004 NSF CAREER award recipient, the 2003 International Neural Network Society Young Investigator award recipient, a 2001 recipient of the IEEE Neural Network Society summer research scholarship, and the recipient of five prize papers with the IEEE Industry Application Society and IEEE Neural Network Society.

**Felix F. Wu** received the BS degree in Electrical Engineering from National Taiwan University, Taipei, Taiwan, R.O.C., the MS degree in Electrical Engineering from the University of Pittsburgh, Pittsburgh, PA, and the PhD degree in Electrical Engineering and Computer Science from the University of California, Berkeley, in 1965, 1969, and 1972, respectively. From 1976 to 1977, he worked for Pacific Gas and Electric as a Computer Applications Engineer. He held a TEPCO (Tokyo Electric Power Company) Professorship at the University of Tokyo, Japan, in 1991. Currently, he is Professor of Electrical Engineering at the University of Hong Kong. Prior to that he was a professor and vice-chair

of Department of Electrical Engineering and Computer Science, University of California, Berkeley. His research interests include electric energy industry restructuring, power system investment planning, design of modern control centers, distribution automation, and distributed processing.

**Aleksandar I. Zecevic** is an Associate Professor in the School of Engineering, Santa Clara University, where he teaches courses in the area of electric circuits. His research interests include graph theoretic decomposition algorithms, parallel computation, and control of large-scale systems. He is particularly interested in the theory and applications of large electric circuits, such as those arising in power systems and VLSI design.

# Chapter 1

## APPLIED MATHEMATICS FOR RESTRUCTURED ELECTRIC POWER SYSTEMS

Joe H. Chow

*Rensselaer Polytechnic Institute*

[chowj@rpi.edu](mailto:chowj@rpi.edu)

Felix F. Wu

*Hong Kong University and University of California, Berkeley*

[ffwu@eee.hku.hk](mailto:ffwu@eee.hku.hk)

James A. Momoh

*Howard University and National Science Foundation*

[jmomoh@nsf.gov](mailto:jmomoh@nsf.gov)

**Abstract** This first chapter summarizes the motivation for holding the November 2003 National Science Foundation Workshop, and provides a listing of the Workshop speakers and their presentations. It also contains an overview of the articles contained in this compilation.

**Keywords:** Large scale power systems, systems engineering, control systems, computational intelligence, power system restructuring, electricity market deregulation.

### 1. Introduction

The achievements in system engineering in advancing power system reliability and security over the last three decades, accomplished by taking full advantages of advances in computer, communication, and control technologies, are truly remarkable. For example, the economic genera-

tion commitment and dispatch with security constraints for large power systems are now routinely solved using efficient Lagrangian-relaxation methods [1] and interior-point methods [2]. State estimation with bad data and topology detection capability [3], has become a mainstay in many control centers, and has gone from being an advisory tool to being used in real-time energy price calculation [4]. Fast stability analysis has benefited from energy function analysis [5, 6, 7], which also contributed to enhanced understanding of modes of instability. Tools for analyzing voltage stability, a phenomenon not noted until the 1970's, have been well-developed [8, 9]. It is now common for control center operators to rely on the power-voltage ( $P$ - $V$ ) sensitivity curve in determining admissible power transfer across major congested interfaces. Small-signal stability has evolved from a power system stabilizer adding damping to the local swing mode to the need to damp interarea mode oscillations based on coherency analysis [10, 11], which drives the development of the wide-area monitoring system (WAMS) installed in the western US system [12]. Flexible AC Transmission Systems (FACTS) [13], based on advances in high-voltage power electronics, allow the control of bus voltages and power flows on transmission lines, as well as provide damping enhancement [14]. More recently, artificial neural networks and genetic algorithms have been applied to several power system problems, including damping control design [15, 16, 17]. From a public policy viewpoint, the work in [18] was singularly significantly in the restructuring of the power industry originally organized as regional monopolies [19, 20].

Such accomplishments were achieved, in part, due to highly focused university research programs supported by the Energy Research and Development Agency (ERDA), Department of Energy (DOE), National Science Foundation (NSF), Electric Power Research Institute (EPRI), and many utilities and manufacturers in the US, as well as their international counterparts. In particular, this very successful research process was driven from two directions: power system problems had motivated the development of new applied mathematical tools, and conversely, advances in applied mathematics were customized to form systematic approaches to complex power system problems.

Although we can point to many successes, the August 14, 2003 Northeast US Blackout [21] is a stark reminder that the increasing complexity of interconnected power systems continues to outstrip the preparedness of automatic control and protection systems and power control centers to deal with extreme contingencies. The unprecedented magnitude of overloading on a group of transmission lines in Ohio and the subsequent redistribution and swings in power flow when these lines were tripped resulted in system conditions not foreseen in any system planning and

operation studies, causing several interconnected systems to separate and collapse.

Power grid control problems, in normal and emergency operating conditions, need to be continuously studied. The task is particularly challenging in deregulated electricity markets where the basic structure of decision-making has moved from centralization towards decentralization. The objective of November 3-4, 2003 NSF Workshop, entitled “Applied Mathematics for Deregulated Electric Power Systems: Optimization, Control, and Computational Intelligence,” was to delineate major technical and engineering issues related to reliability and security of power systems arising from growing system complexities, increased transmission congestions, and structural changes for which basic research can contribute. In particular, such fundamental changes in infrastructures require a reevaluation of issues related to information, coordination, and computation in the analysis and control of power system.

Cross-disciplinary fertilization has benefited the development of power system engineering a great deal in the past and will definitely benefit even more in the future. This Workshop was intended to bring authorities in several relevant disciplines to stimulate discussions on how to bring the latest advances in these disciplines to bear on rethinking and reformulating problems of reliability and security in power systems. The following disciplines, in particular, were identified as potential suppliers of new philosophies and new tools for emerging problems in power systems. They included: Distributed Optimization, Nonlinear Control, Adaptive Control, Dynamical System Theory, and Distributed Artificial Intelligence. Recent developments in these disciplines had been revolutionary and most likely would bring in fresh ideas and new approaches to problems of information, coordination and computation in power system reliability and security.

## 2. Workshop Presentations

The presentations in the Workshop were divided into three groups, as listed in Tables 1.1-1.3. The overhead slides used by all the presenters are available from the web site [www.ecse.rpi.edu/homepages/chowj](http://www.ecse.rpi.edu/homepages/chowj).<sup>1</sup>

The topics of the speakers in the first group (Table 1.1) were on power system issues, such as voltage stability and oscillatory stability. They covered some of the most urgent current planning and operating problems in power systems, and were useful to the non-power attendees at

<sup>1</sup>Due to the lack of time, the last two speakers in Table 1.3 did not get to present their discussion at the Workshop. They had, however, graciously posted their presentations on the web site as well.

the Workshop. The most popular topic among this group, as had been for some time in the power research community, was voltage stability. The

*Table 1.1.* Presentations on power systems.

<i>Speakers and affiliations</i>	<i>Presentation titles</i>
Felix Wu Hong Kong University	Power System Security
Peter Sauer University of Illinois, Urbana-Champaign	Reactive Power and Voltage Control
Marija Ilic Carnegie-Mellon University	Large Scale Dynamic Network Systems Revisited: The Case of Electric Power Systems
Hsiao-Dong Chiang Cornell University	A Novel Deterministic Paradigm for Global Optimal Technology – A Dynamical Trajectory- Based Paradigm
Robert Thomas Cornell University	The August 14 Northeast Blackout
Sujit Mandal Entergy	Identification of Voltage Stability Weak Points in Bulk Power Systems
Venkataramana Ajjarapu Iowa State University	Bifurcation and Manifold Based Approach for Voltage and Oscillatory Stability Assessment and Control
Aleksandar Stankovic Northeastern University	Hilbert Space Approach to Modeling and Compensation of Reactive Power
Efrain O'Neill-Carrillo University of Puerto Rico, Mayaguez	Modern Mathematics Applications in Power System Control, Security, and Restoration
Miguel Velez-Reyes University of Puerto Rico, Mayaguez	Challenges in Modeling and Identification of Power Systems: Dealing with Ill-Conditioning, High Dimensionality and Other Challenges
Lamine Mili Virginia Polytechnic and State University	Challenges in Power System State Estimation
Ronald Harley Georgia Institute of Technology	Report of the EPRI-NSF Workshop in Playacar on Dynamic Optimization of the Electric Power Grid

increased loading of transmission systems and the restructuring of the electricity markets, resulting in sometimes unpredictable flow paths, have greatly increased the concern of system voltage as the limiting factor in stability considerations.

The second group of speakers discussed new advances in Control Systems. By nature, a power system is large, is nonlinear, and undergoes continuous changes. The presentations listed in Table 1.2 touched on these topics. The presented work was more at the conceptualization phase and would require additional investigations to prove their applicability.

The last group of speakers (Table 1.3) focused on the computational intelligence area, which can be defined as the study of the design of intelligent agents. An intelligent agent is a system that acts intelligently. The central scientific goal of computational intelligence is to understand the principles that make intelligent behavior possible, in natural or artificial systems [22]. The interest in using computational intelligence for power system problems had been quite high, as witnessed by the number of recent papers presented in power conferences and journals. The specific topics presented in this Workshop included approximate dynamic programming, neural networks, and genetic algorithms, with applications to energy pricing, risk and portfolio analysis, load forecasting, and power system control design.

*Table 1.2.* Presentations on control systems.

<i>Speakers and affiliations</i>	<i>Presentation titles</i>
Petar Kokotovic University of California, Santa Barbara	Recent Nonlinear Control Design methods and their Applications
Dragoslav Siljak University of Santa Clara	Robust Control of Large Power Systems via Convex Optimization
Gang Tao University of Virginia	Adaptive Actuator Failure Compensation
Eyad Abed University of Maryland	Instability Monitoring and Control of Power Systems
Ian Hiskens University of Wisconsin	Dynamic Embedded Optimization and Shooting Method for Power System Performance Assessment

*Table 1.3.* Presentations on computational intelligence.

<i>Speakers and affiliations</i>	<i>Presentation titles</i>
Dagmar Niebur Drexel University	High Order Statistical Techniques for Power System Signal Estimation and Identification
Shi-Jie Deng Georgia Institute of Technology	Heavy-Tailed GARCH Models: Pricing and Risk Management Application in Power Markets
Benjamin Van Roy Stanford University of Virginia	Approximate Dynamic Programming
Warren Powell Princeton University	Approximate Dynamic Programming for High Dimensional Resource Allocation
Djalma Falcao Federal University of Rio de Janeiro	Placement and Coordinated Tuning of Control Devices for Capacity and Security Enhancement using Genetic Algorithms and Other Metaheuristics
Warren Adams Clemson University	Attractive Mathematical Representation of Decision Problems
Rene Carmona Princeton University	Portfolio Risk in the Power Markets
Donald Wunsch University of Missouri-Rolla	Systems of Systems: Cybersecurity Vulnerabilities and Opportunities Affecting the Power Grid
Eugene Feinberg Stony Brook University	Load Forecasting
Ganesh Venayagamoorthy University of Missouri-Rolla	Approximate Dynamic Programming and Reinforcement Learning for Nonlinear Optimal Control of Power Systems

### 3. Synopses of the Articles in this Compilation

The speakers at the Workshop were invited to write up their presentations and submit them to this edited volume. It was suggested to them that the articles should follow a three-part format: (1) a description of an important power system problem or problems, (2) the current practice and/or particular research approaches to deal with the problem, and (3) future research directions in that problem area. Our intent is to use these articles to motivate further research in these challenging areas.

A total of 12 articles were received, some with a slightly different title than the one used in the presentation. Each of the articles is presented as a chapter in this compilation. They are arranged in an order such

that all articles on similar topics are clustered together and then the first and/or the last articles in the clusters would provide some transitions between the clusters. We hope that this ordering will serve best a reader intending to study all the articles.

The first four articles (Chapters 2-5) are on power system stability. Sauer's article presents an introduction to power system reactive power stability, written in a fashion suitable for non-power engineers. The article by He, *et al.*, provides a method to find "weak" buses in a power system, which are vulnerable to voltage collapse. Such constraints can be accounted for dispatch and be considered for future reactive power support enhancement. Ajjarapu's article provides an analytical overview of voltage and oscillatory stability and defines boundary predictors and correctors that can be used to compute stability margins. The article by Chiang and Li proposes a methodology to compute load margins subject to static and dynamic security constraints for large power systems.

The last article in the first group by Ilic (Chapter 6) discusses a vision of power system hierarchical control utilizing an information technology infrastructure that spans broad ranges of time horizon and system details. The next three articles (Chapter 7-9) are broadly based on control theory and follow the theme of Ilic's hierarchical control. The article by Zečević and Šiljak presents a method to design decentralized controllers using linear matrix inequalities. In the article by Abed, *et al.*, the authors provide an input-to-state participation factor approach to apply probe signals to monitor system stability. In Chapter 9, Hiskens, *et al.*, discusses system performance optimization for continuous analog systems with discrete states and events as a dynamic embedded optimization.

The last set of articles (Chapters 10-13) is on the application of computational intelligence to power systems, of which the first two are also on controls. Venayagamoorthy and Harley discuss in their article the use of neuroidentifiers and neurocontrollers for FACTS controllers, as well as an adaptive critic design. Falcaõ and Taranto use genetic algorithms for optimal protection device placement in distribution networks and coordinated tuning of power system controls. The last two articles are on different aspects of load modeling. Feinberg and Genethliou's article discusses statistical approaches to short- and long-term load forecasting. The article by Niebur, *et al.*, reports successful applications of the independent component analysis techniques for both active and reactive load estimation.

## 4. Conclusions

In this chapter we have provided the background and purpose of this compilation of articles from leading researchers in power systems, control systems, and computational intelligence. The remaining 12 chapters in this book discussed research areas where applied mathematics can have an impact on the reliable operation of large-scale interconnected power systems. A few chapters are of the survey or tutorial type, whereas some others discuss more specific approaches. We hope that the materials, together with suggested research directions, will offer applied mathematicians and power system engineers and researchers ideas for future investigations.

## References

- [1] S. Virmani, E.C. Adrian, K. Imhof, and S. Mukherjee. Implementation of a Lagrangian Relaxation Based Unit Commitment Problem. *IEEE Transactions on Power Systems*, 4:1373–1380, 1989.
- [2] J.A. Momoh and J.Z. Zhu. Improved Interior Point Method for OPF Problems. *IEEE Transactions on Power System*, 14:1114–1120, 1999.
- [3] A. Monticelli. *State Estimation in Electric Power System: a Generalized Approach*. Kluwer Academic Publishers, Boston, 1999.
- [4] NYISO Market Structure Working Group. *Real-Time Scheduling System: Concept of Operations*. June 3, 2002 meeting, available from [www.nyiso.com](http://www.nyiso.com).
- [5] H.-D. Chiang, M.W. Hirsch, and F.F. Wu. Stability Regions of Nonlinear Autonomous Dynamical System. *IEEE Transactions on Automatic Control*, 33:16–27, 1988.
- [6] J. Zaborszky, G. Huang, B. Zheng, and T.-C. Leung. On the Phase Portrait of a Class of Large Nonlinear Dynamic Systems such as the Power System. *IEEE Transactions on Automatic Control*, 33:4–15, 1988.
- [7] M.A. Pai. *Energy Function Analysis for Power System Stability*. Kluwer Academic Publishers, Boston, 1989.
- [8] C.W. Taylor. *Power System Voltage Stability*. McGraw Hill, New York, 1994.
- [9] T. Van Cutsem and C. Vounas. *Voltage Stability of Electric Power Systems*. Kluwer Academic Publishers, Boston, 1998.

- [10] R. Podmore. Identification of Coherent Generators for Dynamic Equivalents. *IEEE Transactions on Power Apparatus and Systems*, PAS-97:1344–1354, 1978.
- [11] J.H. Chow, G. Peponides, P.V. Kokotovic, B. Avramovic, and J.R. Winkelman. *Time-Scale Modeling of Dynamic Networks with Applications to Power Systems*. Lecture Notes in Control and Information Sciences, 46, Springer-Verlag, New York, 1982.
- [12] J. Hauer, D. Trudnowski, G. Rogers, B. Mittelstadt, W. Litzenberger, and J. Johnson. Keeping an Eye on Power System Dynamics. *IEEE Computer Applications in Power*, 10-4:50–54, October 1997.
- [13] N. G. Hingorani and L. Gyugyi. *Understanding FACTS*. IEEE Press/McGraw-Hill, New York, 2000.
- [14] E.V. Larsen and J.H. Chow. SVC Control Design Concepts for System Dynamic Performance. in IEEE Power Engineering Society Publication 87TH0187-5-PWR Application of Static Var Systems for System Dynamic Performance, 1987.
- [15] A.L.B. Do Bomfim, G.N. Taranto, and D.M. Falcao. Simultaneous Tuning of Power System Damping Controllers using Genetic Algorithms. *IEEE Transactions on Power Systems*, 15:163–169, 2000.
- [16] J.-W. Park, G.K. Venayagamoorthy, and R.G. Harley. Adaptive Critic Designs and their Implementations on Different Neural Network Architectures. *Proceedings of the International Joint Conference on Neural Networks*, 3:1879–1884, 2003.
- [17] A.I. Megahed and O.P. Malik. Experimental Testing of a Neural Network Based Digital Differential Relay for Synchronous Generators. *IEEE Transactions on Power Delivery*, 15:80–85, 2000.
- [18] F.C. Schweppe, M.C. Caramanis, R.D. Tabors, and R.E. Bohn. *Spot Pricing of Electricity*. Kluwer Academic Press, Boston, 1988.
- [19] M. Ilic, F. Galiana, and L. Fink. *Power System Restructuring: Engineering and Economics*. Kluwer Academic Publishers, Boston, 1998.
- [20] M. Shahidehpour and M. Alomoush. *Restructured Electrical Power Systems: Operation, Trading, and Volatility*. Marcel Dekker, New York, 2001.
- [21] *Blackout, Can It Happen Again?*. Time, August 25, 2003.
- [22] D. Poole, A. Mackworth, and R. Goebel. *Computational Intelligence: A Logical Approach*. Oxford University Press, New York, 1998.

## Chapter 2

# REACTIVE POWER AND VOLTAGE CONTROL ISSUES IN ELECTRIC POWER SYSTEMS

Peter W. Sauer

*University of Illinois at Urbana-Champaign*

[sauer@ece.uiuc.edu](mailto:sauer@ece.uiuc.edu)

**Abstract** This chapter was prepared primarily for “non power” engineers to introduce reactive power and voltage control concepts, and to identify several issues that remain as research challenges in this area. It begins with basic definitions and information on reactive power, and then focuses on problems that have been known for many years and have surfaced recently in power system operations. These problems are described in the framework of traditional security analysis used in control centers throughout the world. The research challenges identify areas where collaboration between power systems engineers and applied mathematicians could yield major advances in power system reliability.

**Keywords:** Voltage collapse, Maximum power transfer, Var reserves, reactive power, voltage control, security analysis, power transfer capability.

### 1. Introduction

There has been a very large effort to understand reactive power and voltage control issues in power systems in the last 15 years [1, 2, 3, 4, 5]. While this work has produced a significant volume of results that explain various phenomena and propose potential solutions to problems, much of it has not been taken to the stage of useful application software and hardware in actual power systems. In addition, there remain serious issues of how traditional controls impact the interaction between the flow of real and reactive power on a system level when an objective might be to maximize real power transfer capabilities. There has been a strong temptation to try and separate the voltage/MVar problems with

the angle/MW problems. While this separation is valuable because it allows decoupling that might be useful in some computational algorithms and in understanding fundamental phenomena, this separation cannot be made when systems are stressed to their physical limitations. On the contrary, the interaction between real and reactive power (and voltage magnitudes and angles) becomes very complex under these extreme conditions [6]. This chapter begins with an introduction to reactive power and how it relates to voltage control. This is followed by several examples that illustrate problems which remain in the operations environment of electric power systems.

## 2. Reactive Power

Reactive power is a quantity that has become fundamental to the understanding and analysis of AC electric power systems. It is rarely mentioned in physics text books and is often clouded in mystery because of its “imaginary” status in the mathematics that electrical engineers use to describe certain phenomenon in AC circuits. The fundamental definition of reactive power can be explained by first looking at the relationship between a sinusoidal voltage and current waveforms of the same frequency (Figure 2.1). Reactive power has its origin in the phase shift between these two waveforms. When a device consumes real power such that the voltage and current waveforms are in phase with each other, the device consumes zero reactive power. When the current defined “into” a device lags the voltage, it consumes reactive power (this is the case in Figure 2.1). The amount of reactive power consumed by the device depends on the phase shift between the voltage and current.

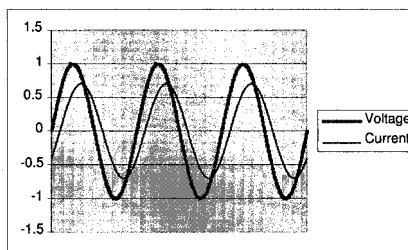


Figure 2.1. Voltage and current waveforms.

To formally see how this works, consider the instantaneous power (simple product of voltage times current) consumed by a device as shown in Figure 2.2. This power has two interesting characteristics. First, it is double the frequency of the original voltages and currents. Second, it is not symmetric above and below the horizontal axis. This power can

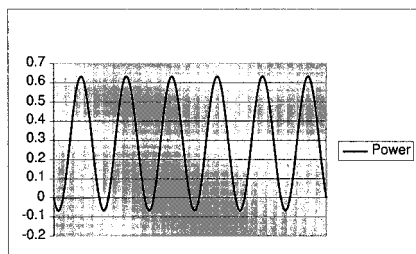


Figure 2.2. Instantaneous power.

be decomposed into two waveforms one that is always positive plus one that is symmetric about the horizontal axis as shown in Figure 2.3.

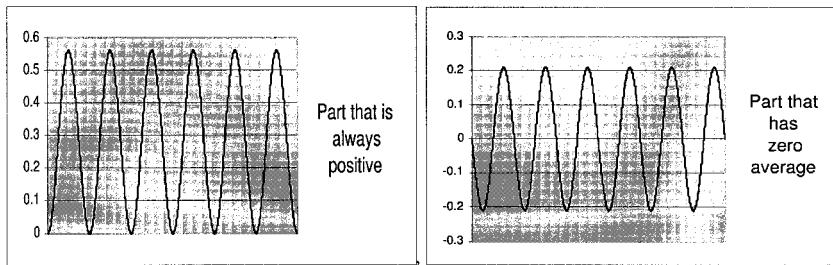


Figure 2.3. Decomposition of instantaneous power.

This decomposition yields the following two terms which formally define real ( $P$ ) and reactive ( $Q$ ) power, where the units of  $Q$  are Volt-Amperes-Reactive (Vars) to distinguish this component from  $P$ :

$$\begin{aligned} P(1 - \cos(2\omega t)) &: P = 0.275 \text{ Per Unit Watts} \\ -Q \sin(2\omega t) &: Q = 0.205 \text{ Per Unit Vars} \end{aligned} \quad (2.1)$$

This definition of reactive power leads to the definition of complex power  $S$  as

$$S = VI^* = P + jQ \quad (2.2)$$

where  $V$  and  $I$  are the complex “Root Mean Square” phasor representations of the voltage and current, and  $*$  denotes conjugation. From this relationship, it is clear that reactive power ( $Q$ ) will have a serious impact on both the voltages in a network and the currents.

### 3. Reactive Power in Operations

Reactive power affects power system operation in numerous ways:

- 1 Loads consume reactive power, so this must be provided by some source.

- 2 The delivery system (transmission lines and transformers) consumes reactive power, so this must be provided by some source (even if the loads do not consume reactive power). Note however that all transmission lines do provide some reactive power from their shunt line charging which offsets their consumption of reactive power in their series line losses.
- 3 The flow of reactive power from the supplies to the sinks causes additional heating of the lines and voltage drops in the network.
- 4 The generation of reactive power can limit the generation of real power.

So, one primary dilemma with reactive power is that a sufficient quantity of it is needed to provide the loads and losses in the network, but having too much reactive power flowing around in the network causes excess heating and undesirable voltage drops. The normal answer to this dilemma is to provide reactive power sources exactly at the location where the reactive power is consumed. And, since strictly speaking it does not take any "fuel" to provide reactive power, it should be possible to distribute reactive power sources (such as capacitors) all around the network to avoid the problem of heating the conductors and causing voltage drops. Unfortunately, this is not practical in the extreme since there are literally millions of lines and loads connected to the grid and so this would require millions of reactive power sources - all controlled to provide exactly the right amount of reactive power at the right time - every second of every day. The best we can do in most cases is work with some type of aggregation of load (say at the feeder leaving a substation) and at terminals of major lines and transformers. This also brings up the issue of the difference between power factor control (trying to exactly provide the right amount of reactive power needed to equal that which is consumed) and voltage control (trying to keep voltage levels at exactly the right level no matter how much reactive power it takes).

Reactive power is both the problem and the solution to network voltage control. The reactance of lines creates a voltage drop which must be compensated for whether the actual line flow is transferring real or reactive power (or both). The reactance also consumes reactive power which must be provided from some source. Serving reactive power to loads is especially difficult because the reactive power must flow from the source to the load - thereby increasing reactive losses - which in turn requires more reactive power from the source. The response of reactive power sources varies from milliseconds to seconds. The use of synchronous machines is the most common source for reactive power

(and also voltage control). The excitation system which provides the dc to the field winding of the machine adjusts the reactive power output (or input) to maintain the desired voltage set point. But, generators also have capability curves which bound the combination of real and reactive power output. The phenomena which bound the output vary from heating of the stator to heating of the rotor, stability, and other physical constraints. In some regions, this curve is simply the bound on the square root of the sum of the squares of  $P$  and  $Q$  (called “apparent power”).

There is a basic concept that is taught in power system analysis that provides an interesting fact about transmission lines and their loading level. The Surge Impedance Load (SIL) of a lossless transmission line is the amount of load delivered to a pure resistance equal to the characteristic impedance (square root of  $L/C$  where  $L$  and  $C$  are the incremental distributed series inductance and shunt capacitance). A line with 1.0 SIL loading will have a flat voltage profile (same voltage from sending to receiving end), and the same current all along the line. The voltage and current will be in phase along the entire line. The reactive power into the line from the shunt capacitance charging is exactly equal to the reactive power consumed by the series inductance losses. Approximate values of 1.0 SIL are given in Table 2.1.

*Table 2.1.* Approximate values of 1.0 SIL.

69 kV	10 MW
138 kV	50 MW
230 kV	150 MW
345 kV	400 MW
500 kV	1000 MW
765 kV	2000 MW

In some sense, 1.0 SIL is the “ideal” loading for a transmission line. In very early work on the analysis of transmission line loading capabilities, St. Clair created a composite curve which provided the maximum loading for transmission lines in terms of SIL and line length in miles [7].

The bounds on loading in the St. Clair curve consider three phenomena – thermal, voltage, and stability. For short lines, the loading is constrained by thermal limits. For medium length lines the loading is constrained by voltage drop. For long lines the loading is limited by steady-state stability (or maximum power transfer). While these limitations are all well known, the composite plot of these constraints for any line length of any voltage is interesting and provides a good physical feeling for line loadability and the possible sources of limitation.

The voltage collapse phenomenon remains a major issue for power system networks. In the words of Carson Taylor [8], “A power system at a given operating state and subject to a given disturbance undergoes voltage collapse if post-disturbance equilibrium voltages are below acceptable limits. Voltage collapse may be total (blackout) or partial.” Similarly, Prabha Kundur says [9], “Voltage stability is the ability of a power system to maintain steady acceptable voltages at all buses in the system under normal operating conditions and after being subjected to a disturbance. A system enters a state of voltage instability when a disturbance, increase in load demand, or change in system condition causes a progressive and uncontrollable drop in voltage.” Prabha Kundur goes on to say, “The main factor causing instability is the inability of the power system to meet the demand for reactive power. The heart of the problem is usually the voltage drop that occurs when active power and reactive power flow through the inductive reactance associated with the transmission network.” He also states, “Voltage collapse is the process by which the sequence of events accompanying voltage instability leads to a low unacceptable voltage profile in a significant portion of the power system.” Finally, he indicates, “A criterion for voltage stability: inject Vars at bus  $k$  and the voltage at bus  $k$  goes up ( $V-Q$  sensitivity is positive).” These collective statements indicate how widely different the interpretation of the issue of “voltage collapse” can be.

Walter Lachs [10] provided a possible scenario for voltage collapse (given in [9]):

- 1 Generating units near load centers out of service. Heavily loaded lines and low Var reserves.
- 2 Loss of a heavily loaded line. Increases other line loadings and Var losses - voltage reduction.
- 3 Load consumption would temporarily lower to stabilize. AVR<sub>s</sub> would act to restore generator voltages, but increased Var flow would lower voltages elsewhere.
- 4 The ULTCs (Under Load Tap Changers) at load centers would increase distribution voltages and so the load would go back up, and EHV voltages would go back down.
- 5 Generators would hit Var limits.

Over the years, a fairly common interpretation of voltage collapse is: “Static” voltage collapse has become synonymous with maximum power transfer and the ability to solve a load flow problem. “Dynamic” voltage collapse involves detailed load models, control and other dynamics.

## 4. A Fundamental Illustration

A very simple illustration reveals several very fundamental issues with reactive power and voltage control as they relate to power system security analysis. Consider a case where two areas with generation are interconnected through multiple transmission lines as shown in Figure 2.4. For simplicity, the lines do not have resistance or shunt capacitive charging elements.

This “Case 1” shows that both areas have adequate voltage control (evident by the voltage levels of 1.0 p.u.). The West area is providing 3,000 MW to the East area through 6 identical transmission lines (500 MW per line). The East generator is providing 150 MVar into the lines and the West generator is also providing 150 MVar into the lines to collectively provide the 300 MVar of reactive power losses. The East generator has a MVar limit of 1,200. The West generator has unlimited Var capability.

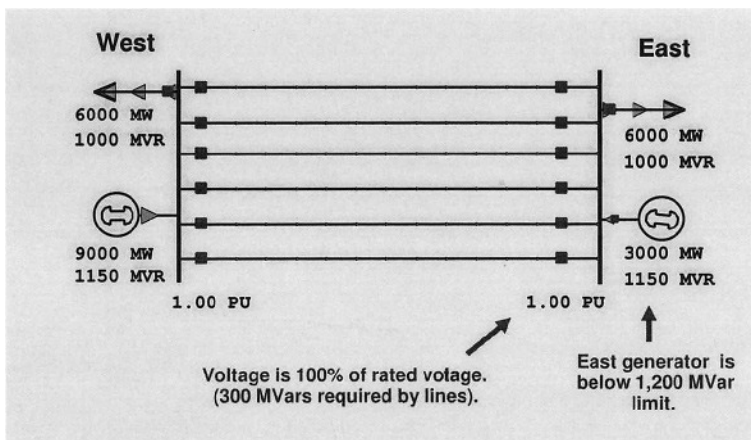


Figure 2.4. Illustration Case 1 (all lines in).

Figure 2.5 shows the situation when one of the transmission lines is removed (perhaps by relay action). The 3,000 MW transfer is now divided equally as 600 MW per line and the voltage at both ends is acceptable (voltage levels of 1.0 p.u.) and the East generator Var supply requirement is still below the 1,200 limit. The reactive power losses in the 5 remaining lines now totals 362 MVar (half from each generator).

Figure 2.6 shows the result of losing 2 lines, which causes the East generator to hit its reactive power supply limit. However, the East voltage has not dropped below 1.0, so this is a critical point where the

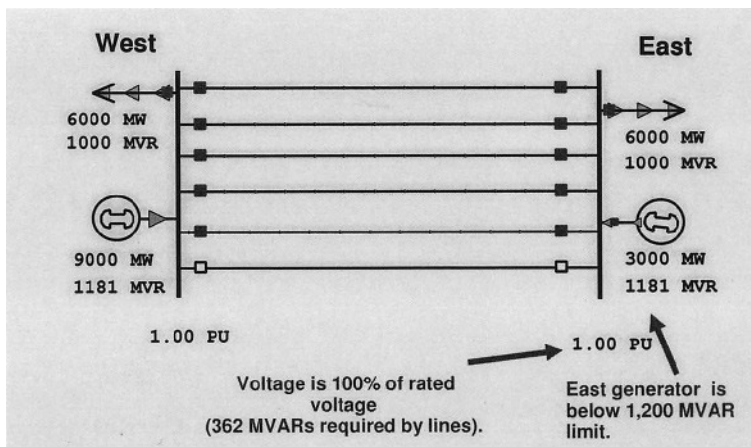


Figure 2.5. Illustration Case 2 (one line out).

reactive power supply available in the East is exhausted, but the voltage is still normal. The reactive power losses in the lines are now 453 MVar.

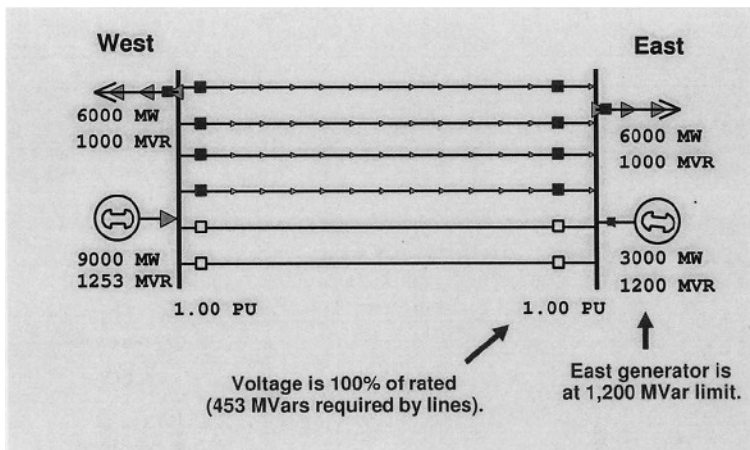


Figure 2.6. Illustration Case 3 (two lines out).

Figure 2.7 shows the result of losing 3 lines. The East voltage is now starting to drop (down to 0.99 p.u.), and the line reactive power losses have increased to 611 MVar.

Figure 2.8 shows the case for four lines out which loads the remaining two lines to 1,500 MW each with an accompanying reactive power total loss of 957 MVar. The East generator bus voltage drops to 0.97 p.u. (still above acceptable levels). One important point here is that with

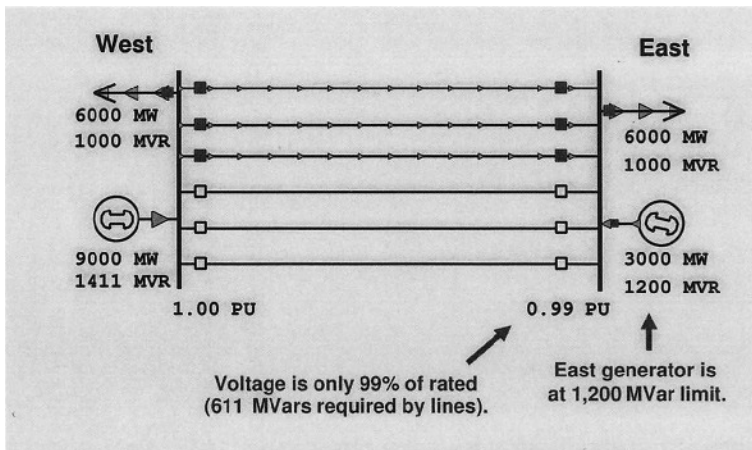


Figure 2.7. Illustration Case 4 (three lines out).

four lines out, the system still seems acceptable in terms of voltage levels (remaining line loadings are not enforced here).

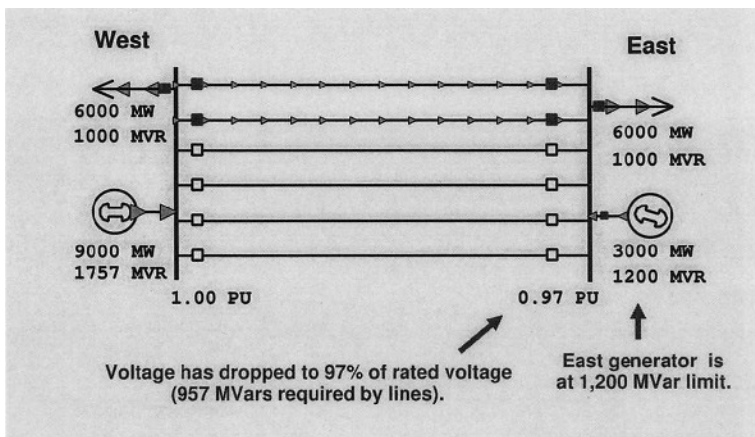
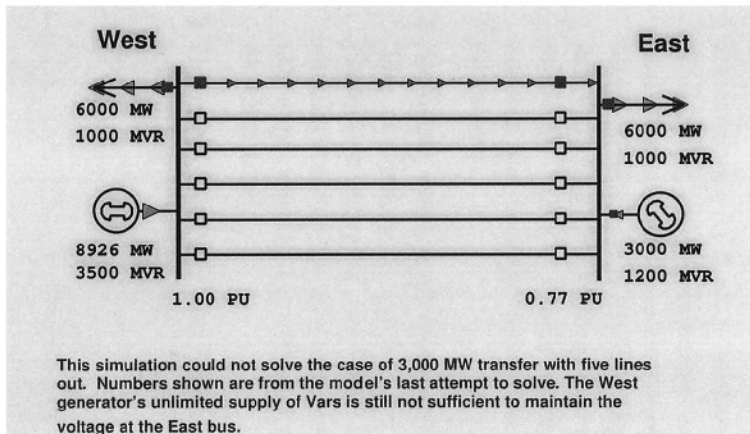


Figure 2.8. Illustration Case 5 (four lines out).

Figure 2.9 shows that when a fifth line is removed, the system can no longer transfer 3,000 MW and the computer solution fails to converge to a solution.

While in the real network, the loads might change under this condition, the computer solution attempts to enforce the 3,000 MW transfer. Some would consider this a voltage collapse, although examination of the “rotor angles” of the East generator indicates that this bus likely



*Figure 2.9. Illustration Case 6 (five lines out).*

has an angle difference which could be considered an “angle stability” problem or a “maximum power transfer” problem. Whatever it is called, this illustrates the importance of reactive power in the cases where lines are lost.

The remaining figures indicate what would happen if unlimited reactive power supply was available in the East.

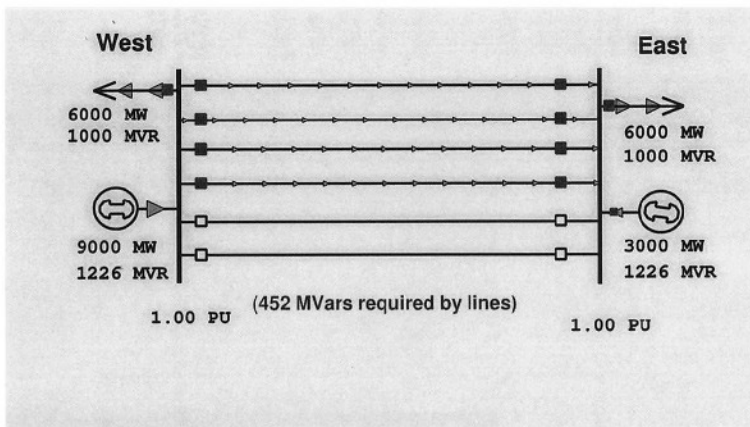


*Figure 2.10. Illustration Case 7 (two lines out - unlimited Vars).*

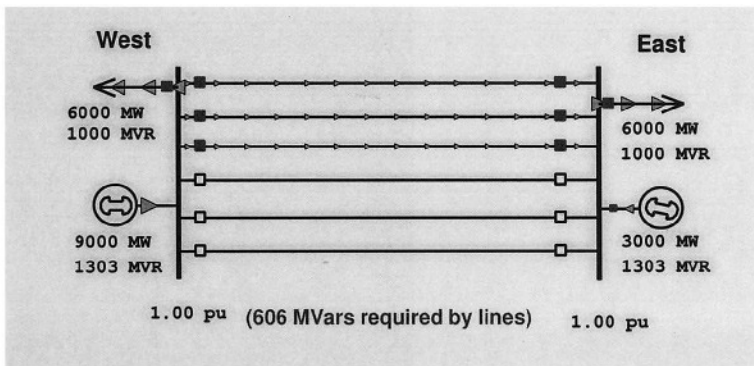


Figure 2.11. Illustration Case 8 (three lines out - unlimited Vars).

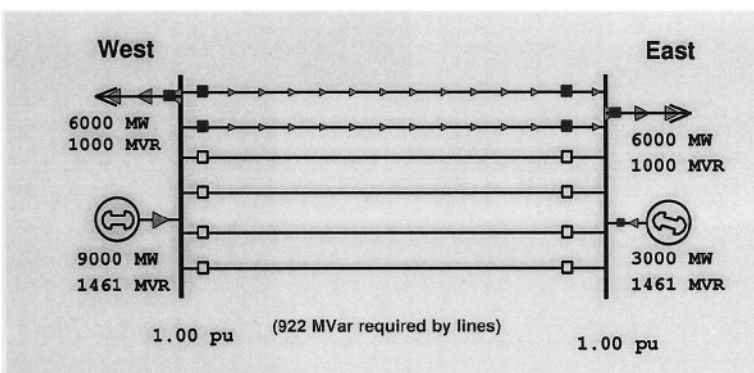


Figure 2.12. Illustration Case 9 (four lines out - unlimited Vars).

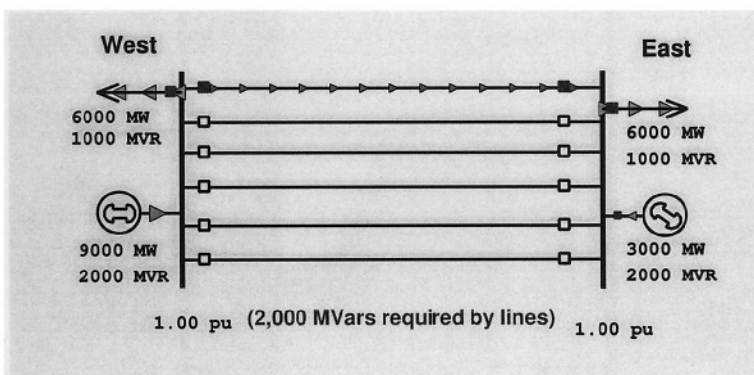


Figure 2.13. Illustration Case 10 (five lines out - unlimited Vars).

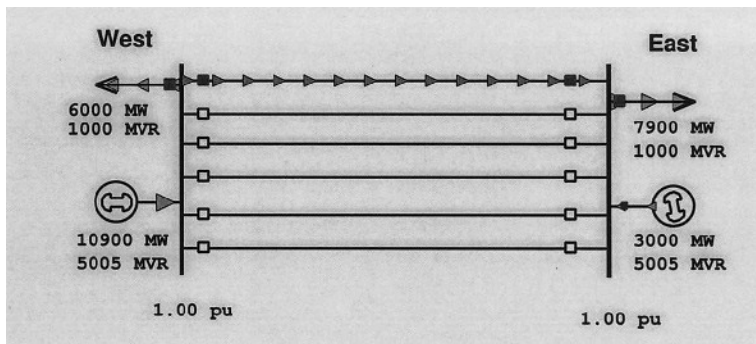


Figure 2.14. Illustration Case 11 (five lines out - unlimited Vars - maximum power transfer).

While line loading may be a thermal problem, there is no “voltage collapse” or “power transfer” problem in the cases where 5 lines are lost. In fact, the absolute maximum power transfer that can be achieved with full voltage control at both ends is shown in Figure 2.14 to be 4,900 MW.

## 5. Challenges in Voltage Control and Related Security

There are many challenges to voltage control and security in power systems. A few of these are indicated below:

- 1 Determining AVR set points and supplementary input signals: The Automatic Voltage Regulator set points for voltage control are normally not currently determined by any global system strategy for some optimal performance. Supplementary signals to enhance stability during disturbances are also based primarily on local considerations. There is a need to formulate a global strategy for voltage control and reactive power dispatch for both static and dynamic situations.
- 2 Modeling what really happens when excitation systems hit limits: The mathematical models for excitation limiters and associated protective relaying need to be incorporated in security analysis simulations. In many cases the excitation limit controls have several steps which yield different results in terms of what is controlled at what time.
- 3 Optimal placement and control of Static Var Compensators (SVC) and other Var sources: There remains a major challenge to deter-

mine the best locations and controls for reactive power devices to provide maximum benefit to the system as a whole during normal operation and contingencies.

- 4 The constraints of “acceptable” margins: Several components of security analysis are based on maintaining a reasonable distance to limits. While several margin concepts have been proposed over the years, these margins have not been properly incorporated into analysis tools that determine secure operation. This is particularly difficult for the margins to voltage collapse and transient stability.
- 5 Determination of “acceptable” Var margins: It is clear that in some cases, even an infinite amount of reactive power may not be enough support to accommodate certain levels of power transfer. Determining the acceptable size, location, and response characteristics of Var support is a major challenge in this area.
- 6 New security concepts: A challenging and useful margin would be to compute the minimum number of things that can be lost without resulting in cascading failure. This departs from the traditional N-1 criteria and characterizes a security margin in terms of number of contingencies required to create a blackout.
- 7 Reactive power computation in fast contingency analysis: Traditional linear contingency analysis completely ignores voltage and reactive power issues. There is an open challenge to rapidly compute the impact of contingencies on voltage and the margin to voltage collapse.

## 6. Conclusions

The purpose of this chapter was to provide background information on the mathematical challenges associated with voltage control and reactive power supplies. Several fundamental properties of reactive power and the consequences of shortages in reactive power reserves have been discussed. Open research issues associated with voltage control and reactive power support have also been discussed. These research issues are especially difficult because of the complex interaction between real and reactive power from an engineering point of view, and from an economic point of view. The power engineering community and industry at large could benefit greatly from the contributions that the mathematical community might make in these areas.

## References

- [1] *Proceedings of Bulk Power System Voltage Phenomena—Voltage Stability and Security.* Potosi, MO, September 19-24, 1988.
- [2] *Proceedings of NSF Workshop on Bulk Power System Voltage Phenomena—Voltage Stability and Security.* Deep Creek Lake, MD, August 4-7, 1991.
- [3] *Proceedings of Bulk Power System Voltage Phenomena III—Seminar on Voltage Stability, Security and Control.* Davos, Switzerland, August 22-26, 1994.
- [4] *Proceedings of the Symposium on Bulk Power System Dynamics and Control IV—Restructuring.* Santorini, Greece, August 24-28, 1998.
- [5] *Proceedings of Bulk Power Systems Dynamics and Control V—Security and Reliability in a Changing Environment.* Onomichi, Japan, August 26-31, 2001.
- [6] C.D. Vournas, P.W. Sauer, and M.A. Pai. Relationships between Voltage and Angel Stability of Power Systems. *International Journal of Electrical Power and Energy Systems*, 18:493–500, 1996.
- [7] H.P. St. Clair. Practical Concepts in Capability and Performance of Transmission Lines. *AIEE Transactions*, 72:1152–1157, 1953.
- [8] C.W. Taylor. *Power System Voltage Stability.* McGraw-Hill, New York, 1994.
- [9] P. Kundur. *Power System Stability and Control.* McGraw Hill, New York, 1994.
- [10] W.R. Lachs. *Voltage Collapse in EHV Power Systems.* Paper A78057-2, 1978 IEEE PES Winter Meeting, New York, January 28-February 3, 1978.

## Chapter 3

# IDENTIFICATION OF WEAK LOCATIONS IN BULK TRANSMISSION SYSTEMS USING VOLTAGE STABILITY MARGIN INDEX

Tao He

*Entergy*

the@entergy.com

Sharma Kolluri

*Entergy*

vkollur@entergy.com

Sujit Mandal

*Entergy*

smandal@entergy.com

Floyd Galvan

*Entergy*

fgalvan@entergy.com

Parviz Rastgoufard

*Tulane University*

pr@eecs.tulane.edu

**Abstract** *PV* curve analysis is widely used in the industry for investigating voltage stability problems. However, *PV* curve analysis does not provide any information about weak facilities with potential voltage problems in the system. This paper presents a new method of finding the weak

locations in a large-scale power system. The new method is based on the relationship between voltage stability and the angle difference between sending- and receiving-end buses. This relationship is derived for a simplified two-bus system and later applied to a large system. For any given operating point, this new approach calculates the Voltage Stability Margin Index (VSMI) of every line in the system. The VSMI provides information about the weak locations and also estimates voltage stability margin from the collapse point - lower VSMI value indicates lower margin and vice versa. The proposed method was applied to one of the critical regions in the Entergy System and was successful in identifying weak facilities. Because of simplified approach and ability to calculate indices quickly, the new approach has the potential of being used in a real time environment.

**Keywords:** Voltage stability, voltage collapse, Voltage Stability Margin Index (VSMI), *PV* curve, voltage stability weak point.

## 1. Introduction

With the increased loading of transmission lines, the voltage stability problem has become a very critical issue for most power system planners and operators. The main challenge of this problem is to pinpoint the locations of voltage instability and to understand the cause of voltage instability [4, 5]. Typically, *PV* curve analysis is widely used in the industry for analyzing voltage stability problems [1]. However, the *PV* curve analysis has the following limitations:

- 1 *PV* curves show the behavior of system bus voltages only when the transmission system is under stressed condition.
- 2 *PV* curves are not very useful in identifying the weak buses in the system.
- 3 *PV* curve analysis is only valid for a particular scenario. If the scenario changes, a new set of *PV* curves needs to be reproduced. This process can be very time consuming.

In this chapter, a new approach for studying voltage stability problem has been developed. The relationship of voltage stability and angle difference between sending- and receiving-end buses is described, and the concept of Voltage Stability Margin Index (**VSMI**) is introduced. Initially **VSMI** is calculated for any given operating condition and subsequently can be quickly recalculated for other operating conditions. The **VSMI** is ultimately used to estimate voltage stability margin and identify the weak transmission lines and buses at any given operating

condition. As the new approach is much faster when compared to *PV* analysis, it has the potential for being applied to real time applications.

The basic mathematical model for the new approach is explained in Section 2. The equations for the mathematical formulation of the new approach are shown in Section 3. The application of the method to a large scale power system is described in Section 4. Simulation results are presented in Section 5. Conclusions are given in Section 6.

## 2. Basic Mathematical Model

The basic concepts of this new approach can be explained with a simple two-bus system. This two-bus system is illustrated in Figure 3.1.

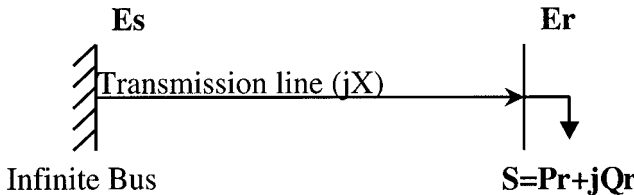


Figure 3.1. A simple two-bus system.

The two-bus system in Figure 3.1 has an infinite bus with the voltage of  $E_s$ , a load bus with the voltage of  $E_r$ , and a transmission line with the impedance of  $jX$ . The basic assumptions for this two-bus system are:

- 1 The sending-end bus is an infinite bus with voltage  $E_s$  always at 1.0 p.u.
- 2 The receiving-end bus is a load bus with voltage  $E_r$ , which can vary with the change of load  $S$ .
- 3 The load  $S$  can be varied with constant power factor.
- 4 The transmission line is lossless.

From the fundamental equations of active power and reactive power for a transmission line [2], the following equations can be derived:

$$E_r = E_s \frac{\cos(\phi_r + \theta)}{\cos \phi_r} \quad (3.1)$$

$$P_r = \frac{1}{2} \frac{E_s^2}{X} \left( \frac{\sin(\phi_r + 2\theta)}{\cos \phi_r} - \tan \phi_r \right) \quad (3.2)$$

where  $\tan \phi_r = Q_r/P_r$ ,  $E_s$  is the sending-end voltage,  $E_r$  is the receiving-end voltage,  $P_r$  is the receiving-end active power,  $Q_r$  is receiving-end reactive power,  $\theta$  is the angular difference between the sending- and receiving-end bus voltages, and  $X$  is the reactance of the transmission line.

From equations (3.1) and (3.2), the equation of maximum  $P_r$ , for any given  $Q_r/P_r$ , can be derived. The corresponding angular difference of the sending- and receiving-end bus voltages,  $\theta$ , and the receiving-end voltage,  $E_r$ , can also be derived as

$$P_{r\max} = \frac{1}{2} \frac{E_s^2}{X} \left( \frac{1}{\cos \phi_r} - \tan \phi_r \right) \quad (3.3)$$

$$E_{r\max} = E_s \frac{\cos(\phi_r + (\pi/2))}{\cos \phi_r} \quad (3.4)$$

when

$$\theta_{r\max} = \frac{\pi/2 - \phi_r}{2} \quad (3.5)$$

The above equations were verified using the two-bus test system given in [1]. From these equations, it can be seen that there is a relationship between voltage stability and angle difference between the sending- and receiving-end buses. When the angle difference approaches  $\theta_{r\max}$ , the corresponding  $P_{r\max}$  and  $V_{r\max}$  are supposed to be at the nose point of the  $PV$  curve. This relationship is clearly illustrated in Figure 3.2. As shown in Figure 3.2, from the Voltage-Angle and Power-Angle curves, the  $PV$  curve can be obtained for any given Q/P ratio.

Because there is a relationship between voltage stability and angle difference of sending- and receiving-end buses, the voltage stability margin can be estimated based on how close  $\theta$  is to  $\theta_{r\max}$ . For any given operating condition, the receiving-end Voltage Stability Margin Index (**VSMI**) [6, 7] can be calculated from

$$\mathbf{VSMI} = \frac{\theta_{r\max} - \theta}{\theta_{r\max}} \quad (3.6)$$

The **VSMI** value indicates how close the angle  $\theta$  is from the maximum angle  $\theta_{r\max}$ . Therefore a higher value of **VSMI** implies that  $\theta$  is farther away from the  $\theta_{r\max}$  and the two-bus system has a larger voltage stability margin. On the other hand, a lower value of **VSMI** means that  $\theta$  is closer to the  $\theta_{r\max}$  and hence, a smaller voltage stability margin.

Equations (3.1) through (3.6) are based on the assumption that sending-end bus is an infinite bus. If, instead of the sending-end bus, the

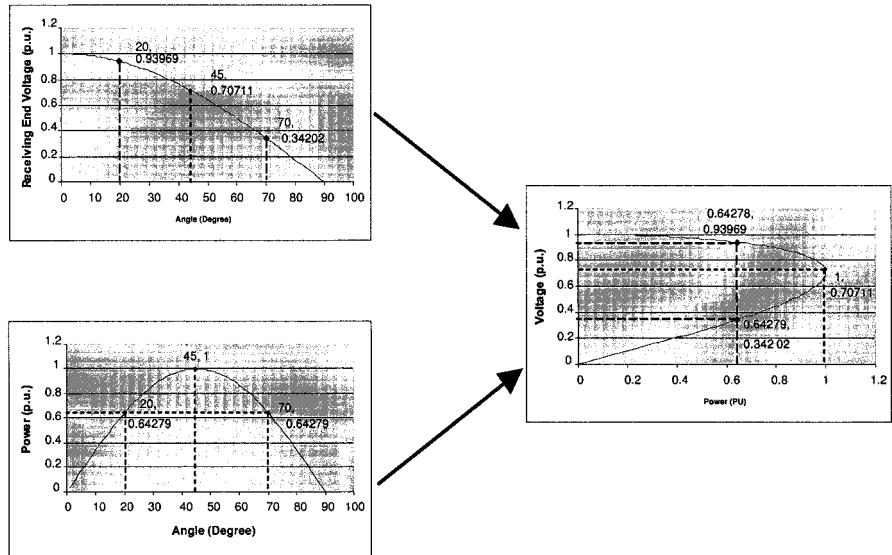


Figure 3.2. Process to develop PV curve from voltage-angle and power-angle curves.

receiving-end bus is considered to be an infinite bus, then the following set of equations can be derived for the sending-end bus:

$$E_s = E_r \frac{\cos(\phi_s - \theta)}{\cos \phi_s} \quad (3.7)$$

$$P_s = \frac{1}{2} \frac{E_r^2}{X} \left( \frac{\sin(2\theta - \phi_s)}{\cos \phi_s} - \tan \phi_s \right) \quad (3.8)$$

where  $\tan \phi_s = Q_s/P_s$ ,  $P_s$  is the sending-end active power, and  $Q_s$  is the sending-end reactive power.

The equations of the maximum  $P_{s\max}$  and corresponding  $\theta_{s\max}$  and  $V_{s\max}$  are

$$P_{s\max} = \frac{1}{2} \frac{E_r^2}{X} \left( \frac{1}{\cos \phi_s} + \tan \phi_s \right) \quad (3.9)$$

$$E_{s\max} = E_r \frac{\cos((\phi_s - (\pi/2))/2)}{\cos \phi_s} \quad (3.10)$$

when

$$\theta_{s\max} = \frac{\pi/2 + \phi_s}{2} \quad (3.11)$$

for any given ratio of  $Q_s/P_s$ .

### 3. Application of the New Method to Large Scale Power Systems

In order to apply this approach to a large-scale transmission system, a two step process was used.

In the first step, to study the voltage stability margin of any transmission line, the system has to be simplified into an equivalent two-bus system for this particular line. This is explained in Figure 3.3. Basically the idea is to keep all operating conditions of the transmission line intact and simply represent the rest of the system as the sending-end infinite bus.

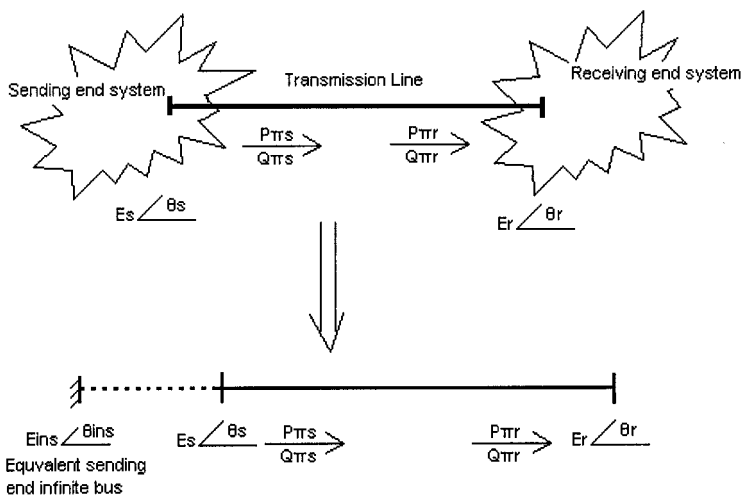


Figure 3.3. Simplify large scale power system to equivalent two-bus system.

As the voltage stability problem is mostly a local area problem, the system can be represented by a two-bus system for the given transmission line, provided the following conditions are kept the same.

- 1 The sending-end voltage  $E_s$ .
- 2 The receiving-end voltage  $E_r$ .
- 3 The angular difference between the sending- and receiving-end bus voltages.
- 4 The sending-end power flow  $P_s + jQ_s$ .
- 5 The receiving-end power flow of  $P_r + jQ_r$ .

The equivalent two-bus system can be obtained, if it is further assumed that:

- 1 Sending-end infinite-bus voltage  $E_s$  is 1.0 p.u.
- 2 The  $X/R$  ratio of the source impedance from the equivalent sending-end infinite bus to the sending-end bus is equal to that of the transmission line.

In the second step, after the equivalent two-bus system is obtained, the **VSMI** of the two-bus system can be calculated by assuming that the  $Q/P$  ratio of the receiving end is kept constant. This **VSMI** value is the voltage stability indicator for the receiving end of the transmission line. The above two-step approach was applied to all the lines in the system for determining the receiving-end **VSMI** values.

In the above discussion, the receiving-end **VSMI** was calculated based on the assumption that the sending-end system can be represented by an infinite bus. Similar approach can be used for calculating the sending-end **VSMI** if assuming the receiving-end system can be represented by an infinite bus.

For any transmission line, there will be two **VSMI** values – one for the sending end and one for the receiving end. The lower of these two **VMSI** values should be selected to indicate the voltage stability margin for any given line. The voltage stability ranking of the lines is provided by comparing the **VSMI** values. The transmission line with a lower **VSMI** value will be ranked higher than those with higher values. Thus relatively weak transmission lines and buses can be identified from the ranking table.

#### 4. Simulation Results

The proposed method was applied to the Amite South Region in the Entergy system for identifying the weak transmission lines and buses. The 2004 summer peak case was used for this study, with an expected peak load of 6,200 MW in this region. There are 5 major 230 kV tie lines into this area and three critical units on the 230 kV system. Loss of one major tie line and one critical unit can lead to severe voltage stability problem in the region. In order to verify the results of the new approach, the *PV* curve analysis was also performed.

By using the *PV* curve approach, the voltage collapse point in this region was identified. For verification purposes, the **VSMI** was calculated at this operating point. The results using the new approach are shown in Table 3.1. Only the transmission lines, for which the **VSMI** is below 10%, are included in the table.

Table 3.1. VSMI at the nose of the PV curve for Amite South Region.

From Bus	To Bus	$E_s$ (p.u.)	$E_r$ (p.u.)	P (MW)	Q/P	VSMI (%)
GYPSY	SOUTH NORCO	0.941	0.914	841.5	0.35	0.9
BAGATELLE	SORROENTO	0.963	0.958	96.7	0.40	2
9MILE	NAPOLEON	0.884	0.876	266.5	0.27	2
LABARRE	PARIS	0.881	0.878	171.1	0.25	3
9MILE	DERBIGNY	0.884	0.876	244.2	0.25	3
KAISER	PACKENHAM	0.865	0.865	131.9	0.24	3
NAPOLEON	MARKET ST.	0.876	0.875	149.3	0.24	3
DONALDSON VILLE	BAYOU VERRET	0.984	0.978	187.5	0.33	6
9MILE	ESTELLE	0.884	0.873	219.5	0.23	7
GYPSY	UNIV. CITY	0.941	0.895	576.0	0.31	7
GYPSY	PONTCHARTR AIN	0.941	0.888	584.3	0.30	7
SLIDELL	MICHoud	0.909	0.900	323.5	0.26	7
SOUTH NORCO	PROSPECT	0.914	0.912	756.2	0.24	8
ESTELLE	PETERS ROAD	0.873	0.870	182.5	0.18	9
SOUTH PORT	JOLIET	0.882	0.879	349.8	0.18	10
PROSPECT	GOODHOPE	0.912	0.911	721.6	0.23	10

The following observations can be made from Table 3.1:

- 1 The lines identified in Table 3.1 are found to be the major tie lines in the Amite South area. The **VSMI** index for these lines is observed to be below 10%, which indicates that they are weak lines.
- 2 The Gypsy to South Norco 230kV line, which carries the most power into this area, was found to have the lowest **VSMI** index (less than 1%). This indicates that the line is heavily loaded and has very low voltage stability margin.
- 3 The results in Table 3.1 are found to be consistent with the *PV* curve analysis.

Because the Gypsy to South Norco 230 kV line is one of the most severely loaded lines in the Amite South region, it is interesting to show how the **VSMI** values for this line change with various operating conditions along the *PV* curve. The simulation results for the Gypsy to South Norco 230 kV line under different operating conditions is shown in Table 3.2.

Table 3.2. **VSMI** for the Gypsy - South Norco 230 kV line.

<i>Unit Output (MW)</i>	$E_s$ (p.u.)	<i>Sending End VSMI (%)</i>	$E_r$ (p.u.)	<i>Receiving End VSMI (%)</i>
550	0.988	16.2	0.967	86.8
450	0.986	15.4	0.964	85.3
350	0.981	13.6	0.958	83.3
300	0.971	10.4	0.947	79.8
260	0.960	6.87	0.935	76.1
210	0.941	0.9	0.914	70.1

The observations from the Table 3.2 are as follows:

- 1 Both the sending- and receiving-end **VSMI** decrease with increasing stress on the interface serving the problem region.
- 2 The sending-end **VSMI** has lower value than the receiving-end **VSMI**. Therefore the sending-end **VSMI** should be used for ranking the voltage stability margin of the line.
- 3 The sending-end **VSMI** decreases from 16.2% to 0.9% as the operating point moves along the *PV* curves. At the nose of *PV* curve, the value of **VSMI** was found to be 0.9%, which is considered to be very low. This indicates that there is no voltage stability margin available for this line to carry more power.

This new approach was applied to the other parts of Entergy system for identifying the voltage stability weak locations. The simulation results show that the weak locations or critical transmission lines in the problem area were successfully identified using the proposed approach.

## 5. Conclusions

This chapter presents a new simplified approach for analyzing voltage stability problem in large scale power systems. The basic concepts

and equations of this new approach are derived from a simplified two-bus system. By using a two-bus system to represent large-scale power systems and by studying some reported research describing voltage stability margins [7,8,9,10], we feel that the new approach can be applied to large-scale power systems. Using this approach, **VSMI** is calculated for all the transmission lines in a given system or area. Based on the values of **VSMI**, the relative strength or weakness of the transmission lines is determined. Transmission lines with low **VSMI** value are considered to be weak lines and give an indication of voltage stability margins in the area.

This new approach was applied to the Amite South area in the Entergy system. The purpose of this analysis was to determine voltage stability margin for this area and identify facilities in the area which can lead to voltage stability problem. The *PV* analysis was performed to verify results using the new approach. For the results, it is observed that

- 1 **VSMI** can be used to indicate the voltage stability margin.
- 2 **VSMI** can provide very useful information to identify the weak points in large-scale power systems.
- 3 **VSMI** will change automatically with different operating condition and does not depend on any particular scenario.
- 4 **VSMI** can be used to for real time operation purpose as it is a simple and faster approach as compared to *PV* analysis.

The simulation results show that this new approach works very well for transmission line of normal *Q/P* ratio. However, the results also show that this new method has some limitation on those transmission lines with high *Q/P* ratios ( $> 1$ ). Some further work has to be carried out to address the following issues:

- 1 Understand the cause and function of those transmission lines with high *Q/P* ratio ( $> 1$ ).
- 2 Modify the equations of **VSMI** for those transmission lines with high *Q/P* ratio ( $> 1$ ).
- 3 Modify the equations to take transformer taps and negative impedance into the consideration.

The investigation reported in this paper is an on-going activity at Entergy Service Inc. and we will publish our findings in subsequent papers as they become available.

## 6. Future Work

During the simulation, the results show that there are always some negative **VSMI** indexes before voltage collapse. Normally the negative **VSMI** index appears on the transmission lines having high  $Q/P > 1$  ratio and most of them are found close to the reactive power sources, such as **SVC** and synchronous condensers. Basically the function of this type of lines is transferring reactive power instead of active power. Even though it give us some indication about the reactive flow situation in large-scale power systems, these transmission lines are not as critical as tie lines for voltage stability problem. It is better to use some screening criteria to find out the important lines, which are critical for voltage stability. There are two parameters, which can be used for this screening purpose: power and line length. Basically, the ideas are:

- 1 If the line transfers more active power, it is more likely to be the critical tie line for either the sending- or receiving-end system, and more prone to have voltage stability problems.
- 2 For a long transmission line, even though the active power flow is low, it is still prone to have voltage stability problem. Therefore the length of transmission line needs to be considered as a screen criterion.

These two parameters have been used as screening criteria for some preliminary studies. The simulation results show this method is very effective. However, some future work still needs to be done on combining these two parameters into one criterion.

Because the **VSMI** calculation is simple and very fast, there are some future works on the real time application of the **VSMI** index:

- 1 Voltage stability is closely related to the maximum loadability of transmission systems. To fully utilize existing transmission assets, the operators need some real time tools to track how close the transmission system is to its loadability limits. The main challenge is that the system maximum loadability changes with the system operation conditions, such as generator dispatch, transmission line outages, load distribution, and unexpected disturbances. All these conditions vary with time. Because the **VSMI** index can be readily and quickly estimated with the changing operation condition, it is a very appropriate index for this real time application. Some software could be developed based on the **VSMI** index and associated with an **EMS** system to provide alarms to the operators about weak locations.

- 2 For many systems, the voltage can appear normal even though the grid is on the verge of voltage instability. Therefore voltage is not a very good indicator. It is very difficult to choose voltage setpoints to shed load in voltage stability problem areas. The **VSMI** index is a much better indicator than voltage for voltage stability problem. Some load shedding schemes could be designed based on the **VSMI** index.
- 3 Under severe operating conditions, it is preferable to disconnect the voltage stability unstable system from the main system to protect the main system. Some special control schemes or relay devices could be developed for this purpose. The **VSMI** index could be programmed in these equipment to detect the voltage instability condition.

## References

- [1] C.W. Taylor. *Power System Voltage Stability*. McGraw-Hill, New York, 1994.
- [2] J.J. Grainger and W.D. Stevenson. *Power System Analysis*. McGraw-Hill, New York, 1994.
- [3] J. Zaborszky and J.W. Rittenhouse. *Electric Power Transmission*, Volumes 1 and 2. The Rensselaer Bookstore, New York, 1969.
- [4] I. Musirin and T.K. Abdul Rahman. Estimating Maximum Loadability for Weak Bus Identification using FVSI. *IEEE Power Engineering Review*, 22(11):50–52, November 2002.
- [5] M.H. Haque. Determination of Steady-State Voltage Stability Limit using P-Q Curves. *IEEE Power Engineering Review*, 22(4):71–72, April 2002.
- [6] P. Rastgoufard, T. He, S. Mandal, S. Kolluri, and F. Galvan. Identification of Weak Voltage Buses for Entergy Transmission System. Entergy Technical Report, May 2003.
- [7] P. Rastgoufard and J. Bian. Voltage Stability Study for Entergy Services. Tulane University Technical Report, August 1993.
- [8] IEEE PES Power System Committee Report. *Voltage Stability of Power Systems: Concepts, Analytical Tools, and Industry Experience*. IEEE Publication 90TH0358-2-PWR, 1990.
- [9] IEEE PES Power System Stability Subcommittee Special Publication. *Voltage Stability Assessment, Procedures and Guides*, January 2001.

- [10] M. Moghavvemi and F.M. Omar. A line Outage Study for Prediction of Static Voltage Collapse. *IEEE Power Engineering Review*, 18(8):52–54, August 1998.

## Chapter 4

# BIFURCATION AND MANIFOLD BASED APPROACH FOR VOLTAGE AND OSCILLATORY STABILITY ASSESSMENT AND CONTROL

Venkataramana Ajjarapu

*Iowa State University*

vajjarap@iastate.edu

**Abstract** This paper presents a framework based on a bifurcation and differential manifold approach that combines identification and tracing of both saddle node and Hopf bifurcation margin boundaries. The bifurcation related margin boundary could be traced along any control scenario in a multi-control parameter space combined with any given loading scenario. This is achieved by moving from one boundary point to the next without re-tracing the entire  $PV$  curve. In addition, to take into account damping, an integration-based approach to trace the critical eigenvalue near the imaginary axis is proposed. Indices are developed to identify the critical eigenvalue to be traced for further analysis. They take into account the rate of change as well as the direction of the movement. This method in combination with maximum real part calculation provides reliable information related to margins with respect to oscillatory stability and minimum damping requirements. Eigenvalue and eigenvector sensitivities (with respect to any explicit/implicit parameters) are by products of this approach. This approach can lead to cost-based fast monitoring and control for voltage and damping related margins.

**Keywords:** Voltage stability, load margin, manifold, saddle-node bifurcation, Hopf bifurcation, damping, margin boundary tracing, DAE, time domain simulation

### 1. Introduction

Voltage collapse is an inherently nonlinear phenomenon that relates to bifurcation from the viewpoint of nonlinear dynamic systems. Sub-

stantial research has been conducted to help understand and analyze the mechanism of this instability based on bifurcation theory and quasi-steady-state analysis [1]-[11], [35]-[39]. A web-based search engine is also available to access the recent work in this area [12].

Voltage collapse is related to saddle-node bifurcation [13]: system equilibrium disappears as system parameters, mostly system load, change slowly.

Oscillatory instability is another constraint to power system operational security and is related to Hopf bifurcations [13]. Improper tuning of generation control parameters may lead to Hopf bifurcation [14]-[16]. Nonlinear load may also lead to Hopf bifurcation [17]. References [7], [18], [19] present an analysis related to the 1992 disturbance on the midwestern segment of the US interconnected power system and the resulting voltage oscillations caused by line tripping. It confirms that the event was indeed related to a Hopf bifurcation.

Continuation based approaches have been proposed to identify these critical points in voltage collapse [20]-[26]. Load margin is a reasonable measure of proximity to the bifurcation related instability. It is defined as the amount of additional load on a specified pattern of load increase that would cause power system instability. This margin can be obtained in a variety of ways. The trivial way to obtain a new margin is to retrace the *PV* curve for a given contingency and scenario. Obviously this method is time consuming and less informative. References [27]-[32] focused on saddle node bifurcation related to voltage stability margin estimation based on linear or quadratic margin sensitivities. Retracing of the entire *PV* curve for each parameter change is avoided. In [14] sensitivity of Hopf bifurcation for various power system parameters is studied. Margin sensitivity based methods are very useful for a quick calculation of the margin for a given change in any parameter. However, the prominent sources of inaccuracy inherently associated with margin sensitivity methods make a significant impact on the reliability of the margin estimation. Parameter changes, sometimes due to a contingency, may not be within a small range and hence higher order non-linearity could not be neglected [25].

Damping also plays an important role in power system oscillations. Margin related to damping can be defined as the amount of additional load on a specified pattern of load increase that would cause the damping ratio to reach its minimum limit. In an oscillatory stability assessment, in order to keep the system far away from the minimum damping limit, the damping ratio margin needs to be checked for each contingency and scenario. WSCC [40] recommends various criteria in determining the safe operating limits with respect to damping.

Oscillatory stability assessment with damping information needs eigenvalue estimation. In the literature very extensive work is available for estimating the eigenvalues. In principle one can calculate all the eigenvalues of any dynamical system. However, it is very computationally expensive to calculate all these values for practical power systems. We may need only one eigenvalue which crosses the imaginary axis first.

References [41] and [42] discuss the robustness and efficiency of existing dominant eigenvalue-computing methods and provide new alternatives. Because only one eigenvalue is calculated each time, these algorithms are very fast.

Reference [18] applies the power method with bilinear transformation to calculate the dominant eigenvalue. In reference [41] the power method is implemented and compared with other dominant eigenvalue-computing algorithms. The authors find that this method belongs to the linear convergence algorithms. Reference [41] also implemented the Newton's method, the inverse power, the Rayleigh quotient iteration, and other methods. The various algorithms are compared and evaluated with regards to convergence, performance, and applicability. In the conclusion, [41] points out that linear convergence algorithms, like the power method with bilinear transformation, are more robust than higher-order methods. However, higher-order methods, such as the quadratic and cubic convergence methods, are much faster. A better result is achieved by combining these two types together.

Reference [43] describes new matrix transformations suited to the efficient calculation of the dominant eigenvalue of large-scale power system dynamic models. Because only the most critical eigenvalue is calculated, all the other eigenvalue information is not provided.

References [44], [45] describe an algorithm which efficiently computes the dominant poles of any specified high-order transfer function. It has the numerical properties of global and ultimately cubic convergence. A numerical example is provided to study low-frequency oscillations in electrical power systems.

In a large-scale power system simulation, using more than one processor will obviously speed up the calculation. References [46]-[48] present an application of parallel computing in eigenvalue calculation. Parallel processing introduces increased complexity in software and algorithm strategies. Thus, the task of converting a sequential algorithm into an efficient parallel procedure is always challenging.

Reference [49] presents two sparsity-based eigenvalue techniques for oscillatory stability analysis of large-scale power systems. These critical eigenvalue calculation algorithms can provide a snapshot at a particular

operating point. To find the stability margin, we have to repeat this process at a series of operating points.

Reference [18] combines dominant eigenvalue calculation with an eigenvalue-based iterative algorithm that calculates the Hopf bifurcation-related segment of the feasibility boundary for a realistically large power system model. Each iteration consists of a parameter estimator and a dominant eigenvalue calculation, also called the eigenvalue corrector. In [18], the secant method is used for the parameter estimator.

Another way to identify a Hopf bifurcation is through the direct method [50]. This method can identify the oscillatory stability margin directly without computing any intermediate operating points. The Hopf bifurcation point is the solution of a set of algebraic nonlinear equations.

References [51] and [52] were the first to apply the direct method in the identification of the power system oscillatory stability margin. The solution of these nonlinear algebraic equations is also complex and sometimes the traditional Newton-based techniques can lead to difficulties or non-convergence. The direct method is very fast for a close initial guess. Reference [53] extended the direct method to include damping margin as a constraint. This reference utilized the dominant eigenvalue/eigenvector [45] as an initial guess. Reference [53] rightly pointed out that this area needs further work. For example, there can be a case where the dominant eigenvalue of the base case is moving away from the imaginary axis, resulting in non-convergence.

Reference [54] proposed a manifold-based indirect method that does not need eigenvalue estimation to identify Hopf bifurcation. This method looks for singularities of  $(A_{total} + A_{total}^T)$ .

Reference [55] presents an approach for tracking all the eigenvalues of a dynamic system Jacobian matrix. It employs an iterative method to update the eigenvalues. As the authors mentioned it may diverge for repeated eigenvalues.

In Figure 4.1, various boundaries (including damping) are conceptually shown. The load level at  $A_0$  after subtracting the base-case load level, is called the voltage stability loading margin. Similarly, the load level at  $A_1$  after subtracting the base-case load level is called the oscillatory stability loading margin. The load level at  $A_2$  after subtracting the base-case load level is called the damping-ratio loading margin.

The respective margin boundaries (as shown by the dashed lines in Figure 4.1) can also be obtained by any control parameter change starting with  $A_1$ ,  $A_2$ , and  $A_0$ .

In the case of a multi-dimensional, implicitly defined manifold  $M$ , specific local parameterizations need to be constructed to trace a cer-

tain sub-manifold with special properties on  $M$ . Saddle node or Hopf bifurcation points form a margin boundary sub-manifold corresponding to the change of control parameters along a specified control scenario. Thus a bifurcation related stability margin boundary could be traced by a specific design of local parameterizations.

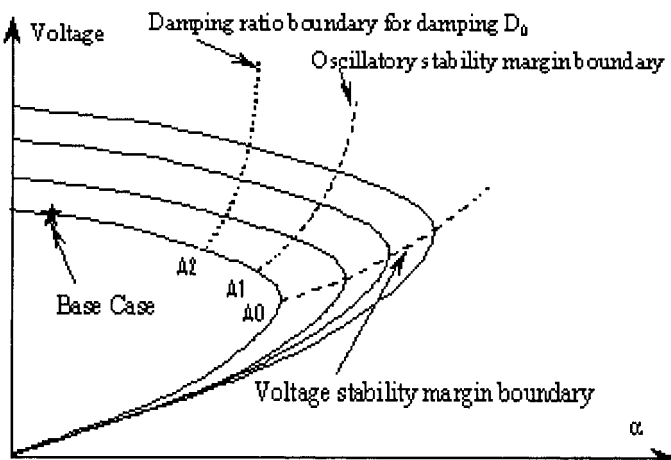


Figure 4.1. Illustration of three types of boundaries.

This chapter provides an overview of the methodology that provides information related to voltage stability, oscillatory stability and damping information for varying system conditions (details are given in [58], [59]). It takes advantage of the differential manifold approach [33], [34] that combines the identification and tracing of both saddle-node and Hopf bifurcation margin boundaries, first without calculating any eigenvalues. Then based on this information an integration-based approach to trace the critical eigenvalue near the imaginary axis is proposed. The eigenvalue index and damping index are defined for critical eigenvalue identification.

## 2. Identification of Saddle Node, Hopf Bifurcation, and Damping Margins

In power systems, the differential together with algebraic equations are commonly known as a DAE representation of the power system.

They can be denoted as

$$\begin{aligned}\dot{X} &= F(X, Y, \alpha, \beta) \\ 0 &= G(X, Y, \alpha, \beta)\end{aligned}\quad X(t_0) = X_0 \quad (4.1)$$

where the vector  $X(\delta, \omega, E'_q, E'_d, P_m, \mu, E_{fd}, V_r, R_f)$  contains all the system state variables and  $Y$  includes the algebraic variables  $(V, \theta)$ .

Based on the loading scenario, the loading parameter space could be parameterized by a scalar  $\alpha$  to characterize the system loading pattern

$$\begin{aligned}P_{li} &= (1 + K_{lpi}\alpha)P_{li0} \\ Q_{li} &= (1 + K_{lqi}\alpha)Q_{li0}\end{aligned}\quad (4.2)$$

where  $P_{li0}$  and  $Q_{li0}$  represent the initial loading condition of the base case where  $\alpha$  is assumed to be zero. The parameters  $K_{lpi}$  and  $K_{lqi}$  indicate the rate of load change at bus  $i$  as  $\alpha$  changes.

The control parameter space ( $U$ ) is parameterized by a scalar  $\beta$

$$U_i = U_{i0} + \beta L_i \quad (4.3)$$

The effects of on-load tap changers are approximately taken into account in (4.1) by adjusting their tap ratios during equilibrium tracing. It should be pointed out that although other dynamic devices such as HVDC and FACTS are not explicitly formulated here, they could be readily included in (4.1).

The following proposition establishes the background needed for the identification of both bifurcations. The proposition is established with the total Jacobian.

**Proposition 1. Identification of Saddle Node:** *If  $G_Y^{-1}$  exists and  $u_X \neq 0$ , then the following equivalent condition is valid*

$$A_{sys}u_X = (F_X - F_Y G_Y^{-1} G_X)u_X = \lambda u_X \quad (4.4)$$

if and only if

$$\begin{bmatrix} F_X - \lambda I & F_Y \\ G_X & G_Y \end{bmatrix} \begin{bmatrix} u_X \\ u_Y \end{bmatrix} = 0 \quad (4.5)$$

where

$$u_Y = -G_Y^{-1} G_X u_X \quad (4.6)$$

and the subscripts  $X$  and  $Y$  denote partial derivatives with respect to the vector variables  $X$  and  $Y$ , respectively.

We define the extended right eigenvector  $u = [u_X^T \ u_Y^T]^T$ . From (4.5), the total Jacobian matrix can be utilized to detect either a saddle-node or Hopf bifurcation.

We define

$$A_{total} = \begin{bmatrix} F_X & F_Y \\ G_X & G_Y \end{bmatrix}$$

From Proposition 1, the condition

$$\begin{bmatrix} F_X & F_Y \\ G_X & G_Y \end{bmatrix} \begin{bmatrix} u_X \\ u_Y \end{bmatrix} = 0 \quad (4.7)$$

will be utilized to detect a saddle-node bifurcation, that is, to detect the singularity of the total Jacobian matrix.

**Proposition 2. Identification of Hopf Bifurcation:** *Let the maximum eigenvalue of*

$$(A_{total} + A_{total}^T) = \begin{bmatrix} F_X + F_X^T & F_Y + G_X^T \\ G_X + F_Y^T & G_Y + G_Y^T \end{bmatrix}$$

be  $\lambda_1$ , then  $\lambda_1 = 0$  is the necessary condition for a Hopf bifurcation associated with the power system DAE model ( $A_{sys}$ ).

From Proposition 2, the identification of a Hopf bifurcation for  $A_{sys}$  is nothing but the identification of the singularity of the matrix  $(A_{total} + A_{total}^T)$ . As a result, without any eigenvalue calculations and iterative algorithms, a Hopf bifurcation could be detected along with a saddle-node bifurcation. It is similar to the continuation power flow algorithm.

## 2.1 Identification of critical eigenvalue

An eigenvalue  $\lambda$  of  $A_{sys}(\alpha)$  and its corresponding right eigenvector  $v$  are related by

$$A_{sys}(\alpha)v = \lambda v, \quad v^T v = 1 \quad (4.8)$$

where  $\alpha$  is the loading parameter (4.2) to trace. To preserve sparsity, an extended eigenvector defined as  $u = -G_Y^{-1}(\alpha)G_X(\alpha)v$  results in the formulation

$$\begin{aligned} F_X v + F_Y u &= \lambda v \\ G_X v + G_Y u &= 0 \end{aligned}$$

Based on the approach in [56, 57], an eigenvalue and its corresponding eigenvector of  $A_{sys}(\alpha)$  as  $\alpha$  varies are described by the differential equation

$$\begin{bmatrix} \lambda I - F_X & -F_Y & v \\ -G_X & -G_Y & 0 \\ v^T & 0 & 0 \end{bmatrix} \begin{bmatrix} \dot{v} \\ \dot{u} \\ \dot{\lambda} \end{bmatrix} = \begin{bmatrix} \dot{F}_X v + \dot{F}_Y u \\ \dot{G}_X v + \dot{G}_Y u \\ 0 \end{bmatrix} \quad (4.9)$$

where the symbol  $\cdot$  denotes the derivative with respect to  $\alpha$ . Because the vector  $(\lambda(\alpha), v(\alpha), u(\alpha))^T$  is in  $C \times C^n \times C^m$ , define

$$v = v_R + jv_I, \quad u = u_R + ju_I, \quad \lambda = \lambda_R + j\lambda_I$$

where

$$v_R, v_I \in R^n, \quad u_R, u_I \in R^m, \quad \lambda_R, \lambda_I \in R$$

With the above notation, (4.9) can be further extended to the form

$$\begin{bmatrix} \lambda_R I - F_X & -\lambda_I I & -F_Y & 0 & v_R & -v_I \\ \lambda_I I & \lambda_R I - F_X & 0 & -F_Y & v_I & v_R \\ -G_X & 0 & -G_Y & 0 & 0 & 0 \\ 0 & -G_X & 0 & -G_Y & 0 & 0 \\ v_R^T & -v_I^T & 0 & 0 & 0 & 0 \\ v_I^T & v_R^T & 0 & 0 & 0 & 0 \end{bmatrix} \begin{bmatrix} \dot{v}_R \\ \dot{v}_I \\ \dot{u}_R \\ \dot{u}_I \\ \dot{\lambda}_R \\ \dot{\lambda}_I \end{bmatrix} = \begin{bmatrix} \dot{F}_X v_R + \dot{F}_Y u_R \\ \dot{F}_X v_I + \dot{F}_Y u_I \\ \dot{G}_X v_R + \dot{G}_Y u_R \\ \dot{G}_X v_I + \dot{G}_Y u_I \\ 0 \\ 0 \end{bmatrix} \quad (4.10)$$

where  $F_{X(ij)}$  is the  $(i, j)$  entry of  $F_X$  and

$$\dot{F}_{X(ij)} = \frac{\partial F_{X(ij)}}{\partial X} \frac{\partial X}{\partial \alpha} + \frac{\partial F_{X(ij)}}{\partial Y} \frac{\partial Y}{\partial \alpha} + \frac{\partial F_{X(ij)}}{\partial \alpha}$$

This formulation leads to a sparsity-preserving algorithm for tracing any eigenvalue and eigenvector of a parameterized matrix.

From the formulation (4.10), one can trace all the eigenvalues of any specified subset or a single eigenvalue of interest. To detect a Hopf bifurcation, we are interested in the complex eigenvalue which crosses the imaginary axis first. To identify this eigenvalue an index is derived.

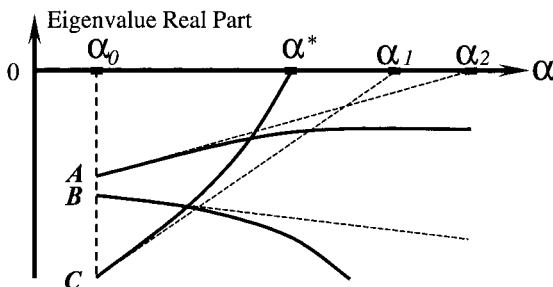


Figure 4.2. Eigenvalue real part vs. parameter  $\alpha$ .

Figure 4.2 shows a conceptual variation of the real parts of three eigenvalues with respect to the parameter  $\alpha$ . From (4.10), any eigenvalue real-part derivative can be obtained. The dashed lines in Figure 4.2 indicate the slopes at the base case parameter value of  $\alpha_0$ . This information is used to define an index to estimate which eigenvalue will cross imaginary axis first. This index is given by

$$\text{Index}_{\text{Eigen}} = -\frac{\lambda_{Re}}{d\lambda_{Re}/d\alpha} = -\frac{\lambda_{Re}}{\dot{\lambda}_{Re}} \quad (4.11)$$

If we assume all the eigenvalues at the base case are in the left half of the complex plane, then  $\text{Index}_{\text{Eigen}}$  positive means that the corresponding eigenvalue moves towards the imaginary axis and negative means that it moves away from the imaginary axis. A low positive index value relative to the others indicates that the corresponding eigenvalue is critical and may be the first one to cross the imaginary axis.

In Figure 4.2, the eigenvalues corresponding to points A and C have positive index values, where as the point B has a negative index value. Between points A and C, C is less positive. In this particular scenario, the Hopf bifurcation can be identified by tracing the real part of the eigenvalue that corresponds to the point C.

## 2.2 Damping margin identification

Actually Hopf bifurcation can be identified from Proposition 2. However, our aim is to estimate damping margin using the damping ratio

$$D = -\cos \left( \tan^{-1} \left( \frac{\lambda_I}{\lambda_R} \right) \right) \quad (4.12)$$

Because  $\dot{\lambda}_R$  and  $\dot{\lambda}_I$  are available, the damping ratio's derivative with respect to the parameter  $\alpha$  is given by

$$\frac{dD}{d\alpha} = \sin \left( \tan^{-1} \left( \frac{\lambda_I}{\lambda_R} \right) \right) \frac{(\lambda_R(d\lambda_I/d\alpha) - \lambda_I(d\lambda_R/d\alpha))}{(\lambda_I^2 + \lambda_R^2)} \quad (4.13)$$

The damping index can be defined as

$$\text{Index}_{\text{damping}} = -\frac{D - D_0}{(dD/d\alpha)}$$

where  $D_0$  is the damping ratio threshold.

Using a similar approach to Hopf identification, the damping ratio of any eigenvalue can be traced. Figure 4.3 shows the process of searching for the damping margin. The slope of the damping ratio curve in Figure 4.3 can be used to predict the parameter value in damping margin identification.

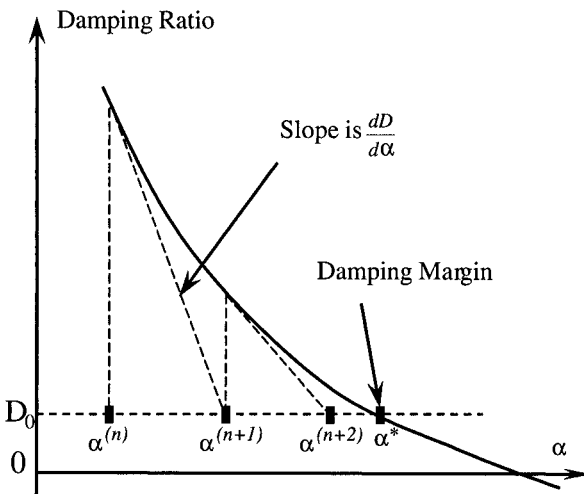


Figure 4.3. Tangent information is used in searching for damping margin.

## 2.3 Example

This approach is demonstrated through a 10-bus, 4-generator system with a two-axis generator model, and the IEEE DC-I excitation system and governor model [21]. There are 9 state variables for each generator. The total system Jacobian dimension is  $55 \times 55$  (35 state variables and 20 algebraic variables). Loads consist of 50% constant power, 30% constant current, and 20% constant impedance. Loads on all buses will increase with the same percentage. The sum of the initial load on all the buses is 1974 MW.

The total number of eigenvalues at any given operating equilibrium is 35, out of which 19 are real and 8 are complex pairs.

Figure 4.4 shows all the complex eigenvalues in the upper half of the complex plane for the base case (total load: 1974 MW). From (2.10), each eigenvalue's  $\dot{\lambda}_R$  and  $\dot{\lambda}_I$  can be calculated. The arrows show the direction of motion of each eigenvalue when the parameter  $\alpha$  increases. The length of arrow shows the relative speed of movement with respect to  $\alpha$ .

Table 4.1 shows the index values  $Index_{damping}$  for all the complex eigenvalues in Figure 4.4. The complex eigenvalues D, E, F, G, and H have negative index values. We include them in Table 4.1 to show the importance of the index. Eigenvalue H is very close to the imaginary axis compared to the other ranked eigenvalues. However, it is moving

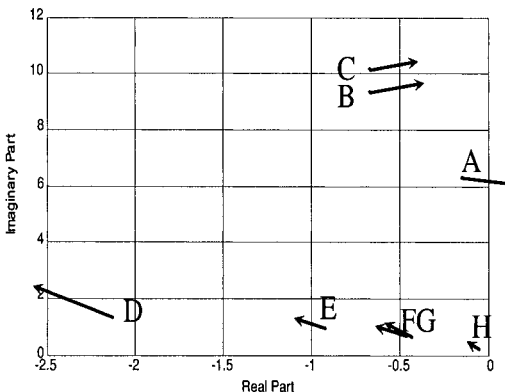


Figure 4.4. All complex eigenvalues in complex plane at base case.

Table 4.1. Index of all complex eigenvalues in Figure 4.4.

<i>Index Ranking</i>	<i>Symbol</i>	<i>Eigenvalue</i>	<i>Index Value</i>
1	A	$-0.1427 \pm j6.2611$	0.2221
2	B	$-0.6634 \pm j10.1385$	0.9122
3	C	$-0.6640 \pm j9.3350$	0.9325
	D	$-2.1291 \pm j1.3082$	-1.3789
	E	$-0.9201 \pm j0.9190$	-2.6855
	F	$-0.4496 \pm j0.6541$	-9.4662
	G	$-0.4291 \pm j0.6383$	-5.8928
	H	$-0.05086 \pm j0.1801$	-10.7757

away from the imaginary axis for increasing load. Using the index, we eliminate this eigenvalue for further tracing. We trace the highest ranked eigenvalue through (2.10) using the fourth order Runge-Kutta method.

Figure 4.5 shows the eigenvalue's real part as a function of the parameter  $\alpha$ . The figure shows that the real part of the eigenvalue becomes zero for a total load increase of 551 MW.

For each load increase of 150 MW, we have to solve a  $2(m+n)+2$  dimensional linear equation four times.

Similar to the oscillatory stability margin identification, the damping margin identification can also be obtained. Figure 4.6 shows the simulation results for a damping ratio limit ( $D_0$ ) of 1%. Here the highest ranked eigenvalue damping ratio is traced. The damping threshold  $D_0$  limits the load increase to a total of 307 MW.

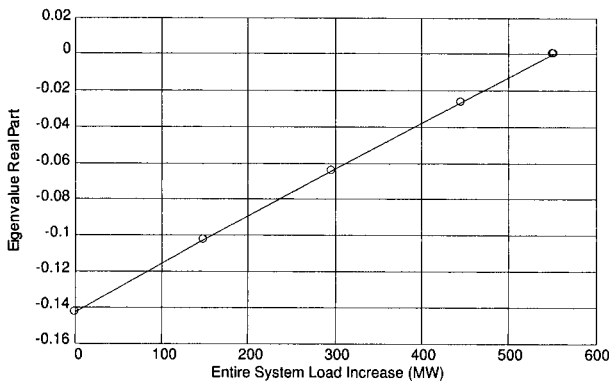


Figure 4.5. Integrated eigenvalue with total load increase.

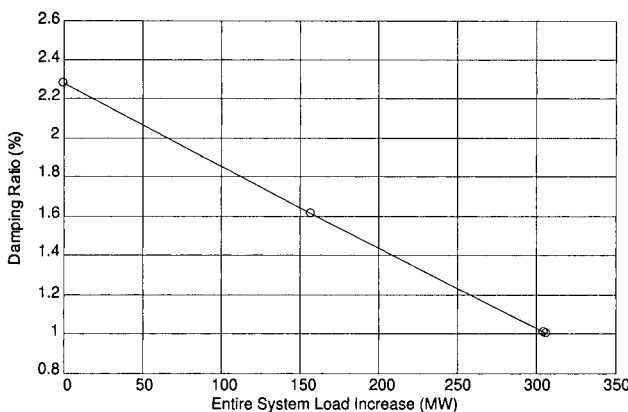


Figure 4.6. Damping ratio vs. entire system load increase.

### 3. Tracing Margin Boundaries

In the previous section we described a procedure to identify saddle-node, Hopf bifurcation, and damping boundaries. Further tracing of these boundaries for any changes in control parameters can be obtained by the solution manifold

$$B(X, Y, \mu, \alpha) = \begin{bmatrix} F(X, Y, \alpha, \beta) \\ G(X, Y, \alpha, \beta) \\ c(X, Y, \alpha, \beta) \end{bmatrix} = 0 \quad (4.14)$$

as defined in (4.14) [34]. The cut function  $c$  in (4.14) defines the saddle-node bifurcation (SNB) or Hopf bifurcation condition.

For SNB-related voltage collapse margin boundary,  $c$  is defined as

$$c(X, Y, \mu, \alpha) = \gamma_{SNB}(X, Y, \mu, \alpha) \quad (4.15)$$

such that its derivatives with respect to the variables of  $c$ , denoted by  $D$ , follow as

$$Dc(X, Y, \mu, \alpha) = D\gamma_{SNB} \quad (4.16)$$

A cut function for oscillatory stability (Hopf bifurcation related) margin boundary is defined as

$$c(X, Y, \mu, \alpha) = \gamma_{H1}(X, Y, \mu, \alpha) \quad (4.17)$$

$$Dc(X, Y, \mu, \alpha) = D\gamma_{H1} \quad (4.18)$$

For a given change in the control parameter, the solution of (4.14) is always related to either a saddle-node or Hopf bifurcation point. This in turn provides the margin change for any particular perturbation in the control vector.

Equation (4.14) can be solved based on the predictor-corrector approach implemented in the equilibrium tracing program (EQTP) [21]. The solution is always on the bifurcation boundary. The basic solution procedure is described in the following section.

#### 3.1 Boundary predictor

The total augmented equations for margin boundary tracing are

$$H(X, Y, \alpha, \beta) = \begin{bmatrix} B(X, Y, \alpha, \beta) \\ [X^T \ Y^T \ \alpha \ \beta] e_k - \eta \end{bmatrix} = \begin{bmatrix} F(X, Y, \alpha, \beta) \\ G(X, Y, \alpha, \beta) \\ c(X, Y, \alpha, \beta) \\ [X^T \ Y^T \ \alpha \ \beta] e_k - \eta \end{bmatrix} \quad (4.19)$$

$$DH(X, Y, \mu, \alpha) = \begin{bmatrix} DF \\ DG \\ Dc \\ e_k^T \end{bmatrix} \quad (4.20)$$

where  $\eta = [ X_{pre}^T \ Y_{pre}^T \ \alpha_{pre} \ \beta_{pre} ] e_k$  is obtained from the tangent vector calculated by the boundary predictor. With  $\delta$  as the step size,

$$DH(X, Y, \alpha, \beta) \begin{bmatrix} dX \\ dY \\ d\alpha \\ d\beta \end{bmatrix} = \begin{bmatrix} 0 \\ 0 \\ 0 \\ \pm 1 \end{bmatrix} \text{ and } \begin{bmatrix} X_{pre} \\ Y_{pre} \\ \alpha_{pre} \\ \beta_{pre} \end{bmatrix} = \begin{bmatrix} X \\ Y \\ \alpha \\ \beta \end{bmatrix} + \delta \begin{bmatrix} dX \\ dY \\ d\alpha \\ d\beta \end{bmatrix} \quad (4.21)$$

The Jacobian matrix of the augmented system is nonsingular with a properly chosen continuation parameter.

### 3.2 Boundary corrector

The Newton method is employed to perform the boundary correction as

$$\begin{bmatrix} X \\ Y \\ \alpha \\ \beta \end{bmatrix}^{new} = \begin{bmatrix} X \\ Y \\ \alpha \\ \beta \end{bmatrix} - DH^{-1}(X, Y, \alpha, \beta) H(X, Y, \alpha, \beta) \quad (4.22)$$

For damping boundary tracing, a technique based on the direct method is proposed in [60].

#### Steps involved in boundary Tracing Procedure

- Specify a loading scenario.
- Start the direct equilibrium tracing at the current operating point for the first boundary point under the current fixed control configuration and the specified loading scenario.
- Specify the control scenario that describes the change of control configuration or contingencies.
- Compute the boundary prediction using (4.21).
- Compute the boundary correction using (4.22).

### 3.3 Computation result

Figure 4.7 shows the *PV* curve for a given control configuration for the 30-bus New England test system. A Hopf bifurcation is identified for a total load increase of 809 MW (by observing simultaneous sign changes of  $\gamma_{H1}$  and  $\gamma_{H2}$ ). A saddle-node bifurcation is observed for a total load increase of 1370 MW.

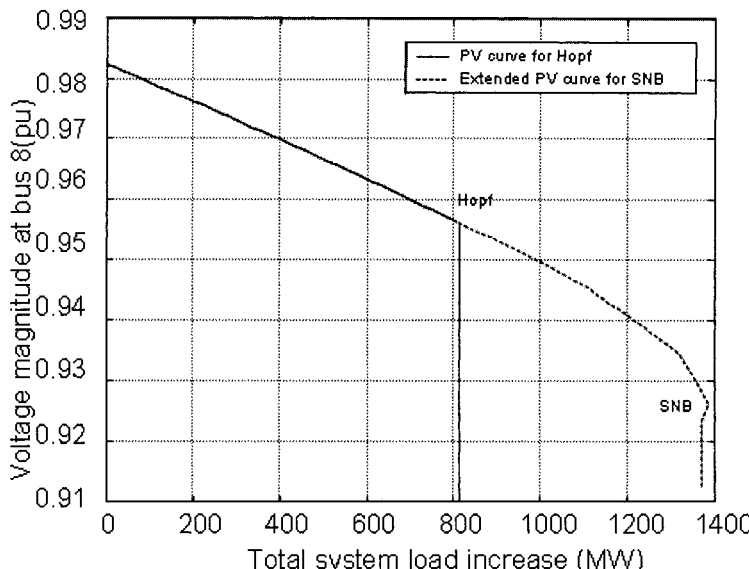


Figure 4.7. Hopf and SNB detection in *PV* curve tracing for base case control.

These Hopf and saddle-node bifurcations can be further traced for changes in various system parameters. For the Hopf bifurcation, 800 MW is the starting point, whereas for the saddle-node bifurcation, it is around 1400 MW. Figure 4.8 shows the effect of load shedding on voltage as well as oscillatory stability boundaries. In this case, load shedding increases both the margins.

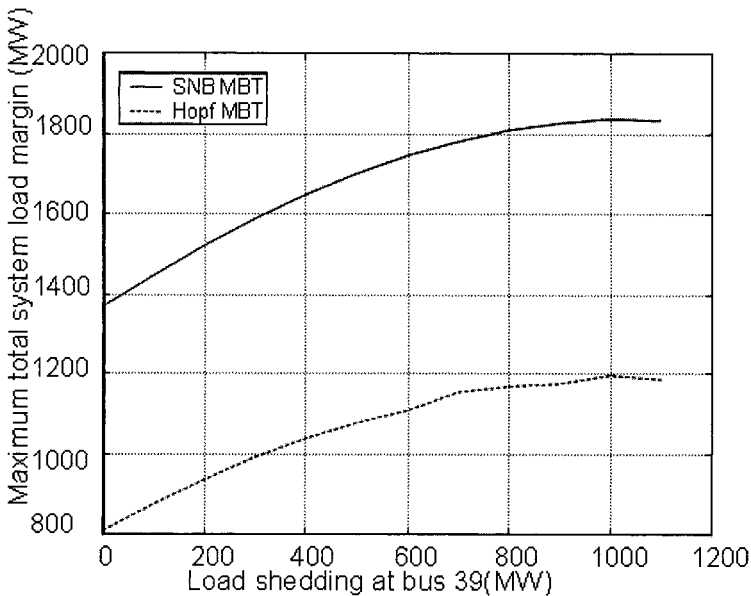


Figure 4.8. Margin boundary tracing (MBT) vs. load shedding.

## 4. Further Extensions

### 4.1 Optimal margin boundary: cost based security

This formulation can be further extended to optimal margin boundary tracing. As we can see from the previous section, the same margin increase can be obtained by different control strategies. We need to know the minimum control cost strategy to achieve a given amount of margin. The problem definition is given below:

*For a sequence of specified margin levels, minimize a cost function*

$$f(U)$$

*subject to:*

*Equality Conditions : F, G*

*Inequality constraints : I*

*Optimality conditions  
Margin boundary conditions }  $C^{obt}$*

This formulation results in a set of nonlinear equations of the form

$$\begin{bmatrix} F(X, Y, \mu, U) \\ G(X, Y, \mu, U) \\ I(X, Y, \mu, U, s_\ell, s_h) \\ C^{\text{obt}}(f_u, \lambda, F_x, \dots) \end{bmatrix} = 0$$

The main advantage of this formulation is that we can explicitly include margin constraints in the optimization. Details are provided in [61]-[63].

## 4.2 Fast and slow time scales

Continuation-based techniques have been extended to capture short-term and long-term voltage stability (Figure 4.9). The integration step-size is varied according to variation of short-term and long-term variables: small steps for fast dynamics and large steps for slow dynamics. There are no singularity problems due to singularity induced bifurcation during the time domain simulations. The details are given in [35, 36].

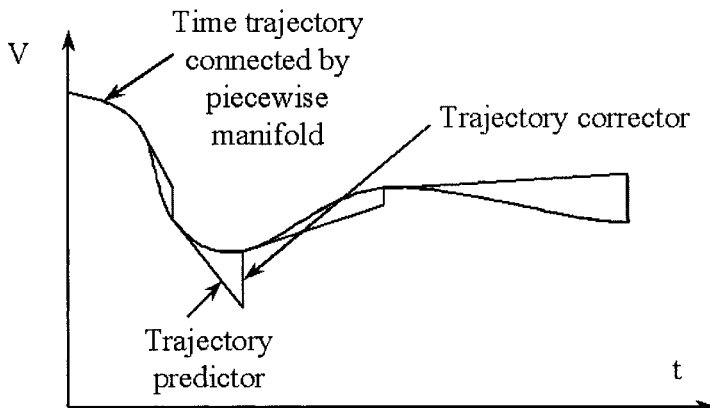


Figure 4.9. Continuation-based time domain simulation using locally parameterized time trajectory tracing.

## 4.3 Impact on power system security

The work presented in this paper leads to:

- Cost-based preventive and corrective strategies that are very effective for stressed power systems.

- When, where, and how much control to maintain required margins.
- A single tool can be adapted for steady state optimization as well as time domain simulation.
- Byproducts
  - Various sensitivities
    - \* Margin sensitivities.
    - \* Eigenvalue and eigenvector sensitivities.
  - Index to indicate the movement of eigenvalues.
  - What-if analysis.

## 5. Research Needs

The recent August 14, 2003 Northeast US Blackout amply demonstrated the need for better assessment of power system security. Various factors contributed to that system collapse. The following discussion briefly identifies some critical aspects that future research should concentrate to improve overall security.

**Integration of protection systems into power system security analysis:** Protection system plays an important role in the overall security of the power system. There should be a balance between individual component protection versus system protection. In [65], it is reported that incorrect relay operations contributed to the most of the voltage related large disturbances. In some cases the apparent impedance seen by the low voltage buses with high currents may fall into the protected zone of impedance relays, resulting in unnecessary trips. Research is needed to explore the design of protection schemes that can tune each relay operation bias continuously and intelligently by taking into account relevant system vulnerability indices.

**Dynamic versus static Var compensation:** Proper reactive power coordination is needed to improve both the voltage profile and voltage security. At present we do not have any systematic procedure to allocate dynamic and static Vars for the overall improvement of voltage profile and security. Research is needed to come up with a procedure to allocate the reactive power with respect to how fast, how much, and where to locate these static and dynamic reactive power devices. The relevance of FACTS controllers should become part of this investigation.

**Fast power system security assessment tools:** To assess the system security with respect to transient stability, voltage stability, and oscillatory stability for every contingency and scenario is a very time

consuming process. New analytical tools in combination with emerging computer technology and numerical techniques should be explored to speed up the process without losing accuracy. This chapter has made an attempt to address some of these concerns.

**Cost of power system security:** We also have to consider the cost of system security in a deregulated environment. It costs money to maintain certain security margins to prevent a loss of load. Because reactive power plays an important role in voltage security, how to price this reactive power (both dynamic and static) to maintain a proper voltage profile as well as voltage stability is a challenging problem for further research. Instead of purely cost based, some form of cost/benefit analysis can be incorporated.

## References

- [1] IEEE Power System Stability Subcommittee. *Voltage Stability Assessment: Concepts, Practices, and Tools*. IEEE/PES Publication SP101PSS, ISBN: 0780378695, 2002.
- [2] IEEE System Dynamic Performance Subcommittee. *Voltage Stability of Power Systems: Concepts, Analytical Tools, and Industry Experience*. IEEE/PES Publication 90TH0358-2-PWR, 1990.
- [3] Y. Mansour, ed. *Suggested Techniques for Voltage Stability Analysis*. IEEE PES Working Group on Voltage Stability, Publication 93TH0620-5-PWR, 1993.
- [4] C.W. Taylor. *Power System Voltage Stability*. McGraw-Hill, New York, 1994.
- [5] P. Kundur. *Power System Stability and Control*. McGraw-Hill, New York, 1994.
- [6] T. Van Cutsem and C. Vournas. *Voltage Stability of Electric Power Systems*. Kluwer Academic Publishers, Norwell, MA, 1990.
- [7] M. Ilic and J. Zaborszky. *Dynamics and Control of Large Electric Power Systems*. John Wiley & Sons, New York, 2000.
- [8] *Proceedings of Bulk Power System Voltage Phenomena III—Seminar on Voltage Stability, Security, and Control*. Davos, Switzerland, August 22-26, 1994.
- [9] *Proceedings of the Symposium on Bulk Power System Dynamics and Control IV—Restructuring*. Santorini, Greece, August 24-28, 1998.
- [10] *Proceedings of Bulk Power System Dynamics and Control V—Security and Reliability in a Changing Environment*. Onomichi, Japan, August 26-31, 2001.

- [11] V. Ajjarapu and B. Lee. Bibliography on Voltage Stability. *IEEE Transactionz on Power Systems*, 13:115–125, 1998.
- [12] V. Ajjarapu. *Iowa State University's Web Based Voltage Stability Search Engine*. Accessible at <http://design-2.ee.iastate.edu/biblio/>.
- [13] B.D. Hassard, N.D. Kazarinoff, and Y.-H. Wan. *Theory and Applications of Hopf Bifurcation*. Cambridge University Press, Cambridge, 1981.
- [14] I. Dobson, F. Alvarado, and C.L DeMarco. Sensitivity of Hopf Bifurcations to Power System Parameters. *Proceedings of the 31<sup>st</sup> IEEE Conference on Decision and Control*, 3:2928–2933, 1992.
- [15] C.D. Vournas, M.A. Pai, and P.W. Sauer. The Effect of Automatic Voltage Regulation on the Bifurcation Evolution in Power Systems. *IEEE Transactions on Power Systems*, 11:1683–1688, 1996.
- [16] W. Zhu, R.R. Mohler, R. Spee, W.A. Mittelstadt, and D. Maratukulam. Hopf Bifurcations in a SMIB Power System with SSR. *IEEE Transactions on Power Systems*, 11:1579–1584, 1996.
- [17] V. Ajjarapu and B. Lee. Bifurcation Theory and its Application to Nonlinear Dynamical Phenomena in an Electrical Power System. *IEEE Transactions on Power Systems*, 7:424–431, 1992.
- [18] K. Kim, H. Schattler, V. Venkatasubramanian, J. Zaborszky, and P. Hirsch. Methods for Calculating Oscillations in Large Power Systems. *IEEE Transactions on Power Systems*, 12:1639–1648, 1997.
- [19] F. Howell and V. Venkatasubramanian. Transient Stability Assessment with Unstable Limit Cycle Approximation. *IEEE Transactions on Power Systems*, 14:667–677, 1999.
- [20] V. Ajjarapu and C. Christy. The Continuation Power Flow: a Tool for Steady State Voltage Stability Analysis. *IEEE Transactions on Power Systems*, 7:416–423, 1992.
- [21] Z. Feng, V. Ajjarapu, and B. Long. Identification of Voltage Collapse through Direct Equilibrium Tracing. *IEEE Transactions on Power Systems*, 15:342–349, 2000.
- [22] C.A. Canizares, A.C.Z. De Souza, and V.H. Quintana. Comparison of Performance Indices for Detection of Proximity to Voltage Collapse. *IEEE Transactions on Power Systems*, 11:1441–1450, 1996.
- [23] C.A. Canizares and F.L. Alvarado. Point of Collapse and Continuation Methods for Large AC/DC Systems. *IEEE Transactions on Power Systems*, 8:1–8, 1993.
- [24] A.C.Z. De Souza, C.A. Canizares, and V.H. Quintana. New Techniques to Speed Up Voltage Collapse Computations using Tangent Vectors. *IEEE Transactions on Power Systems*, 12:1380–1387, 1997.

- [25] A.J. Flueck and J.R. Dondeti. A New Continuation Power Flow Tool for Investigating the Nonlinear Effects of Transmission Branch Parameter Variations. *IEEE Transactions on Power Systems*, 15:223–227, 2000.
- [26] H.D. Chiang, A.J. Flueck , K.S. Shah, and N. Balu. CPFLOW: A Practical Tool for Tracing Power System Steady-State Stationary Behavior due to Load and Generation Variations. *IEEE Transactions on Power Systems*, 10:623–634, 1995.
- [27] I. Dobson and L. Lu. Computing an Optimal Direction in Control Space to Avoid Saddle Bifurcation and Voltage Collapse in Electrical Power Systems. *IEEE Transactions on Automatic Control*, 37:1616–1620, 1992.
- [28] S. Greene, I. Dobson, and F.L. Alvarado. Contingency Ranking for Voltage Collapse via Sensitivities from a Single Nose Curve. *IEEE Transactions Power Systems*, 14:232–240, 1999.
- [29] S. Greene, I. Dobson, and F.L. Alvarado. Sensitivity of the Loading Margin to Voltage Collapse with respect to Arbitrary Parameters. *IEEE Transactions on Power Systems*, 12:262–272, 1997.
- [30] B. Long and V. Ajjarapu. The Sparse Formulation of ISPS and its Application to Voltage Stability Margin Sensitivity and Estimation. *IEEE Transactions on Power Systems*, 14:944–957, 1999.
- [31] A. Berizzi, P. Finazzi, D. Dosi, P. Marannino, and S. Corsi. First and Second Order Methods for Voltage Collapse Assessment and Security Enhancement. *IEEE/PES Publication PE-422-PWRS-0-01-1997*, IEEE PES Winter Meeting, New York, 1997.
- [32] J. Barauin, T. Gomez, and F.L. Pagola. Estimating the Loading Limit Margin Taking into Account Voltage Collapse Areas. *IEEE Transactions on Power Systems*, 10:1952–1962, 1995.
- [33] W.C. Rheinboldt. *Numerical Analysis of Parameterized Nonlinear Equations*. John Wiley & Sons, New York, 1986.
- [34] R. Dai and W.C. Rheinboldt. On the Computation of Manifolds of Fold Points for Parameter-Dependent Problems. *SIAM Journal of Numerical Analysis*, 27:437–446, 1990.
- [35] Y. Zhou and V. Ajjarapu. Local Parameterization Approach for Unified Time Domain Simulation of Power System Dynamics. *Proceedings of IEEE Winter Power Meeting*, New York, January 2002.
- [36] T. Van Cutsem. An Approach to Corrective Control of Voltage Instability using Simulation and Sensitivity. *IEEE Transactions on Power Systems*, 10:616–622, 1995.

- [37] T. Van Cutsem and C.D. Vournas. Voltage Stability Analysis in Transient and Mid-Term Time Scales. *IEEE Transactions on Power Systems*, 11:146–154, 1996.
- [38] T. Van Cutsem. Voltage Instability: Phenomena, Countermeasures, and Analysis Methods. *Proceedings of the IEEE*, 88:208–227, 2000.
- [39] T. Van Cutsem, Y. Jacquemart, J.N. Marquet, and P. Pruvot. A Comprehensive Analysis of Mid-Term Voltage Stability. *IEEE Transactions on Power Systems*, 10:1173–1182, 1995.
- [40] D. Kosterev, B. Mittelstadt, M. Viles, B. Tuck, J. Burns, M. Kwok, J. Jardim, and G. Garnett. *Model Validation and Analysis of WSCC System Oscillations following Alberta Separation on August 4, 2000*. Final Report, January 2001.
- [41] G. Angelidis and A. Semlyen. Improved Methodologies for the Calculation of Critical Eigenvalues in Small Signal Stability Analysis. *IEEE Transactions on Power System*, 11:1209–1217, 1996.
- [42] G. Angelidis and A. Semlyen. Efficient Calculation of Critical Eigenvalue Clusters in the Small Signal Stability Analysis of Large Power Systems. *IEEE Transactions on Power System*, 10:427–432, 1995.
- [43] L.T.G. Lima, L.H. Bezerra, C. Tomei, and N. Martins. New Method for Fast Small-Signal Stability Assessment of Large Scale Power Systems. *IEEE Transactions on Power Systems*, 10:1979–1985, 1995.
- [44] N. Martins, L.T.G. Lima, and H.J.C.P. Pinto. Computing Dominant Poles of Power System Transfer Function. *IEEE Transactions on Power Systems*, 11:162–170, 1996.
- [45] N. Martins. The Dominant Pole Spectrum Eigensolver. *IEEE Transactions on Power Systems*, 12:245–254, 1997.
- [46] J.M. Campagnolo, N. Martins, J.L.R. Pereira, L.T.G. Lima, H.J.C.P. Pinto, and D.M. Falcao. Fast Small-Signal Stability Assessment using Parallel Processing. *IEEE Transactions on Power Systems*, 9:949–956, 1994.
- [47] J.M. Campagnolo, N. Martins, and D.M. Falcao. Refactored Bi-Iteration: A High Performance Eigensolution Method for Large Power System Matrices. *IEEE Transactions on Power Systems*, 11:1228–1235, 1996.
- [48] J.M. Campagnolo, N. Martins, and D.M. Falcao. An Efficient and Robust Eigenvalue Method for Small-Signal Stability Assessment in Parallel Computers. *IEEE Transactions on Power Systems*, 10:506–511, 1995.

- [49] L. Wang and A. Semlyen. Application of Sparse Eigenvalue Techniques to the Small Signal Stability Analysis of Large Power Systems. *IEEE Transactions on Power Systems*, 5:635–642, 1990.
- [50] M. Kubicek and M. Marek. *Computational Methods in Bifurcation Theory and Dissipative Structures*. Springer Series in Computational Physics, Springer-Verlag, New York, 1983.
- [51] Y.V. Makarov, Z.Y. Dong, and D.J. Hill. A General Method for Small Signal Stability Analysis. *IEEE Transactions on Power System*, 13:979–985, 1998.
- [52] D.J. Hill and Z.Y. Dong. Nonlinear Computation and Control for Small Disturbance Stability. Panel Session on Recent Applications of Small-Signal Stability Techniques, *Proceedings of IEEE Summer Power Meeting*, Seattle, July 2000.
- [53] S. Gomes Jr., N. Martins, and C. Portela. Computing Small-Signal Stability Boundaries for Large-Scale Power Systems. *IEEE Transactions on Power Systems*, 18:747–752, 2003.
- [54] Y. Zhou and V. Ajjarapu. Identification and Tracing of Voltage and Oscillatory Stability Margins. *Proceedings of IEEE PES Winter Meeting*, 1:250–255, 2002.
- [55] R.T.H. Alden and F.A. Qureshy. Eigenvalue Tracking due to Parameter Variation. *IEEE Transactions on Automatic Control*, 30:923–925, 1985.
- [56] R. Kalaba, K. Spingarn, and L. Tesfatsion. Variational Equations for the Eigenvalues and Eigenvectors of Nonsymmetric Matrices. *Journal of Optimization Theory and Applications*, 33:1–8, 1981.
- [57] R. Kalaba, K. Spingarn, and L. Tesfatsion. Individual Tracking of an Eigenvalue and Eigenvector of Parameterized Matrix. *Nonlinear Analysis: Theory, Methods and Application*, 54:337–340, 1981.
- [58] Y. Zhou and V. Ajjarapu. Local Parameterization Based Tracing for Stability Boundary, Optimal Margin Control and Time Domain Simulation. *Proceedings of Bulk Power System Dynamics and Control V*, Onomichi, Japan, August 2001.
- [59] X. Wen and V. Ajjarapu. Critical Eigenvalue Trajectory Tracing for Power System Oscillatory Stability Assessment. *Proceedings of IEEE PES General Meeting*, Denver, June 2004.
- [60] Y. Zhou, X. Wen, and V. Ajjarapu. Identification and Tracing of Oscillatory Stability Margin Boundaries. Presented at IEEE Panel Session on Recent Applications of Linear Analysis Techniques, IEEE PES General Meeting, Toronto, Canada, 2003.

- [61] Z. Zhou and V. Ajjarapu. Optimal Margin Boundary Tracing With Continuation Optimal Power Flow. *Proceedings of the 34<sup>th</sup> North American Power Symposium*, Tempe, AZ, 2002.
- [62] Z. Zhou and V. Ajjarapu. A Novel Approach for Cost Based Optimization with Variable Voltage Stability Margins. *Proceedings of the 35<sup>th</sup> North American Power Symposium*, Rolla, MO, 2003.
- [63] Z. Zhou and V. Ajjarapu. A Novel Approach for Cost Based Optimization With Variable Oscillatory Stability Limits. *Proceedings of the 36<sup>th</sup> North American Power Symposium*, Moscow, Idaho, 2004.
- [64] Z. Zhou and V. Ajjarapu. A Novel Approach to Trace Time Domain Trajectories of Power Systems in Multiple Time Scales. Accepted for publication in IEEE Transactions on Power Systems, 2004.
- [65] J. Huang, S.S. Venkata, V. Ajjarapu, and Z. Zhou. Adaptive Wide Area Protection to Mitigate Voltage Collapse. *Proceedings of the 35<sup>th</sup> North American Power Symposium*, Rolla, MO, 2003.

## Chapter 5

# ON-LINE ATC EVALUATION FOR LARGE-SCALE POWER SYSTEMS: FRAMEWORK AND TOOL

Hsiao-Dong Chiang

*Cornell University*

Hua Li

*Cornell University*

**Abstract** A framework for accurate determination of Available Transfer Capability (ATC) of interconnected power systems with respect to a set of proposed power transactions is presented. A full AC nonlinear modeling of power systems including the effects of control devices is employed in the framework. Both static and dynamic security constraints under a list of credible contingencies are taken into account in the framework. A computer package implementing this framework for ATC evaluation of large-scale power systems is developed. One distinguished feature of this tool is that it provides a list of the topmost severe contingencies in terms of ATC and identifies the associated violated constraints. This feature offers a platform for the development of effective migration schemes to increase ATC. This tool was applied to compute the ATC satisfying the static security constraints of a 15,000-bus system with promising results.

**Keywords:** Available transfer capability, large scale power systems, dynamic security analysis, transient stability constraints.

### 1. Introduction

Open transmission access requires transmission network owners (or providers) to provide unbundled services (including ancillary services) necessary to support power transactions and to maintain reliable opera-

tion of transmission networks. To enforce the open transmission access policy, FERC defined the term “available transfer capability” (ATC) to be posted in the open-access same-time information system (OASIS) to inform all energy market participants of the maximum power transfer capability for a power system. The FERC requires that ATC information be made publicly available on hourly and daily basis. The speed requirement is one of the factors that make the task of ATC evaluation rather challenging. The other factor is the accuracy requirement that the ATC calculation be performed on nonlinear power system models subject to static security and dynamic security constraints under a list of credible contingencies. Hence, the ability to accurately determine on-line ATC is essential under the open-access environment of power systems. A practical computer package for determining ATC will be an important tool for all transmission providers. Significant progress has been made in developing such a tool; however, one remaining major challenge is to accurately evaluate on-line ATC under varying loading conditions, taking into account the static as well as dynamic security limits of multiple contingencies [1], [2].

Within the last several years the area of ATC evaluation has become a subject of great interest to many researchers in the power system community. A number of methods have been proposed in the literature. They can be categorized into three classes of methods: (i) linear approximation methods [34], (ii) optimal power flow (OPF)-based methods [16], and (iii) continuation power flow (CPFLOW)-based methods [3], [10], [11]. Among these classes of methods, linear approximation methods are faster than the other two classes of methods at the expense of accuracy. Linear approximation methods solve DC power flow equations and linear constraints. OPF-based methods can handle nonlinear power flow equations and nonlinear constraints such as the constraints of thermal limit and voltage violations. Both linear approximation methods and OPF-based approach cannot directly handle the constraints of voltage stability and transient stability. Most OPF-based methods use a simplified approach, translating these (dynamic) stability constraints based on off-line studies into algebraic inequality constraints in terms of either voltage angle differences between several selected buses or MW flow interface constraints in some selected inter-ties. CFPFLOW-based methods can handle the constraints of thermal limits, voltage violations as well as voltage collapse for each study contingency. However, effective schemes are needed to handle these constraints under a list of credible contingencies. We note that these classes of methods cannot effectively handle the transient stability constraint. The task of ATC evaluation subject to

the constraint of transient stability under a list of credible contingencies remains challenging. Of the proposed methods for ATC evaluation, very few methods can handle the transient stability constraints of credible contingencies. While the transient stability constraints can be handled in a straightforward manner by incorporating a time-domain stability program into an ATC evaluation engine, this approach becomes very slow relative to the speed requirement when there is a sizable list of credible contingencies.

ATC is, in fact, an estimate of the near-future transmission network's capability of additional power transfer over the existing committed usage. As such, there are several uncertainties associated with the parameters and forecasting quantities used in the ATC evaluation. The following types of uncertainties are some examples: the uncertainty in the base-case operating conditions, the uncertainty in the area-to-area bilateral power transactions that are different from those assumed in the base-case, the uncertainty in the contingency list, the uncertainty in the generation dispatch patterns that are different from those assumed in the base-case, the uncertainty in the control schemes that are different from those assumed in the base case, the uncertainty in the projected load demand, the uncertainty in scheduled power transfers, the uncertainty in the base-case system configuration, and uncertainties of market activities that include demand variations, demand-side management, and ancillary services.

Current ATC posting in the OASIS uses a deterministic approach based on an assumed set of system condition and certain safety margins to accommodate these uncertainties in the ATC calculation. It is, however, unclear regarding how to determine an adequate amount of safety margin. To deal with uncertainties, several techniques are used in conjunction with a deterministic approach for ATC evaluation. For instance, an optimal power flow method in conjunction with Monte-Carlo simulations was proposed to evaluate ATC and associated risks [15]-[17]. The technique of Monte-Carlo simulation was used to deal with the uncertainty of forecasted system conditions in evaluating ATC. This technique requires the data with uncertainty be assigned a probability distribution of the expected variability in the data. In [33], a simple bootstrap procedure was proposed to deal with uncertainties in the power transactions and bus injections for the determination of the probability distribution of ATC. The derived ATC distribution can then be used to evaluate the risk of curtailment for each transmission service reservation. We focus in this chapter on the development of a deterministic framework for accurate determination of ATC with both static and dynamic security constraints for a list of credible contingencies taken into account. We

note that the proposed deterministic framework can be used in conjunction with other tools for statistical inference to derive the probability distribution of ATC. By applying the deterministic framework to ATC evaluation over sufficient time, the probability density and cumulative distribution of ATC can be obtained.

The task of ATC evaluation is very complex. Furthermore, the speed and accuracy requirements for on-line ATC evaluation make the task even harder. Unfortunately, these two factors, accuracy and speed, associated with general numerical methods often conflict with each other, making a compromise between accuracy and speed a popular choice. Indeed, a majority of the existing proposed methods for ATC calculation achieves the speed requirement at the expense of accuracy. In this chapter, the proposed framework is focused on the accuracy of ATC evaluation (to the accuracy of underlying power system model) as well as comprehensive static and dynamic security constraints. We develop a computer package based on this framework with the aim of providing accurate ATC evaluation with relatively fast speed. This tool evaluates ATC subject to the following static as well as dynamic security constraints of credible contingencies:

- 1 line thermal limits
- 2 bus voltage limits
- 3 steady-state stability limits
- 4 transient stability limits

We term the first two limits *soft limits*, because a power system can be operated under the violation of soft limits for a period. The last two limits are termed *hard limits*, since power system instability occurs when either one of the hard limits is violated. We consider preventive-mode ATC calculation, which considers both soft and hard limits, as well as corrective-mode ATC calculation, which considers only hard limits. In order to effectively handle static security constraints of credible contingencies, three look-ahead load margin estimators for steady-state stability, line thermal limits and voltage violation limits are developed and integrated into the tool. In order to effectively handle dynamic security constraints of credible contingencies, one look-ahead load margin estimators for transient stability limits is proposed and will be integrated into the tool.

The tool offers the following features:

#### Functional viewpoint

- It evaluates ATC and identifies the corresponding (the most severe) contingency (including the location and type of the contingency), and the associated binding constraint (voltage violation, thermal limit, steady-state stability limit, or transient stability limit).
- It identifies and ranks the most severe contingencies in terms of their impacts on ATC.
- For each ranked contingency, it computes the corresponding ATC and the associated binding constraints.
- It pinpoints the system bottlenecks of ATC in terms of the locations of bottlenecks, types of binding constraints, and the associated binding contingency.
- It checks all the static security constraints of credible contingencies.
- It checks all the dynamic security constraints of credible contingencies.
- It determines the required ancillary services.

#### Modeling viewpoint

- It uses a full AC nonlinear modeling.
- It takes the general characteristics of power system operating environments into account.
- It includes the effects of control devices.

#### Control viewpoint

- It allows the development of a migration scheme to increase ATC and FCITC.
- It provides a platform to take proactive action in evaluating ATC and FCITC and to prepare a remedy control, should a contingency occur.

#### Probabilistic analysis

- It allows a probabilistic treatment of each contingency and the associated risk management.

The tool has been applied to two realistic power system models, a 646-bus and a 15,000-bus power system, to compute their ATC's (both preventive-mode ATC and corrective-mode ATC) with respect to several proposed power transactions under static security constraints of credible contingencies. The tool also determines the required ancillary services such as VAR control and service components that facilitate power transfers.

## 2. Transfer Capability

Transfer capability refers to the ability of a transmission network to transfer electric power reliably from an area of supply to an area of demand by way of all transmission lines (or paths) between two areas under a given operating condition. The operating condition includes several projected factors such as the expected load demands, real generation dispatch policy, the system configuration, and the scheduled power transfers among the interconnected systems.

The transfer capabilities proposed by NERC are the first contingency incremental transfer capability (FCITC) or first contingency total transfer capability (FCTTC) for predicted peak load conditions. FCITC is the amount of electric power incremental above a normal base power that can be transferred in a reliable manner based on the following conditions [4]:

- (1) for the existing or planned system configuration, and with normal (pre-contingency) operating procedures in effect, all facility loadings are within normal ratings and all voltages are within normal limits,
- (2) the electric system is capable of absorbing the dynamic power swings, and remains stable following a disturbance that results in the loss of any single electric system element, such as a transmission line, transformer, or generation unit,
- (3) after the dynamic power swings subside following a disturbance that results in the loss of any single electric system element as described in (2) above, and after the operation of any automatic operating systems, but before any post-contingency operator-initiated system adjustments are implemented, all transmission facility loadings are within emergency ratings and all voltages are within limits.

Note that Condition (1) is related to the static security constraints under the first contingency of the pre-contingency operating conditions while Condition (3) is concerned with the static security constraints of

the post-contingency operating conditions. Condition (2) is the typical (angle) transient stability constraint and may not include the voltage dip problem during transients as constraints. FCTTC is the total amount of electric power (net of normal base power transfers plus first contingency incremental transfers, i.e. the ATC) that can be transferred between two areas of the interconnected systems in a reliable manner based on Conditions (1), (2), and (3) in the FCITC defined above.

Due to the nonlinear nature of interconnected electric systems, ATC's between two areas and their associated binding constraints depend on the system operating condition. The ATC's and their associated binding constraints can be significantly different for different system operating condition, such as a different pattern of system load demands, a different network configuration, or a different generation dispatch policy. Hence, ATC evaluations must be sufficient in system modeling and scope to ensure that all equipments as well as system limits of the entire interconnected systems network are properly taken into account.

### 3. Transaction-Dependent ATC

Given a set of proposed power transactions (and transmission service), the transaction-dependent ATC is the maximum transfer capability of the interconnected power system with respect to the proposed power transactions, or simultaneous power transactions. The system model upon which the evaluation of transaction-dependent ATC is based must satisfy the following three conditions:

- (C1) it represents a realistic operating condition or expected future operating condition,
- (C2) it conforms to the requirements of ATC definition,
- (C3) it considers single contingency facility outages that result in conditions most restrictive to electric power transfers.

The information of calculated transaction-dependent ATC then forms the basis to approve or disapprove the proposed power transactions, or to suggest another transfer value for the proposed power transactions. One by-product of the developed tool for calculating the transaction-dependent ATC is the security margin after the proposed power transactions (or the suggested power transactions).

To achieve Condition (C1), activation of control devices should be included in the system model. The control devices include: (i) Switchable shunts and static VAR compensators, (ii) ULTC Transformers, (iii) ULTC phase shifters, (iv) Static tap changer and phase shifters, (v) DC

network and the associated control strategy. In order to accurately simulate the actual power flow in the interconnected systems and the parallel power flows on adjacent systems, a detailed nonlinear power flow analysis of the interconnected system must be performed. To achieve Condition (C2), it is important to accurately represent a proposed power transaction. Given a load demand vector, i.e., the real and reactive load demands at each load bus, and a real generation vector, i.e., the real power generation at each generator bus, one can compute the state of the power system (the complex voltage at each bus), by solving the set of power flow equations. Let  $P_i \equiv P_{gi} - P_{di}$  and  $Q_i \equiv Q_{gi} - Q_{di}$ . The lowercase  $g$  represents generation, the lowercase  $d$  represents load demand, and  $i$  is the bus index. The set of power flow equations can be represented in compact form as

$$f(x) \equiv \begin{bmatrix} P(x) - P \\ Q(x) - Q \end{bmatrix} = 0, \quad x = \begin{bmatrix} V \\ \theta \end{bmatrix} \quad (5.1)$$

where the vector  $P$  (resp.  $Q$ ) represents the real (resp. reactive) power injection at each bus.

Next, it will be explained how one can examine the power system steady-state behavior under slowly varying loading and real power re-dispatch conditions. For example, if one needs to trace the power system state from the base-case load-generation condition specified by the following vector  $[P_d^0, Q_d^0, P_g^0]$  to a new load-generation condition specified by the following vector  $[P_d^1, Q_d^1, P_g^1]$ , then one can parameterize the set of power flow equations as the following parameterized power flow equations

$$F(x, u, \lambda) \equiv f(x, u) - \lambda b = 0 \quad (5.2)$$

where  $u$  is the control vector,  $\lambda \in [0, 1]$ , and the load-generation vector  $b$  is

$$b \equiv \begin{bmatrix} P^1 - P^0 \\ Q^1 - Q^0 \end{bmatrix} \quad (5.3)$$

It is clear that the set of the parameterized power flow equations (5.2) become the base-case power flow equations when  $\lambda = 0$ ,

$$F(x, 0) = \begin{bmatrix} P(x) - P^0 \\ Q(x) - Q^0 \end{bmatrix} = 0$$

and when  $\lambda = 1$ , the set of parameterized power flow equations describes the power system steady-state behavior at the new load-generation condition  $[P_d^1, Q_d^1, P_g^1]$  and is described by

$$F(x, 1) = f(x) - b = \begin{bmatrix} P(x) - P^0 \\ Q(x) - Q^0 \end{bmatrix} = 0$$

Thus, one can investigate the effects of varying real power generations as well as varying load demands on power system steady-state behaviors via solving the set of parameterized power flow equations (5.2). In fact, one can parameterize any change in  $PQ$  loads in conjunction with any change in  $P$  generations by selecting an appropriate vector  $b$ .

We next apply the above general setting to the problem of computing ATC of interconnected power systems. In this application, the vector  $b$  is used to represent one or several of the following power transactions and transmission service:

- Point-to-point MW transaction - the real power at one load bus of the receiving area varies while the others remain fixed and the real power at one generator bus of the sending area varies while the others remain fixed,
- Slice-of-the-system sale - both the real and reactive power demand at a load bus of the receiving area vary and the real power generation at some collection of generators of the sending bus varies while the others are fixed,
- Network service - the real and/or reactive power demands at some collection of load buses of the receiving area vary and the real power generation at some collection of generators of the sending bus varies while the others are fixed.

We shall call the vector  $b$  the proposed power transaction vector when the parameterized power flow equations (5.2) are used for ATC evaluation, and the scalar  $\lambda$ , the load-generation margin. The proposed power transaction vector  $b$  can be used to represent a power transaction involving simultaneous power transfers by summing each power transaction vector, i.e.,  $b = \sum b_i, i = 1, 2, \dots$ , where the vector represents the  $i^{\text{th}}$  power transaction. The introduction of the power transaction vector and the load-generation margin enables us to evaluate ATC with respect to proposed multiple power transactions of an interconnected power system satisfying the general characteristics (C1), (C2), and (C3) stated above.

## 4. System Modeling

Electric power transfers between two control areas will be distributed among all parallel transmission paths according to the laws of physics. Power transfers cannot be forced through pre-determined transmission paths, unless the paths are physically controlled by control devices such as phase-shifters. To accurately compute ATC's, all the relevant physical constraints as well as engineering constraints must be modeled; hence,

the power system model must take into account physical limitations on transmission lines and equipment/facilities, static security constraints such as thermal limits, voltage violation limits, and steady-state stability and dynamic security constraints. Moreover, a full AC detailed power system model including the sending area, the receiving area, as well as, all neighboring areas (to a lesser extent) is needed for accurate calculation of ATC.

The modeling capability of the developed tool includes:

### 1 Generators

Generators are modeled as active and reactive power sources that also provide voltage control. The MVar output of each on-line generator is adjusted during power flow solutions in order to control the voltage of the local bus (the bus where the generator is connected to) or a remote bus. The generator's MW output has fixed limits, and the generator's MVar output is limited by defining so-called capability curves.

### 2 Loads

Loads can be modeled as constant power ( $P-Q$ ), constant current ( $I$ ), constant impedance ( $Z$ ), or any linear combination of them. The tool can also accept nonlinear load models as long as they are expressed as nonlinear functions of voltage.

### 3 Control Devices

The following control devices are modeled

- Switchable shunts and static VAR compensators
- Interchange schedules
- ULTC transformers
- ULTC phase shifters
- Static tap changer and phase shifters

### 4 DC Network

The basic information required for ATC evaluations include the following:

- 1 the current operating condition (obtained from the state estimator and the topological analyzer),
- 2 a base-case power system model with control devices, reactive power generation limits,

- 3 load forecast for the next period (say, next 15 minutes) of each bus,
- 4 a set of proposed power transactions, such as (i) a point-to-point MW transaction, (ii) a slice-of-the-system sale, or (iii) a network service, for the next period,
- 5 generation scheduling (or generation participation factor) to accommodate load increases or/and to accommodate power transactions,
- 6 a list of credible contingencies  $\{l_1, \dots, l_{total}\}$ .

In addition to the above basic information, the information of how to model the control actions during the process of the step increases of loads and generations is required. These control actions include static Var compensator, TCSC, tap changers, synchronous condenser voltage/MVar, LTC transformer voltage control, phase-shifter control, capacitor/reactor voltage control, etc.

It has been well recognized that the selection of delivery buses in the sending area and of receiving buses in the receiving area that participate in the proposed power transactions is a critical assumption in ATC evaluation. Another critical assumption is the generation scheduling (or generation participation factor) for each participating generator. There are several schemes available for generation scheduling (or generation participation factor) such as generation scheduling based on the AGC, economic dispatch, governor response, or capacity limits. However, different schemes can lead to significantly different ATC values. A fixed participation factor based on capacity limits for each participating generator is a widely used scheme for ATC evaluation. Evidently, ATC values will change if a user specifies different participation factors or select different generators to participate in the power transfer.

Each contingency in the list is composed of elementary contingency events such as branch opening/closing, generator outage, load transfer, etc. It is common that each contingency is specified with up to 30 elementary contingency events.

We next state the problem of ATC calculation in mathematical terms. Two modes of ATC are considered: preventive-mode ATC and corrective-mode ATC. The key difference between these two modes is the inclusion of soft limits of security constraints.

## Preventive-mode ATC

$$\max \lambda \quad (5.4)$$

subject to

- the parameterized power flow equations

$$F(x, u, \lambda) \equiv f(x, u) - \lambda b = 0$$

derived from information (1)-(3)

- soft limits of credible contingencies  $\{l_1, \dots, l_{total}\}$ 
  - (1) line thermal limits
  - (2) bus voltage limits
- hard limits of credible contingencies  $\{l_1, \dots, l_{total}\}$ 
  - (3) steady-state stability limits
  - (4) transient stability limits

The control allows the participation of generators, loads, ULTC taps, phase-shifter settings, shunt capacitors, and DC links as either active control or passive control to maximize simultaneous power transfer.

Because a violation of a hard limit will immediately result in system instability, preventive controls are essential for hard limits while timely corrective controls may prove appropriate for soft limits. Hence, if the soft limits of a study system are correctable, then another mode of ATC evaluation is presented below:

## Corrective-mode ATC

$$\max \lambda \quad (5.5)$$

subject to

- the parameterized power flow equations derived from information (1)-(3)

$$F(x, u, \lambda) \equiv f(x, u) - \lambda b = 0$$

- soft limits of credible contingencies  $\{l_1, \dots, l_{total}\}$ 
  - (1) steady-state stability limits
  - (2) transient stability limits

## 5. Identify Critical Contingencies for Static Security

It is imperative in determining the ATC to take into account all the soft limits as well as hard limits under credible contingencies. This task

however is computationally intensive. The strategy of using effective schemes to rank all credible contingencies and of applying detailed analysis programs only to critical contingencies is widely accepted. In order to identify critical contingencies, which will severely violate static security constraints, we developed three look-ahead ranking schemes which are to be incorporated into the tool. The first look-ahead scheme ranks the set of all credible contingencies in terms of load margin to system collapse and to select the top few critical contingencies. The second look-ahead scheme ranks the set of all credible contingencies in terms of branch MVA violation and selects the top few critical contingencies. The third scheme ranks all credible contingencies in terms of bus voltage violation and selects the top few critical contingencies.

Given (i) the current operating condition (obtained from the state estimator and the topological analyzer), (ii) a set of proposed power transactions, and (iii) a list of credible contingencies, we will develop three look-ahead schemes for estimating the load margins, along the proposed power transaction vector  $b$ , with respect to steady-state stability limits (nose-point load margin), bus voltage magnitude limits, and line flow thermal limits for the power system with the proposed power transactions, i.e., the parameterized power system (parameterized along the direction of the proposed power transactions), subject to the list of credible contingencies. The three load margins are defined as follows.

**Definition:** The *nose-point load margin* of a power system (1) under a contingency with respect to a load-generation vector (3) is the distance (in terms of MW and/or MVar) from the current operating condition to the nose point of the parameterized power system (2) subject to the contingency (see Figures 5.1 and 5.2).

Mathematically speaking, the nose point of the parameterized power system with respect to a load-generation vector can be due to a saddle-node bifurcation or a limit-induced bifurcation. Physically speaking, in the context of transfer capability evaluation, the saddle-node bifurcation is closely related to the transfer capability limit of the study power system with respect to the load-generation vector. On the other hand, the limit-induced bifurcation is closely related to the reactive power generation limit of one or some generators involved in the load-generation vector.

The nose-point load margin with respect to a contingency can be negative. Under this situation, the study power system will undergo voltage collapse should the contingency occur. This contingency is termed as an insecure contingency. One numerical scheme to identify whether or not a contingency is insecure is the numerical check of the existence of the post-contingency power flow solution which lies in a neighborhood of the

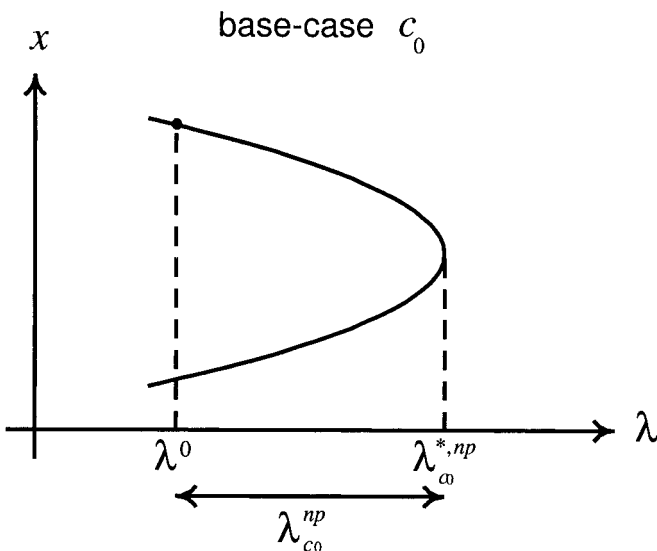


Figure 5.1. The nose point load margin  $\lambda_{C_0}^{np}$  for the base case power system  $C_0$ .

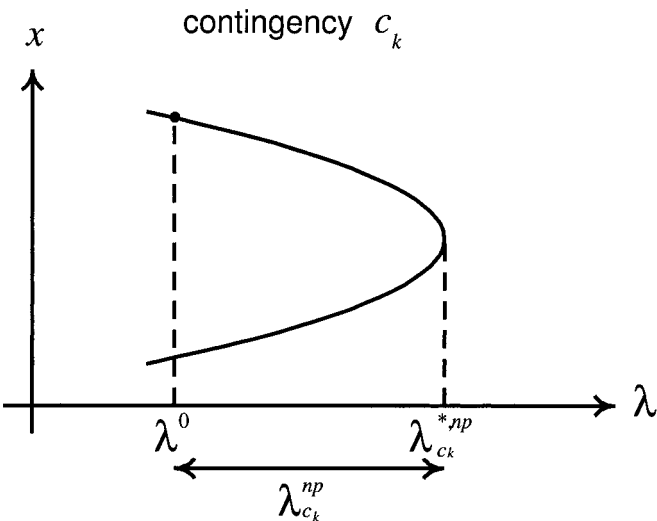


Figure 5.2. The nose point load margin  $\lambda_{C_k}^{np}$  for the power system under contingency  $C_k$ .

base-case power flow solution. If a nearby post-contingency power flow solution does not exist, then it can be concluded, with certain conservativeness, that the study power system will undergo a voltage collapse should the contingency occur. However, the task of checking existence

of the post-contingency power flow solution which lies in a neighborhood of the base-case power flow solution is difficult.

A widely used approach, in the power industry to compute the nose point, with respect to a given parameter increase pattern, is the use of repetitive power flow calculations to generate the so-called  $P$ - $V$  or  $Q$ - $V$  curve along the parameter increase direction. In this approach, an operating point is claimed to be the nose point if it is the first point (along the parameter increase direction) where power flow calculation does not converge. Several issues arise regarding this approach. First, the point where the power flow calculations diverge (which is determined by a numerical failure) does not represent the nose point (which is a physical limitation). The nose point should not be determined based on the mathematical limitation of a numerical method. Second, the point where power flow calculations fail to converge may vary, depending on which method was used in the calculation. For instance, it is likely that the point where the Newton method fails to converge is different from the point where the decoupled Newton method fails to converge. It is known that the set of power flow equations is ill-conditioned near its nose point, making the Newton method diverge in the neighborhood of nose points. From the viewpoint of numerical analysis, this is due to the fact that, at the nose point, i.e., the saddle-node bifurcation point, the corresponding Jacobian matrix has one zero eigenvalue, causing the set of power flow equations to be ill-conditioned. Recently, considerable progress has been made in generating  $P$ - $V$  and  $Q$ - $V$  curves using an approach based on continuation methods (continuation power flow). Continuation methods, sometimes called curve tracing or path following, are useful tools to generate solution curves for general nonlinear algebraic equations with a varying parameter. In summary, a non-converged solution may be due to physical limitations or due to the solution algorithm itself or due to a poor initial guess.

Another caution of a converged power flow solution: the converged power flow solution may not correspond to the actual post-fault operating point. From a nonlinear dynamical system viewpoint, the actual post-fault operating point depends on the location of the initial guess and the size and nature of stability regions of post-fault stable equilibrium points. From a numerical method viewpoint, the converged power flow solution depends on the location of the initial guess and the size and nature of convergent region of post-fault stable equilibrium points with respect to the employed solution algorithm.

**Definition:** The *voltage-limit load margin* of a power system (1) under a contingency with respect to a load-generation vector (3) is the (minimum) distance (in terms of MW and/or MVar) from the current

operating point to the state vector, of the parameterized power system (2) subject to the contingency, at which the voltage constraint at some bus is violated (see Figures 5.3 and 5.4).

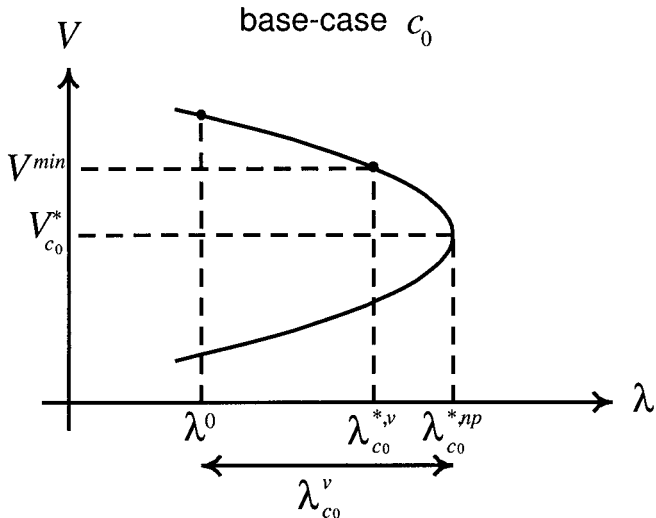


Figure 5.3. The voltage-limit load margin  $\lambda_{C_0}^v$  for the base case power system  $C_0$ .

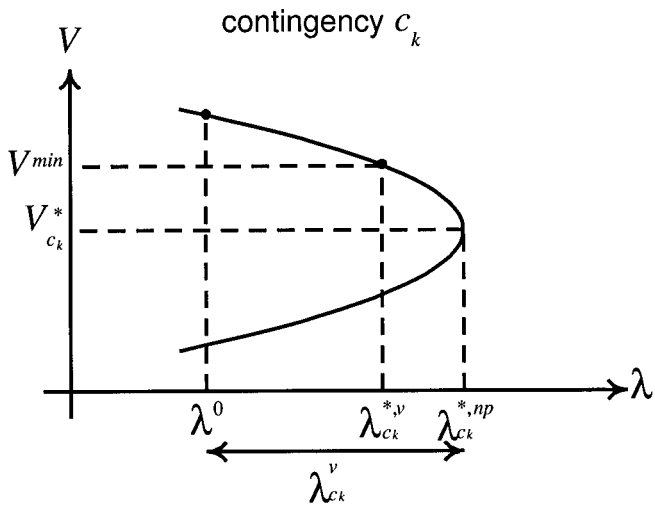


Figure 5.4. The voltage-limit load margin  $\lambda_{C_k}^v$  for the power system under contingency  $C_k$ .

**Definition:** The *thermal-limit load margin* of a power system (1) under a contingency with respect to a load-generation vector (3) is the (minimum) distance (in terms of MW and/or MVar) from the current operating point to the state vector, of the parameterized power system (2) subject to the contingency, at which the thermal limit constraint of some transmission line is violated (see Figures 5.5 and 5.6).

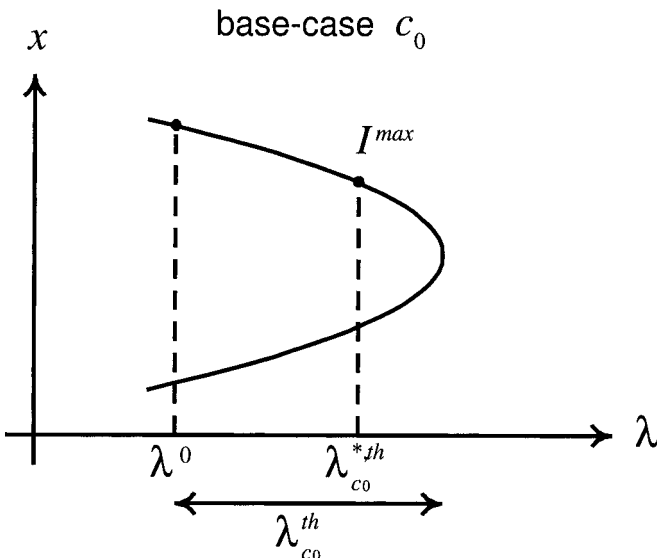


Figure 5.5. The thermal-limit load margin  $\lambda_{C_0}^{th}$  for the base case power system  $C_0$ .

The objective of look-ahead contingency screening and ranking is two-fold: (1) to rapidly screen out, from a large set of credible contingencies on a power system with committed power transactions, the set of insecure contingencies and severe contingencies. Insecure contingencies will result in immediate voltage collapse while severe contingencies will result in very small load margins with respect to committed power transactions; and (2) to rank the set of severe contingencies according to their impacts on the power systems with committed power transactions. One physically meaningful impact is the look-ahead load margin of the power system to its voltage collapse point, the voltage-violation point, or the thermal-limit point.

The schemes for estimating the three load margins will be presented in the next section. Each estimated load margin is then used to rank all the contingencies on the contingency list. The following three look-ahead ranking lists are thus obtained:

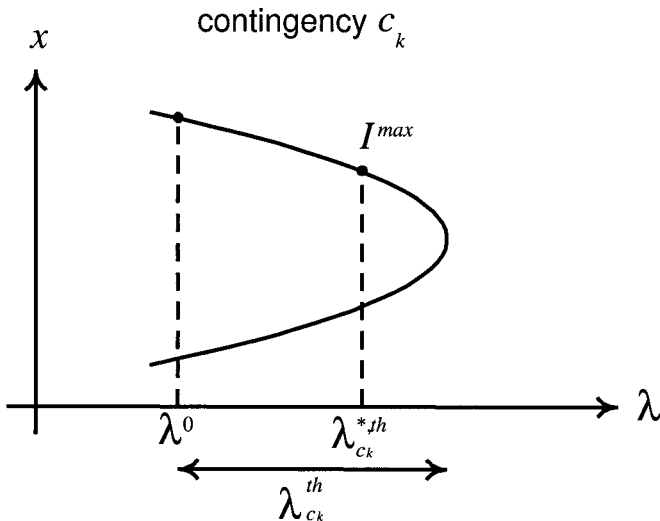


Figure 5.6. The thermal-limit load margin  $\lambda_{C_k}^{th}$  for the power system under contingency  $C_k$ .

- 1 look-ahead ranked list of contingencies for steady-state stability limit,
- 2 look-ahead ranked list of contingencies for voltage limit,
- 3 look-ahead ranked list of contingencies for thermal limit.

## 6. Estimating Load Margins to Nose Points

A large number of performance indices intended to measure the severity of voltage collapse under a study contingency have been proposed in the literature, see for example [20], [21], [22]. They can be classified into two categories: the state-space-based approach and the parameter-space-based approach, i.e., the approach is developed in the load or load-generation space [20]. The state-space-based approach cannot provide a direct measure because the state-space-based performance indices generally do not exhibit any obvious relation between their values and the amount of the underlying mechanism that the system can withstand before collapse. Development of performance indices in the parameter space, i.e., performance indices for estimating look-ahead load margins, is a relatively new concept that may have been spurred by the local bifurcation theory. In [20], a new performance index for estimating look-ahead load margins to nose point was developed. From an analytical viewpoint, this performance index is based on the normal form of

saddle-node bifurcation points and its computation was formulated as a generalized curve-fitting problem. Some improvements on this performance index can be found in [11], [12], [24]-[26]. Recent works on the parameter-space-based performance indices include the study of linear profile of these indices [27].

However, existing methods proposed in the literature for estimating the look-ahead load margin to nose point still require further improvements before entering practical application stages. For instance, the accuracy of their estimations is not satisfactory yet. Furthermore, these methods do not address the limit-induced bifurcation points. Consequently, the estimated load margins by these methods are optimistic for those contingencies that result in limit-induced bifurcation points. This overestimation of load margins to nose point can lead to missing alarms in contingency ranking for voltage security assessment.

The theoretical basis under the parameter-space-based approach is the normal form theory [5]. It can be analytically shown that, in the context of power flow equations, the power flow solution curve passing through the saddle-node bifurcation point is a quadratic curve, at least locally. Hence, in the neighborhood of saddle-node bifurcation point, the power flow solution curve can be approximated by a quadratic curve. The saddle-node bifurcation point of the power flow solution curve can be estimated using a curve-fitting technique via two power flow solutions close to the nose point and a characteristic equation for the nose point. This is the basis for all the curve-fitting-based performance indices developed for estimating the load margin to the saddle-node bifurcation point. We next present an overview of the look-ahead curve-fitting technique. Starting from a power flow solution, say  $x_1$  with the corresponding load-generation level  $\lambda_1$ , we compute the next power flow solution along the load/generation curve specified by the predicted near-term load demands and the scheduled real power generations at a higher load-generation level, say at  $\lambda_2$ , by using CPFLOW. Let the power flow solution be  $x_2$ , and its derivative with respect to the parameter  $\lambda$  be  $\dot{x}_2$ . We select the load bus whose drop in voltage magnitude is the largest, and let this bus be labeled  $i$ . That is, we define

$$\Delta V_i = \frac{(V_i|_{\lambda=\lambda_1} - V_i|_{\lambda=\lambda_2})}{V_i|_{\lambda=\lambda_1}} \quad (5.6)$$

and use  $\Delta V_i$  as a quantitative criterion to choose the bus whose drop in voltage magnitude is the largest. This means that if  $\Delta V_i$  is the maximum value among  $\{\Delta V_1, \Delta V_2, \dots, \Delta V_n\}$ , then the  $\lambda$ - $V$  curve of  $i^{\text{th}}$  load bus is chosen to derive the load margin. We then use the quadratic curve

$$\lambda = \alpha + \beta V_i + \gamma V_i^2 \quad (5.7)$$

to approximate the  $V\text{-}\lambda$  curve of bus  $i$  passing through two points, say  $(V_{i,1}, \lambda_1)$  and  $(V_{i,2}, \lambda_2)$ . By using the information of the derivative  $\dot{V}_{i,2}$  at the second point, we can obtain the values for the parameters  $\alpha$ ,  $\beta$  and  $\gamma$  from

$$\begin{aligned}\lambda_1 &= \alpha + \beta V_{i,1} + \gamma V_{i,1}^2 \\ \lambda_2 &= \alpha + \beta V_{i,2} + \gamma V_{i,2}^2 \\ 1 &= \beta \dot{V}_{i,2} + 2\gamma \dot{V}_{i,2} V_{i,2}\end{aligned}\quad (5.8)$$

From the quadratic function (5.8), we get the following load margin measure, called look-ahead load margin, as

$$\bar{\lambda}_{V_{max}} = \alpha - \frac{\beta^2}{4\gamma}$$

### Analysis of inaccurate estimation

Inaccurate estimation of load margins to nose point can arise if the two power flow solutions are not sufficiently close to the nose point of interest. From a computational viewpoint, the first power flow solution can be the current operating point, which can be obtained from a state estimator. The second power flow solution should be placed as close to the nose point as possible. However, if the first power flow solution is far away from the nose point, then the resulting load margin estimation can be very optimistic even if the second power flow is close to the nose point. Furthermore, the accuracy of estimation highly depends on the location of the second power flow solution. The farther the distance between the nose point and the second solution, the greater the estimation error becomes.

To enhance the accuracy in estimating the nose points, we use a sensitivity-based scheme to determine a suitable step-size for the computation of the second power flow solution [28]. For each contingency, this scheme determines an adaptive step-size, instead of fixed step-size in computing the second power flow solution. We then apply CPFLOW [11] to compute the second power flow solution with the determined (adaptive) step-size. After obtaining the second power flow solution, we then check whether it is sufficiently close to the nose point by the distance between the second computed power flow solution and the estimated nose point. If the second power flow solution lies sufficiently close to the nose point in the parameter space, then the accuracy of the estimated load margin to nose point is verified for the contingency; otherwise, a reselection scheme is used to compute the third power flow solution and applies the curve fitting technique again using the second power flow solution and the third power flow solution to estimate the location of the nose point in the parameter space. This process is repeated, if necessary, to obtain accurate load margin estimation to collapse for each contingency.

The following “closeness” criterion to check whether or not the computed power flow solution is close to the nose point was proposed in [28]:

$$\frac{\lambda_b - \lambda_2}{\lambda_2} < \beta \quad (5.9)$$

where  $\lambda_b$  is the estimated load margin to the saddle-node bifurcation point based on the (second) computed power flow solution,  $\lambda_2$  is the parameter value associated with the computed power flow solution, and  $\beta$  is a pre-defined value, say 0.15. When this criterion is satisfied, it implies that the second power flow solution is close to the estimated saddle-node bifurcation point and the estimated load margin is expected to be quite accurate. If the computed power flow solution is far away from the estimated saddle-node bifurcation point, i.e., the criterion (5.9) is not satisfied, then another power flow solution closer to the bifurcation point than the current one is needed. Under this situation, we set this second solution as the first solution point and use the step-size

$$\lambda_{step} = \alpha(\lambda_b - \lambda_2) \quad (5.10)$$

to compute next power flow solution, where  $\alpha$  is step-size factor smaller than 1.0. This scheme may require the computation of three or more power flow solutions. Our numerical experience on several test systems indicates that only a few contingencies in a contingency list will require this scheme.

There is another type of voltage collapse caused by the so-called limit-induced bifurcation. The limit point is induced primarily due to the generator reactive power limits [24]. It should be pointed out that all the curve-fitting based performance indices can give inaccurate estimation of load margins caused by the limit-induced bifurcation point. To overcome this difficulty, we estimate the location of the limit-induced bifurcation point in the parameter space via a procedure in computing power flow solutions [28]. The computation of the limit-induced bifurcation point is significant when its location is far away from the saddle-node bifurcation point in the parameter space (see Figure 5.7); otherwise, the load margin to the limit-induced bifurcation point is close to the load margin to the saddle-node bifurcation point (see Figure 5.8) and then the estimation of load margin to the saddle-node bifurcation point can be used to approximate the load margin to the limit-induced bifurcation point.

A step-by-step description of the proposed method for estimating the load margin to nose point is given below.

**Given:** A study power system with a load/generation vector, and a list of contingencies.

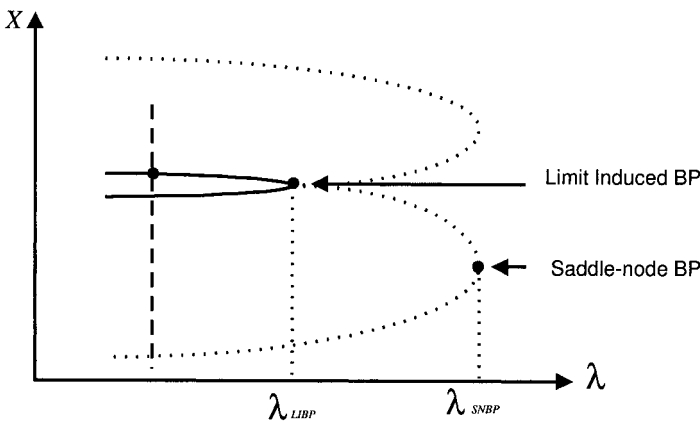


Figure 5.7. The limit-induced bifurcation point is far away from the saddle-node bifurcation point.

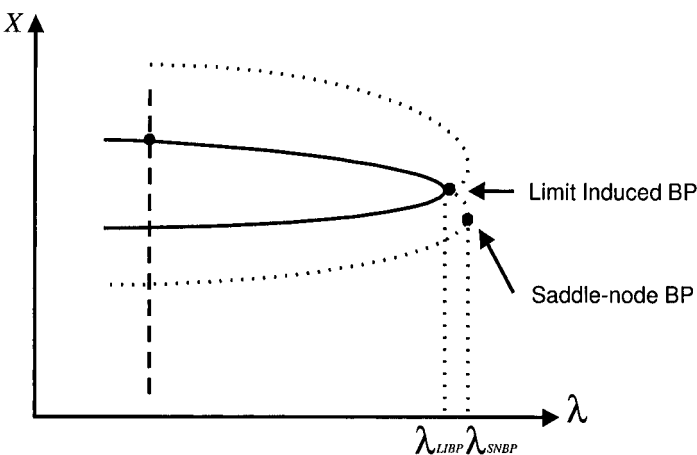


Figure 5.8. The limit-induced bifurcation point is close to the saddle-node bifurcation point.

**Goal:** Estimate the load margin to the nose point (along the load/generation vector) of the parameterized power system under each contingency.

- *Step 1:* For the given load/generation variation direction, apply CPFLOW to compute the exact nose point of base case.
- *Step 2:* For each contingency, say contingency  $i$ , compute a suitable step length for the contingency. If load margins of all the contingencies have been estimated, go to Step 4; otherwise, go to Step 3.

- *Step 3:* For contingency  $i$ , compute the estimated load margin  $\lambda_{i,b}$  via the following seven steps.
  - *Step 3.1:* Use a reliable solver to compute the power flow solution of the post-contingency system. If a power flow solution is found, set this solution  $x_1$  as the first point and go to Step 3.2; if the power flow diverges, this contingency is insecure and set  $\lambda_{i,b} = 0$  and go to Step 2.
  - *Step 3.2:* Compute the second power flow solution  $x_2$  by CPFLOW using the step length obtained at step 2.
  - *Step 3.3:* If the power flow solution cannot be found, then compute the second power flow solution by using the automatic step length shrinking technique until a solution is obtained.
  - *Step 3.4:* If the second power flow solution  $x_2$  obtained is very close to the first power flow solution  $x_1$ , then set the estimated load margin  $\lambda_{i,b}$  by using the load margin to the second power flow solution  $\lambda_{i,2}$  as the estimated load margin for this contingency (i.e.  $\lambda_{i,b} = \lambda_{i,2}$ ) and go to Step 2; otherwise, go to Step 3.5.
  - *Step 3.5:* Use the curve-fitting technique to estimate the load margin  $\lambda_{i,b}$  for this contingency. Check whether the estimated load margin  $\lambda_{i,b}$  is satisfied with the closeness criterion. If the criterion is satisfied; then the estimation for this contingency is obtained and go to Step 2; otherwise, go to Step 3.6.
  - *Step 3.6:* Set this second point as the first point and compute a new second point by using a reduced step-length and go to Step 3.3.
- *Step 4:* Rank the contingency list based on the estimated load margin  $\lambda_{i,b}$ .

For a contingency which leads to a limit-induced bifurcation point, the above method estimates the load margin to the nose point (in this case, it is a limit-induced bifurcation point) in the following way: if the limit-induced bifurcation point is close to the nose point, then the estimated load margin is set to be the estimated load margin to the nose point; otherwise, we use Step 3.3 and Step 3.4 to estimate its load margin.

## 7. Estimating Load Margins to Static Security Violations

The look-ahead scheme for voltage-violation load margin is based on the scheme developed in [5]. Let the  $\lambda$ - $V$  curve of the  $i^{\text{th}}$  load bus be chosen to derive the load margin. We then use the quadratic curve described by (5.7) to approximate the  $\lambda$ - $V$  curve of bus  $i$  passing through two points, say  $(\lambda_1, V_{i,1})$  and  $(\lambda_2, V_{i,2})$ . By using the information of the derivative  $\dot{\lambda}_{i,2}$  at the second point, we can obtain the values for the parameters  $\alpha$ ,  $\beta$  and  $\gamma$  from (5.8). The point with the maximal value of  $\gamma$  on the curve (5.7) corresponds to the nose point; hence the corresponding value  $\lambda_{max}$  can be used to estimate the nose-point load margin. To estimate the voltage-violation load margin, we consider a load bus, say bus  $j$ , and use  $\lambda_1$ ,  $V_{j,1}$ ,  $\lambda_2$ ,  $V_{j,2}$ ,  $\lambda_{max}$ , and a characteristic equation to determine the corresponding quadratic curve, to calculate the bus voltage at  $\lambda_{max}$ , denoted by  $V_{max,j}$ , from

$$\begin{aligned}\lambda_1 &= \alpha_j + \beta_j V_{j,1} + \gamma_j V_{j,1}^2 \\ \lambda_2 &= \alpha_j + \beta_j V_{j,2} + \gamma_j V_{j,2}^2 \\ \lambda_{max} &= \alpha_j + \beta_j V_{max,j} + \gamma_j V_{max,j}^2 \\ 0 &= \beta_j + 2\gamma_j V_{max,j}\end{aligned}\tag{5.11}$$

The last equation in (5.11), which is a characteristic equation for the nose point of the  $P$ - $Q$ - $V$  curve, states that the sensitivity of the voltage with respect to the load increase at the nose point is infinite. From the four equations in (5.11), one can obtain the values  $\alpha_j$ ,  $\beta_j$ ,  $\gamma_j$ , and  $V_{max,j}$ . If the lower voltage, say  $V_j$ , of bus  $j$  is less than  $V_{max,j}$ , then the voltage-violation load margin of the bus equals the nose-point load margin of the bus. If the lower voltage  $V_j$  is higher than  $V_{max,j}$ , then the voltage-limit load margin,  $\lambda_v$  is derived from

$$\lambda_v = \min \left\{ \alpha_j + \beta_j V_j + \gamma_j V_j^2 \right\}, \quad \forall j$$

As to the look-ahead thermal limit analysis, which is needed to predict the point at which the power flow through a transmission line reaches its limit, one must look ahead at the behavior of line flow that requires knowing the bus voltage magnitude as well as the bus angle. This piece of information can be obtained from both  $\lambda$ - $V$  and  $\lambda$ - $\delta$  curves. In general, the  $\lambda$ - $\delta$  curve is more complicated than the  $\lambda$ - $V$  curve, especially for the portion that corresponds to the lower part of the  $\lambda$ - $V$  curve. However, we observe that the upper part of the  $\lambda$ - $\delta$  curve has a shape that is approximately either a straight line or a quadratic curve. Since we are only interested in the upper part of the  $\lambda$ - $\delta$  curve, this piece of

information is useful in the development of the following algorithm to obtain the  $\lambda$ - $\delta$  curve.

To approximate the  $\lambda$ - $\delta$  curve of bus  $i$ , we present the following scheme. Suppose we have two points  $(\lambda_{i,1}, V_1)$  and  $(\lambda_{i,2}, V_2)$ , and the derivative  $\dot{\delta}_{i,2}$  at the second point. We use the following guidelines:

- 1 If the gradient  $\frac{\delta_{i,1} - \delta_{i,2}}{\lambda_{i,1} - \lambda_{i,2}}$  is very close to  $\dot{\delta}_{i,2}$ , then the  $\lambda$ - $V$  curve is approximately a straight line, which can be expressed as

$$\delta_i = \frac{\delta_{i,1} - \delta_{i,2}}{\lambda_{i,1} - \lambda_{i,2}} \lambda + \frac{\lambda_1 \delta_{i,2} - \lambda_2 \delta_{i,1}}{\lambda_{i,1} - \lambda_{i,2}} \quad (5.12)$$

- 2 Otherwise, the  $\lambda$ - $\delta$  curve is approximately a quadratic curve, which can be expressed as

$$\lambda = \alpha + \beta V_i + \gamma V_i^2 \quad (5.13)$$

The coefficients  $\alpha$ ,  $\beta$ , and  $\gamma$  can be obtained simultaneously

$$\begin{aligned} \lambda_1 &= \alpha + \beta \delta_{i,1} + \gamma \delta_{i,1}^2 \\ \lambda_2 &= \alpha + \beta \delta_{i,2} + \gamma \delta_{i,2}^2 \\ 0 &= \beta \dot{\delta}_{i,2} + 2\gamma \delta_{i,2} \dot{\delta}_{i,2} \end{aligned} \quad (5.14)$$

With the above formula, one can estimate the load margin to thermal-limit of a transmission line based on the  $\lambda$ - $V$  and  $\lambda$ - $\delta$  curves at end buses of the transmission line. Using this procedure for each transmission line, one can estimate the thermal-limit load margin for the interconnected power system under the proposed power transactions.

## 8. Identify Critical Contingencies for Dynamic Security

The ATC of an interconnected power system with respect to a set of proposed power transactions can be constrained by dynamic security limits. The task of computing ATC subject to dynamic security constraints, however, is very challenging due to the nonlinear nature of interconnected power systems and the tremendous computation requirements for stability analysis of credible contingencies. The dynamic security limit considered in this paper is the transient stability limit. To put this dynamic security limit into the framework of ATC, we next define transient-stability-limit load margin.

**Definition:** The *transient-stability-limit load margin* of a power system dynamical model under a contingency with respect to a load-generation vector (5.3) is the (minimum) distance (in terms of MW and/or MVar)

from the current operating point to the state vector of the parameterized power system dynamical model subject to the contingency, at which transient instability occurs (See Figure 5.9).

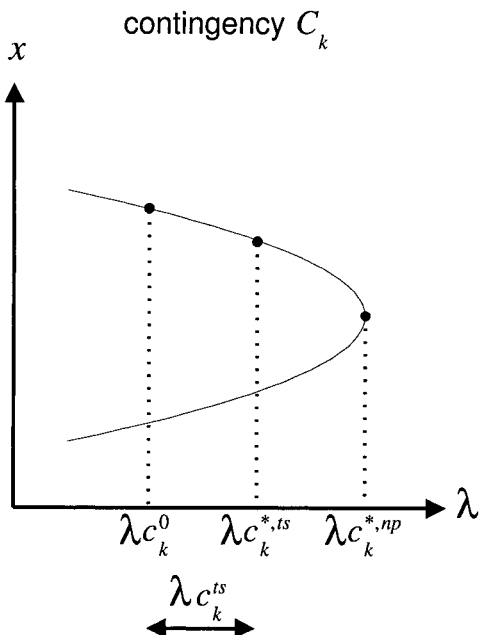


Figure 5.9. The transient-stability-limit load margin  $\lambda_{C_k}^{ts}$  for the power system subject to  $C_k$ .

We note that the transient-stability-limit load margin should be smaller than the nose-point load margin of the base-case power system because the transient-stability-limit load margin is not defined when its value is greater than the nose-point load margin of the base-case power system. In brief, transient instability is not an issue when the steady-state instability occurs.

The task of computing transient-stability-limit load margin with respect to a set of credible contingencies is challenging. We present a tool, termed BCU limiter, which can quickly compute ATC limited by the transient stability limits of credible contingencies. This tool computes, given a proposed power transaction, the amount of power transfers that a power system can withstand before its transient stability limit is reached. In addition, BCU limiter can rank a given list of contingencies in terms of their load margins to transient stability limits and compute the corresponding ATC. The BCU limiter is an integrated computer package of

CPFLOW, BCU method, BCU classifiers, and BCU-guided time-domain simulation [29], [30]. The combined BCU method and BCU classifiers, given an operating point, not only perform power system dynamic security assessments and ranking but also compute the load margin to transient stability limit under a list of credible contingencies [18], [19].

## 9. Solution Algorithm

A solution algorithm for computing the ATC with respect to a set of proposed power transactions, i.e., transaction-dependent ATC, for an interconnected power system subject to static as well as dynamic security constraints is presented below. We note that there is a significant difference in the required computational efforts between the static security assessment and dynamic security assessment of a list of credible contingencies. On-line security assessment requires evaluating the static as well as dynamic effects of hundreds or even thousands of credible contingencies on power systems. Static security assessment (SSA) checks all relevant static constraints of post-fault (post-contingency) steady states. From a computational viewpoint, SSA needs to solve a large set of nonlinear algebraic equations. Dynamic security assessment (DSA) requires the handling of a large set of nonlinear differential equations in addition to the nonlinear algebraic equations involved in the SSA. The computational effort required in on-line DSA is roughly three orders of magnitude higher than that for the SSA. This three orders of magnitude computational requirement has traditionally prompted the task of performing DSA in an off-line mode. Due to this consideration, the proposed solution algorithm examines security constraints in two stages. The static security constraints are handled in Stage I while the dynamic security constraints are handled in Stage II.

The four look-ahead ranking schemes, described in the previous two sections, for identifying the critical contingencies for each type of security limits play an important role in the proposed solution algorithm. Detailed studies of these critical contingencies indeed provide the top binding contingencies, the associated binding constraints and, ultimately, the corresponding ATC's. The solution algorithm first computes at Stage I the load margin to static security limits under the list of contingencies. The solution algorithm then checks the look-ahead operating point of the load margin calculated at Stage I against the transient stability constraint by performing the transient stability assessment at the look-ahead operating point. If the transient stability constraint is satisfied, then the look-ahead operating point of the load margin satisfies both the static and dynamic security constraints under a list of contingencies and

the corresponding load margin is the ATC; otherwise the BCU limiter is applied to compute the load margin to the transient-stability-limit with respect to a set of credible contingencies. Under this situation, the load margin to the transient-stability-limit is the ATC and the limiting constraint is the transient stability constraint and the corresponding contingency is the binding contingency.

- **Stage 1:** Initialization

- **1.1** Build the power transfer vector  $b$  to represent (mathematically) the proposed power transfer transactions.
- **1.2** Form the parameterized power flow equations by incorporating the power transfer vector  $b$  into the base-case power flow equations

$$f(x) - \lambda b = 0.$$

- **1.3** Initialize the parameter (i.e., load-generation condition number)  $\lambda$  by setting  $\lambda = 0$  to the base case.

- **Stage 2:** Look-ahead contingency ranking for static security violation

- **2.1** Use a look-ahead scheme to rank the set of contingencies  $L$  in terms of branch MVA violation.
- **2.2** Use a look-ahead scheme to rank the set of contingencies  $L$  in terms of bus voltage violation.
- **2.3** Use a look-ahead scheme to rank the set of contingencies  $L$  in terms of load margins.

- **Stage 3:** Compute first-contingency ATC and identify the corresponding binding contingency.

Select the top critical contingencies from each of the ranked contingencies obtained in Stage 2.1-2.3; say the total number of contingencies is  $\mu$ . Apply CPFLOW to those contingencies for calculating the corresponding ATC and identifying the corresponding constraint violations.

- **Stage 4:** Rank selected contingencies in terms of ATC

Rank the set of contingencies according to each value  $\hat{\lambda}_j$  obtained in Stage 3. Rename the set of contingencies such that the ranked contingency set is  $\hat{L} \equiv \{l_1, l_2, \dots, l_\mu\}$  with  $\hat{\lambda}_1 \geq \hat{\lambda}_2 \geq \dots \geq \hat{\lambda}_\mu$ . The ATC subject to static voltage stability constraints and static security constraints of the contingency set  $L$  is  $\hat{\lambda}_\mu$ , the binding contingency is  $l_\mu$  and the associated violated constraint is  $C^*$ .

- **Stage 5:** Check the transient stability constraint

Apply the BCU method to the look-ahead operating point of the load margin  $\hat{\lambda}_\mu$  and identifying, if any, the unstable contingencies. If there are no unstable contingencies, then the ATC subject to both static and dynamic security constraints of the contingency set  $L$  is  $\hat{\lambda}_\mu$  and go to Stage 7; otherwise, go to Stage 6.

- **Stage 6:** Look-ahead contingency ranking for dynamic security violation

Use a look-ahead scheme to rank the set of contingencies  $L$  in terms of load margin to transient instability. If there are unstable contingencies, then apply both the CPFLOW and BCU-DSA to these unstable contingencies for calculating the corresponding ATC and identifying the corresponding binding contingency.

- **Stage 7:** Output analysis

Output each ATC with respect to the corresponding binding contingency and the associated violated constraint.

We explain the physical meaning of the value  $\hat{\lambda}_j$  in Stage 4 (or in Stage 5) which is the transaction-dependent ATC for the power system subject to the contingency, say,  $j$ . Physically, if  $\hat{\lambda}_j$  is greater than 1.0, then it means that the transmission network is able to transfer the proposed power transactions, should the contingency  $j$  occur. In addition, the (normalized) static security margin of the power system with the proposed power transactions is  $\hat{\lambda}_j - 1.0$ . On the other hand, the transmission network would be unable to transfer the proposed power transactions, should the contingency  $j$  occur, if  $\hat{\lambda}_j$  is less than 1.0. In this case, the suggested maximum value of reliable power transfer is  $\hat{\lambda}_j$  of the proposed power transactions. For example, if  $\hat{\lambda}_j$  equals 0.7, then the maximum available transfer capability for the proposed power transactions is 70% of the proposed power transactions. Note that even though these ranking schemes do not consider the physical limits of control devices, the solution algorithm does take these physical limits into account during the process of solving the parameterized power flow equations via CPFLOW [11].

## 10. Numerical Studies

We have developed a computer package based on the solution algorithm presented in the previous section and on the platform of CPFLOW.

The overall architecture of the computer package developed for evaluating maximum simultaneous transfer capability for a set of proposed power transactions and the required ancillary services of interconnected power systems in the FERC's open-access transmission environment is shown in Figure 5.10.

### Preventive-mode ATC

We consider a 15,005-bus interconnected power system containing about 2,400 generators, 16,000 transmission lines, 8,000 loads, 4,000 fixed transformers, 2,400 fixed shunts, 3,000 ULTC transformers, 800 switchable shunts, and other control devices such as fixed and ULTC phase shifters, etc. Given a base case of the interconnected power system with a secure operating point, a proposed power transaction described by transmitting 1,300 MW real power from area A to area B by decreasing all the real power generations of area B uniformly to zero (24 generators are scaled down to 0 MW) and increasing real power generations of area A uniformly to supply the loads of Area B (the area-wide generation of Area A is scaled properly), we apply the tool to evaluate the real power transfer capability from area A to area B of the interconnected power system subject to a list of contingencies which is a set of transmission line or generator outages. Three cutsets of 500 kV transmission lines were selected and the corresponding sum of the line flows was defined as the interface line flows.

ATC can be expressed in several ways. It is sometimes useful to represent ATC in terms of pre-contingency interface power flow, i.e., the base-case interface power flow, at the limit point. In this numerical study, the ATC was constrained by one of the limitations: the nose point of the  $P$ - $Q$ - $V$  curve (steady-state stability limits), voltage-violation limits and thermal limits. The transient stability limit is not considered in this numerical study. ATC is expressed in terms of either (i) available power transfer between the sending area and the receiving area, or (ii) the pre-contingency power flow of the three interface flows.

The three fast look-ahead estimators were applied to the list of credible contingencies. The top 5 most serious contingencies captured by each look-ahead scheme and the corresponding load margin are listed respectively in Tables 5.1, 5.2, and 5.3. In these three tables, a contingency marked with \* indicate a generator trip. For instance, contingency 32-6830 is the most severe contingency in terms of load margin to voltage collapse because its corresponding load margin to voltage collapse is 933 MW while contingency 4364-6831 is the second most severe contingency whose corresponding load margin to voltage collapse is 1043 MW. Table 5.1 lists the top five most severe contingencies in terms of load margin to voltage collapse. On the other hand, contingency 89389-89392 is the

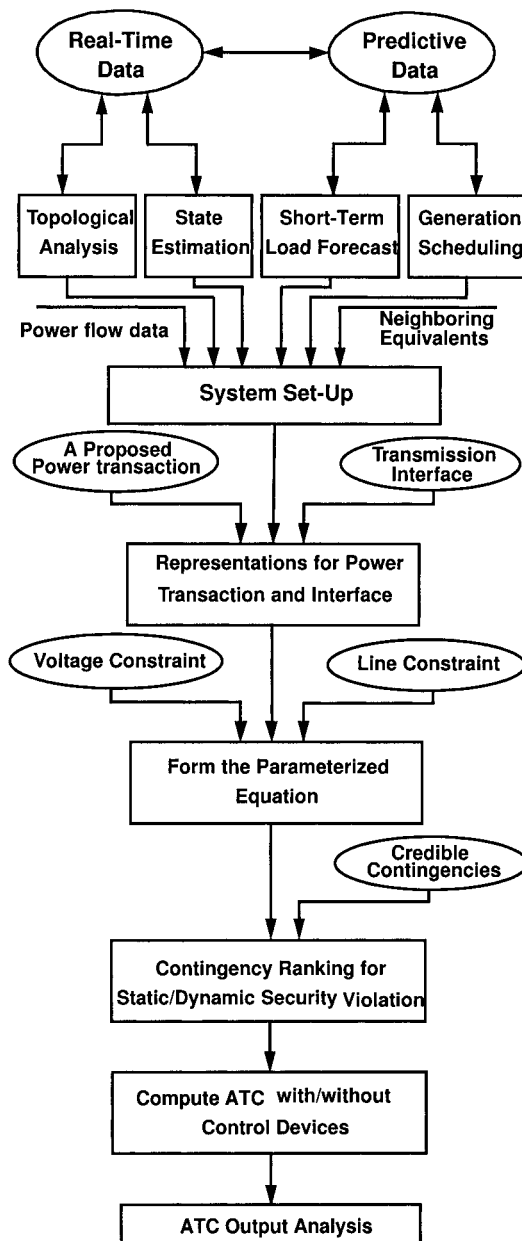


Figure 5.10. The overall architecture of the proposed tool for accurate evaluation of ATC.

most severe contingency in terms of load margin to thermal limit because its corresponding load margin to thermal limit is 194 MW while contingency \*289 is the second most severe contingency whose corresponding load margin to thermal limit is 566 MW. Table 5.2 lists the top five most severe contingencies in terms of load margin to thermal limit. In terms of load margin to voltage violation, contingency 4364-6831 is the most severe whole contingency 85-4323 is the second most severe. Table 5.3 lists the top five most severe contingencies in terms of load margin to voltage violation.

*Table 5.1.* The five most serious contingencies ranked by load margin to system collapse.

<i>Contingency</i>	<i>Estimated load margin (MW)</i>	<i>Estimated <math>\lambda_n</math></i>
32-6830	933	0.728
4364-6831	1043	0.808
85-4323	1053	0.81
*4523	1053	0.81
*4496	1057	0.813

*Table 5.2.* The five most serious contingencies ranked by load margin to thermal limit.

<i>Contingency</i>	<i>Estimated load margin (MW)</i>	<i>Estimated <math>\lambda_t</math></i>
89389-89392	194	0.149
*289	566	0.435
89394-104	681	0.524
*7498	746	0.574
*89418	785	0.604

*Table 5.3.* The five most serious contingencies ranked by load margin to voltage violation.

<i>Contingency</i>	<i>Estimated load margin (MW)</i>	<i>Estimated <math>\lambda_v</math></i>
4364-6831	680	0.523
85-4323	748	0.575
32-6830	754	0.58
*7498	759	0.584
89386-89387	759	0.584

The tool then performed detailed analysis based on the continuation power flow for each of these 11 contingencies to compute the corresponding ATC and to identify the binding constraints and the associated binding constraint. We note that because 4 of these top 15 contingencies are duplicated, only 11 contingencies require further detailed analysis. Note that the participation of all control devices and the physical constraints of these control devices are taken into account in the process of continuation power flow study. The final results of ATC with respect to the proposed power transaction along with a list of binding contingencies and the corresponding binding constraints are summarized in Table 5.4.

Table 5.4. Output Analysis of ATC evaluation.

<i>The top eight serious contingency</i>	<i>Contingency</i>	<i>Pre-contingency interface power flow of three interfaces (MW)</i>		
		<i>Eastern</i>	<i>Central</i>	<i>Western</i>
Base Case	Base Case	5552	2247	4473
The most serious	89389-89392	5422	2203	4445
2 <sup>nd</sup> most serious	89394-104	5478	2218	4452
3 <sup>rd</sup> most serious	4364-6831	5531	2237	4465
4 <sup>th</sup> most serious	32-6830	5537	2240	4467
5 <sup>th</sup> most serious	*7498	5538	2241	4468
6 <sup>th</sup> most serious	85-4323	5541	2242	4468
7 <sup>th</sup> most serious	*4496	5543	2243	4469
8 <sup>th</sup> most serious	89386-89387	5549	2246	4472

<i>The top eight serious contingency</i>	<i>Contingency</i>	<i>ATC (MW)</i>	<i>Binding constraints</i>	
			<i>Type</i>	<i>Location</i>
Base Case	Base Case	913	Voltage	7084
The most serious	89389-89392	234	Thermal	3687-3337
2 <sup>nd</sup> most serious	89394-104	584	Thermal	37-276, 37-277
3 <sup>rd</sup> most serious	4364-6831	820	Voltage	6807, 6808, 7804
4 <sup>th</sup> most serious	32-6830	845	Voltage	6808, 68087, 7804
5 <sup>th</sup> most serious	*7498	857	Thermal	37-276, 37-277
6 <sup>th</sup> most serious	85-4323	869	Voltage	7804
7 <sup>th</sup> most serious	*4496	883	Thermal	37-276, 37-277
8 <sup>th</sup> most serious	89386-89387	898	Thermal	37-276, 37-277

It is clear that the ATC of the system for the proposed power transaction, under the assumed condition and the list of credible contingencies, is 234 MV between the sending area and the receiving area, which is

much smaller than the proposed 1300 MW of power transaction. The corresponding contingency, 89389-89392, is the binding contingency that leads to a thermal limit violation at the transmission line between Buses 3687 and 3337. Equivalently, the ATC for the proposed power transaction is 5422 MW for the eastern interface, 2203 MW for the central interface, and 4445 MW for the western interface. It is interesting to note that the constrained eastern interface line flow under this contingency is the smallest among the constrained eastern interface line flows of all the contingencies considered. This is also true for the constrained central interface line flow and the constrained western interface line flow.

Because ATC is the system transfer capability under the most severe contingency, it may prove useful to compute ATC under the top most severe contingencies. To this end, this tool can compute ATC with the corresponding binding contingency as a by-product and the associated violated constraint in an “increasing” order as shown in Table 5.4. This piece of information is useful to decision-making personnel and can enable a proactive approach to measure the transfer capability of the network. For instance, the ATC of the study system without the consideration of the contingency (89389-89392) is 584 MW. If the probability of the occurrence of contingency 89389-89392 is very low, then it may be reasonable to post the ATC as 584 MW and, in the meantime, a remedial control scheme can be prepared in advance should contingency 89389-89392 occur.

### **Corrective-mode ATC**

A corrective-mode ATC is the maximum available transfer capability defined by the system’s hard limits such as steady-state stability limits and transient stability limits. Computing the corrective-mode ATC is of significant importance in ATC evaluation. We next consider a 646-bus interconnected power system with a total generation of 28,500 MW. The scope of the tested system is: 98 generators, 482 transmission lines, 224 loads, 489 ULTC transformers, 158 switchable shunts, and 3 areas. A power transaction is proposed to transfer 250 MW from the central region to the northern region by decreasing Generator 211 in the northern region to zero and increasing Generator 1083 in the central region to support the load demand in the northern region. A cluster of 6 tie-lines between the central and northern regions was monitored and the corresponding sum of the line flows was defined as the interface line flows.

We applied the tool to evaluate the corrective-mode ATC subject to a list of credible contingencies on the test system. It turns out that the corrective-mode ATC of the base-case system for the proposed power transaction is 217.98 MW. This indicates that the system’s ATC cannot meet the request of the 250 MW power transaction even without the con-

sideration of possible contingencies. Under the list of credible contingencies, the corrective-mode ATC of the test system is 77.01 MW with the binding contingency 1500-1501. Under the list of credible contingencies without the binding contingency 1500-1501, the corrective-mode ATC of the test system is 77.02 MW with the binding contingency 1750-1900. This tool computes the corrective-mode ATC with the corresponding binding contingency as a by-product and the associated violated constraint in an “increasing” order as shown in Table 5.5. Again, this table allows a probabilistic treatment of each contingency and the associated risk management as well.

Table 5.5. Summary of corrective-mode ATC of 600-bus system.

Severity	Contingency	Interface power Flow (MW)	ATC (MW)	Weakest Bus
1 <sup>st</sup>	1500-1501	6526.66	77.01	4214
2 <sup>nd</sup>	1750-1900	6531.55	77.01	4002
3 <sup>rd</sup>	1750-1761	6549.36	87.78	3243
4 <sup>th</sup>	1750-1910	6537.02	89.82	4410
5 <sup>th</sup>	3321-3361	6506.09	110.61	4410
6 <sup>th</sup>	1900-2000	6533.99	122.06	4410
7 <sup>th</sup>	1700-1900	6517.43	143.99	4410
8 <sup>th</sup>	1910-2000	6519.14	150.71	4410
	Base case	6499.90	217.98	4214

## 11. Conclusions

We have presented a framework and described a practical tool for accurate evaluation of ATC of an interconnected power system with respect to a set of proposed power transactions. A full AC nonlinear modeling of power systems including the effects of control devices is employed in the framework. Both static and dynamic security constraints under a list of credible contingencies are taken into account in the framework. A computer package implementing this framework for ATC evaluation of large-scale power systems is developed. This tool has comprehensive modeling capability and can determine the maximum simultaneous transfer capability between several exporting and importing companies, zones, areas, or individual buses under various power transactions and transmission service. In order to effectively handle credible contingencies, the strategy of using effective schemes to rank all credible contingencies and of applying detailed analysis programs only to critical contingencies is adopted in the tool. We have developed three look-ahead margin estimators for estimating the load margin to steady-state stability limit, thermal-limit

load margin and voltage-violation load margin and integrated these three load margin estimators into the tool.

The theoretical basis behind these three look-ahead margin estimators is the normal form theory. To handle the possible inaccurate estimation of load margins due to limit-induced bifurcation points, we estimate the location of the limit-induced bifurcation point in the parameter space via a refined procedure in computing power flow solutions. It should be pointed out that all the curve-fitting based performance indices can give inaccurate estimation of load margins due to limit-induced bifurcation points which are caused by generator reactive power capability limits. The computation of limit-induced bifurcation point is significant when its location is far away from the saddle-node bifurcation point in the parameter space.

This tool has the ability to identify top binding contingencies and their associated binding constraints, and to compute the corresponding ATC subject to static security constraints. The developed framework provides a platform to take dynamic security constraints into account. Further development of this tool for computing on-line ATC with both static and dynamic security constraints is being investigated. We have applied this tool with promising results to compute the ATC with respect to a proposed power transaction considering static security constraints of a 15,000-bus power system. This tool identified the top eight binding contingencies, the associated binding constraints (some are thermal limit constraints and others are voltage violation constraints), and computed the corresponding ATC for each binding contingency, from which the system ATC is readily determined. Hence, this tool allows the development of a migration scheme to increase ATC and provides a platform to take a proactive action in evaluating ATC and to prepare a remedy control, should a contingency occur. It allows a probabilistic treatment of each contingency and the associated risk management.

ATC is in fact an estimate of the near-future transmission network's capability of additional power transfer over the existing committed usage. As such, there are several uncertainties associated with the parameters and forecasting quantities used in the ATC evaluation that can significantly affect the ATC values. To deal with uncertainty, several techniques are used in conjunction with a deterministic approach for ATC evaluation. Further development of techniques to deal with uncertainties in the context of ATC evaluation is desirable. We focus in this paper on the development of a deterministic framework for accurate determination of ATC with both static and dynamic security constraints with a list of credible contingencies taken into account. We note that the proposed deterministic framework can be used in conjunction with

other tools for statistical inference to derive the probability distribution of ATC.

There are several factors related to modeling that affect the accuracy of ATC evaluation. For instances, how to model the step increases of system load, area load, zone loads, and bus loads. The current practice of using constant  $P$ - $Q$  load to model the step increases can lead to rather conservative results. Using ZIP loads to model the step increases can be a good compromise [35]. The question of what types of load models should be used to model the step increases of loads deserves further investigation. Another uncertainty is how to model the generation scheduling to meet the load increases and proposed power transactions. The generation scheduling can be AGC-based, economic dispatch-based, governor response-based, or capacity limits-based, and it should be properly modeled in the ATC evaluation.

A limiting contingency is the most severe contingency in the contingency list that determines the ATC value with respect to an assumed set of participating generators and the associated fixed participation factor. A practical question naturally arises: will the limiting contingency continue to be the limiting contingency with respect to multiple combinations of participating generators and participating factors? Another related question is: what are the possible range of ATC values due to the different schemes of generation scheduling and to the different participation factors? This possible range obviously ties closely with the value of Transmission Reliability Margin (TRM), which is the amount of transmission capability necessary to ensure that the interconnected network is secure under a reasonable range of uncertainties in system conditions.

A widely used approach in the power industry to compute the nose point is the use of repetitive power flow calculations to generate the so-called  $P$ - $V$  or  $Q$ - $V$  curve along the parameter increase direction. In this approach, an operating point is claimed to be the nose point if it is the first point (along the parameter increase direction) where power flow calculation does not converge. We have identified in this paper several issues regarding this approach. First, the point where the power flow calculations diverge (which is determined by a numerical failure) does not necessarily represent the nose point (which is a physical limitation). Second, the point where power flow calculations fail to converge may vary, depending on which method was used in the calculation. Another caution of a converged power flow solution is that the converged power flow solution may not correspond to the actual post-fault operating point. From a nonlinear dynamical system viewpoint, the actual post-fault operating point depends on the location of the initial guess

and the size and nature of stability regions of post-fault stable equilibrium points. From a numerical method viewpoint, the converged power flow solution depends on the location of the initial guess and the size and nature of the convergence region of post-fault stable equilibrium points with respect to the employed solution algorithm. The question of how to relate a computed power flow solution to the actual operating point, under the condition that the underlying model is accurate, deserves further investigations.

## References

- [1] P.W. Sauer. Technical Challenges of Computing Available Transfer Capability (ATC) in Electric Power Systems. *Proceedings of IEEE 30<sup>th</sup> Hawaii International Conference on System Science*, Maui, Hawaii, January 1997.
- [2] M.H. Gravener and C. Nwankpa. Available Transfer Capability and First Order Sensitivity. *IEEE Transactions on Power Systems*, 14:512–518, 1999.
- [3] J. Tong. Real Time Transfer Limit Calculations. *Proceedings of IEEE PES Winter Power Meeting*, 0-7803-6423-6, 2000.
- [4] Transmission Transfer Capability Task Force. *Transmission Transfer Capability*. North American Reliability Council, Princeton, New Jersey, May 1995.
- [5] H.D. Chiang, C.S. Wang, and A.J. Flueck. Look-Ahead Voltage and Load Margin Contingency Selection Functions for Large-Scale Power Systems. *IEEE Transactions on Power Systems*, 12:173–180, 1997.
- [6] X.Y. Chao, R.R. Austria, N.D. Reppen, D.E. Welsh, J.A. Uhrin, and J.B. Shultz. Practical Determination of Operating Transfer Limits. *Proceedings of the 1995 IEEE Power Industry Computer Applications Conference*, 271–277, Salt Lake City, Utah, 1995.
- [7] S. Wunderlich, T. Wu, R. Fischl, and R. O’Connell. An Inter-Area Transmission and Voltage Limitation (TVLIM) Program. *IEEE Transactions on Power Systems*, 10:1257–1263, 1995.
- [8] G.W. Rosenwald and C.C. Liu. Consistency Evaluation in an Operational Environment Involving Many Transactions. *IEEE Transactions on Power Systems*, 11:1757–1762, 1996.
- [9] R. Baldick and E. Kahn. A Linear Model of Voltage Limited Transmission Interface Constraints. *IEEE Transactions on Power Systems*, 10:476–482, 1995.

- [10] A.J. Flueck, H.-D. Chiang, and K.S. Shah. Investigating the Installed Real Power Transfer Capability of a Large Scale Power System under a Proposed Multiarea Interchange Schedule using CPFLOW. *IEEE Transactions on Power Systems*, 11:883–889, 1996.
- [11] H.D. Chiang, A.J. Flueck, K.S. Shah, and N. Balu. CPFLOW: A Practical Tool for Tracing Power System Steady-State Stationary Behavior Due to Load and Generation Variations. *IEEE Transactions on Power Systems*, 10:623–634, 1995.
- [12] G.C. Ejebe, G.D. Irisarri, S. Mokhtari, O. Obadina, P. Ristanovic, and J. Tong. Methods for Contingency Screening and Ranking for Voltage Stability Analysis of Power Systems. *IEEE Transactions on Power Systems*, 11:350–356, 1996.
- [13] S. Greene, I. Dobson, and F.L. Alvarado. Sensitivity of the Loading Margin to Voltage Collapse with respect to Arbitrary Parameters. *IEEE Transactions on Power Systems*, 12:262–272, 1997.
- [14] G.T. Heydt and B.M. Katz. A Stochastic Model in Simultaneous Interchange Capacity Calculations. *IEEE Transactions on PAS*, 94:350–359, 1975.
- [15] F. Xia and A.P.S. Meliopoulos. A Methodology for Probabilistic Simultaneous Transfer Capability Analysis. *IEEE Transactions on Power Systems*, 11:1269–1278, 1996.
- [16] J.C.O. Mello, A.C.G. Melo, and S. Granville. Simultaneous Transfer Capability Assessment by Combining Interior Point Methods and Monte Carlo Simulation. *IEEE Transactions on Power Systems*, 12:736–742, 1997.
- [17] B.C. Lesieutre and J. Hockenberry. Uncertainty Analysis of Power System Simulations and ATC Calculations Using the Probabilistic Collocation Method. *Proceedings of Bulk Power System Dynamic and Control IV-Restructuring*, Santorini, Greece, August 1998.
- [18] H.D. Chiang, C.S. Wang, and H. Li. Development of BCU Classifiers for On-Line Dynamic Contingency Screening of Electric Power Systems. *IEEE Transactions on Power Systems*, 14:660–666, 1999.
- [19] H.D. Chiang and H. Li. On-Line Dynamic Contingency Classifications for Large Power Systems: BCU Classifiers. *Proceedings of the 30<sup>th</sup> North American Power System Symposium*, 311–316, Cleveland, Ohio, 1988.
- [20] H.D. Chiang and R. Jean-Jumeau . Toward a Practical Performance Index for Predicting Voltage Collapse in Electric Power System. *IEEE Transactions on Power Systems*, 10:584–592, 1995.

- [21] C.A. Canizares, A.C.Z. de Souza, and V.H. Quintana. Comparison of Performance Indices for Detection of Proximity to Voltage Collapse. *IEEE Transactions Power systems*, 11:1441–1447, 1996.
- [22] H.D. Chiang. Power System Stability. Webster J.G. (ed.) Wiley Encyclopedia of Electrical and Electronics Engineering, 104–137, John Wiley & Sons, New York, 1999.
- [23] S. Greene, I. Dobson, and F.L. Alvarado. Contingency Analysis for Voltage Collapse via Sensitivities from a Single Nose Curve. *IEEE Transactions on Power Systems*, 14:232–240, 1999.
- [24] I. Dobson and L.M. Lu. Voltage Collapse Precipitated by the Immediate Change in Stability When Generator Reactive Power Limits are Encountered. *IEEE Transactions on Circuits and Systems I: Fundamental Theory and Applications*, 39:762–766, 1992.
- [25] A.J. Flueck, R. Gonella, and J.R. Dondeti. A New Power Sensitivity Method of Ranking Branch Outage Contingencies for Voltage Collapse. *IEEE Transactions on Power Systems*, 17:265–270, 2002.
- [26] E. Vaahedi, C. Fuchs, W. Xu, Y. Mansour, H. Hamadanizadeh, and G.K. Morison. Voltage Stability Contingency Screening and Ranking. *IEEE Transactions on Power Systems*, 14:256–265, 1999.
- [27] Z. Jia and B. Jeyasurya. Contingency Ranking for On-line Voltage Stability Assessment. *IEEE Transactions on Power Systems*, 15:1093–1097, 2000.
- [28] J. Zhao, H.-D. Chiang, and H. Li. Enhanced Look-Ahead Load Margin Estimation for Voltage Collapse Assessment. *International Journal of Electrical Power and Energy Systems*, to appear, 2004.
- [29] Y. Tada, A. Kurita, Y. Zhou, K. Koyanagi, H.-D. Chiang, and Y. Zheng. BCU-guided Time-Domain Method for Energy Margin Calculation to Improve BCU-DSA System. *Proceedings of IEEE/PES T&D Conference and Exhibition 2002*, 366–371, Yokohama, Japan, October 2002.
- [30] H.-D. Chiang, Y. Tada, H. Okamoto, Y. Zhou, and K. Koyanagi. A BCU-guided Time-Domain Method for Energy Margin Calculation of Practical Power Systems. *Proceedings of the 14<sup>th</sup> Power Systems Computation Conference*, Sevilla, Spain, June 2002.
- [31] *Available Transfer Capability Definitions and Determination*. North American Electric Reliability Council, June 1996.
- [32] J. Flory. Electricity Transactions in an Open Access Market. *Power Engineering Review*, 16(1):15–18, January 1996.
- [33] R.F. Chang, C.Y. Tsai, C.L. Su, and C.N. Lu. Method for Computing Probability Distributions of Available Transfer Capability.

- IEE Proceedings on Generation, Transmission and Distribution*, 149:427–431, 2002.
- [34] B.S. Gisin, M.V. Obessis, and J.V. Mitsche. Practical Methods for Transfer Limit Analysis in the Power Industry Deregulated Environment. *IEEE Proceedings of Power Industry Computer Applications*, PICA-1999, 261–266, May 1999.
- [35] H. Li, H.-D. Chiang, H. Yoshida, Y. Fukuyama, and Y. Nakanishi. The Generation of ZIP-V Curves for Tracing Power System Steady State Stationary Behavior due to Load and Generation Variation. *Proceedings of IEEE PES Summer Meeting*, 647–651, Edmonton, Canada, July 1999.

## Chapter 6

# AUTOMATING OPERATION OF LARGE ELECTRIC POWER SYSTEMS OVER BROAD RANGES OF SUPPLY/DEMAND AND EQUIPMENT STATUS

Marija Ilic

*Carnegie Mellon University*

[milic@ece.cmu.edu](mailto:milic@ece.cmu.edu)

**Abstract** One of the ultimate challenges in operating today's electric power grids is in designing automation for managing the system as demand varies over broad ranges and the status of major equipment changes. These changes are often hard to predict and it is, therefore, fundamentally impossible to design for the worst case scenarios; such scenarios are not known due to the very combinatorial nature of the problem. One possible way forward is to pursue automation for facilitating system's adjustments as the conditions vary. In this chapter we propose an extension of today's hierarchical control of electric power grids as one direction toward such automation. The approach is strongly motivated by the recognition that it has become insufficient to rely solely on operators' decisions; instead, more on-line information gathering and active decision making at various layers of the grid are needed. The proposed generalization is introduced by relaxing some critical assumptions underlying current operating practices, and by deriving layers of models so that each model can capture the events and phenomena in the power grid at the spatial and temporal scales that are appropriate for each level of decision. These models are used for quasi-stationary state estimation and automated control for the system to adjust smoothly to on-going changes. This is in sharp contrast to today's approach in which automation is only used during normal operation, while during abnormal conditions major decisions are made by the humans.

The resulting layered-architecture should reduce the complexity of the problem significantly. More important, it should provide the decision makers at each layer with the most relevant dynamic information that is needed for their own decision level, and at the same time provide the information necessary for the decision makers to respond and ad-

just to the overall system objectives. The layered models form a basis for an information technology (IT) infrastructure that can be proven to ensure pre-specified performance at various layers and in the system as a whole. An important observation is that when the assumptions typically made in today's system control are met, the proposed control generalization closely resembles current Supervisory Control and Data Acquisition (SCADA) and operating practices. In this sense, the approach is a natural outgrowth of what is already in place and should be considered for ensuring reliable and efficient operation over the broad ranges of conditions and equipment status.

**Keywords:** IT infrastructure, multi-layered electric power system models, quasi-stationary estimation, quasi-stationary electric power systems control, large-scale computations.

## 1. Introduction

Possibly one of the biggest causes of insecure and inefficient operation of today's electric power systems comes from a sub-optimal use of available resources because of hard-to-predict demand variations and equipment failures. Current operating practices in dealing with both types of uncertainties have been mainly preventive and off-line, without resorting to automated responses to the events and uncertainties. The system has been automated only to respond to relatively small demand fluctuations around historic patterns. We suggest here that this is one of the major distinctions between what it is and what it might be in the future electric power systems. These systems must become more automated over wide ranges of supply/demand patterns and equipment status. While the communications and control hardware are readily available, it is essential to pursue this inevitable automation based on systematic modeling, estimation, and control.

However, moving toward more automation could defeat its own purpose unless an IT infrastructure is in place to facilitate formation and coupling of sub-networks within the grid as they define sub-objectives according to their own needs and the changing system-wide conditions.

Moreover, depending on particular organizational industry structures in place, the nature of complexity of this automation varies significantly. At least three structures are of direct interest here:

- The partitioning of the large electric power grid is given a priori. The main problem here is to introduce an IT infrastructure in support of monitoring and control for providing pre-cursors of extreme conditions, and to adjust available resources so that the system is

adapting smoothly as the operating conditions and equipment status vary. The major portion in this chapter concerns this problem.

- A more futuristic problem of automation is the one in which the boundaries of sub-networks are allowed to evolve according to their distributed sub-objectives. The main problem here is to introduce an IT infrastructure for facilitating both distributed decision making by these sub-networks and, at the same time, provide dynamic coupling with the other sub-networks so that performance objectives are met at several higher layers of the industry organization.
- Finally, the most complex problem of automation is the one in which economic and regulatory and organizational signals are modeled as endogenous together with the physical and IT infrastructures. This is the problem of long-term evolution of the electric power grid as driven by regulatory, economic, and technological signals. The IT infrastructure here, in contrast with the previous two, is heterogeneous and spans broad range of time horizons and system details.

The starting issue for all three cases is the fact that the overall network complexity is outside of human's ability to master at the right time and the right level of detail necessary for best decision making. The boundaries between automation and human decision making are different in the three cases above. In this chapter we conceptualize an approach to the IT infrastructure for the first case. In our view, this automation for enhanced performance over a broad range of supply/demand patterns and equipment status is critical for avoiding unexpected system-wide failures such as the August 14, 2003 Northeast US blackout. In the last part of this chapter we provide ideas for extending our proposed approach to the other two cases.

In this chapter we explore fundamentals of possible next generation automation for managing electric power systems over a broad range of demand/supply and equipment status. The approach builds upon today's operating practices by conceptualizing sufficiently adaptive models with respect to time and space needed to capture relevant phenomena even when critical assumptions under which today's control is designed fail to hold. These models are grouped according to: (1) the type of operating problems they capture; and (2) rigorous temporal- and spatial-model reductions of the initially very large models for quasi-stationary estimation of the changing conditions and for the regulation of the set-points of all available controllers according to the information provided through the estimation. Based on these models, a multi-layered multi-rate IT infrastructure is proposed in support of protocols for (1) auto-

mated estimation of on-going changes in operating ranges and equipment status using carefully placed sensors and communications equipment; (2) automated multi-layered communication of state-estimation results to the controllers; and (3) automated control logic adjustments based on the provided information. A multi-layered modeling, estimation and control approach proposed lends itself to choosing the type of data to be measured, rate at which the information needs to be processed and locations for measurements. At present there is no systematic methodology for this purpose. The operators do not know what is happening and are not able to make informed decisions when the system finds itself outside the operating ranges previously simulated and/or experienced.

This chapter is organized as follows. In Section 2 we briefly review today's hierarchical control and critical assumptions. We identify the challenges in this design when these critical assumptions do not hold. To suggest how one might go about relaxing these critical assumptions, we take a step back in Sections 3 and 4 to review the basic structure of the electric power system dynamics. Based on this review, we introduce in Section 5 a conceptual flow chart for model simplifications when the system conditions vary significantly. It is suggested that it is possible to develop a family of models whose granularity varies with space and time, and which can be used according to the systematic logic in a proposed flowchart for monitoring the system and controlling reliably and efficiently over a very broad range of conditions. In the remainder of this chapter major components of the flow-chart underlying the multi-layered estimation and control are described in some detail. Finally, in Section 7, ideas for further extensions of the proposed approach to model, estimate, and regulate dynamics of non-technical signals are briefly outlined.

## 2. Electric Power Grids as Complex Network Systems

We begin by emphasizing the network system nature of electric power grids. Inputs into these network systems are the demand and supply at the nodes. These inputs are served by a vast, complex network that enables the delivery of supply and demand among users and suppliers. The delivery is in terms of power flowing through the network branches. The flows are, in turn, subject to the network constraints.

While the electric power grids generally provide reliable and high quality of electricity service to the end users, the system from time to time experiences extreme stress and blacks out. It was recognized several decades ago that in order to avoid such blackouts more coordination

and on-line monitoring would be needed. Consequently, the field of electric power systems engineering (EPSE) has emerged [1]. The industry has established control centers, each utility and/or a pool of utilities has these, and they support today's hierarchical monitoring and control of the grid. More recently, there has been an additional trend to operate the system outside the ranges for which the network was designed as a result of increased tendencies to purchase the least expensive power. Competitive provision of electricity has in effect revived the technical question concerning optimization for efficiency in using available resources to supply customers. We show in what follows how our proposed automation would help optimize system-wide resources through on-line control and get away with all together less expensive stand-by capacity.

However, while particular elements of the needed automation are known and have been implemented, there have been no systematic frameworks for ensuring a pre-specified performance in the complex network systems of interest here. This situation is a result of many factors, including: (1) the evolution and operation of these systems; (2) an overwhelming complexity of the problem as a whole; (3) historical lack of fast reliable monitoring and critical information collection programs, as well as a lack of communications, control, and computer methods for systems of this complexity; and (4) lack of financial incentives to encourage investments in their computer-aided on-line management. The important consequence of this situation is that these real-life networks require systematic integration of monitoring, computing, and control for improved performance. Without such integration, which would facilitate timely use of on-line critical information, managing these systems is simply too complex and leads to complex operating failures, such as blackouts in electric power grids. While specific technologies are beginning to be available for effective on-line gathering of real-time data in such systems and the case for their use is being made [2], it remains critically important to develop methodologies for differentiating between the information necessary to make decisions in order to prevent undesired performance, on one side, and excessive data gathering, on the other. Such methodologies are not available at present, and this creates a major obstacle to enhancing the performance of electric power grids.

## 2.1 Assumptions underlying today's operation of hierarchical systems

Complex power grids are currently operated as hierarchical systems under strong assumptions concerning temporal and spatial separation. Both temporal and spatial simplifications are fundamentally based on

weak interconnections between the sub-networks potentially achieved through the network design. Consequently, the supporting models for sub-networks and the network as a whole exhibit general properties of monotone dynamic systems [3]. At the equilibrium, monotone systems decrease the magnitude of their state response when the magnitude of the disturbance increases. For example, when electric demand increases, voltage decreases. This must be accounted for when designing the controllers. Controllers then need to have gains that decrease the demand in order to bring voltage up. Temporal separation in hierarchical network systems is further induced by: (1) the operation of *fast* controllers to stabilize the system dynamics by controlling the local outputs of the individual components; and (2) *slower* adjustments of the setpoints of these controllers for each sub-network to achieve stationary performance. Further adjustments of the stationary interactions between the sub-networks are made through off-line agreements and with no on-line information about the equipment status outside one's own sub-network [3].

The class of monotone systems lends itself to many convenient simplifications of the monitoring and control logic, as well as to the supporting computer algorithms. To start with, monotone systems are effectively controlled in a distributed way, because the effects of each disturbance can be compensated locally for the operating conditions for which the network design is done [4]. In addition, no qualitative change in their logic is needed to ensure stabilization as the operating conditions vary, as long as their system response remains monotone. That is, as long as a linearized matrix of such system preserves the Metzler-matrix properties over the range of operating conditions of interest, at least the sign in the controllers' logic is correct, and the system is stabilizable without requiring fast communications between the components. The same properties favorable to decentralized regulation are seen in the models characterizing equilibria of monotone electric power network systems [5, 6].

This property of localized response to the inputs/disturbances of both the dynamic responses of these systems and their equilibria has served as the basis for: (1) decomposition of the system as a whole into sub-networks; (2) decomposition of the sub-networks for slow regulation; and (3) fast stabilization of the local primary controllers on the individual equipment components. Much of the state-of-the-art theoretical work for large-scale network systems relies on this property. In linear control theory, the monotone network property is known as the block-diagonal dominance property of the system matrix or as the property of weak interconnections between the sub-networks. Fundamentally, this is the same property which allows for: (1) robust decentralized sta-

bilization; (2) aggregation into sub-systems; and (3) their decentralized control without requiring system-wide top-down coordination. Similarly, computer algorithms for decomposing the network into sub-networks for parallel computing are based on the same property; more recently, the ideas of amorphous computing have drawn on the same property.

## 2.2 Implications of violating monotone response

As the electric power grids are operated away from the conditions for which they were initially designed, they may lose the properties of monotone networks. Consequently, the layered-managed system may fail to meet its objectives. The variations in system conditions are generally caused by both significant variations in operating conditions and/or by the major equipment failures. There is no black-and-white line between the effects of these two, i.e., one cannot say that the system remains monotone for any changes in operating conditions as long as there is no topological change in the network caused by the equipment failures, and, vice-versa, that any topological change would cause violations of system properties favorable to its decomposition. As a matter of fact, it is well documented that often qualitative changes occur as the controllers reach their limits and the degree of controllability gets lost [7]. It is plausible that similar problems may take place if a critical measurement becomes unavailable, and the system is less observable.

Independent of the actual root causes of such changes in qualitative response of an electric power system, when weak interconnection conditions generally cease to hold, the hierarchical decomposition-based operation may result in very unpredictable events. It is our conjecture that this was the case during the August 2003 blackout. The current approach is to rely on complicated off-line simulations of similar scenarios and to use these to assist human operators with the decision making under such conditions. These off-line studies are very time-consuming and are done for pre-screened most-critical equipment failures. This preventive approach requires expensive stand-by reserves that, no matter how large, do not ensure guaranteed performance [8, 9, 10].

## 2.3 The major challenge: monitoring and control outside monotone response system conditions

Based on the above discussion, we conjecture that electric power networks require major enhancements for more accurate and transparent monitoring and for the use of this information for adjusting controllers. The enhanced monitoring requires that the correct options be exercised

relating to: (1) placement and choice of type of sensors; (2) information architectures; and (3) on-line communications technologies. These will provide timely and easy-to-process information to the controllers throughout the system and to the human operators. Within a complex infrastructure, an enhanced dynamic and adaptive decision making framework is also needed, which is capable of responding to the available measurements over the wide range of input/disturbance conditions and to potential topological changes. None of the changes are straightforward to predict, and it is, therefore, necessary to rely on feedback-based automation. A particular question is how to accommodate distributed decision making within a typically multi-layered IT infrastructure in an on-line manner, with minimal coordination of various layers, while ensuring desired performance for the system as a whole, for its sub-networks and for the individual components. The fundamental challenge then becomes one of developing an IT framework to support the operation of a complex infrastructure in a seamless way over a wide range of operating conditions. Of particular interest are extensions of current hierarchical system concepts to relax the assumption concerning weak coupling. It is suggested in this chapter that the very need to relax this assumption requires more complex IT architectures in which physical and IT signals do not necessarily map in a direct way.

### **3. Current Operating Practice: Problems and Open Questions**

The use of electric power network systems exhibiting monotone response has a far reaching impact on the actual near real-time management of electric power grids; it underlines much of current operating practices. The system operators keep routinely this characteristic in mind in their decision-making [11]. Assuming stable operation, the system is stabilized by means of fast, local primary controllers. These eliminate the need for near real-time, split-millisecond communications. On the other hand, the setpoints on some of these primary controllers are slowly adjusted by the sub-networks in an automated way based on few slow output variables within the sub-networks themselves. Finally, the flow exchanges between the sub-networks are generally not coordinated; this does not deteriorate the quality of the system response significantly as long as the basic nature of *monotone* response is preserved.

Complex electric power networks are operated as hierarchical systems under strong assumptions concerning temporal and spatial separation. The highest layer is managed in a feed-forward way. The lower levels are automated, but the controllers are not adjusted as the inputs and

disturbances vary over broad ranges. Theoretical justification for the spatial separation has its roots in the general localized response property and block-diagonal dominance.

### 3.1 Historic problems of operating under stress

Disturbances have major effects at the location where they occur, and dissipate with the spatial distance. This is an implied assumption that when violated, creates a real challenge to the entire hierarchical concept [12, 7, 13]. A long history of sporadic blackouts in the electric power grids has indicated the following fundamental characteristics:

- The system response to disturbances was not localized; instead, a sequence of cascading events contributed to the ultimate failure of major portions of the backbone grid.
- The constant-gain primary controllers were generally inadequate during the blackout conditions when the system departed from its monotone response characteristic; these controllers contributed in a major way to the overall system failure [14].
- Actions by the system operators during the blackout were largely inadequate because the system response exhibited a qualitatively different response than expected by the operators; for example, reduction in demand contributed to further reduction in voltage, contrary to the the operators' experience.
- Finally, a typical sequence of cascading events was characterized by a gradually deteriorating slow response over several hours [2]. This is again contrary to the common thinking that blackouts take place extremely fast.

A close look into the sequence of events preceding the actual blackout shows that: (1) slow system input variations from those assumed were not monitored or used for re-scheduling other resources; (2) several discrete events, related to changes in network topology (consecutive failures of three transmission lines, i.e., network branches), over the range of 2-3 hours were not identified before it was too late and went largely undetected; and (3) the primary controllers and protective devices did not adjust their control logic to drastically different conditions, and were, therefore, ineffective in preventing the grid from complete destabilization [8, 9, 10].

An important aspect of the electric power grid blackout is the fact that the inability to detect topological failures and to correct for their effects was a combination of: (1) inadequate control logic [14]; (2) lack

of critical measurements [22]; and (3) malfunctioning sensors, and computer system software and hardware. This scenario clearly points into the need for comprehensive approaches in which sensors, control, on-line measurements, and computer logic supporting on-line decisions interact to provide a required performance. Moreover, the approach must be capable of accounting for failures of any of these sub-functions, and therefore, be robust with respect to logic, measurement, and real-time signal failures.

### **3.2 Some possible solutions and their shortcomings**

One of the main proposals for enhancing operation of network infrastructures under stress is redundancy-based, achieved by installing more resources and by building stronger network interconnections. However, this solution is very expensive. A more systematic design is needed to provide capacity at the points in the system that are most vulnerable. One must also recognize that equipment failures are state dependent and that simple redundancy will not ensure reliable service.

The other approach under consideration is to effectively reduce quality of service (QoS) by means of a more aggressive demand re-scheduling when there is not enough supply and/or network capacity to serve the entire forecasted load. While some of the experiments of this type are on-going, the amount of demand reduction needed to save the system under emergencies may not be socially acceptable. Most important, the demand scheduling should be done at the places where its effects on system-wide reliability are minimized. This, in turn, requires the careful combination of: (1) off-line probabilistic sensitivity studies; and (2) on-line monitoring and decision making techniques of the type that are currently not available.

Finally, there have been proposals for processing more information to support appropriate control actions [2]. Sample measurements in recent work following the electric power grid blackout show that warning signs of abnormal operation existed much before the system entered the time-critical situation [2]. However, in order for these measurement technologies to be cost effective and useful to the operators as difficult conditions evolve, much needs to be done toward selecting the best locations for such measurements, and for their on-line use for decision making. An aggressive monitoring everywhere within the complex system would not do much good, because, among other problems, one would quickly run into the challenge of huge data management.

#### 4. Multi-Layered Modeling, Estimation and Control Approach to Managing Electric Power Networks Over Broad Ranges of Operating Conditions

In this section we introduce fundamental modeling for managing complex electric power networks over broad ranges of operating conditions and equipment status. Our modeling is structure-based, and it represents an outgrowth of our structure-based modeling initially developed for the enhanced operation of the electric power grids [12, 13]. Moreover, our modeling approach builds upon existing hierarchical models by explicitly relaxing the conditions of *monotone* response. The monotone response conditions are conceptually relaxed in two steps: (1) by enhancing the logic of the local equipment controllers [15, 16] to ensure stabilization over broad ranges of quasi-stationary conditions; and (2) by adaptively changing on-line the settings of the equipment controllers, in order to re-direct the existing resources as the operating conditions vary outside the acceptable ranges. A version of this two-level approach (adjusting the setpoints on-line and better logic in fast equipment controllers) has been shown to contribute to significant enhancements of the electric power grid under major equipment failures [17]. Particularly important for developing structure-based protocols is the fact that closed-loop dynamics with the enhanced local controllers are fully decoupled from the rest of the system—i.e., we have complex dynamics with non-interacting control [19]. We make sure that, because the basic monotonic system assumptions are generally true, there is no need to fully re-work the existing architecture currently used during normal conditions. In the next section, we provide detailed modeling ideas.

The concepts proposed in this section are fairly complex. In order to avoid confusion, we have attempted to pose current control practices and our proposed approach to monitoring and control of electric power networks using systems control language. We believe that this helps to identify fundamental problems and would open doors to more systematic future research and very much needed technology transfer.

In what follows, we briefly review the system dynamics of interest. This is followed by posing the system stabilization and optimization problem building upon the current operating practices and identifying fundamental improvements needed for enhancing its performance.

## 4.1 Full non-linear dynamics of electric power systems

A very complex electric power network system is generally represented as a set of differential algebraic equations (DAEs)[20]. The dynamics of its components connected to the nodes in the network with the primary (local) controllers at individual components, subject to network constraints generally results in a very high order of algebraically coupled differential algebraic equations of the following form:

$$\dot{x}_N = f_N(x_N, u_N, y, d_N, \Pi_N), \quad x(o) = x_0 \quad (6.1)$$

$$0 = f_B(x_N, x_B, u_B, y, d_B, \Pi_B) \quad (6.2)$$

where  $x_N$ ,  $u_N$ ,  $w_N$ ,  $\Pi_N$ , and  $f_N$  represent the state variables, primary control, disturbances, parameters, and dynamics associated with each node (N) in a network-type system, and  $y$ ,  $x_B$ ,  $u_B$ ,  $d_B$ ,  $\Pi_B$ , and  $f_B$  represent the flows, states, control, disturbances, parameters, and flow-type constraints for all branches (B) in this network. Depending on the level of details, the primary (node and branch) controllers in place, and the types of disturbances considered, the specifics of model (6.1)-(6.2) vary. The dynamics of this type have been the subject of much investigation by many researchers. Many difficult phenomena including bifurcations related to non-existence of the solution to the algebraic constraints (6.2) and the instabilities of the system dynamics (6.1), have been studied. Also, methods of finding equivalent system dynamics in complex systems using coherency- and synchrony-properties have been explored for overcoming the overall complexity of these systems. Much progress has been made in this direction. These questions have been a subject of research over several decades; no literature survey on this subject is provided in this chapter, see [7].

To introduce the structural properties of interest, express flow variables  $y$  in (6.2) in terms of  $x_N$ ,  $u_B$ ,  $d_B$  and  $\Pi_B$ .<sup>1</sup> Consolidate next the nodal and branch variables into single vectors

$$\underline{x} = \begin{bmatrix} x_N \\ x_B \end{bmatrix}, \quad \underline{u} = \begin{bmatrix} u_N \\ u_B \end{bmatrix}, \quad \underline{d} = \begin{bmatrix} d_N \\ d_B \end{bmatrix}, \quad \underline{\Pi} = \begin{bmatrix} \Pi_N \\ \Pi_B \end{bmatrix}$$

Using this notation, system (6.1)-(6.2) takes on the form

$$\dot{\underline{x}} = \underline{F}(\underline{x}, \underline{u}, \underline{d}, \underline{\Pi}) \quad (6.3)$$

<sup>1</sup>The most difficult challenge arises when the system is almost at the point at which the function  $f_B$  is not invertible (point of singular bifurcation). For this situation carefully designed techniques can be used in order to ensure that the system is stabilizable. A primary controller of this type would ensure that the system-wide dynamics are stabilizable.

This non-linear system can be further thought of as a generalized linearized system over the family of operating conditions of interest, i.e.,

$$\dot{\underline{x}} = A\underline{x} + B\underline{u} + M\underline{d} + N\Pi \quad (6.4)$$

## 4.2 Disturbance- and control-driven multi-layered models

As the operating conditions and the equipment status vary, the properties of the system matrices  $A$ ,  $B$ ,  $M$ , and  $N$  vary. These variations are not critical as long as their basic characteristics such as stabilizability, controllability, and observability do not change.

In order to more specifically define multi-layered models of interest we recall that the system defined in the model (6.3) above constantly varies in response to both its disturbances  $d$  and in response to discrete-event changes in its parameter  $\Pi$ . The multi-temporal separation of the complex dynamics measured in real-life electric power grids is a result of the multi-periodic as well as random disturbances. The major unexpected deviations are generally caused by the unplanned parameter changes.

The total demand at each node  $j$  in the power grid can be expressed as [12, 22]

$$d_j(t) = \hat{d}_j + \tilde{d}_j \quad (6.5)$$

where  $\hat{d}(t)$  represents the predictable component of the actual demand and  $\tilde{d}(t)$  represents the fast deviations around the predictable component. For purposes of relating our approach to today's operating practices, we further decompose the predictable demand component  $\hat{d}_j$  as

$$\hat{d}_j(t) = \hat{D}_j[KT] + \hat{D}_j[KhT] \quad (6.6)$$

where  $\hat{D}_j[KT]$  and  $\hat{D}_j[KhT]$  are demand variations at node  $j$  for each 5-15 minutes and each hour, respectively. Similarly, the unpredictable component of demand deviations  $\tilde{d}_j$  is further decomposable into truly dynamic, fast fluctuations  $\tilde{d}_j[kt_p]$  and the quasi-stationary deviations evolving on a minute-by-minute basis  $\tilde{d}_j[kT_s]$ , i.e.,

$$\tilde{d}_j = \tilde{d}_j[kt_p] + \tilde{d}_j[kT_s] \quad (6.7)$$

Similarly, the major equipment status can be represented as a set of parameters characterizing the status of each piece of equipment connected to node  $i$  as  $\Pi_i$ , where  $\Pi_i = 1$  if the component is connected to the system and  $\Pi_i = 0$  if the component has failed. Similarly, if a transmission line connected between nodes  $i$  and  $j$  is characterized by

its parameter  $\Pi_{ij}$  so that  $\Pi_{ij} = 1$  if the line is connected and  $\Pi_{ij} = 0$  if the line is disconnected. It is further possible to differentiate between planned (predictable) equipment failures  $\hat{\Pi}_i$  and/or  $\hat{\Pi}_{ij}$  and hard-to-predict, low probability rare-event-type equipment failures  $\tilde{\Pi}_i$  and/or  $\tilde{\Pi}_{ij}$ . The envisioned automation using these models is based on a multi-rate sampling ranging from near real-time [ $kt_p$ ], second-by-second [ $kT_s$ ], minute-by-minute [ $KT$ ], to hour-by-hour [ $K_hT$ ].

Our multi-layered approach is based on the idea to ensure that local and/or sub-network layers are stabilizable by means of control. Once this is ensured, the higher-layers (sub-networks, the entire network) are regulated by changing the setpoints of their controllers at the slower rates with a well-defined control objective at each layer. The fastest transients are hard to monitor and control through on-line coordination. Reasons for this are many, but in particular it is extremely hard to process split-second system-wide information when the system is already unstable or very close to its stability boundary. The idea in this approach is, instead, to develop a framework for on-line monitoring of sequences of equilibria driven by relatively slow variations in system inputs and disturbances, and to perform quasi-stationary state estimation for detecting discrete events  $\hat{\Pi}[KT]$  and  $\hat{\Pi}[K_hT]$ . This information will be used to implement slow corrective actions which shape this quasi-stationary process according to well-understood performance objectives. Among others, one of the results of this is keeping the system away from the stability boundaries, beyond which it is effectively impossible to stabilize the system.

Assuming that the system-wide dynamics are stabilizable locally over a wide range of changes enables us to introduce a well-defined notion of a quasi-stationary model. This is done in the next subsection.

### 4.3 A large-scale quasi-stationary model

Consider next a sequence of equilibria of the complex network system whose dynamics are given in (6.1)-(6.2). This model is simply obtained by assuming that transients between equilibria are stabilizable, therefore  $\dot{x} = 0$  in model (6.4). A quasi-stationary model representing sequence of equilibria sampled each  $T$  interval is obtained by: (1) using model (6.4) to express the states at a sampling time [ $nT$ ] as a function of disturbances and inputs at the same sampling time [ $nT$ ]; (ii) expressing the states at the next sampling time [ $(n+1)T$ ] as a function of disturbances and inputs at the next sampling time [ $(n + 1)T$ ]; and (iii) subtracting these two equilibria relations. Applying this process to model (6.4) after taking

$\dot{\underline{x}} = 0$ , one obtains

$$\begin{aligned} \underline{0} &= A\underline{x}_n + B\underline{u}_n + M\underline{d}_n + N\underline{\Pi}_n \\ \underline{0} &= A\underline{x}_{n+1} + B\underline{u}_{n+1} + M\underline{w}_{n+1} + N\underline{\Pi}_{n+1} \end{aligned} \quad (6.8)$$

Solving further for  $\underline{x}_n$  and  $\underline{x}_{n+1}$ , respectively, and subtracting the two expressions results in a full-order model which defines a sequence of state equilibria as affected by the input and disturbance increments  $\Delta\underline{u}_n = \underline{u}_{n+1} - \underline{u}_n$  and  $\Delta\underline{d}_n = \underline{d}_{n+1} - \underline{d}_n$ , respectively, and parameter increments  $\Delta\underline{\Pi}_n = \underline{\Pi}_{n+1} - \underline{\Pi}_n$ . The resulting model takes on the form

$$\underline{x}_{n+1} = \underline{x}_n - A^{-1}B\Delta\underline{u}_n - A^{-1}M\Delta\underline{d}_n - A^{-1}N\Delta\underline{\Pi}_n \quad (6.9)$$

Quasi-stationary models of this type were used in [22] to model hierarchically decomposed demand balancing in large-scale electric power grids, and have led to some of the state-of-art voltage control implementations in the French electric power grid. Here we will use these models as the starting models for system monitoring over broad ranges of operating conditions. The corresponding output variables (measurements) of interest are expressed as<sup>2</sup>

$$\underline{m}_{n+1} = K\underline{x}_{n+1} + L\underline{u}_{n+1} + Q\underline{d}_{n+1} + F\underline{\Pi}_{n+1} \quad (6.10)$$

#### 4.4 Multi-layered system constraints

The dynamics described in the previous section are a result of the *unconstrained* system response to a variety of disturbances and local controllers<sup>3</sup>. The basic objective of monitoring and controlling system dynamics is to ensure that the system is stabilizable within constraints imposed on both the control and output/state variables. Defining control constraints is fairly straightforward. However, defining meaningful constraints on the output/state variables is conceptually a challenging task. A meaningful set of constraints is the one which ensures pre-specified performance with respect to both system reliability and efficiency. A basic lack of understanding of observability for candidate output variables in electric power systems has a direct practical implication of not

<sup>2</sup>Throughout this chapter notations for outputs  $y$  and  $m$  are used interchangeably; initially the only output variable referred to was line flow  $y$ . However, the concepts extend to all relevant outputs/measurements  $m$ .

<sup>3</sup>We recognize that not every node is equipped with fast controllers. One of the important questions is how to aggregate a large network in order to get away with fewer measurements/outputs when designing stabilizing control. Very little is known on this subject. As an aggressive campaign is set in place for on-line monitoring and wide area measurements, more research must be done to decide on the most critical measurements in order to ensure system-wide stabilization.

knowing what is critical to measure for what purpose. This, further, raises the question of the basic rationale for defining constraints on the output/state variables. At least in principle, these constraints are three-fold, namely:

- They are caused by the need to ensure that the individual equipment components are operated within the manufacturer specifications (turbine blades are not spun faster than specified; currents do not exceed design limits, etc).
- The quality of service (QoS) in terms of frequency and voltage deviations and the rate of interruptions is met.
- Finally, the system as a whole is robust with respect to both small disturbances as well as with respect to major equipment failures. Robustness has traditionally been measured in the electric power networks in terms of steady-state, small-signal, and transient stability [7].

Depending on the system design and the range of operating conditions over which it is operated, the most critical constraints could be one of the above. If the limiting constraints are determined by the limitation of the system as a whole, it is very difficult to compute these constraints once and for all. Current industry practices have been to re-compute the output limits for what is believed to be the worst conditions in terms of demand and equipment status. Moreover, the basic approach has been preventive, so that enough control capacity is kept in a stand-by mode in case one of the worst-case events takes place so that the customers are not interrupted. It is important to notice that these computations do not rely on real-time corrective actions and feedback. Unfortunately, as the system is beginning to be operated in ranges previously not experienced nor studied, it becomes impossible to understand the worst case scenario and to actually pre-plan for guaranteed performance. Moreover, the preventive planning approach is also one of the major causes of inefficiencies. Our proposed approach introduces basic logic for updating the output constraints.

In what follows it is assumed that the state/output constraints are updated in a quasi-stationary way, i.e.  $\underline{y}^{\min}[K_h]$ ,  $\underline{y}^{\max}[K_h]$ ,  $\underline{y}^{\min}[K]$ , and  $\underline{y}^{\max}[K]$ , are updated on-line in order to ensure reliable control without any of the system-wide constraints being violated.

## 5. Multi-Layered Estimation and Control

Because it is impossible to predict well for rare events, one must rely on estimation of operating ranges and corrective feedback at the right

sampling rate; steady-state problems during which system dynamics are not critical are corrected for at a slower rate than situations which need extremely fast stabilization. In what follows we describe such a multi-layered approach to estimation and control using multi-layered modeling from the previous section. These models can be used to support measurement, estimation, and control protocols for flexible system operation. Particular emphasis is on the quasi-stationary monitoring and control needed to adjust setpoints of local controllers. The basic information flow in such multi-layered estimation and control IT infrastructure is shown in the flowchart in Figure 6.1 (which will be referred to as Flowchart 6.1 hereafter).

The fundamental need for a quasi-stationary estimator comes from the fact that currently used estimators for fault detection in large-scale network systems are based on strictly static information, and do not exploit slow trends in system conditions observable during blackouts as documented in [2]. True dynamic observers, on the other hand, would require fast communications over vast spatial distances [23, 24, 25, 26]. Future work on estimating time-critical changes may be based on the recent ideas in [27].

The basic idea is to:

- Introduce state estimators which detect qualitative changes in quasi-stationary operating conditions.
- Use this information to adjust local control logic of fast continuous controllers on various pieces of controllable equipment to ensure that they stabilize the system-wide fast dynamics over a broad range of changes in power demand and equipment conditions.
- Use this information to adjust the logic of re-setting the setpoints of discrete-type controllers and/or setpoints of the continuous controllers.

This approach then leads to a multi-layered approach to monitoring and controlling complex power network, which is systems engineering in its basic nature and it is characterized as follows:

- Formulate limits on control (actuators).
- Formulate bounds on disturbances (demand deviations and/or classes of equipment failures).
- Design a multi-rate state estimators for providing the information about the type of operating ranges for which the quasi-stationary control (scheduling) and stabilizing feedback are needed.

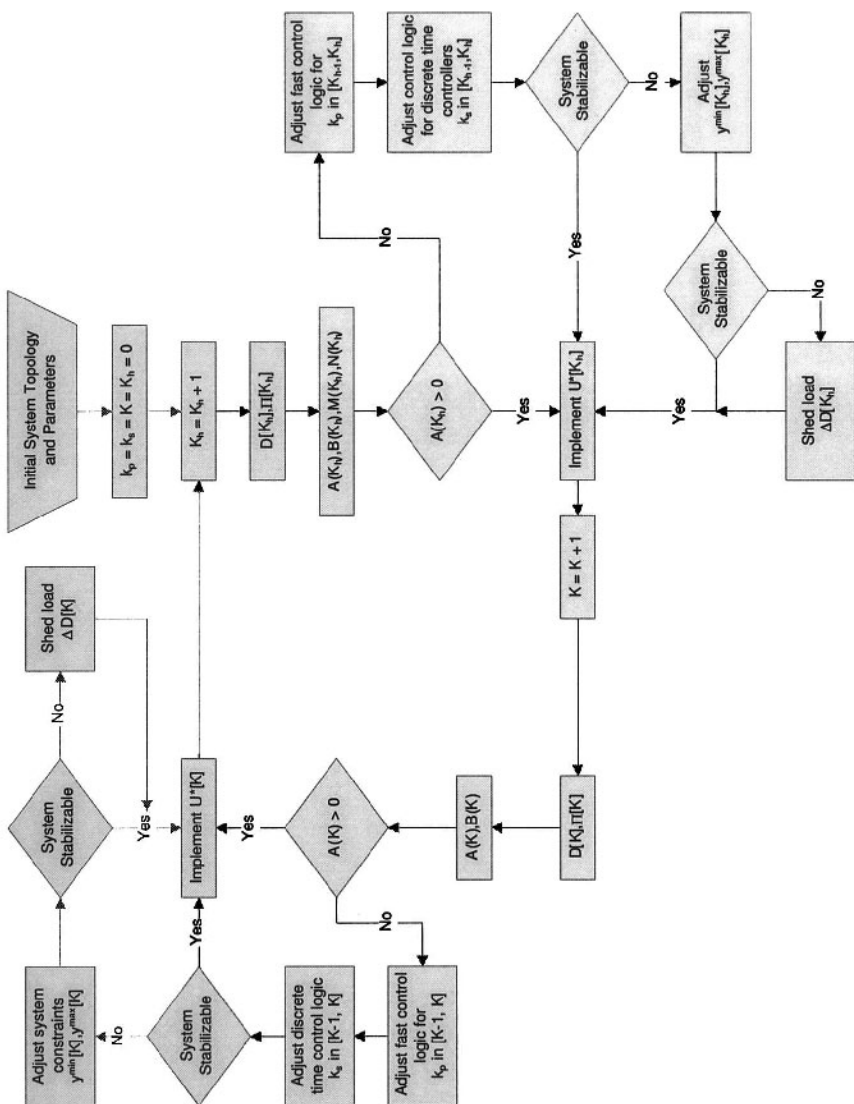


Figure 6.1. Basic IT infrastructure flow for multi-layered automated estimation and control

- Use the information from the state estimators to automate on-line corrective actions for optimizing the use of available controls.
- Use the information from the state estimators to adjust the control logic of the primary fast controllers on individual pieces of

equipment (power plants, transformers, and transmission lines in particular).

- Use the information from the state estimators to adjust the constraints on the output variables so that the system stabilization is ensured as the system is optimized in a quasi-stationary way.

Shown in Flowchart 6.1 is a possible IT infrastructure for automated on-line monitoring and control over broad ranges of changing conditions. The scheme is first initialized for time  $K_h = 0$ , then the clock is incremented each hour [ $K_h$ ] for optimal turning on/off available controllers (unit commitment (UC)) in order to meet an hourly demand  $\hat{D}[K_h]$  for given (estimated) system parameters for that hour  $\hat{\Pi}[K_h]$ . Based on these increments/changes, the system matrices are re-computed with the new data, and the positive definiteness of system matrix  $A[K_h]$  is assessed. Depending on the result, automated UC is performed to compute the optimal on/off status of controllers, with or without changing the logic of fast controllers. Furthermore, if the system is not stabilizable for the given controls and output constraints, either these constraints get further adjusted or partial load is shed. Observe that fast control, both continuous and discrete-time, serve the same purpose as today. The only difference is that their control logic is adjusted on an hourly basis as the UC is computed. This is critical in order to ensure stabilizability over the broad range of conditions. Also, notice that both unit commitment (hourly base) and security constrained economic dispatch (15 minutes, or so) are automated taking into consideration quasi-stationary system model. Quasi-stationary estimators estimate parameters  $\Pi[K_h]$  and hourly demand variations  $\hat{D}[K_h]$ , and check potential abnormalities in system matrices,  $A[K_h]$  in particular. This information is actively used for adjusting the logic of faster controllers. Similar automated actions are repeated on a shorter time-scale [ $K$ ].

## 5.1 Quasi-stationary state estimators

The key concept to making large-scale systems adaptive over a wide range of conditions hinges on the ability to extract critical timely information out of a huge amount of data monitored. State estimators currently used to detect discrete-event type failures are ineffective in assisting the system under stress for several reasons. To start with, they can at best be used to advise a human operator of the nature and location of fault, so he can draw on his expert knowledge and base follow-up actions on the earlier off-line simulations closest to the situation at hand. Today's state estimators do not generate information relevant

for quickly recognizing the need for communication beyond control area boundaries and for adjustments of decision making by the control areas in response to the situation at hand. They are not used to change the settings nor the logic of primary controllers. What is needed, instead, are estimators capable of identifying qualitative changes in operating conditions and/or fault occurrence that requires adjustments in information processing, control logic and coordination beyond hierarchical decomposition. It is worthwhile attempting the design of estimators based on key measurements to reduce both the complexity and cost of their deployment.

Our basic approach to developing effective quasi-stationary estimators uses the quasi-stationary models derived above, at the right time scale. For example, unit commitment and security constrained economic dispatch would need data at the hourly and 5-15 minute time scales  $[K_h]$  and  $[K]$ , respectively, and the corresponding models to be used for quasi-stationary estimation take on the following general form:

$$\begin{aligned} \underline{x}[K_h + 1] = & \underline{x}[K_h] - A^{-1}([K_h])B([K_h])\Delta\underline{u}[K_h] \\ & - A^{-1}([K_h])M([K_h])\Delta\underline{d}[K_h] \\ & - A^{-1}([K_h])F([K_h])\Delta\underline{\Pi}[K_h] \end{aligned} \quad (6.11)$$

and the sufficiently rich model for detecting topological changes as

$$\begin{aligned} \underline{x}[K + 1] = & \underline{x}[K] - A^{-1}([K])B([K])\Delta\underline{u}[K] \\ & - A^{-1}([K])M([K])\Delta\underline{d}[K] \\ & - A^{-1}([K])F([K])\Delta\underline{\Pi}[K] \end{aligned} \quad (6.12)$$

The static state-estimator introduced many years ago by the late Fred Schweppe represents the heart of SCADA in modern day utility control centers. It is based on highly redundant flow measurements in all branches of the very large-scale model (6.1)-(6.2) at equilibrium (single snap shot) and the comparison of the estimated model variables (power inputs) with those measured. If the discrepancy is beyond an acceptable threshold, a fault has occurred. Observe, however, that this state estimator is hard to use because (1) it does not relate prior measurements  $[(n-2)T], [(n-1)T]$ , etc., to the current measurements  $[nT]$ , and (2) it is of very high order, and therefore, too combinatorial to effectively detect the fault in a timely manner. What is needed, instead, is a quasi-stationary estimator which overcomes both of these problems and would make the fault identification a more manageable problem. The estimators of interest here are based on the models given in (6.11) and (6.14). Using model (6.14) one can combine techniques from observers [27] with recent work on system identification and state estimation for

hybrid systems [28, 29, 30] to develop a novel state estimator. It is important to recognize that discrete-time methods are directly applicable to the quasi-stationary models derived here.

**5.1.1 New quasi-stationary state estimator as the observability problem in hybrid systems.** The question of how to create a reduced-order model (6.14) that is sufficiently complex for identifying discrete events within this complex network system, while keeping complexity at a manageable level also could be posed as the problem of hybrid systems [31]. This then becomes effectively the problem of finding the minimal order model for a fully observable hybrid system. This model will then be used to implement a novel quasi-stationary state estimator (observer), based on well-defined measurements, to identify discrete events in near-real time. The state estimator then reports the discrete event to the family of nested models used for controlling the states within the cutsets and for coordinating their interactions. We close this section by re-iterating that the emphasis here is on quasi-stationary phenomena as directly motivated by the recent blackout of the US Northeast electric power grid in August 2003.

## 5.2 Multi-layered control approach

An important aspect of the multi-layered approach described in this chapter is the control logic and the type of information needed for the adaptive controllers to stabilize the largest range of disturbances within given control capacity limits necessary to:

- Regulate setpoints of the local controllers in a quasi-stationary way as the operating conditions vary.
- Provide information from the higher system layers to the local controllers concerning a *qualitative* change of the ranges of operating conditions for which the control logic of primary controllers must be adjusted.

An example of the basic multi-layered control idea in which the setpoint of the controllers is regulated from a higher layer and a highly nonlinear (feedback-linearizing, sliding mode) type primary controllers are stabilizing to the slower changing regulated setpoints of the same controllers can be found in [18, 17, 15, 16]. This idea underlies the fundamentals of a multi-layered adaptive control approach described here. In what follows, particular control blocks supporting multi-layered control shown in Flowchart 6.1 are described.

### 5.2.1 Adaptive control for stabilizing fast system dynamics.

The problem of fast stabilization of system dynamics in large electric power networks remains one of the most difficult challenges. The efforts have been somewhat sporadic over the years. Instead, major long-term efforts by the power systems community seem to have been targeted toward analyzing the dynamics in response to small deviations as well as during large equipment failures. Despite these efforts it remains very difficult to perform this analysis on-line because of complexity of the underlying dynamics. As a result, the area of dynamic security assessment is still a real challenge.

*The approach envisioned here is to, instead, simplify the problem through careful control design.* This is an extension of the hierarchical control in place today, but based on the recognition that as the operating conditions vary and technologies advance, the assumptions made must be relaxed and the control paradigms of complex electric power grids must evolve. Because of the time criticality, fast stabilization is critical in order to prevent the system from massive fast collapses. However, local stabilizing controllers must be designed with full awareness of the overall system conditions. In particular, it is possible to regulate the setpoints of these controllers so that the system as a whole can manage larger ranges of unpredictable demand deviations  $\tilde{d}$  and changes in the equipment status  $\tilde{\Pi}$ . The objective here is to automate slow system regulation, much the same way as this is being done in several European countries during normal operations. This multi-temporal automation needs to be done carefully when assumptions under which the design is done no longer hold. Much more information is needed in order to ensure robust performance. The ideas in this chapter can be interpreted in light of these extensions.

For example, one must identify the type of instability that is being controlled. In some sense the most difficult is the problem when (6.2) can not be solved for output variables in terms of states and control in order to transform the complex DAE model (6.1)-(6.2) into an ODE model (6.3). The stabilization control in the operating ranges close to the bifurcation points is a challenge in its own right. Generally in such situations one cannot rely on strictly local controllers and truly dynamic observers may be needed [23, 24].

In any other situations it is possible to start with a nonlinear model (6.3) and design fast primary controllers to guarantee system stabilization for a well-understood range of hard-to-predict fast disturbances  $\tilde{d}(t)$  within the given control capacity limits. There has been considerable effort toward such designs [21, 15, 17, 16, 18]. Most recently, an idea of designing an “all DC power system” by implementing nonlin-

ear primary controllers on transmission lines and various reactive power compensating devices has been introduced as a promise of making the analysis of such closed-loop electric power system fairly straightforward [32]. These ideas hold a tremendous promise for facilitating systematic robust multi-layered control of complex electric power systems as the cost of distributed controllers decreases.

### 5.2.2 Adaptive scheduling of discrete mechanical

**controllers.** The rate at which discrete mechanical controllers in electric power networks can be controlled generally falls somewhere in between the very fast power-electronically managed primary devices needed for fast dynamics stabilization on one side, and the rates at which setpoints of these fast controllers can be regulated using higher layer information on the other side. These controllers have been widely used and it is important to ensure that they are also managed systematically. In [14] the quasi-stationary changes of operating conditions driven by the unpredictable component of the demand variations on minute-by-minute basis are regulated by changing the settings on these mechanically-switched devices, and in particular on-load-tap-changing transformers (OLTCs). It is illustrated in [14] how a typical voltage collapse situation of the type experienced in early 1980 in France and Belgium due to “malfunctioning” of the OLTCs could be avoided by:(1) monitoring at the system level the nature of the operating region within which the OLTC is regulating load voltage, and (2) by using this information to reverse the control logic when the operating region is qualitatively different than during normal operation. In this work normal conditions are characterised by the system matrix relating slow changes in demand deviations and slow regulation of OLTC setpoints being a positive definite matrix, and therefore, a discrete-time model representing these slow variations being stabilizable. An extension of the ideas in [14] can be found in [33] which gives a sliding-mode type interpretation of OLTC control with the adaptive logic, based on a similar switching criterion as in the original work.

It can be seen from this previous work that one possible characterization of a qualitatively different range of operating conditions can be in terms of positive definiteness of the system matrix relating quasi-stationary regulation and disturbances evolving at the same rate. This is not to say that this is the only characterization, because these are only sufficient conditions for the multi-layered adjustments to work.

### 5.3 Automated short-term dispatch and unit commitment over broad ranges of conditions and equipment status

Assuming that fast primary controllers are sufficiently adaptive to stabilize system dynamics in response to unpredictable deviations in the demand  $\tilde{d}(t)$  and the rare equipment failures  $\tilde{\Pi}_i$  and/or  $\tilde{P}i_{ij}$  to the quasi-stationary states  $x[K_h]$  and outputs  $x[K]$  and  $y[K]$ , the objective of short-term quasi-stationary optimization is to:

- Turn on/off pieces of equipment (power plants, in particular) so that the number of available controllers is sufficient to supply the predictable component of demand  $\hat{d}(t)$ ,  $\hat{D}_i[K_h]$ .
- Optimize the amount of control needed to supply the demand component  $\hat{D}_i[K]$ .

The turning on/off in anticipation of longer-term predictable demand component  $\hat{D}_i[K_h]$  is done so that there is enough least expensive total control capacity to balance this demand component. This turning on and off of the available control capacity can be viewed as one type of (controlled) discrete events in an electric power grid. Once the total number of control units is turned on for the coming period  $[K_h]$ , this control capacity is scheduled so that the short-term performance criterion representing the total cost of quasi-stationary control is optimized, i.e.,

$$\min_{u[KT]} \Sigma_K J[KT] = \min_{u[KT]} \Sigma_K \Sigma_i c_i(u_i[KT]) \quad (6.13)$$

subject to the quasi-stationary system model (6.14), i.e.,

$$\begin{aligned} \underline{x}[(K+1)] &= \underline{x}[K] - A^{-1}([K])B([K])\Delta\underline{u}[K] \\ &\quad - A^{-1}([K])M([K])\Delta\underline{d}[K] \\ &\quad - A^{-1}([K])F([K])\Delta\underline{\Pi}[K] \end{aligned} \quad (6.14)$$

and subject to the output constraints, i.e.

$$y_j^{\min}[KT] \leq \hat{y}_j[KT] \leq y_j^{\max}[KT] \quad (6.15)$$

and

$$y_{ij}^{\min}[KT] \leq \hat{y}_{ij}[KT] \leq y_{ij}^{\max}[KT] \quad (6.16)$$

for the nodal output variables at each network node  $j$ ,  $\hat{y}_j[KT]$ , and through each branch  $\hat{y}_{ij}[KT]$  connecting nodes  $i$  and  $j$ , respectively.

As discussed earlier, determining meaningful constraints on the output variables  $y_j^{\min}$ ,  $y_j^{\max}$ ,  $y_{ij}^{\min}$ , and  $y_{ij}^{\max}$  for all nodes  $j$  and all branches  $ij$

in a large electric power network is a challenge in its own right. However, it is critically important to understand that the more accurately these limits are updated (with the objectives of making them non-conservative and reliable in the sense that they would ensure that the system is stabilizable and/or no physical damage is done to the equipment), the less conservative the short-term optimization is. If these limits are somewhat arbitrary, everything else will be arbitrary, no matter how accurate the numerical optimization algorithm for solving the problem (6.13)-(6.16) is. The proposed multi-layered approach is intended to get around this conceptual roadblock to achieve efficient usage of the available control by estimating these limits on-line. Yet, it is recognized that the shortest time-scale does not lend itself readily to the optimization, but only to stabilization.

## 5.4 Particular case: Today's hierarchical control

It is important to recognize that the envisioned approach is not very radical. It is, actually, a natural extension of today's hierarchical control, in which system stabilization is done by the fully decentralized fast controllers tuned to stabilize the local dynamics and a secondary-control area level automated control is a bit slower (such as automatic generation control (AGC) and automatic voltage control (AVC) [12, 22]) and it is intended to regulate control area frequency deviations and voltage deviations at the key (pilot point) loads back to the pre-scheduled levels which are done in a feed-forward manner.

However, there are several key distinctions from what is being proposed here. In particular, the control logic of the fast controllers is not being adjusted as system conditions deviate significantly from those at the planning stages, and therefore, cannot be assumed to be fully effective when the system is operated in unusual operating ranges, either because of the unusual supply/demand patterns and/or because of the large equipment failures. Moreover, the output constraints, in particular, are not being re-computed on-line at the required rate in order to ensure robust performance of the system as a whole and to make the most use out of the available control capacity.

As a result, today's hierarchical control of large-scale electric power systems is automated during what is referred to as a normal operating mode and is not intended for use when the system is undergoing extreme, often previously unexperienced stress, frequently referred to as the emergency mode or in extremis mode. The intent of the proposed approach is to make the monitoring and control of the system more automated and not to have to rely on a human expert during stress.

## 6. Structural Spatial Aggregation: Managing Large Network Complexity by Means of Systematic Estimation and Control

In addition to managing temporal complexity, a significant part of the ultimate quest for automation design lies in managing the spatial complexity of the electric power grid. In the regulated industry boundaries between various different entities such as utility companies and power pools, are pre-set and the spatial complexity is managed assuming that the interactions between these entities are relatively weak. The vast interconnected power grid has worked well without system-wide on-line coordination of these entities. Instead, each control area (utility, power pool) has implemented ingenuous means of balancing supply and demand in an entirely decentralized way on a minute-by-minute basis in response to demand fluctuations  $\tilde{d}[kT_s]$ , by means of AGC. Similarly, the individual pieces of equipment are protected for safety using relays, and/or have primary local controllers intended to stabilize fast dynamics of each control area during normal operation in response to the very fast deviations  $\tilde{d}(t)$ . Only very recently, as the use of the grid has extended beyond the objectives of each control area relying solely on its own resources to balance hard-to-predict demand deviations  $\tilde{d}$ , the real need for on-line coordination across multi-control areas is in sight [10].

The main objective of simplifications with respect to space is very similar as with respect to time. Assuming that the system is stabilizable using adaptive controllers described above, an IT framework is needed for on-line management of large-scale complex networks for guaranteed quasi-stationary performance. However, because of the inherently large interconnection, it is important to draw on unique structural characteristics of this class of network systems in order to reduce this complexity as well.

In what follows we briefly describe these structural characteristics and the basis for multi-layered spatial simplifications. We then explain how this overall concept can be incorporated in Flowchart 6.1 for simplifying quasi-stationary estimation and control of large electric power networks.

### 6.1 Quasi-stationary state estimators

High-order dynamical systems of the form (6.3) exhibit the following characteristics of fundamental interest here.

- Structural separation of slow and fast dynamics within a complex network

It is known that complex network systems generally lend themselves to the non-standard singularly perturbed form [21] given as

$$\epsilon \dot{\underline{x}} = A(\epsilon) \underline{x} \quad (6.17)$$

where  $0 \leq \epsilon \ll 1$ . This form supports a structural separation of the dynamic process in a complex network into slow and fast sub-processes, because  $A(0)$  is structurally (not numerically) always singular. This enables a sub-grouping of states into very fast sub-states internal to each sub-network, and sub-states defining slow(er) interactions between the sub-networks. These properties form the basis for defining so-called interaction variables between the sub-networks in [12, 13].

- (a) **Definition of interaction variables associated with a subnetwork cutset.** The interaction variables associated with any subnet of a complex network are a linear combination of state variables internal to the cutset defining the subnet, and remain constant whenever the subnet is disconnected from the rest of the network. They cannot be changed by control internal to the subnetwork. Their existence is a direct consequence of the structural singularity of matrix  $A(0)$  in the model (6.17) above.

We denote these interaction variables associated with each subnet  $R^i$  as  $\underline{z}^i$ . According to their definition above there exists a transformation  $C^i$ , which when applied to states inside the subnet,  $\underline{x}^i$  gives output variables  $z^i$  which remain constant, i.e.,

$$\underline{z}^i = C^i \underline{x}^i \quad (6.18)$$

For an example of a construction algorithm for transformation  $C^i$ , see [12, 13].

- (b) **Variables relevant for inter-control area interactions.** These interaction variables are the main representatives to be used for the aggregation of the inter-dependencies between the control areas. At the subnet level they are relevant for decentralized decision making between each control area and the neighboring control areas. At the system-wide level an IT layer model defining interdependencies of these variables is essential [22, 10].

- **Structure-based network response to system disturbances.** Yet another structural notion in complex network systems comes from the tri-diagonal structure of system matrix  $A$  in the model

(6.17) [5, 7]. It is straightforward to recognize this when the network nodes where the disturbance occurs is denoted as Tier I, nodes directly connected to Tier I nodes as Tier II, and so on, until all nodes in the network are visited. The tier-wise enumeration of nodes of the system matrix results in a tri-diagonal structure. This structure lend itself to proving localized response of the system to the disturbance as long as system matrix remains a Metzler matrix [3, 5]. Tracking its Metzler property will be a feature one can use to detect faults at subnetworks. One of the major challenges is development of fast algorithms for tracking how far the response propagates through the network when the matrix loses its Metzler conditions properties, while still relying on the tri-diagonal structure of the system matrix. The findings would form the basis for understanding the structure of fault effects when the system response ceases to be monotone. This is the major simplification when monitoring qualitative changes in system response according to Flowchart 6.1.

**6.1.1 Particular case: Today's hierarchical control in multi-control area interconnections.** Today's hierarchical control assumes separability among the control areas' dynamics during small disturbances  $\vec{d}$ . The settings are scheduled for power exchanges among the control areas in a cooperative way, so that good balance is reached between economic transfers during normal conditions and exchange of power for reliability during equipment failures.

**6.1.2 Open questions in today's multi-control area interconnections.** Both temporal and spatial separation are possible when the system as a whole has monotone response. Serious reliability problems have been known to take place when this property fails to hold [14, 8]. Therefore, further enhancements of today's operating practices are needed in order to automate coordination of several control areas within an electric power interconnection in order to have reliable operation during the large variation in demand and/or equipment status. Using structural characteristics for on-line assessment if the system is monotone or not, and depending on the outcome, switching to one or the other type of control (See Flowchart 6.1) would go a long way toward a multi-layered estimation and control, in which the models used are multi-layered themselves with respect to both time and space. One of the critical open questions is the development of the algorithms for monitoring monotone response characteristics of the entire interconnection using a minimal set of measurements. The set of measurements used

for this purpose would be needed to build so-called tertiary layer model (defining exchanges between the control areas) for minimal system-wide monitoring, estimation, and optimization. An example of such tertiary layer model for reactive power monitoring and control can be found in [22].

The net effect of decomposition is that the decentralized stabilization through primary controllers is generally sub-optimal with respect to (some norm measure of) control needed to meet the pre-specified performance for the range of given disturbances. Efficiency is attempted, instead, by each control area for feed-forward actions of pre-scheduling settings of these primary controllers in anticipation of changes in system inputs by performing static optimization. This is, furthermore, done for the assumed scheduled exchanges with the neighboring control areas, without any formal optimization of the overall system resources. In this sense, a typical complex network system operated hierarchically is sub-optimal, because more control resources (stand-by reserves) are needed in order to meet a pre-specified performance for the given range of changes in input conditions than if optimal scheduling of exchanges among the control areas themselves were carried out [34].

## 7. Conclusions and Open Questions

The approach in this chapter is motivated by our observation that the challenge of operating electric power networks outside the ranges in which they exhibit a monotone response is huge. The analysis is very difficult, because the required models are truly nonlinear. The main idea here is to suggest that one could get around this fundamentally difficult problem by means of carefully designed multi-rate state estimation and control. If carefully done, it would be possible to introduce methods which smoothly manage variations in operating conditions without having to rely excessively on human operators and large reserves. We explain how it is possible to have a sufficient set of measurements, which, if sensed and processed at the right sampling rate and at the right level of spatial detail, could provide the critical information to the automated controllers dispersed throughout the complex system to adjust their logic and operate the system as reliably as possible, without sacrificing efficiencies. This means moving from today's preventive practices, to the corrective, automated practices. The approach must be, however, carefully put in place in order not to make matters worse. A possible vision for such setup is offered in this chapter.

The objective is to provide sufficiently informative state estimators over a variety of time horizons concerning the *qualitative changes* of sys-

tem conditions; as the complex system undergoes these changes, right controllers (at the right system layer and at the right time) would change their logic to help out with the overall system conditions. Some examples of such logic adjustments are provided in context of control of the existing equipment in today's power networks.

Open research concerns extending the proposed multi-layered approach to estimation and control in large electric power systems so that economic and policy considerations are included. The motivation for this generalization is multi-fold. To start with, it is unrealistic to attempt the best technical solutions without consideration of their cost tradeoffs. The evolution of electric power grids is greatly determined by both physical and economic factors. Furthermore, as the electric power systems begin to re-organize, once single operating and design objective is unbundled into a set of often conflicting sub-objectives. One needs to compare (1) the effects of the distributed decision making by the sub-networks without any coordination (no coordinating IT layer) on the economic performance of the system as a whole, with (2) the system-wide performance in which the IT layer performs minimal coordination for optimizing system-wide resources subject to flow exchange constraints between the sub-networks. At least theoretically, the second solution would be more efficient, but the efficiency should account for the cost of coordination. These comparisons lend themselves well to widely open areas of decentralized optimization in complex network systems. However, in order to include economic and regulatory feedback one must extend the strictly technical state space to include economic and regulatory states. One can then pursue the proposed approach to this generalized state space, see [34]. The generalized models derived in [34] are potentially instrumental to capturing the interdependencies between the technical, economic, and policy states.

### Acknowledgments

The author greatly appreciates partial financial support for this work by the National Science Foundation under the Electric Power Network Efficiency and Security (EPNES) Program. Also several technical discussions with Professors Jose Moura and Bruce Krogh at the ECE Department at Carnegie Mellon University have been very helpful, and are greatly appreciated.

## References

- [1] M. Ilic and J. Zaborzsky. Electric Power Systems Engineering. In *Encyclopedia of Energy*, Academic Press, New York, 2004.
- [2] C. Wells and C. Russo. Analysis of East Coast Frequency Data August 14, 2003. January 9 presentation, Toronto, CA, <http://www.osisoft.com>.
- [3] D. Siljak. *Large-Scale Dynamic Systems: Stability and Structure*. North-Holland, New York, 1978.
- [4] M. Araki. Applications of M-matrices to the Stability Problems of Composite Nonlinear Systems. *Journal of Mathematical Analysis and Applications*, 52:309–321, 1975.
- [5] M. Ilic-Spong, M. Spong, and R. Fischl. The No-gain Theorem and Localized Response for the Decoupled  $P-\theta$  Network with Active Power Losses Included. *IEEE Transactions on Circuits and Systems*, 32:170–177, 1985.
- [6] M. Ilic-Spong, J. Thorp, and M. Spong. Localized Response Performance of the Decoupled Q-V Network. *IEEE Transactions on Circuits and Systems*, 33:316–322, 1986.
- [7] M. Ilic and J. Zaborszky. *Dynamics and Control of Large Electric Power Systems*. John Wiley & Sons, New York, 2000.
- [8] M. Ilic. Technologies and Management Structures to Support Reliable and Efficient Operation over a Broad Range of Generation and Demand. First Energy, Inc. WWW site, November, 2003. (also New Electricity Transmission Software (NETSS), Inc. WP03-01, December 2003.)
- [9] M. Ilic. Engineering Needs for Enhancing Performance of the U.S. Electric Power Grid: Regulated Industry, Performance Measures and R&D Needs. First Energy, Inc. WWW site, January 2004. (also NETSS WP04-01, January 2004.)
- [10] M. Ilic. Regulatory/Market and Engineering Needs for Enhancing Performance of the U.S. Electric Power Grid: Alternative Architectures and Methods for Their Implementation. First Energy, Inc. WWW site, January 2004. (also *Proceedings of the 8<sup>th</sup> World Multi-Conference on Systematics, Cybernetics and Informatics*, XII:353–361, Orlando, FL, July 2004.)
- [11] J. Zaborszky, K.W. Whang, and K.V. Prasad. Fast Contingency Evaluation using Concentric Relaxation. *IEEE Transactions on Power Apparatus and Systems*, 99:28–36, 1980.

- [12] M.D. Ilic and X.S. Liu. Hierarchical Power Systems Control: Its Value in a Changing Electric Power Industry. *Advances in Industrial Control*, Springer-Verlag, London, 1996.
- [13] M.D. Ilic and X.S. Liu. A Modelling and Control Framework for Operating Large-Scale Electric Power Systems Under Present and Newly Evolving Competitive Industry Structures. *Journal on Mathematical Problems in Engineering*, 1:317–340, 1995.
- [14] J. Medanic, M.D. Ilic, and J. Christensen. Discrete Models of Slow Voltage Dynamics for Under Load Tap-Changing Transformers. *IEEE Transaction on Power Systems*, 2:873–882, 1987.
- [15] J.W. Chapman, M.D. Ilic, C.A. King, L. Eng, and H. Kaufman. Stabilizing a Multimachine Power System via Decentralized Feedback Linearizing Excitation Control. *IEEE Transactions on Power Systems*, 8:830–839, 1993.
- [16] E.H. Allen, J.W. Chapman, and M.D. Ilic. Effects of Torsional Dynamics on Nonlinear Generator Control. *IEEE Transactions on Control Systems Technology*, 4:125–140, 1996.
- [17] C.A. King, J.W. Chapman, and M.D. Ilic. Feedback Linearizing Excitation Control on a Full-Scale Power System Model. *IEEE Transactions on Power Systems*, 9:1102–1111, 1994.
- [18] M.D. Ilic and J.W. Chapman. Decentralized Excitation Control for an Electrical Power Utility System. U.S. patent number 5 483 147, 1996.
- [19] G. Quazza. Large-Scale Control Problems in Electric Power Systems. *IFAC Automatica*, 13:579–593, 1973.
- [20] S.L. Campbell. *Singular Systems of Differential Equations*. Pitman, 1980.
- [21] J.H. Chow, B. Avramovic, P.V. Kokotovic, and J.R. Winkelman. *Singular Perturbations, Coherency, and Aggregation of Dynamic Systems*. Springer-Verlag, Berlin, Germany, 1982.
- [22] M. Ilic, S.X. Liu, B.D. Eidson, C. Vialas, and M. Athans. A New Structure-Based Approach to the Modelling and Control of Electric Power Systems in Response to Slow Reactive Power/Voltage Load Variations. *Automatica*, 33:515–531, 1997.
- [23] E. Scholtz. *Observer-Based Monitors and Distributed Wave Controllers for Electromechanical Disturbances in Power Systems*. MIT, PhD Thesis, August 2004.
- [24] E. Scholtz, P. Sonthikorn, G.C. Verghese, and B.C. Lesieutre. Observers for Swing-State Estimation of Power Systems. *Proceedings*

- of the 34<sup>th</sup> Annual North American Power Symposium, Tempe, Arizona, October 2002.
- [25] H.-L. Pei and B.H. Krogh. Stability Regions for Systems with Mode Transitions. *Proceedings of the 2001 American Control Conference*, 6:25–27, June 2001.
  - [26] L. Sha, L. Xue, and R. Chandra. On the Schedulability of Flexible and Reliable Real Time Control Systems. *Journal of Real-Time Systems*, 2000.
  - [27] Z. Gajic and M. Lim. *Optimal Control of Singularly Perturbed Linear Systems with Applications: High Accuracy Techniques*. Marcel Decker, New York, 2001.
  - [28] J. Thomas, D. Dumur, J. Buisson, C.M. Falinower, and P. Bendotti. Moving Horizon State Estimation of Hybrid Systems. Application to Fault Detection of Sensors of a Steam Generator. *Proceedings of the 2003 IEEE Conference on Control Applications*, 2:1375–1380, 2003.
  - [29] R. Vidal, A. Chiuso, and S. Soatto. Observability and Identifiability of Jump Linear Systems. *Proceedings of the 41<sup>st</sup> IEEE Conference on Decision and Control*, 4:3614–3619, 2000.
  - [30] A. Bemporad, J. Roll, and L. Ljung. Identification of Hybrid Systems via Mixed-Integer Programming. *Proceedings of the 40<sup>th</sup> IEEE Conference on Decision and Control*, 1:786–792, 2001.
  - [31] Z. Han and B. Krogh. Reachability Analysis of Hybrid Control Systems using Reduced-Order Models. *Proceedings of the 2004 American Control Conference*, 1183–1189, Boston, MA, June 2004.
  - [32] J. Zaborszky and M. Ilic. Exploring the Potential of the All DC (ADC) Bulk Power Systems. *Proceedings of Bulk Power System Dynamics and Control V*, Onomichi, Japan, August 2001.
  - [33] K.K. Lim and M. Ilic. Control Coordination on the Distribution Power Network. *Proceedings of IEEE International Symposium on Circuits and Systems*, 1232–1235, Singapore, June 1992.
  - [34] M. Ilic, et al. *Optimal Decision Making and Working Electricity Markets*. Kluwer Academic Publishing, 2004 (to appear).

## Chapter 7

# ROBUST CONTROL OF LARGE POWER SYSTEMS VIA CONVEX OPTIMIZATION

A. I. Zečević

*Santa Clara University*

[azecevic@scu.edu](mailto:azecevic@scu.edu)

D. D. Šiljak

*Santa Clara University*

[dsiljak@scu.edu](mailto:dsiljak@scu.edu)

**Abstract** The reliable and efficient operation of large electric power systems requires the development of appropriate robust control strategies. In designing such a control, it is necessary to ensure that only locally available information is utilized, and that stability can be guaranteed over a wide range of operating conditions and disturbances. This chapter demonstrates that such requirements can be satisfied using linear matrix inequalities, which provide a natural framework for computing feedback laws with information structure constraints.

**Keywords:** Exciter control, robustness, decentralized output control, large-scale systems, linear matrix inequalities.

### 1. Introduction

Any successful strategy for the control of large-scale power systems must satisfy two fundamental requirements. In the first place, the control must be *decentralized*, since only local measurements are normally available to any given machine. Secondly, the control needs to be *robust*, in the sense that it must guarantee satisfactory performance over a wide range of operating conditions and disturbances. This requirement is particularly important in a deregulated environment, where the sys-

tem tends to be more stressed and the power flow paths are virtually impossible to anticipate.

The last decade has seen a number of new developments in the design of robust power system control, including both decentralized turbine/governor and decentralized exciter control designs [1]-[16]. Much of the recent work related to robust control has been based on the concept of direct feedback linearization, which transforms the original nonlinear model into a linear one. After such a transformation, the control design becomes quite straightforward, but the implementation is complicated by the fact that the resulting controller is nonlinear. This difficulty has motivated several recent attempts to develop techniques for designing robust control laws that are *linear* [3, 5, 6, 16]. Among these techniques, the approach proposed in [16] is of particular interest for this chapter, and its various generalizations will be examined in the following sections.

This chapter has two main objectives, the first of which is to describe a systematic method for designing robust decentralized exciter control. The design is based on Linear Matrix Inequalities (LMI) [17]-[20] and the general mathematical framework developed in [6, 16, 21, 22]. Our second objective is to extend this approach to systems with information structure constraints. In this context, particular attention will be devoted to the issue of decentralized output control, and the problem of feedback design in cases where limited amounts of information are exchanged between subsystems.

Among the principal advantages of the proposed approach, we single out the following:

- The design utilizes convex optimization techniques that can be applied efficiently to large-scale systems. Only a modest number of LMI variables need to be computed, due to the special structure of the gain matrix.
- Nonlinear models and robustness requirements are naturally incorporated into the optimization.
- The proposed LMI framework is not restricted to decentralized control, and can accommodate a number of other structures for the gain matrix (such as overlapping blocks and bordered block diagonal forms). These structures are well suited for minimizing interprocessor communication, and can easily be mapped onto appropriate parallel architectures.
- The design scheme can produce decentralized static output feedback.

The features described above are well suited for power system applications, and provide a basis for different types of control design.

## 2. Exciter Control Design using Linear Matrix Inequalities

Let us consider a nonlinear system described by the differential equations

$$\begin{aligned}\dot{x} &= Ax + h(x) + Bu \\ y &= Cx\end{aligned}\quad (7.1)$$

where  $x \in R^n$  is the state of the system,  $u \in R^m$  is the input vector and  $y \in R^q$  is the output.  $A$ ,  $B$  and  $C$  are constant  $n \times n$ ,  $n \times m$  and  $q \times n$  matrices, and  $h : R^n \rightarrow R^n$  represents a piecewise-continuous nonlinear function satisfying  $h(0) = 0$ . It is assumed that the term  $h(x)$  can be bounded by a quadratic inequality

$$h^T(x)h(x) \leq \alpha^2 x^T H^T H x \quad (7.2)$$

where  $H$  is a constant matrix, and  $\alpha > 0$  is a scalar parameter.

Given a linear feedback control law  $u = Kx$ , the global asymptotic stability of the closed-loop system can be established using a Lyapunov function

$$V(x) = x^T P x, \quad (7.3)$$

where  $P$  is a symmetric positive definite matrix. Sufficient conditions for stability are well known, and can be expressed as a pair of inequalities

$$\begin{aligned}x^T P x &> 0 \\ \begin{bmatrix} x \\ h \end{bmatrix}^T \begin{bmatrix} (A + BK)^T P + P(A + BK) & P \\ P & 0 \end{bmatrix} \begin{bmatrix} x \\ h \end{bmatrix} &< 0\end{aligned}\quad (7.4)$$

Defining  $Y = \tau P^{-1}$  (where  $\tau$  is a positive scalar),  $L = KY$ , and  $\gamma = 1/\alpha^2$ , the control design can now be formulated as an LMI problem in  $\gamma$ ,  $\kappa_Y$ ,  $\kappa_L$ ,  $Y$  and  $L$  [6, 21].

**Problem 1** Minimize  $a_1\gamma + a_2\kappa_Y + a_3\kappa_L$  subject to

$$Y > 0 \quad (7.5)$$

$$\begin{bmatrix} AY + YA^T + BL + L^T B^T & I & YH^T \\ I & -I & 0 \\ HY & 0 & -\gamma I \end{bmatrix} < 0 \quad (7.6)$$

$$\gamma - 1/\bar{\alpha}^2 < 0 \quad (7.7)$$

and

$$\begin{bmatrix} -\kappa_L I & L^T \\ L & -I \end{bmatrix} < 0, \quad \begin{bmatrix} Y & I \\ I & \kappa_Y I \end{bmatrix} > 0 \quad (7.8)$$

Several comments need to be made regarding this design procedure.

**Remark 1** *The control design is formulated as a convex optimization problem, which ensures computational efficiency. The gain matrix is obtained directly as  $K = LY^{-1}$ , with no need for trial and error procedures.*

**Remark 2** *The norm of the gain matrix is implicitly constrained by inequalities (8), which imply that  $\|K\| \leq \sqrt{\kappa_L \kappa_Y}$ . This is necessary in order to prevent unacceptably high gains that an unconstrained optimization may otherwise produce [21].*

**Remark 3** *If the optimization problem (5)-(8) is feasible, the resulting gain matrix stabilizes the closed-loop system for all nonlinearities satisfying (2). Condition (7) additionally secures that  $\alpha$  is greater than some desired value  $\bar{\alpha}$ .*

**Remark 4** *The obtained controllers are linear, so their implementation is straightforward and cost effective.*

The proposed LMI-based design can be extended to a wider class of problems, in which the nonlinearities satisfy a *generalized* constraint of the form

$$h^T(x) h(x) \leq x^T H^T(x) H(x) \quad (7.9)$$

The elements of matrix  $H(x)$  in (9) can be unbounded functions of  $x$ , and our only assumption is that there exists a constant matrix  $\bar{H}$  and a region  $\Omega \subset R^n$  such that  $0 \in \Omega$ , and

$$h^T(x) h(x) \leq \alpha^2 x^T \bar{H}^T \bar{H} x, \quad \forall x \in \Omega \quad (7.10)$$

It has been shown in [16] that if (10) holds, optimization Problem 1 with  $H = \bar{H}$  produces a gain matrix  $K$  that *locally* stabilizes the system. The corresponding region of attraction can be estimated using the Lyapunov function (3), as the largest set

$$\Pi(r) = \{x : x^T P x \leq r\} \quad (7.11)$$

that satisfies  $\Pi(r) \subset \Omega$  (*e.g.* [23]-[24]).

The mathematical framework outlined above can be used for designing robust exciter control. To obtain an appropriate state space description for such a design, we will represent the machine dynamics by two axis generator models (*e.g.* [25])

$$\begin{aligned}\dot{\delta}_i &= \omega_i \\ M_i \dot{\omega}_i &= P_{m_i}^0 - P_{e_i} - D_i \omega_i \\ T'_{d_{0i}} \dot{E}_{q_i} &= -E_{q_i} - (x_{d_i} - x'_{d_i}) I_{d_i} + E_{fd_i} \\ T'_{q_{0i}} \dot{E}_{d_i} &= -E_{d_i} + (x_{q_i} - x'_{d_i}) I_{q_i}\end{aligned}\tag{7.12}$$

where

$$\begin{aligned}I_{d_i} &= \sum_k [G_{ik} \cos(\delta_i - \delta_k) + B_{ik} \sin(\delta_i - \delta_k)] E_{d_k} \\ &\quad + \sum_k [G_{ik} \sin(\delta_i - \delta_k) - B_{ik} \cos(\delta_i - \delta_k)] E_{q_k}\end{aligned}\tag{7.13}$$

and

$$\begin{aligned}I_{q_i} &= \sum_k [B_{ik} \cos(\delta_i - \delta_k) - G_{ik} \sin(\delta_i - \delta_k)] E_{d_k} \\ &\quad + \sum_k [G_{ik} \cos(\delta_i - \delta_k) + B_{ik} \sin(\delta_i - \delta_k)] E_{q_k}\end{aligned}\tag{7.14}$$

In the following, we will assume that  $E_{fd_i} = E_{fd_i}^0 + u_i$  and that the control has the form

$$u_i = k_{1i}(\delta_i - \delta_i^r) + k_{2i}(\omega_i - \omega_i^r) + k_{3i}(E_{q_i} - E_{q_i}^r) + k_{4i}(E_{d_i} - E_{d_i}^r)\tag{7.15}$$

where  $\{\delta_i^r, \omega_i^r, E_{q_i}^r, E_{d_i}^r\}$  represent user-defined reference values, and  $\{k_{1i}, k_{2i}, k_{3i}, k_{4i}\}$  are the gains. Defining the new states  $\{x_{1i}, x_{2i}, x_{3i}, x_{4i}\}$  as deviations from the equilibrium values  $\{\delta_i^e, \omega_i^e, E_{q_i}^e, E_{d_i}^e\}$ , the model in (12) can be rewritten as

$$\begin{aligned}\dot{x}_{1i} &= x_{2i} \\ M_i \dot{x}_{2i} &= -D_i x_{2i} - \Delta P_{e_i}(x) \\ T'_{d_{0i}} \dot{x}_{3i} &= -x_{3i} - (x_{d_i} - x'_{d_i}) \Delta I_{d_i}(x) + u_i \\ T'_{q_{0i}} \dot{x}_{4i} &= -x_{4i} + (x_{q_i} - x'_{d_i}) \Delta I_{q_i}(x)\end{aligned}\tag{7.16}$$

where

$$\Delta I_{d_i}(x) = I_{d_i}(x) - I_{d_i}^e\tag{7.17}$$

$$\Delta I_{q_i}(x) = I_{q_i}(x) - I_{q_i}^e\tag{7.18}$$

$$\Delta P_{e_i}(x) = (E_{d_i} I_{d_i} + E_{q_i} I_{q_i}) - (E_{d_i}^e I_{d_i}^e + E_{q_i}^e I_{q_i}^e) \quad (7.19)$$

As shown in [16], the nonlinear term

$$h_i(x) = [0 \quad \Delta P_{e_i}(x) \quad \Delta I_{d_i}(x) \quad \Delta I_{q_i}(x)]^T \quad (7.20)$$

can be bounded as

$$\begin{aligned} h_i^T(x) h_i(x) &\leq x^T [F_{i1}^T (D_{i1} + 2D_{i3}) F_{i1}] x \\ &+ x^T [F_{i1}^T 2\phi_i(x) D_{i2} F_{i1} + 2\phi_i^2(x) F_{i2}^T F_{i2}] x \end{aligned} \quad (7.21)$$

which conforms to the constraint defined in (9). The function  $\phi_i(x)$  in (21) can be expressed as

$$\phi_i(x) = \sum_{k \neq i} \sqrt{v_{ik}} (|x_{4k}| + |x_{3k}|) + \sum_{k \neq i} 2\sqrt{r_{ik}} |\sin(x_{1i} - x_{1k})/2| \quad (7.22)$$

and the constant matrices  $D_{ij}$ ,  $j = 1, 2, 3$ , and  $F_{ij}$ ,  $j = 1, 2$ , are readily constructed from the system data. The same holds true for the scalar constants  $r_{ik}$  and  $v_{ik}$ .

From the standpoint of decentralized control, the multimachine model (16) can be viewed as a collection of interconnected subsystems

$$\dot{x}_i = A_i x_i + B_i u_i + G_i h_i(x), \quad i = 1, 2, \dots, N \quad (7.23)$$

where

$$G_i = \begin{bmatrix} 0 & 0 & 0 & 0 \\ 0 & -1/M_i & 0 & 0 \\ 0 & 0 & -\Delta x_{di}/T'_{d0i} & 0 \\ 0 & 0 & 0 & -\Delta x_{qi}/T'_{q0i} \end{bmatrix} \quad (7.24)$$

To obtain decentralized feedback laws

$$u_i(x) = K_i x_i, \quad i = 1, 2, \dots, N \quad (7.25)$$

the only additional requirement in Problem 1 is for matrices  $Y$  and  $L$  to be *block-diagonal*. In the case of two axis generator models, it is easily verified that the diagonal blocks of  $Y$  and  $L$  have dimensions  $4 \times 4$  and  $1 \times 4$ , respectively. Since matrix  $Y$  must also be symmetric, the total number of LMI variables amounts to 14 per generator. This represents a very modest computational requirement, considering that existing software packages can solve LMI problems with several thousand variables.

### 3. Some Simulation Results

The LMI - based control design proposed in the previous sections was applied to the IEEE 39 bus system [26]. Two axis generator models with IEEE Type I exciters were used in all the simulations, with field voltage limits  $-3 \leq E_{fd_i} \leq 6$ ,  $i = 1, 2, \dots, N$ . In our experiments we considered a variety of short circuit faults, and simulated the transient responses and critical clearing times. Different fault locations were modeled using the scalar quantity  $\sigma$ , which represents the fraction of the transmission line between the lower-numbered bus and the fault. In all cases, the following fault sequence was assumed:

- 1) The system is in the pre-fault state.
- 2) The fault occurs at  $t = 0.1$  seconds.
- 3) The fault is cleared by removing the line.

In Figure 7.1–7.2 we show the rotor angle and terminal voltage corresponding to Generator 8, for a fault on line (25, 26) with  $\sigma = 0.05$  (the fault was cleared after 0.15 seconds). These responses indicate that the proposed exciter control performs well from the standpoint of transient stability.

In addition to the simulation results, it is also necessary to discuss a number of practical issues related to the implementation of the proposed control. We begin by recalling that the feedback scheme in (15) uses the deviation of the local states with respect to the arbitrarily chosen reference values  $\{\delta_i^r, \omega_i^r, E_{q_i}^r, E_{d_i}^r\}$ . A natural way to select these reference values is to equate them to the pre-fault steady state values obtained from the most recent power flow; this is the way they were computed in all our simulations. Since the operating point of the system varies continuously due to load fluctuations and topological changes in the system, the reference values will typically differ from the system equilibrium.

Several further remarks need to be made regarding the relationship between reference values and the equilibrium.

**Remark 5** *The proposed LMI-based control guarantees that all states tend to their equilibrium values  $\{\delta_i^e, \omega_i^e, E_{q_i}^e, E_{d_i}^e\}$ , although these values needn't be known explicitly.*

**Remark 6** *Since the main objective of the proposed control is to preserve stability following a large disturbance, the post-fault equilibrium should not be expected to be optimal. This is not a serious limitation, since the system operator can subsequently move the system to a desired operating point.*

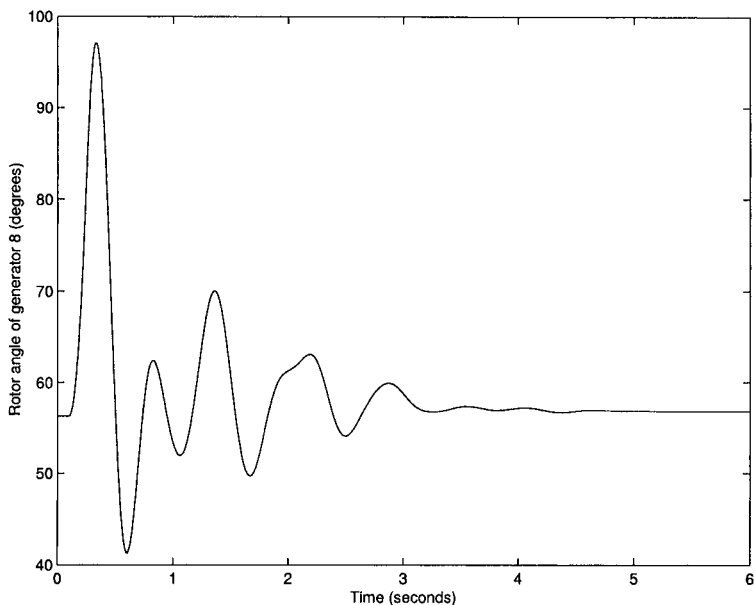


Figure 7.1. Rotor angle of Generator 8.

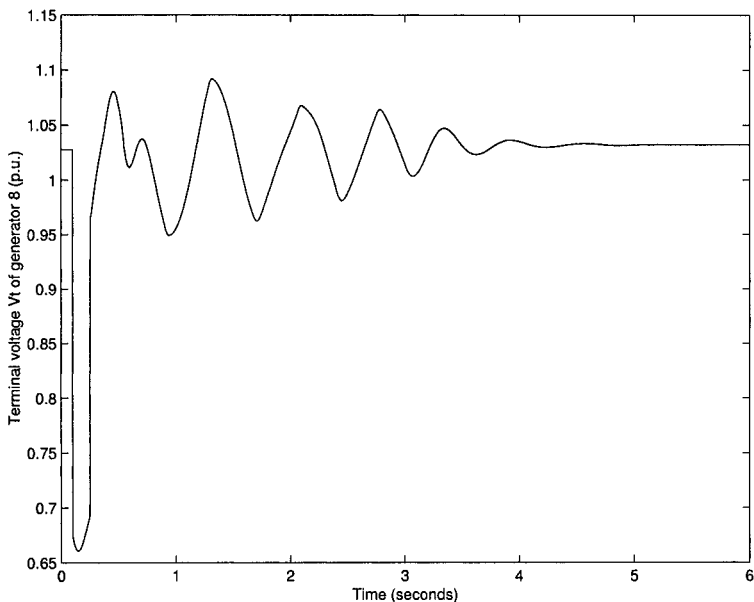


Figure 7.2. Terminal voltage  $V_t$  of Generator 8.

**Remark 7** From a practical standpoint, it is prudent to periodically update the local reference values, based on the most recent power flow results. Such a strategy would reduce the discrepancy between the equilibrium and the reference values. It is important to recognize, however, that this is only an added convenience, and that there is no need for frequent updates.

**Remark 8** The gains obtained using the LMI optimization are computed for a nominal operating point. Since the control strategy is robust, the same gains can be used for a range of operating conditions. If the system were to significantly deviate from its nominal configuration, the performance of the controller could be improved by recomputing the gains. It is possible to do this off-line, based on load forecasts and/or contingency studies.

## 4. New Research Directions

As pointed out in [27], despite advances made in recent years the design of primary generator control still faces a number of unresolved problems. The following two deserve particular attention.

- 1 In most realistic systems, it cannot be assumed that all state variables are available for control purposes. This constraint ultimately necessitates the design of *decentralized static output feedback*, which is a difficult problem in general (e.g. [27]-[30]).
- 2 In a large power system, a decentralized control scheme may not be sufficient to ensure stability over a wide range of operating conditions. It is therefore of interest to consider control schemes with a limited amount of *information exchange* among different subsystems.

In the following, we will consider possible extensions of the LMI design procedure that address these issues.

### 4.1 Design of decentralized output control

Before turning to the question of decentralized output control, let us make two assumptions regarding notation.

**Assumption 1** Let  $y_i = C_i x_i$  denote the subset of states that are available for the control of the  $i$ -th machine.

**Assumption 2** Let  $L_i$  and  $Y_i$ ,  $i = 1, 2, \dots, N$ , denote the  $i$ -th diagonal blocks of matrices  $L$  and  $Y$  that appear in the decentralized LMI optimization.

Given this notation, our objective will be to determine matrices  $L_i$  and  $Y_i$  such that the product  $L_i Y_i^{-1}$  can be expressed as

$$L_i Y_i^{-1} = K_i C_i \quad (7.26)$$

If this can be accomplished, the corresponding input will obviously have the desired decentralized output feedback form  $u_i = K_i y_i$ . With that in mind, we propose to look for a solution of optimization Problem 1 in the form

$$Y = Y_0 + U Y_C U^T, \quad L = L_C U^T \quad (7.27)$$

with the following additional requirements:

**Requirement 1**  $U = \text{diag}\{U_1, \dots, U_N\}$  is a fixed, user-defined block diagonal matrix, with blocks  $U_i$  of dimension  $n_i \times q_i$ .

**Requirement 2**  $Y_0 = \text{diag}\{Y_0^{(1)}, \dots, Y_0^{(N)}\}$  and  $Y_C = \text{diag}\{Y_C^{(1)}, \dots, Y_C^{(N)}\}$  are unknown symmetric block diagonal matrices. The dimensions of  $Y_0^{(i)}$  and  $Y_C^{(i)}$  are  $n_i \times n_i$  and  $q_i \times q_i$ , respectively.

**Requirement 3**  $L_C = \text{diag}\{L_C^{(1)}, \dots, L_C^{(N)}\}$  is an unknown block diagonal matrix, with blocks  $L_C^{(i)}$  of dimension  $m_i \times q_i$ .

To see the connection between (27) and the desired output feedback structure, we should observe that  $Y^{-1}$  can be expressed using the Sherman-Morrison formula as (e.g. [31])

$$Y^{-1} = Y_0^{-1} - S R U^T Y_0^{-1} \quad (7.28)$$

where

$$S = Y_0^{-1} U Y_C, \quad R = [I + U^T S] \quad (7.29)$$

It is now easily verified that condition

$$U^T Y_0^{-1} = C \quad (7.30)$$

ensures that  $LY^{-1} = KC$ , with

$$K = L_C (I - U^T S R) \quad (7.31)$$

Note also that Requirements 1-3 imply that the matrix

$$I - U^T S R \quad (7.32)$$

must have a block diagonal structure, with blocks of dimension  $q_i \times q_i$ .

Regarding condition (30), we should point out that it can be incorporated into the LMI optimization (5)-(8) by adding the equality constraint

$$Y_0 C^T = U \quad (7.33)$$

This condition is *automatically* satisfied if we set  $U = C^T$ , and look for  $Y_0$  in the form

$$Y_0 = QY_QQ^T + C^T(CC^T)^{-1}C \quad (7.34)$$

where  $Q = \text{diag}\{Q_1, \dots, Q_N\}$  is a block diagonal  $n \times (n - q)$  matrix such that

$$Q^T C^T = 0 \quad (7.35)$$

In that case, the LMI optimization does not require an explicit equality constraint, and the corresponding design procedure can be summarized as follows.

## Design Procedure

Step 1. Compute an  $n \times (n - q)$  block diagonal matrix  $Q$  of full rank that satisfies (35).

Step 2. Set  $U = C^T$ , and solve the decentralized optimization Problem 1 for  $\gamma$ ,  $\kappa_Y$ ,  $\kappa_L$ ,  $Y_Q$ ,  $Y_C$  and  $L_C$ , with

$$Y = QY_QQ^T + C^T(CC^T)^{-1}C + UY_CU^T, \quad L = L_CU^T \quad (7.36)$$

In this process, the structure of matrices  $U$ ,  $Y_Q$ ,  $Y_C$  and  $L_C$  must conform to Requirements 1-3.

Step 3. Compute the gain matrix  $K$  using (29) and (31).

## 4.2 Coordinated design of power system stabilizers and robust feedback

To illustrate how the proposed design strategy can be applied to power systems, in the following we will consider the problem of designing power system stabilizers and robust feedback in a coordinated manner. In this case it is essential to use decentralized output feedback, since only a subset of local states is available for control purposes.

We begin by observing that the dynamics of a fast exciter can be described by treating  $E_{fd_i}$  as a state variable, and adding equation

$$T_{E_i} \dot{E}_{fd_i} = -K_{E_i} E_{fd_i} + K_{A_i} \left( V_{ref_i} - V_{t_i} + u_{pss}^{(i)} + u_i \right) \quad (7.37)$$

to the model in (12). In (37),  $V_{t_i}$  is the terminal voltage of the  $i$ -th machine, while  $u_i$  denotes the input associated with the robust feedback control. We will assume that each generator in the system has an input  $u_i$ , while  $u_{pss}^{(i)}$  is added only to those machines that are equipped with power system stabilizers.

The standard description of a power system stabilizer involves a third order transfer function of the form [25]

$$G_i(s) = \frac{u_{pss}^{(i)}}{\omega_i} = K_{PSS}^{(i)} \frac{(1+sT_{1i})(1+sT_{3i})}{(1+sT_{2i})(1+sT_{4i})} \frac{sT_{wi}}{1+sT_{wi}} \quad (7.38)$$

where the time constants  $\{T_{1i}, T_{2i}, T_{3i}, T_{4i}, T_{wi}\}$  and gain  $K_{PSS}^{(i)}$  can be obtained using any number of different techniques [32]-[39]. For our purposes, it will be convenient to rewrite  $G_i(s)$  as

$$G_i(s) = K_i^* + \frac{\beta_{2i}s^2 + \beta_{1i}s + \beta_{0i}}{s^3 + a_{2i}s^2 + a_{1i}s + a_{0i}} \quad (7.39)$$

where

$$K_i^* = K_{PSS}^{(i)} \frac{T_{1i}T_{3i}}{T_{2i}T_{4i}} \quad (7.40)$$

and the coefficients  $\{\beta_{0i}, \beta_{1i}, \beta_{2i}\}$  and  $\{a_{0i}, a_{1i}, a_{2i}\}$  are explicit functions of the time constants. The corresponding observable state space realization introduces states  $\xi_{1i}$ ,  $\xi_{2i}$  and  $\xi_{3i}$ , which satisfy

$$\begin{aligned} \dot{\xi}_{1i} &= -a_{2i}\xi_{1i} + \xi_{2i} + \beta_{2i}\omega_i \\ \dot{\xi}_{2i} &= -a_{1i}\xi_{1i} + \xi_{3i} + \beta_{1i}\omega_i \\ \dot{\xi}_{3i} &= -a_{0i}\xi_{1i} + \beta_{0i}\omega_i \end{aligned} \quad (7.41)$$

and

$$u_{pss}^{(i)} = K_i^*\omega_i + \xi_{1i} \quad (7.42)$$

In view of (41) and (42), the dynamics of the  $i$ -th generator can now be described by an eighth order model, with states  $\{\delta_i, \omega_i, E_{q_i}, E_{d_i}, E_{fd_i}, \xi_{1i}, \xi_{2i}, \xi_{3i}\}$ .

If we define a new set of states

$$\begin{aligned} x_{1i} &= \delta_i - \delta_i^e \\ x_{2i} &= \omega_i - \omega_i^e \\ &\vdots \\ x_{8i} &= \xi_{3i} - \xi_{3i}^e \end{aligned} \quad (7.43)$$

as deviations from the equilibrium values (which needn't be known explicitly), we can rewrite the overall model for the  $i$ -th machine as

$$\begin{aligned}\dot{x}_{1i} &= x_{2i} \\ M_i \dot{x}_{2i} &= -D_i x_{2i} - \Delta P_{e_i}(x) \\ T'_{d_{0i}} \dot{x}_{3i} &= -x_{3i} - (x_{d_i} - x'_{d_i}) \Delta I_{d_i}(x) + x_{5i} \\ T'_{q_{0i}} \dot{x}_{4i} &= -x_{4i} + (x_{q_i} - x'_{d_i}) \Delta I_{q_i}(x) \\ T_{E_i} \dot{x}_{5i} &= -K_{E_i} x_{5i} + K_{A_i} K_i^* x_{2i} + K_{A_i} x_{6i} \\ &\quad - K_{A_i} \Delta V_{t_i} + K_{A_i} (u_i - u_i^e) \\ \dot{x}_{6i} &= -a_{2i} x_{6i} + x_{7i} + \beta_{2i} x_{2i} \\ \dot{x}_{7i} &= -a_{1i} x_{6i} + x_{8i} + \beta_{1i} x_{2i} \\ \dot{x}_{8i} &= -a_{0i} x_{6i} + \beta_{0i} x_{2i}\end{aligned}\tag{7.44}$$

where

$$\begin{aligned}\Delta V_{t_i} &= V_{t_i} - V_{t_i}^e \\ \Delta I_{d_i}(x) &= I_{d_i}(x) - I_{d_i}^e \\ \Delta I_{q_i}(x) &= I_{q_i}(x) - I_{q_i}^e\end{aligned}\tag{7.45}$$

and

$$\Delta P_{e_i}(x) = (E_{d_i} I_{d_i} + E_{q_i} I_{q_i}) - (E_{d_i}^e I_{d_i}^e + E_{q_i}^e I_{q_i}^e)\tag{7.46}$$

Assuming a linear control of the form

$$u_i = k_{1i}(\delta_i - \delta_i^r) + \dots + k_{8i}(\xi_{3i} - \xi_{3i}^r)\tag{7.47}$$

it is straightforward to show that

$$u_i - u_i^e = \sum_{j=1}^8 k_{ji} x_{ji} \equiv K_i x_i\tag{7.48}$$

which corresponds to standard decentralized state feedback. In this context, we should also note that  $\Delta V_{t_i}$ ,  $\Delta P_{e_i}(x)$ ,  $\Delta I_{d_i}(x)$  and  $\Delta I_{q_i}(x)$  can all be bounded along the lines of inequality (9).

The control law (47) is not suitable for practical implementation, since it is unlikely that all eight local states are available for control purposes. As a result, it is necessary to consider an appropriate decentralized output feedback strategy. In order to do that, let us assume that an initial PSS transfer function has been determined by some appropriate technique, and that the corresponding state space realization has the form (41). We will then introduce additional inputs  $u_{2i}$ ,  $u_{3i}$  and  $u_{4i}$  into (44), obtaining

$$\begin{aligned}\dot{x}_{6i} &= -a_{2i} x_{6i} + x_{7i} + \beta_{2i} x_{2i} + u_{2i} \\ \dot{x}_{7i} &= -a_{1i} x_{6i} + x_{8i} + \beta_{1i} x_{2i} + u_{3i} \\ \dot{x}_{8i} &= -a_{0i} x_{6i} + \beta_{0i} x_{2i} + u_{4i}\end{aligned}\tag{7.49}$$

It is important to recognize that these inputs are *not* physical, and are simply an auxiliary step in the design process. The corresponding feedback will subsequently be interpreted as an adjustment to the time constants in the PSS transfer function.

If we consider a feedback law of the form

$$\begin{bmatrix} u_{2i} \\ u_{3i} \\ u_{4i} \end{bmatrix} = \begin{bmatrix} \eta_{2i} \\ \eta_{3i} \\ \eta_{4i} \end{bmatrix} x_{6i} \quad (7.50)$$

and assume that only states  $\{x_{1i}, x_{2i}, x_{3i}, x_{4i}\}$  are available for input  $u_{1i}$ , the overall control law for the  $i$ -th machine can be expressed as

$$u_i = K_i C_i x_i \quad (7.51)$$

where  $x_i = \{x_{1i}, \dots, x_{8i}\}$ ,

$$C_i = \begin{bmatrix} 1 & 0 & 0 & 0 & 0 & 0 & 0 & 0 \\ 0 & 1 & 0 & 0 & 0 & 0 & 0 & 0 \\ 0 & 0 & 1 & 0 & 0 & 0 & 0 & 0 \\ 0 & 0 & 0 & 1 & 0 & 0 & 0 & 0 \\ 0 & 0 & 0 & 0 & 0 & 1 & 0 & 0 \end{bmatrix} \quad (7.52)$$

and

$$K_i = \begin{bmatrix} k_{1i} & k_{2i} & k_{3i} & k_{4i} & 0 \\ 0 & 0 & 0 & 0 & \eta_{2i} \\ 0 & 0 & 0 & 0 & \eta_{3i} \\ 0 & 0 & 0 & 0 & \eta_{4i} \end{bmatrix} \quad (7.53)$$

It is not difficult to show that the structure in (52) and (53) can be incorporated into the decentralized output control framework proposed earlier in this section. Note also that if a different subset of states is used for  $u_{1i}$ , the only necessary adjustments would involve simple modifications of matrices  $C_i$  and  $K_i$ .

The closed-loop system with feedback (53) takes the form

$$\begin{aligned} \dot{x}_{1i} &= x_{2i} \\ M_i \dot{x}_{2i} &= -D_i x_{2i} - \Delta P_{e_i}(x) \\ T'_{d_{0i}} \dot{x}_{3i} &= -x_{3i} - (x_{d_i} - x'_{d_i}) \Delta I_{d_i}(x) + x_{5i} \\ T'_{q_{0i}} \dot{x}_{4i} &= -x_{4i} + (x_{q_i} - x'_{d_i}) \Delta I_{q_i}(x) \\ T_{E_i} \dot{x}_{5i} &= -K_{E_i} x_{5i} + K_{A_i} K_i^* x_{2i} + K_{A_i} x_{6i} \\ &\quad - K_{A_i} \Delta V_{t_i} + K_{A_i} \sum_{j=1}^4 k_{ji} x_{ji} \\ \dot{x}_{6i} &= -(a_{2i} - \eta_{2i}) x_{6i} + x_{7i} + \beta_{2i} x_{2i} \\ \dot{x}_{7i} &= -(a_{1i} - \eta_{3i}) x_{6i} + x_{8i} + \beta_{1i} x_{2i} \\ \dot{x}_{8i} &= -(a_{0i} - \eta_{4i}) x_{6i} + \beta_{0i} x_{2i} \end{aligned} \quad (7.54)$$

A simple inspection of (54) indicates that the effect of the auxiliary inputs  $u_{2i}$ ,  $u_{3i}$  and  $u_{4i}$  is equivalent to a modification of coefficients  $\{a_{0i}, a_{1i}, a_{2i}\}$ . Since these coefficients are directly related to the time constants in (38), the corresponding adjustments in the PSS design can be determined by solving equations

$$a_{2i} - \eta_{2i} = \frac{1}{T_{2i}} + \frac{1}{T_{4i}} + \frac{1}{T_{wi}} \quad (7.55)$$

$$a_{1i} - \eta_{3i} = \frac{1}{T_{2i}T_{4i}} + \frac{1}{T_{4i}T_{wi}} + \frac{1}{T_{2i}T_{wi}} \quad (7.56)$$

$$a_{0i} - \eta_{4i} = \frac{1}{T_{2i}T_{4i}T_{wi}} \quad (7.57)$$

Note that in this process  $K_{PSS}^{(i)}$  will need to be adjusted as well, in order to keep  $K_i^*$  unchanged.

### 4.3 Control design with information exchange between subsystems

To illustrate how LMI control design can be generalized to include information exchanges between subsystems, let us consider a four machine system in which each generator has its own decentralized output control of the form

$$u_i(x) = K_{ii}y_i \quad (7.58)$$

If we additionally assume that Generators 1 and 3 can exchange their output information through an appropriate communication channel, a possible control law for such a system would be

$$\begin{aligned} u_1 &= K_{11}y_1 + K_{13}y_3 \\ u_2 &= K_{22}y_2 \\ u_3 &= K_{33}y_3 + K_{31}y_1 \\ u_4 &= K_{44}y_4 \end{aligned} \quad (7.59)$$

The corresponding gain matrix would then have the structure

$$K = \begin{bmatrix} K_{11} & 0 & K_{13} & 0 \\ 0 & K_{22} & 0 & 0 \\ K_{31} & 0 & K_{33} & 0 \\ 0 & 0 & 0 & K_{44} \end{bmatrix} \quad (7.60)$$

with blocks  $K_{ij}$  of dimension  $1 \times q_j$ , where  $q_j$  represents the number of outputs associated with the  $j$ -th machine.

To see how the proposed LMI design procedure can produce such a gain matrix, it will suffice to recall that matrix (32) consists of  $q_i \times q_i$  diagonal blocks, by virtue of Requirements 1-3. As a result, if  $L_C$  is chosen to have the same structure as the matrix in (60), the gain matrix defined by (31) is guaranteed to have the same form.

It is also important to note that this approach can be extended to any gain matrix with the nested BBD structure shown in Figure 7.3.

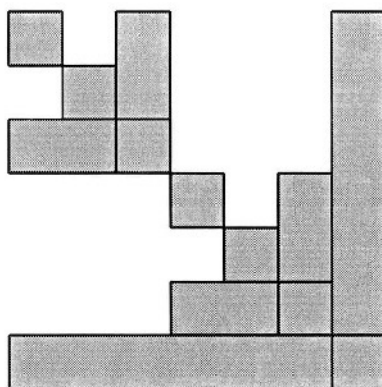


Figure 7.3. Matrix  $K$  with a nested BBD structure.

This kind of control is inherently hierarchical, and can be easily embedded into a tree-type multiprocessor architecture. In such a scheme, the only communication tasks are single node gather and scatter operations, which results in low overhead (*e.g.* [40]).

A crucial step in the identification of an appropriate BBD structure for  $K$  is the development of a decomposition that *simultaneously* permutes matrix  $A$  into the BBD form *and* secures a compatible block-diagonal structure for matrices  $B$  and  $C$ . A graph-theoretic algorithm for this purpose has recently been proposed in [41], based on a modification of the balanced BBD decomposition method [42]. This algorithm was found to be effective for a wide range of large, sparse systems, particularly when used in conjunction with epsilon decomposition [43]-[47].

## 5. Conclusions

In this chapter we presented a new strategy for exciter control design. The proposed method represents a generalization of the LMI-based approach formulated in [16] and [6], which allows for the inclusion of a wider class of nonlinearities. The resulting control law is linear and the

gain matrix can be obtained directly, using standard convex optimization techniques. We also considered possible extensions of this method to systems with output information structure constraints. It was established that LMI optimization can be used to design decentralized output control, as well as feedback laws that incorporate information exchange between subsystems. Other possible applications include the coordinated design of robust control and power system stabilizers.

## References

- [1] Z. Qu, J. Dorsey, J. Bond, and J. McCalley. Application of Robust Control to Sustained Oscillations in Power Systems. *IEEE Transactions on Circuits and Systems*, 39:470–476, 1992.
- [2] S. Jain and F. Khorrami. Robust Decentralized Control of Power System Utilizing Only Swing Angle Measurements. *International Journal of Control*, 66:581–601, 1997.
- [3] H. Jiang, H. Cai, J. Dorsey, and Z. Qu. Toward a Globally Robust Decentralized Control for Large-Scale Power Systems. *IEEE Transactions on Control Systems Technology*, 5:309–319, 1997.
- [4] Y. Wang, D. Hill, and G. Guo. Robust Decentralized Control for Multimachine Power Systems. *IEEE Transactions on Circuits and Systems*, 45:271–279, 1998.
- [5] H. Cai, Z. Qu, D. Gan, and J. Dorsey. A Comparison and Simulation Study of Nonlinearly Designed Robust Controllers for Power System Transient Stability. *International Journal of Electrical Power and Energy Systems*, 22:15–28, 2000.
- [6] D.D. Šiljak, D.M. Stipanović, and A.I. Zečević. Robust Decentralized Turbine/Governor Control using Linear Matrix Inequalities. *IEEE Transactions on Power Systems*, 17:715–722, 2002.
- [7] L. Gao, L. Chen, Y. Fan, and H. Ma. A Nonlinear Control Design for Power Systems. *Automatica*, 29:975–979, 1992.
- [8] J.W. Chapman, M.D. Ilić, C.A. King, L. Eng, and H. Kaufman. Stabilizing a Multimachine Power System via Decentralized Feedback Linearizing Excitation Control. *IEEE Transaction on Power Systems*, 8:830–839, 1993.
- [9] C.A King, J.W. Chapman, and M.D. Ilić. Feedback Linearizing Excitation Control on a Full-Scale Power System Model. *IEEE Transaction on Power Systems*, 9:1102–1109, 1994.
- [10] H. Cai, Z. Qu and J. Dorsey. Robust Decentralized Excitation Control for Large Scale Power Systems. *Proceedings of the 13<sup>th</sup> IFAC Congress*, 217–222, San Francisco, CA, 1996.

- [11] M. Djukanović, M. Khammash, and V. Vittal. Application of the Structured Singular Value Theory for Robust Stability and Control Analysis in Multimachine Power Systems. *IEEE Transactions on Power Systems*, 13:1311–1316, 1998.
- [12] J.K. Shiau, G.N. Taranto, J.H. Chow, and G. Boukarim. Power Swing Damping Controller Design using an Iterative Linear Matrix Inequality Algorithm. *IEEE Transactions on Control Systems Technology*, 7:371–381, 1999.
- [13] G. Guo, Y. Wang, and D. Hill. Nonlinear Output Stabilization Control for Multimachine Power Systems. *IEEE Transactions on Circuits and Systems*, 47:46–53, 2000.
- [14] Y. Guo, D. Hill, and Y. Wang. Nonlinear Decentralized Control of Large-Scale Power Systems. *Automatica*, 36:1275–1289, 2000.
- [15] S. Xie, L. Xie, Y. Wang, and G. Guo. Decentralized Control of Multimachine Power Systems with Guaranteed Performance. *IEE Proceedings of Control Theory Applications*, 147:355–365, 2000.
- [16] A.I. Zečević, G. Nešković, and D.D. Šiljak. Robust Decentralized Exciter Control with Linear Feedback. *IEEE Transactions on Power Systems*, 19:1096–1103, 2004.
- [17] S. Boyd, L. El Ghaoui, E. Feron, and V. Balakrishnan. *Linear Matrix Inequalities in System and Control Theory*. SIAM, Philadelphia, PA, 1994.
- [18] J.C. Geromel, J. Bernussou, and P. Peres. Decentralized Control through Parameter Space Optimization. *Automatica*, 30:1565–1578, 1994.
- [19] J.C. Geromel, J. Bernussou, and M.C. de Oliveira.  $H_\infty$ -Norm Optimization with Constrained Dynamic Output Feedback Controllers: Decentralized and Reliable Control. *IEEE Transactions on Automatic Control*, 44:1449–1454, 1999.
- [20] L. El Ghaoui and S. Niculescu (Eds.). *Advances in Linear Matrix Inequalities Methods in Control*. SIAM, Philadelphia, PA, 2000.
- [21] D.D. Šiljak and D.M. Stipanović. Robust Stabilization of Nonlinear Systems: The LMI approach. *Mathematical Problems in Engineering*, 6:461–493, 2000.
- [22] A.I. Zečević and D.D. Šiljak. Stabilization of Nonlinear Systems with Moving Equilibria. *IEEE Transactions on Automatic Control*, 48:1036–1040, 2003.
- [23] D.D. Šiljak. *Large-Scale Dynamic Systems: Stability and Structure*. North Holland, New York, 1978.

- [24] D.D. Šiljak. *Decentralized Control of Complex Systems*. Academic Press, Cambridge, 1991.
- [25] P.W. Sauer and M.A. Pai. *Power System Dynamics and Stability*. Prentice Hall, Englewood Cliffs, 1998.
- [26] M.A. Pai. *Energy Function Analysis for Power System Stability*. Kluwer, Boston, 1989.
- [27] M. Ilić and J. Zaborszky. *Dynamics and Control of Large Electric Power Systems*. John Wiley & Sons, New York, 2000.
- [28] V.L. Syrmos, C.T. Abdallah, P. Dorato, and K. Grigoriadis. Static Output Feedback—A Survey. *Automatica*, 33:125–137, 1997.
- [29] D. Bernstein. Some Open Problems in Matrix Theory arising in Linear Systems and Control. *Linear Algebra Applications*, 164:409–432, 1992.
- [30] V. Blondel, M. Gevers, and A. Lindquist. Survey on the State of Systems and Control. *European Journal of Control*, 1:5–23, 1995.
- [31] G. Golub and C. van Loan. *Matrix Computations*. Johns Hopkins University Press, Baltimore, 1996.
- [32] P. Kundur. *Power System Stability and Control*. McGraw-Hill, New York, 1994.
- [33] P. Kundur, M. Klein, G. Rogers, and M. Zywno. Application of Power System Stabilizers for Enhancement of Overall System Stability. *IEEE Transactions on Power Systems*, 4:614–626, 1989.
- [34] M. Klein, G. Rogers, S. Moorty, and P. Kundur. Analytical Investigation of Factors Influencing Power System Stabilizer Performance. *IEEE Transactions on Energy Conversion*, 7:382–388, 1992.
- [35] J.H. Chow, L.P. Harris, M.A. Kale, H.A. Othman, J.J. Sanchez-Gasca, and G.E. Terwilliger. Robust Control Design of Power System Stabilizers using Multivariable Frequency Domain Techniques. *International Journal of Robust Nonlinear Control*, 2:123–138, 1992.
- [36] S. Chen and O.P. Malik.  $H_\infty$  Based Power System Stabilizer Design. *IEE Proceedings on Generation, Transmission and Distribution*, 142:179–184, 1995.
- [37] M.A. Pai, C.D. Vournas, A.N. Michel, and H. Ye. Application of Interval Matrices in Power System Stabilizer Design. *International Journal on Electrical Power and Energy Systems*, 19:179–184, 1997.
- [38] A.J. Simões Costa, F.D. Freitas, and A.S. Silva. Design of Decentralized Controllers for Large Power Systems considering Sparsity. *IEEE Transactions on Power Systems*, 12:144–152, 1997.

- [39] T.C. Yang, J.H. Zhang, and H. Yu. A New Decentralized Controller Design Method with Application to Power System Stabilizer Design. *Control Engineering Practice*, 7:537–545, 1999.
- [40] D.P. Bertsekas and J.N. Tsitsiklis. *Parallel and Distributed Computation*. Prentice Hall, Englewood Cliffs, 1989.
- [41] A.I. Zečević and D.D. Šiljak. A Decomposition-Based Control Strategy for Large, Sparse Dynamic Systems. *Mathematical Problems in Engineering* (to appear).
- [42] A.I. Zečević and D.D. Šiljak. Balanced Decompositions of Sparse Systems for Multilevel Parallel Processing. *IEEE Transactions on Circuits and Systems—Part I*, 41:220–233, 1994.
- [43] M.E. Sezer and D.D. Šiljak. Nested  $\epsilon$  Decompositions and Clustering of Complex Systems. *Automatica*, 22:321–331, 1986.
- [44] M.E. Sezer and D.D. Šiljak. Nested Epsilon Decompositions of Linear Systems: Weakly Coupled and Overlapping Blocks. *SIAM Journal of Matrix Analysis and Applications*, 12:521–533, 1991.
- [45] M. Amano, A.I. Zečević, and D.D. Šiljak. An Improved Block-Parallel Newton Method via Epsilon Decompositions for Load Flow Calculations. *IEEE Transactions on Power Systems*, 11:1519–1527, 1996.
- [46] A.I. Zečević and N. Gaćić. A Partitioning Algorithm for the Parallel Solution of Differential-Algebraic Equations by Waveform Relaxation. *IEEE Transactions on Circuits and Systems—Part I*, 46:421–434, 1999.
- [47] A.I. Zečević and D.D. Šiljak. A Block-Parallel Newton Method via Overlapping Epsilon Decompositions. *SIAM Journal of Matrix Analysis and Applications*, 15:824–844, 1994.

## Chapter 8

# INSTABILITY MONITORING AND CONTROL OF POWER SYSTEMS

Eyad H. Abed

*University of Maryland, College Park*

[abed@umd.edu](mailto:abed@umd.edu)

Munther A. Hassouneh

*University of Maryland, College Park*

[munther@umd.edu](mailto:munther@umd.edu)

Mohamed S. Saad

*University of Maryland, College Park*

[mssaad@umd.edu](mailto:mssaad@umd.edu)

**Abstract** Today's electric power systems are often subject to stress by heavy loading conditions, resulting in operation with a small margin of stability. This has led to research on estimating the distance to instability. Most of these research efforts are solely model-based. In this work, a signal-based approach for real-time detection of impending instability is considered. The main idea pursued here involves using a small additive white Gaussian noise as a probe signal and monitoring the spectral density of one or more measured states for certain signatures of impending instability. Input-to-state participation factors are introduced as a tool to aid in selection of locations for probe inputs and outputs to be monitored. Since these participation factors are model-based, the chapter combines signal-based and model-based ideas toward achieving a robust methodology for instability monitoring.

**Keywords:** Monitoring, power systems, stability, instability, precursors, bifurcation, voltage collapse, participation factors.

## 1. Introduction

Today's electric power systems are often subject to stress due to heavy loading conditions. Under such conditions, a power system that appears to be functioning well could actually be very vulnerable to loss of stability. Stability loss can, in turn, trigger a chain of events leading to failure of the system. Stability loss can occur in several forms, but the most common one resulting from heavy load conditions is voltage instability, which leads to voltage collapse through cascading of system events [11]. This differs markedly from transient instability following a system contingency, because this type of instability usually results from slow changes in system parameters, such as loading or generation. There is an inherent difficulty in predicting voltage instability, because the parameter values at which it occurs depend on component dynamics in an uncertain and complex interconnected system. Inaccurate system models can easily yield incorrect results for the stability envelope of the system. When a system must be operated near its stability limits, any model uncertainty can result in the system exiting its stable operating regime without warning. Even the most detailed calculations are insufficient in these circumstances.

In this chapter, instability monitoring using (noisy) probe signals is considered. The use of probe signals is shown to help reveal an impending loss of stability. This is because probe signals propagate in the power system and give certain signatures near an instability that can be used as warning signals for possible impending voltage collapse. Such warning signals are needed to alert system operators of a situation that may require preventive control, and to provide the operators with valuable additional time to take necessary preventive (rather than corrective) measures.

The chapter proceeds as follows. In Section 2, participation factors for linear systems are discussed. This includes both the modal participation factors, and newly introduced input-to-state participation factors. In Section 3, a signal-based approach to instability monitoring is presented. In Section 4, three case studies are given that demonstrate the proposed approach to instability monitoring. Concluding remarks are collected in Section 5.

## 2. Participation Factors

As mentioned above, the approach to instability monitoring presented in this chapter involves injecting probe signals at certain locations in a power network and monitoring the effects on measured output variables. Participation factors, specifically input-to-state participation factors in-

troduced in this section, play an important role in selection of sites for probe signal injection and output measurement. Because of this, a brief summary of modal participation factors is given first, along with a derivation of input-to-state modal participation factors. This will be helpful background in the discussion of precursor-based monitoring in the next section.

Participation factors are nondimensional scalars that measure the interaction between the modes and the state variables of a linear system [9, 12, 2]. Since their introduction in [9, 12], participation factors have been used for analysis, order reduction, and controller design in a variety of fields, especially electric power systems.<sup>1</sup>

## 2.1 Modal participation factors

Consider a general continuous-time linear time-invariant system

$$\dot{x} = Ax(t) \quad (8.1)$$

where  $x \in \mathbb{R}^n$ , and  $A$  is a real  $n \times n$  matrix. Suppose that  $A$  has a set of  $n$  distinct eigenvalues  $(\lambda_1, \lambda_2, \dots, \lambda_n)$ . Let  $(r^1, r^2, \dots, r^n)$  be right eigenvectors of the matrix  $A$  associated with the eigenvalues  $(\lambda_1, \lambda_2, \dots, \lambda_n)$ , respectively. Let  $(l^1, l^2, \dots, l^n)$  denote left (row) eigenvectors of the matrix  $A$  associated with the eigenvalues  $(\lambda_1, \lambda_2, \dots, \lambda_n)$ , respectively.

The right and left eigenvectors are taken to satisfy the normalization

$$l^i r^j = \delta_{ij}$$

where  $\delta_{ij}$  is the Kronecker delta

$$\delta_{ij} = \begin{cases} 1 & i = j \\ 0 & i \neq j \end{cases}$$

The definition of modal participation factors is as follows. The participation factor of the  $i$ -th mode in the  $k$ -th state is defined to be the complex number

$$p_{ki} := l_k^i r_k^i$$

This formula also gives the participation of the  $k$ -th state in the  $i$ -th mode. Participation factors measure the level of participation of modes in states and the level of participation of states in modes. The participation factors are dimensionless quantities that are independent of the units in which state variables are measured [9, 12, 2].

<sup>1</sup>In [2], a new approach to defining modal participation factors was presented. The new approach involved taking an average or a probabilistic expectation of a quantitative measure of relative modal participation over an uncertain initial state vector. The new definitions were shown to reduce to the original definition of participation factors of [9, 12] if the initial state obeys a symmetry condition.

## 2.2 Input-to-state participation factors

The concept of participation factors of modes in states and vice versa has been extended to linear time invariant systems with inputs [16]

$$\dot{x} = Ax + Bu \quad (8.2)$$

$$y = Cx. \quad (8.3)$$

We consider the case where the input is applied to one component, say the  $q$ -th component, of the right side of (8.2) and only one state, say the  $k$ -th state, is measured. That is, in (8.2)-(8.3),  $B$  and  $C$  take the form

$$B = e^q = [0 \dots 0 \underbrace{1}_{q\text{-th}} 0 \dots 0]^T$$

$$C = (e^k)^T = [0 \dots 0 \underbrace{1}_{k\text{-th}} 0 \dots 0] \quad (8.4)$$

With this choice of  $C$  and  $B$ , in steady state the output in (8.3) (in the frequency domain) is given by

$$\begin{aligned} y(s) = x_k(s) &= C(sI - A)^{-1}Bu \\ &= \sum_{i=1}^n \frac{Cr^i l^i B}{s - \lambda_i} u(s) \\ &= \sum_{i=1}^n \frac{r_k^i l_q^i}{s - \lambda_i} u(s) \end{aligned} \quad (8.5)$$

We take

$$p_{qk}^i = |Cr^i l^i B| = |r_k^i l_q^i| \quad (8.6)$$

as the participation factor of mode  $i$  in state  $k$  when the input is applied to state  $q$ . We call this quantity the *input-to-state participation factor (ISPF)* for mode  $i$ , with measurement at state  $k$  and input applied to state  $q$ . Note that the ISPF is dimensionless given that the input and output vectors  $B$  and  $C$  take the special form in (8.4). In [8], the quantity  $p_{qk}^i = r_k^i l_q^i$  is called a generalized participation.

## 3. Precursor-Based Monitoring

As noted by Hauer [5], the recurring problems of system oscillations and voltage collapse are due in part to system behavior not well captured by the models used in planning and operation studies. In the face of component failures, system models quickly become mismatched to the physical network, and are only accurate if they are updated using a

powerful and accurate failure detection system. Therefore, it is important to employ nonparametric techniques for instability monitoring. In this work, noisy probe signals are used to help detect impending loss of stability.

Recently, Kim and Abed [7] developed monitoring systems for detecting impending instability in nonlinear systems. The work builds on Wiesenfeld's research on "noisy precursors of bifurcations," which were originally introduced to characterize and employ the noise amplification properties of nonlinear systems near various types of bifurcations [14, 15]. Noisy precursors are features of the power spectral density (PSD) of a measured output of a system excited by additive white Gaussian noise (AWGN). In [7], the noisy precursors concept was extended from systems operating at limit cycles to systems operating near equilibria, and closed-loop monitoring systems were developed to facilitate use of noisy precursors in revealing impending loss of stability for such systems. It was shown in [7] that systems driven by white noise and operating near an equilibrium point exhibit sharply growing peaks near certain frequencies as the system nears a bifurcation. In particular, it was shown that for stationary bifurcation where an eigenvalue passes through the origin (as in the case of pitchfork or transcritical bifurcation), the peak in the PSD occurs at zero frequency. Analogously, for the case of Hopf bifurcation (complex conjugate pair of eigenvalues crossing the imaginary axis transversely), the peak in the PSD occurs near  $\omega_c$ , the critical frequency of the Hopf bifurcation.

In this work, we show that noisy precursors can be used as a warning signal indicating that the power system is operating dangerously close to instability. We also show that the spectrum of a measured state of the system is proportional to the square of the input-to-state participation factors. Thus, ISPFs can be used to determine the best location for applying the probe signal and for choosing which state to measure where the noisy precursor would be most apparent. Figure 8.1 shows a schematic diagram of our instability monitoring technique.

Consider a nonlinear dynamic system ("the plant")

$$\dot{x} = f(x, \mu) + \xi(t) \quad (8.7)$$

where  $x \in R^n$ ,  $\mu$  is a bifurcation parameter, and  $\xi(t) \in R^n$  is a zero-mean vector white Gaussian noise process [7]. Let the system possess an equilibrium point  $x_0$ . For small perturbations and noise, the dynamical behavior of the system can be described by the linearized system in the vicinity of the equilibrium point  $x_0$ . The linearized system corresponding to (8.7) with a small noise forcing  $\xi(t)$  is given by

$$\dot{x} = Df(x_0, \mu)x + \xi(t) \quad (8.8)$$

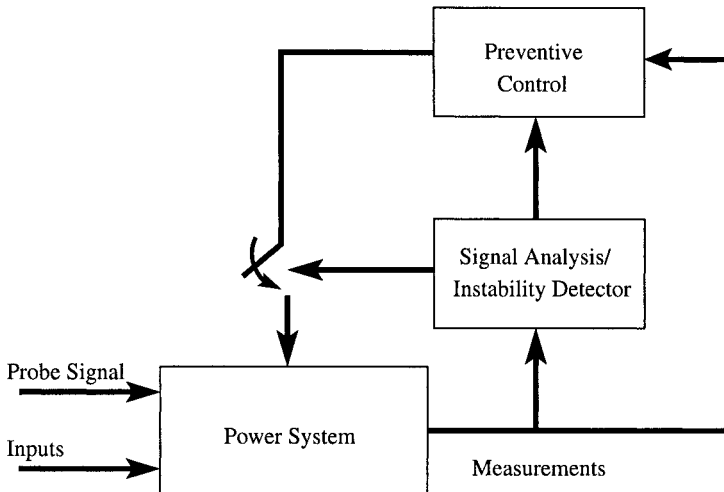


Figure 8.1. Precursor-based instability monitor with external probe signal.

where  $x$  now denotes  $x - x_0$  (the state vector referred to  $x_0$ ). For the results of the linearized analysis to have any bearing on the original nonlinear model, we must assume that the noise is of small amplitude.

The noise  $\xi(t)$  can occur naturally or can be injected using available controls. We consider the case where the noise is applied to one state and the power spectral density of another state is calculated. That is, we consider the case where  $\xi(t) = B\eta(t)$  with  $B = e^q = [0 \dots 0 \underbrace{1}_{q-th} 0 \dots 0]^T$ ,

$\eta(t)$  is a scalar white Gaussian noise with zero mean and power  $\sigma^2$ , and the output is given by  $y = Cx$  with  $C = (e^p)^T = [0 \dots 0 \underbrace{1}_{p-th} 0 \dots 0]$ .

In steady state, the output of system (8.8) forced by a small AWGN is given by

$$\begin{aligned}
 y(s) = x_p(s) &= \sum_{i=1}^n \frac{Cr^i l^i B}{s - \lambda_i} \eta(s) \\
 &= \sum_{i=1}^n \frac{r_p^i l^i}{s - \lambda_i} \eta(s)
 \end{aligned} \tag{8.9}$$

The power spectral density of the output of a linear system with the transfer function  $H(j\omega)$  is related to the power spectral density of the input by [6]

$$S_y(\omega) = H(j\omega)H(-j\omega)S_\eta(\omega) \tag{8.10}$$

Thus, the power spectrum of the  $p$ -th state is given by

$$\begin{aligned} S_{x_p} &= \left( \sum_{i=1}^n \frac{r_p^i l_q^i}{j\omega - \lambda_i} \right) \left( \sum_{k=1}^n \frac{r_p^k l_q^k}{-j\omega - \lambda_k} \right) \sigma^2 \\ &= \sigma^2 \sum_{i=1}^n \sum_{k=1}^n \frac{r_p^i l_q^i}{j\omega - \lambda_i} \frac{r_p^k l_q^k}{-j\omega - \lambda_k} \end{aligned} \quad (8.11)$$

Suppose that the system is nearing a Hopf bifurcation. Specifically, assume that a complex conjugate pair of eigenvalues is close to the imaginary axis, and has relatively small negative real part in absolute value compared to other system eigenvalues. Denote this pair as  $\lambda_{1,2} = -\epsilon \pm j\omega_c$ , with  $\epsilon > 0$  small and  $\omega_c > 0$ :

$$|Re(\lambda_i)| \gg \epsilon, \quad i = 3, \dots, n. \quad (8.12)$$

Under this assumption,  $S_{x_p}(\omega)$  can be approximated as

$$\begin{aligned} S_{x_p}(\omega) &\approx \sigma^2 \sum_{i=1}^2 \sum_{k=1}^2 \frac{r_p^i l_q^i}{j\omega - \lambda_i} \frac{r_p^k l_q^k}{-j\omega - \lambda_k} \\ &= \sigma^2 \left( \frac{1}{\epsilon + j(\omega - \omega_c)} \frac{1}{\epsilon - j(\omega + \omega_c)} (r_p^1 l_q^1)^2 \right. \\ &\quad + \frac{1}{\epsilon + j(\omega + \omega_c)} \frac{1}{\epsilon - j(\omega - \omega_c)} (r_p^2 l_q^2)^2 \\ &\quad + \frac{1}{\epsilon + j(\omega - \omega_c)} \frac{1}{\epsilon - j(\omega - \omega_c)} r_p^1 l_q^1 r_p^2 l_q^2 \\ &\quad \left. + \frac{1}{\epsilon + j(\omega + \omega_c)} \frac{1}{\epsilon - j(\omega + \omega_c)} r_p^1 l_q^1 r_p^2 l_q^2 \right) \\ &= \sigma^2 \left( \frac{|r_p^1 l_q^1|^2}{\epsilon^2 + (\omega - \omega_c)^2} + \frac{|r_p^1 l_q^1|^2}{\epsilon^2 + (\omega + \omega_c)^2} \right. \\ &\quad \left. + 2\text{Re} \left\{ \frac{1}{\epsilon + j(\omega - \omega_c)} \frac{1}{\epsilon - j(\omega + \omega_c)} (r_p^1 l_q^1)^2 \right\} \right) \end{aligned} \quad (8.13)$$

Here,  $r_p^i$  denotes the  $p$ -th component of the  $i$ -th right eigenvector  $r^i$  (the eigenvector corresponding to  $\lambda_i$ ), and  $l_q^i$  denotes the  $q$ -th component of the  $i$ -th left eigenvector  $l^i$ . Note that all terms containing  $\lambda_i$ ,  $i = 3, \dots, n$  have been neglected and only terms containing the critical eigenvalues  $\lambda_1$  and  $\lambda_2$  have been retained. After algebraic manipulation and substituting  $(r_p^1 l_q^1)^2 = \alpha + j\beta$  where  $\alpha = |r_p^1 l_q^1|^2 \cos(2\theta_{pq})$  and  $\beta = |r_p^1 l_q^1|^2 \sin(2\theta_{pq})$ , with  $\theta_{pq} = \tan^{-1}(\text{Im}\{r_p^1 l_q^1\}/\text{Re}\{r_p^1 l_q^1\})$ , the power

spectral density of  $x_p$  can be rewritten as

$$\begin{aligned}
 S_{x_p}(\omega) &= \sigma^2 |r_p^1 l_q^1|^2 \left( \frac{1}{\epsilon^2 + (\omega - \omega_c)^2} + \frac{1}{\epsilon^2 + (\omega + \omega_c)^2} \right) \\
 &\quad + \sigma^2 \frac{(\beta\epsilon + \alpha\omega_c)(\omega - \omega_c) + \epsilon(\epsilon\alpha - \omega_c\beta)}{(\epsilon^2 + \omega_c^2)(\epsilon^2 + (\omega - \omega_c)^2)} \\
 &\quad - \sigma^2 \frac{(\beta\epsilon + \alpha\omega_c)(\omega + \omega_c) - \epsilon(\epsilon\alpha - \omega_c\beta)}{(\epsilon^2 + \omega_c^2)(\epsilon^2 + (\omega + \omega_c)^2)} \\
 &= \sigma^2 |r_p^1 l_q^1|^2 \left[ (1 + G_1(\omega)) \frac{1}{\epsilon^2 + (\omega - \omega_c)^2} \right. \\
 &\quad \left. + (1 - G_2(\omega)) \frac{1}{\epsilon^2 + (\omega + \omega_c)^2} \right] \tag{8.14}
 \end{aligned}$$

where

$$G_1(\omega) = \frac{(\epsilon \sin(2\theta_{pq}) + \omega_c \cos(2\theta_{pq}))(\omega - \omega_c) + \epsilon(\epsilon \cos(2\theta_{pq}) - \omega_c \sin(2\theta_{pq}))}{\epsilon^2 + \omega_c^2}$$

$$G_2(\omega) = \frac{(\epsilon \sin(2\theta_{pq}) + \omega_c \cos(2\theta_{pq}))(\omega + \omega_c) - \epsilon(\epsilon \cos(2\theta_{pq}) - \omega_c \sin(2\theta_{pq}))}{\epsilon^2 + \omega_c^2}$$

For  $\omega = \omega_c$  and sufficiently small  $\epsilon$  ( $\epsilon \ll \omega_c$ ), the power spectral density of  $x_p$  is given by

$$S_{x_p}(\omega) = \sigma^2 |r_p^1 l_q^1|^2 \left( \frac{1}{\epsilon^2} + O\left(\frac{1}{\epsilon}\right) + O(1) \right) \tag{8.15}$$

Note that the ISPFs are related to the spectral densities of the states of a system driven by small AWGN as in (8.14). The amplitude of the spectrum is proportional to the square of the ISPFs. The input-to-state participation factors can be used to determine the best location for applying the probe signal and also the state that will have the highest spectral peak.

## 4. Case Studies

Below, the instability monitoring technique presented above is demonstrated on sample power system models. First, a single generator with dynamic load is considered. Then, a single generator with an infinite bus together with excitation control is considered. Finally, a three-generator nine-bus power system model is considered.

## 4.1 Single-generator system with dynamic load

Consider the single-generator power system model with induction motor load [13]

$$\dot{\delta}_m = \omega \quad (8.16)$$

$$M\dot{\omega} = -d_m\omega + P_m - E_m V Y_m \sin(\delta_m - \delta) \quad (8.17)$$

$$K_{q\omega}\dot{\delta} = -K_{qv2}V^2 - K_{qv}V + Q(\delta_m, \delta, V) - Q_0 - Q_1 \quad (8.18)$$

$$\begin{aligned} TK_{q\omega}K_{pv}\dot{V} &= K_{pw}K_{qv2}V^2 + (K_{pw}K_{pv} - K_{q\omega}K_{pv})V \\ &\quad + K_{q\omega}(P(\delta_m, \delta, V) - P_0 - P_1) \\ &\quad - K_{pw}(Q(\delta_m, \delta, V) - Q_0 - Q_1) \end{aligned} \quad (8.19)$$

The state variables are  $\delta_m$  (the generator phase angle, closely related to the mechanical angle of the generator rotor),  $\omega$  (the rotor speed),  $\delta$  (the load voltage phase angle), and  $V$  (the magnitude of the load voltage). The load includes a constant  $PQ$  load in parallel with an induction motor. The real and reactive powers supplied to the load by the network are

$$\begin{aligned} P(\delta_m, \delta, V) &= -E'_0 V Y'_0 \sin(\delta) + E_m V Y_m \sin(\delta_m - \delta) \\ Q(\delta_m, \delta, V) &= E'_0 V Y'_0 \cos(\delta) + E_m V Y_m \cos(\delta_m - \delta) \\ &\quad - (Y'_0 + Y_m)V^2 \end{aligned}$$

where

$$\begin{aligned} E'_0 &= \frac{E_0}{\sqrt{1 + C^2 Y_0^{-2} - 2CY_0^{-1} \cos \theta_0}} \\ Y'_0 &= Y_0 \sqrt{1 + C^2 Y_0^{-2} - 2CY_0^{-1} \cos \theta_0} \\ \theta'_0 &= \theta_0 + \tan^{-1} \left\{ \frac{CY_0^{-1} \sin \theta_0}{1 - CY_0^{-1} \cos \theta_0} \right\} \end{aligned}$$

The values of the parameters for this model are given in the appendix.

It has been shown that a supercritical Hopf bifurcation occurs in this power system model as the reactive load  $Q_1$  is increased through the critical value  $Q_1^* = 2.980138$  [13].

Next, we consider the system operating at loads close to the Hopf bifurcation, say at  $Q_1 = 2.9$ . The corresponding operating point is  $x_0 = [0.2473, 0, 0.0398, 0.9248]$ . The Jacobian of the system at this

operating point is

$$A = \begin{bmatrix} 0 & 1 & 0 & 0 \\ -324.5254 & -3.4153 & 324.5254 & -73.8611 \\ 33.3333 & 0 & -29.2479 & 72.7220 \\ -3.3656 & 0 & 1.5180 & -11.1529 \end{bmatrix}$$

The eigenvalues of  $A$  are  $\{-0.7923 \pm j6.6318, -21.1157 \pm j10.9959\}$ .

To monitor the system, an AWGN probe signal is applied to the mechanical power  $P_m$ . Figure 8.2 depicts the spectral densities for the four states  $\delta_m$ ,  $\omega$ ,  $\delta$ , and  $V$  for  $Q_1 = 2.9$  and  $\sigma = 0.001$ . As it is clear from this figure, the state  $\omega$  has a higher peak than all other states. Figure 8.3 demonstrates the variation of the spectral density peak near  $\omega = \omega_c \approx 6.6$  rad/s as a function of the bifurcation parameter  $Q_1$ . The values of the input-to-state participation factors of the critical mode in all states are given in Table 8.1. As predicted by the analysis in Section 3, the ordering of the peaks of the spectral densities of all states at  $\omega_c$  can be predicted from the values of the ISPFs.

Table 8.1. Input-to-state participation factors and spectral peaks at  $\omega_c$ .

States	Spectral peak at $\omega_c \approx 6.6318$	Input-to-state participation factors (ISPFs)
$\delta_m$	$9.528 \times 10^{-4}$	$p_{21}^1 = 2.8992$
$\omega$	$40.38 \times 10^{-4}$	$p_{22}^1 = 19.364$
$\delta$	$6.616 \times 10^{-4}$	$p_{23}^1 = 2.4013$
$V$	$0.305 \times 10^{-4}$	$p_{24}^1 = 0.4981$

## 4.2 Single generator connected to an infinite bus

Consider a synchronous machine connected to an infinite bus together with excitation control [1]. It was shown [1] that this system undergoes a Hopf bifurcation as the control gain in the excitation system is increased beyond a critical value. The dynamics of the generator are given by

$$\dot{\delta} = \omega \quad (8.20)$$

$$2H\dot{\omega} = -D\omega + \omega_0(P_m - P_e) \quad (8.21)$$

$$\tau'_d \dot{E}'_q = E_{FD} - E'_q - (X_d - X'_d)i_d \quad (8.22)$$

with the algebraic equations

$$P_e = E_q i_q$$

$$E_q = E'_q + (X_q - X'_d)i_d$$

$$i_d = x(E_q - E \cos \delta) - rE \sin \delta$$

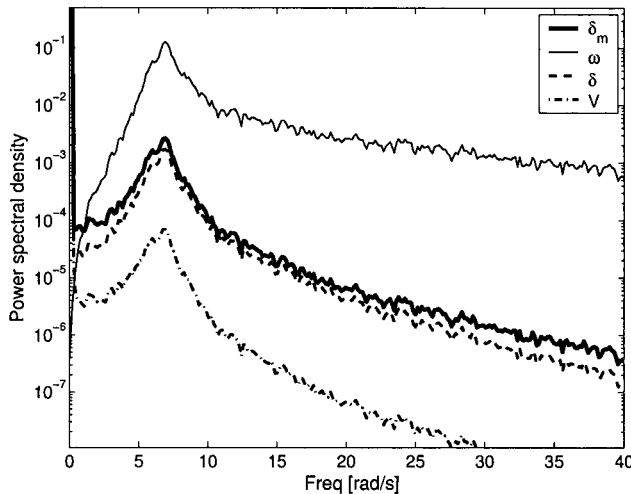


Figure 8.2. Power spectral densities of the states of the model given in (8.16)-(8.19). The bifurcation parameter was set to  $Q_1 = 2.9$ . White Gaussian noise of zero mean and  $(0.001)^2$  power was added to  $P_m$ .

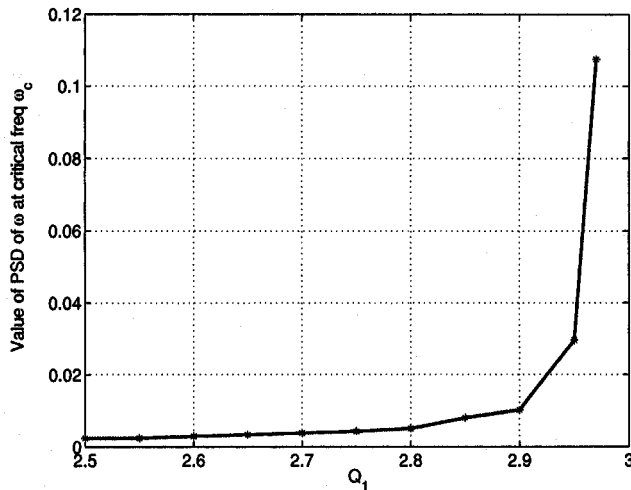


Figure 8.3. Variation of the peak value of the power spectral density of  $\omega$  as a function of the bifurcation parameter  $Q_1$ . White Gaussian noise of zero mean and  $(0.001)^2$  power was added to  $P_m$ .

$$\begin{aligned}
 i_q &= r(E_q - E \cos \delta) + xE \sin \delta \\
 x &= \frac{X_l + X_q}{R_l^2 + (X_l + X_q)^2} \\
 r &= \frac{R_l}{R_l^2 + (X_l + X_q)^2}
 \end{aligned}$$

The subscripts  $d$  and  $q$  refer to the direct and quadrature axes, respectively. The dynamics of the excitation control are given by

$$\tau_E \dot{E}_{FD} = -K_E E_{FD} + V_R - E_{FD} S_E(E_{FD}) \quad (8.23)$$

$$\tau_F \dot{V}_3 = -V_3 + \frac{K_F}{\tau_E} (-K_E E_{FD} + V_R - E_{FD} S_E(E_{FD})) \quad (8.24)$$

$$\tau_A \dot{V}_R = -V_R + K_A (V_{REF} - V_t - V_3) \quad (8.25)$$

Here  $V_t$  is the terminal voltage and is given by

$$V_t^2 = v_d^2 + v_q^2$$

where

$$-v_d = \psi_q = -X_q i_q, \quad v_q = \psi_d = E'_q - X'_d i_d.$$

The saturation function  $S_E(E_{FD})$  is usually approximated as  $S_E(E_{FD}) = A_{EX} \exp(B_{EX} E_{FD})$ . An equilibrium point of this system is denoted by  $x^0 = (\delta^0, \omega^0, E'_q{}^0, E_{FD}^0, V_3^0, V_R^0)$ . The values of the parameters that appear in this power system model are given in Table 8.A.1.

For  $P_m = 0.937$ ,  $V_{REF} = 1.130$ ,  $\lambda = 2$ , it has been shown that a subcritical Hopf bifurcation occurs at  $K_A^* = 193.74$  [1].

Next, we consider the system operating before the Hopf bifurcation, say at  $K_A = 185$ . The corresponding operating point is given by  $x^0 = [1.3515, 0, 1.1039, 2.3150, 0, 0.5472]^T$ . The Jacobian of the system at this operating point is

$$A = \begin{bmatrix} 0 & 1 & 0 & 0 & 0 & 0 \\ -62.2 & -0.2 & -79.7 & 0 & 0 & 0 \\ -0.2 & 0 & -0.4 & 0.2 & 0 & 0 \\ 0 & 0 & 0 & -1.1 & 0 & 2 \\ 0 & 0 & 0 & 0 & -1.7 & 0.1 \\ 125.9 & 0 & -1157.6 & 0 & -1850 & -10 \end{bmatrix}$$

The eigenvalues of  $A$  are  $\{-0.0139 \pm j7.7707, -4.5832 \pm j12.6178, -2.1029 \pm j0.9417\}$ .

Note that for this model, there are two physically feasible locations for applying the probe signal. The probe signal can be either applied to  $V_{ref}$  or to  $P_m$ . The input-to-state participation factors are used to determine the best location for applying the probe signal. From the values of the ISPFs (see Table 8.2), it is clear that mode 1 has higher participation in other states when the probe signal is applied to  $P_m$  than when applied to  $V_{ref}$ . This can be also seen from the power spectral densities shown in Figures 8.4 and 8.5. Also, the ISPFs give an indication of which state

to monitor. The higher the participation factor of the critical mode in a state, the higher the peak of the spectrum for that state. Figure 8.6 shows the variation of the power spectral peak at the critical frequency as a function of the bifurcation parameter when noise is added to  $P_m$ .

Table 8.2. Input-to-state participation factors and spectral peaks at  $\omega_c$  for the single generator connected to an infinite bus.

State	Spectral peak at $\omega \approx 7.8$ (noise added to $P_m$ )	ISPFs	Spectral peak at $\omega \approx 7.8$ (noise added to $V_{ref}$ )	ISPFs
$\delta$	0.0226	$p_{21}^1 = 0.0648$	0.0019	$p_{61}^1 = 0.0024$
$\omega$	1.2880	$p_{22}^1 = 0.4923$	0.1084	$p_{62}^1 = 0.0185$
$E'_q$	$0.75938 \times 10^{-4}$	$p_{23}^1 = 0.0038$	$0.68651 \times 10^{-5}$	$p_{63}^1 = 0.0001$
$E_{FD}$	0.2326	$p_{24}^1 = 0.2084$	0.0210	$p_{64}^1 = 0.0078$
$V_3$	$2.4644 \times 10^{-4}$	$p_{25}^1 = 0.0068$	$2.2288 \times 10^{-5}$	$p_{65}^1 = 0.0003$
$V_R$	3.3923	$p_{26}^1 = 0.8006$	0.3064	$p_{66}^1 = 0.0301$

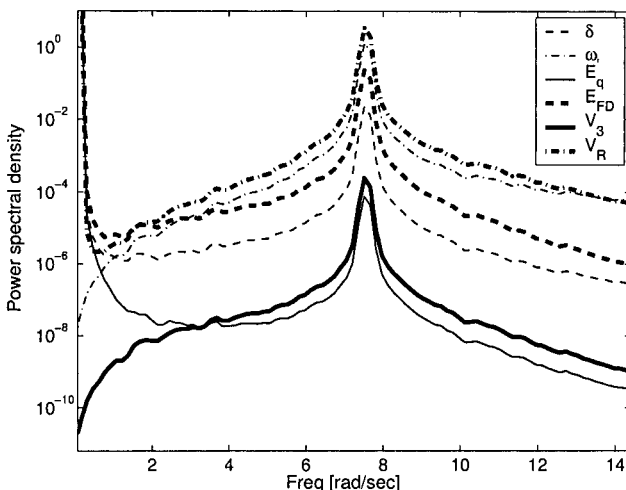


Figure 8.4. Power spectral densities of the states of the single generator connected to an infinite bus system. The bifurcation parameter was set to  $K_A = 185$ . White Gaussian noise of zero mean and  $(0.000032)^2$  power was added to  $P_m$ .

#### 4.3 Three-generator nine-bus power system

Below, we consider the Western System Coordinating Council (WSCC) 3-machine, 9-bus power system model, which is widely used in the literature [10, pp. 170–177],[3]. The dynamics of this model includes three

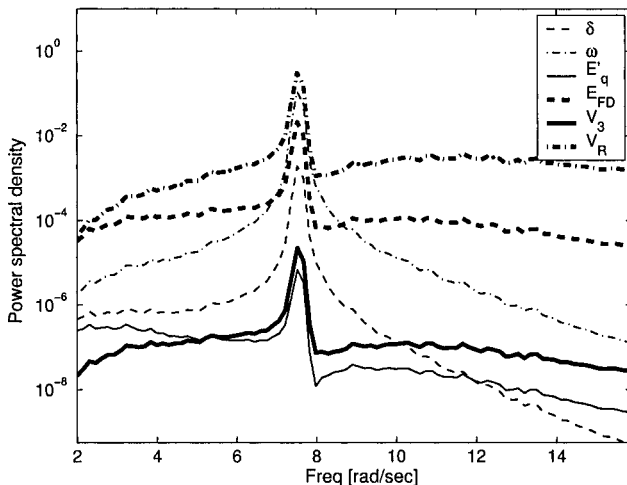


Figure 8.5. Power spectral densities of the states of the single generator connected to an infinite bus system. The bifurcation parameter was set to  $K_A = 185$ . White Gaussian noise of zero mean and  $(0.000032)^2$  power was added to  $V_{ref}$ .

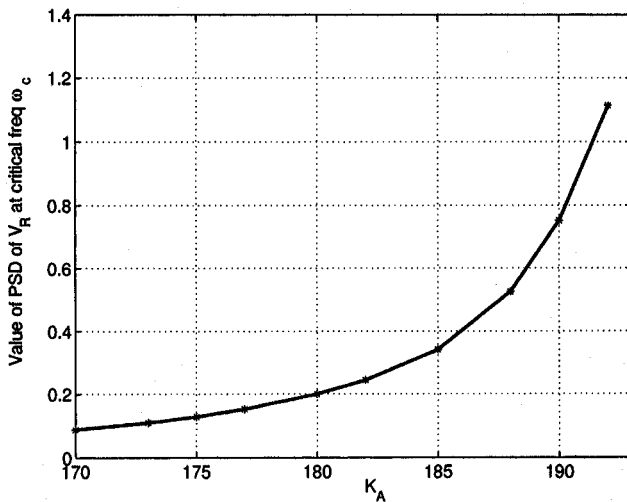


Figure 8.6. Variation of the peak value of the power spectral density of  $V_R$  as a function of the bifurcation parameter  $K_A$ . White Gaussian noise of zero mean and  $(0.000032)^2$  power was added to  $P_m$ .

identical IEEE-Type I exciters for the three machines. The machine data and the exciter data are given in [10, 3].

In this model, a subcritical Hopf bifurcation occurs as the load on Bus 5 is increased beyond 4.5 pu [10]. Our goal in this case study is to de-

tect this impending loss of stability by using an AWGN probe signal and continuously monitoring the power spectral densities of certain states. This would give the system operator (or an automatic controller) valuable time to take appropriate preventive measures (e.g., shedding loads at certain buses). The simulations of this model were conducted using PSAT [3]. For values of the load on Bus 5 close to 4.0 pu, the linearization of the system at the operating point has two complex conjugate pair of eigenvalues close to the imaginary axis,  $\lambda_{1,2} = -0.17665 \pm j8.184$  and  $\lambda_{3,4} = -0.3134 \pm j1.7197$ . As the load on Bus 5 is increased further, the pair  $\lambda_{3,4}$  approaches the imaginary axis, while the other pair  $\lambda_{1,2}$  changes only slightly. For example, when the load at Bus 5 is 4.4 pu,  $\lambda_{1,2} = -0.18231 \pm j8.0978$  and  $\lambda_{3,4} = -0.04602 \pm j2.1151$ . Increasing the load on Bus 5 beyond 4.5 pu causes the pair  $\lambda_{3,4}$  to cross the imaginary axis from left to right.

From the values of the ISPFs calculated for this system, we found that both of the critical modes have higher participation when the probe signal is applied to  $P_{m_3}$ , the mechanical power of generator 3. Also, we found that these modes have high participation in the field voltage of the excitors. Therefore, in the following simulations, the probe signal is added to  $P_{m_3}$  and the power spectral densities of the field voltages of the three excitors (i.e.,  $E_{fd_i}, i = 1, 2, 3$ ) are monitored. Figures 8.7 and 8.8 show the power spectral densities of  $E_{fd_i}, i = 1, 2, 3$ , when the load on Bus 5 ( $P_{L_5}$ ) is 4.0 p.u. and 4.4 p.u., respectively. It is clear from Figure 8.7 that when the load on Bus 5 is 4.0 p.u., the spectrum has two peaks at 0.28 Hz and 1.3 Hz. These two frequencies correspond to the complex eigenvalues  $\lambda_{3,4}$  and  $\lambda_{1,2}$ , respectively. Note that the peak at 1.3 Hz that corresponds to the pair of complex eigenvalues  $\lambda_{1,2}$  is higher than the peak at 0.28 Hz. However, when the load at Bus 5 is increased to 4.4 p.u., the peak at 0.28 Hz becomes much larger than the one at 1.3 Hz (see Figure 8.8), which is an indicator that an instability is being approached. Figure 8.9 shows the power spectral density of  $E_{fd_1}$  for three values of  $P_{L_5}$ : 4.0 p.u., 4.25 p.u., and 4.4 p.u.

## 5. Conclusions and Suggested Future Research

An instability monitoring technique that aims at detection of impending instability has been described and illustrated in several example systems. The theme of the approach is to provide a warning when the margin of stability of a power system is compromised, without dependence on availability of an accurate system model. The approach consists of using additive white Gaussian noise probe signals and monitoring the spectral densities of certain measured states. Models are used in the ap-

Table 8.3. Input-to-state participation factors for the 3-machine nine-bus system (partial listing). The load at Bus 5 is 4.4 p.u.

Input noise added to	States measured					
	$E_{fd_1}$	$E_{fd_2}$	$E_{fd_3}$	$\omega_1$	$\omega_2$	$\omega_3$
$P_{m_1}$	3.0017	2.6973	2.1357	0.0033	0.0028	0.0031
$P_{m_2}$	2.6113	2.3465	1.858	0.0029	0.0024	0.0027
$P_{m_3}$	4.7816	4.2967	3.4022	0.0052	0.0044	0.0049
$V_{ref_1}$	0.0155	0.014	0.0111	0.0000169	0.0000143	0.000016
$V_{ref_2}$	0.0233	0.021	0.0166	0.0000255	0.0000215	0.00002409
$V_{ref_3}$	0.0475	0.0427	0.0338	0.0000519	0.000043	0.000049

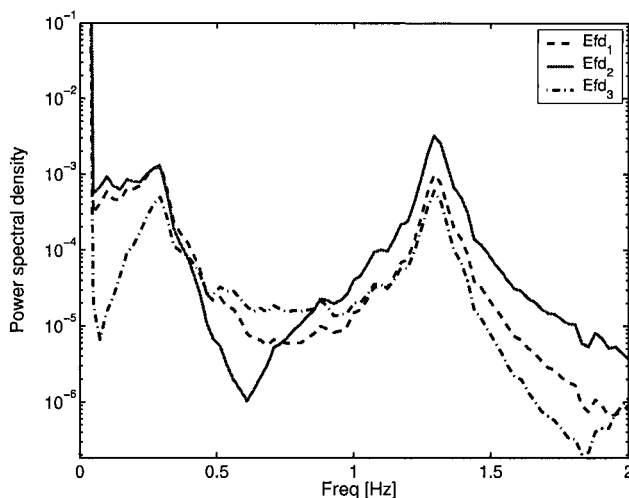


Figure 8.7. Power spectral densities of the states  $E_{fd_1}$ ,  $E_{fd_2}$ , and  $E_{fd_3}$ . The load on Bus 5 was used as a bifurcation parameter. The load value is 4.0 p.u. White Gaussian noise of zero mean and 0.05 power was added to  $P_{m_3}$ , the mechanical power of generator 3.

proach in the selection of sites for probe signal injection and monitored output signal measurement (akin to actuator and sensor placement in control design). Input-to-state participation factors were presented and used as a tool for selection of probe and measurement siting.

The methods presented here are mathematically based but address engineering problems that are not easily defined in a crisp form. There are several directions that can be pursued for furthering the aims of this chapter.

A particularly challenging problem involves detection not only of the fact that an instability is near, but also detecting the severity of the

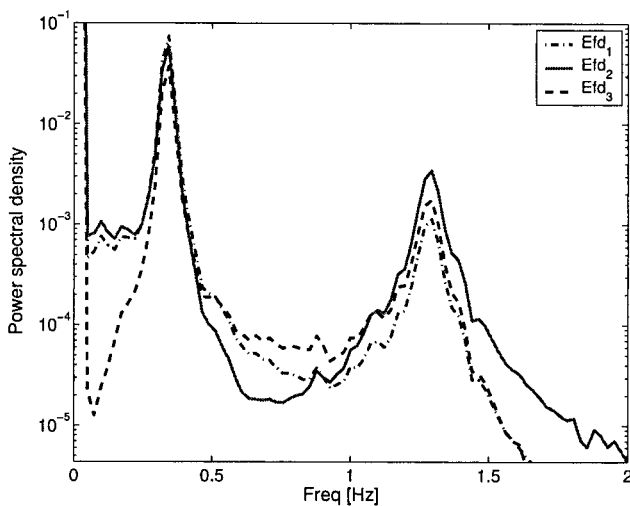


Figure 8.8. Power spectral densities of the states  $E_{fd_1}$ ,  $E_{fd_2}$ , and  $E_{fd_3}$ . The load on Bus 5 was used as a bifurcation parameter. The load value is 4.4 p.u. White Gaussian noise of zero mean and 0.05 power was added to  $P_{m_3}$ , the mechanical power of generator 3.

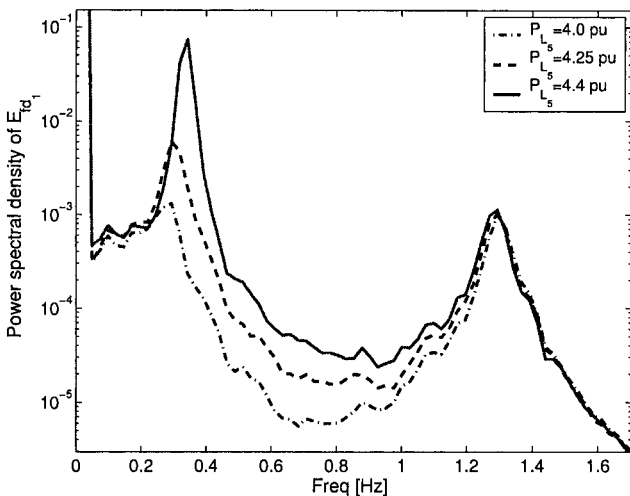


Figure 8.9. Power spectral density of  $E_{fd_1}$  for three values of  $P_{L_5}$  (the load on Bus 5):  $P_{L_5} = 4.0$  p.u. (dash-dotted line),  $P_{L_5} = 4.25$  p.u. (dashed line), and  $P_{L_5} = 4.4$  p.u. (solid line). White Gaussian noise of zero mean and 0.05 power was added to  $P_{m_3}$ , the mechanical power of generator 3.

impending instability from the point of view of nonlinear system behavior. For example, an oscillatory instability can be of the hunting type,

in which small amplitude oscillations occur, or it can be divergent, resulting in complete loss of operation. Although this can be determined using analytical models using known methods of bifurcation analysis, it is not known how this can be achieved using a signal-based approach.

Another direction involves studying use of other probe signals in addition to AWGN. Examples include periodic signals, chaotic signals covering an appropriate frequency range, and colored noise signals. The relative advantages and disadvantages of the various probe signals should be considered. In this regard, connections to past work in real-time probing of power systems and aircraft dynamics should be studied. In research aircraft, for example, it is common to use “chirp” signals to probe the aircraft for its stability properties in various parts of its flight envelope.

The integration of stability monitoring and fault detection is an important long-term research goal. In the meantime, it will be useful to pursue case studies that will shed light on what will be required to achieve this integration.

Finally, we mention the application of closed-loop monitoring systems to electric power system models. These designs, as described in [7], may provide added flexibility and surety to the conclusions reached regarding the presence of impending instability.

### Acknowledgments

This research was supported in part by the National Science Foundation under Grants ECS-01-15160 and ANI-02-19162.

## Appendix: Parameter Values for the Generators in Sections 4.1 and 4.2

### Parameters for the single generator model with dynamic load:

$M = 0.01464$ ,  $C = 3.5$ ,  $E_m = 1.05$ ,  $Y_0 = 3.33$ ,  $\theta_0 = 0$ ,  $\theta_m = 0$ ,  $K_{p\omega} = 0.4$ ,  $K_{pv} = 0.3$ ,  $K_{q\omega} = -0.03$ ,  $K_{qv} = -2.8$ ,  $K_{qv2} = 2.1$ ,  $T = 8.5$ ,  $P_0 = 0.6$ ,  $P_1 = 0.0$ ,  $Q_0 = 1.3$ ,  $E_0 = 1.0$ ,  $Y_m = 5.0$ ,  $P_m = 1.0$ ,  $d_m = 0.05$ .

All values are in per unit except for angles, which are in degrees.

### Parameters for the single generator model with an infinite bus:

The parameter values are given in Table 8.A.1.

Table 8.A.1. Parameter values for the single generator connected to an infinite bus model.

Synchronous machine	Exciter	Transmission line
$H = 2.37 \text{ s}$	$K_E = -0.05$	$R_l^0 = 0.02$
$D = 1 \text{ pu}$	$K_F = 0.02$	$X_l^0 = 0.40$
$X_d = 1.7$	$\tau_E = 0.50 \text{ s}$	$R_l = \lambda R_l^0$
$X'_d = 0.245$	$\tau_F = 0.60 \text{ s}$	$X_l = \lambda X_l^0$
$X_q = 1.64$	$\tau_A = 0.10 \text{ s}$	
$\omega_0 = 377.0 \text{ rad/s}$	$A_{EX} = 0.09$	
$\tau'_{d0} = 5.9 \text{ s}$	$B_{EX} = 0.50$	

## References

- [1] E.H. Abed and P.P. Varaiya. Nonlinear Oscillations in Power Systems. *International J. Electrical Power and Energy Systems*, 6:37–43, 1984.
- [2] E.H. Abed, D. Linsley, and W.A. Hashlamoun. On Participation Factors for Linear Systems. *Automatica*, 36:1489–1496, 2000.
- [3] F. Milano. *Power System Analysis Toolbox Documentation for PSAT, Version 1.3.0*. 2004 (available online at <http://www.power.uwaterloo.ca/~fmilano/>).
- [4] M.A. Hassouneh, H. Yaghoobi, and E.H. Abed. Monitoring and Control of Bifurcations using Probe Signals. In *Dynamics, Bifurcations and Control*, Lecture Notes in Control and Information Sciences, 273:51–65, F. Colonius and L. Gruene, Eds., Springer Verlag, Berlin, 2002.
- [5] J.F. Hauer and M.J. Beshir. Dynamic Performance Validation in the Western Power System. *Association of Power Exchanges*, Kananaskis, Alberta, Oct. 2000.
- [6] C.W. Helstrom. *Probability and Stochastic Processes for Engineers*, Second Edition. Macmillan, London, 1991.
- [7] T. Kim and E.H. Abed. Closed-Loop Monitoring Systems for Detecting Impending Instability. *IEEE Transactions on Circuits and Systems I: Fundamental Theory and Applications*, 47:1479–1493, 2000.
- [8] F.L. Pagola, I.J. Perez-Arriaga, and G.C. Verghese. On Sensitivities, Residues and Participations: Applications to Oscillatory Stability Analysis and Control. *IEEE Transactions on Power Systems*, 4:278–285, 1989.
- [9] I.J. Perez-Arriaga, G.C. Verghese, and F.C. Schweppe. Selective Modal Analysis with Applications to Electric Power Systems, Part I: Heuristic Introduction. *IEEE Transactions on Power Apparatus and Systems*, 101:3117–3125, 1982.

- [10] P.W. Sauer and M.P. Pai. *Power System Dynamics and Stability*. Prentice Hall, Englewood Cliffs, New Jersey, 1998.
- [11] T. Van Cutsem. Voltage Instability: Phenomena, Countermeasures, and Analysis Methods. *Proceedings of the IEEE*, 88:208–227, 2000.
- [12] G.C. Verghese, I.J. Perez-Arriaga and F.C. Schweppe. Selective Modal Analysis with Applications to Electric Power Systems, Part II: The Dynamic Stability Problem. *IEEE Transactions on Power Apparatus and Systems*, 101:3126–3134, 1982.
- [13] H.O. Wang, E.H. Abed, and A.M.A. Hamdan. Bifurcation, Chaos, and Crises in Voltage Collapse of a Model Power System. *IEEE Transactions on Circuits and Systems I*, 41:294–302, 1994.
- [14] K. Wiesenfeld. Noisy Precursors of Nonlinear Instabilities. *Journal of Statistical Physics*, 38:1071–1097, 1985.
- [15] K. Wiesenfeld. Virtual Hopf Phenomenon: A New Precursor of Period Doubling Bifurcations. *Physical Review A*, 32:1744–1751, 1985.
- [16] H. Yaghoobi and E.H. Abed. Optimal Actuator and Sensor Placement for Modal and Stability Monitoring. *Proceedings of the American Control Conference*, 3702–3707, San Diego, CA, June 1999.

## Chapter 9

# DYNAMIC EMBEDDED OPTIMIZATION AND SHOOTING METHODS FOR POWER SYSTEM PERFORMANCE ASSESSMENT

Ian A. Hiskens

*University of Wisconsin - Madison*

[hiskens@engr.wisc.edu](mailto:hiskens@engr.wisc.edu)

Jung-Wook Park

*University of Wisconsin - Madison*

[jungwookpark@ieee.org](mailto:jungwookpark@ieee.org)

Vaibhav Donde

*University of Illinois at Urbana-Champaign*

[donde@ieee.org](mailto:donde@ieee.org)

**Abstract** Power system dynamic performance enhancement can often be formulated as a dynamic embedded optimization problem. The associated cost function quantifies performance and involves dynamically evolving state variables. The dynamic model is embedded within the constraints. Power systems form an important example of hybrid systems, with interactions between continuous dynamics and discrete events playing a fundamental role in behavior. However, it is shown that for a large class of problems, the cost function is smooth even though the underlying dynamic response is non-smooth. Complementing this design-oriented optimization framework, techniques for assessing power system performance and vulnerability can often be expressed as boundary value problems, and solved using shooting methods. It is shown that performance limitations are closely related to grazing phenomena. Techniques are presented for determining parameter values that induce limit cycles and grazing.

**Keywords:** Power system dynamics, dynamic embedded optimization, boundary value problems, limit cycles, grazing phenomena, shooting methods.

## 1. Introduction

Design processes are inherently optimization problems, involving trade-offs between competing objectives, whilst ensuring constraints are satisfied. Such problems are not always established formally, nevertheless underlying optimization principles apply. Design questions arising from system dynamic behavior can also be thought of in an optimization framework. However, the optimization formulation in this case must capture the processes driving dynamics. This class of problems has come to be known as *dynamic embedded optimization*.

Examples of such problems abound in power systems. System operators are often faced with maximizing transmission utilization subject to stability constraints. Voltage collapse can be prevented by shedding load, but determining the correct amount and location involves trade-offs. Shedding too much load incurs the wrath of consumers, but insufficient shedding may not alleviate the problem. The August 2003 blackout in North America illustrated the potential consequences in the latter case [1].

Even the tuning of traditional controllers such as power system stabilizers (PSSs) involves trade-offs. The role of PSSs is to provide damping, so controller tuning focuses on small-signal conditions. As a consequence, performance during the transient period immediately following a large disturbance may be degraded. PSS output limiters attempt to balance these competing effects. It will be shown later that the tuning of these limiter values can be formulated as a dynamic embedded optimization problem.

In contrast to design, analysis of system dynamics is more aligned with understanding extremes of system behavior. Many analysis questions take the form of boundary value problems, which are solved using shooting methods. Two cases will be considered in the sequel, limit cycles and grazing phenomena.

Limit cycle behavior has been observed in power system operation [2]. Such behavior is usually undesirable, and tends to be induced by interactions between generator controllers. In many cases, linear techniques can be used to identify contributing factors, and to retune controls accordingly [3]. Other cases though are truly nonlinear, and may even involve controller limits, making them non-smooth. An example will be considered in Section 4.1. Often nonlinear limit cycles are unsta-

ble, and partially bound the region of attraction of the stable operating point. Linear analysis techniques are inappropriate in such cases. Also reverse-time simulation is unreliable, because it is common for such limit cycles to have saddle characteristics, i.e., attracting in some directions and repelling in others. However, it will be shown in Section 4.1 that limit cycles (even those that are non-smooth) can be formulated as a boundary value problem, and solved using a shooting method.

Power system dynamic behavior is generally subject to performance constraints that seek to ensure appropriate post-fault response. Otherwise excessive transients may trigger protection devices, outaging items of equipment, and possibly leading to cascading system failure [1]. Bounding cases, where the system trajectory just (tangentially) encounters a performance constraint, separate regions of desirable and undesirable behavior. Such tangential encounters are referred to as *grazing*.

Vulnerability to event triggering can be assessed by comparing given (nominal) parameter values with values that induce grazing. If a sufficient margin exists between actual and grazing values, then dynamic performance is guaranteed. Crucial to this assessment is the ability to determine grazing values. This problem can again be formulated as a boundary value problem. An appropriate shooting method is developed in Section 4.2.

## 2. Model

### 2.1 Hybrid systems

Interactions between continuous dynamics and discrete events are an intrinsic part of power system dynamic behavior. Devices that obey physical laws typically exhibit continuous dynamics; examples include generators and their controllers. On the other hand, event-driven discrete behavior is normally associated with rule-based components. Examples in this latter category include protection devices [4], tap-changing transformers [5] and supervisory control [6]. Limits within physical devices also fall into this category; an event occurs when a controller signal saturates, or a FACTS device encounters its maximum/minimum firing angle.

Power systems therefore provide an important application area for *hybrid systems*, i.e., systems that are characterized by:

- continuous and discrete states
- continuous dynamics
- discrete events, or triggers

- mappings that define the evolution of discrete states at events.

A simplified hybrid system representation has the form

$$\dot{x} = f_\rho(x), \quad \rho \in \mathcal{P} \quad (9.1)$$

with  $x(0) = x_0$ ,  $f_\rho : \mathbb{R}^n \rightarrow \mathbb{R}^n$ , and  $\mathcal{P}$  is some finite index set. An event occurs at time  $\tau$ , with the system in discrete state  $\rho(\tau) = i$ , if

$$s_{ij}(x(\tau)) = 0 \quad (9.2)$$

where  $s_{ij} : \mathbb{R}^n \rightarrow \mathbb{R}$  is the event triggering function. For well defined behavior, it must be assumed that event triggers are encountered transversally<sup>1</sup>,

$$\nabla s_{ij}^T \dot{x} = \nabla s_{ij}^T f_i \neq 0 \quad (9.3)$$

that event triggering cannot initiate an infinitely fast switching sequence (chattering)<sup>2</sup>, and that accumulation (Zeno) effects do not occur [8]. Under those conditions, event triggering results in

$$\rho(\tau^+) = j \quad (9.4)$$

$$x(\tau^+) = h_{ij}(x(\tau)) \quad (9.5)$$

where  $\tau^+$  refers to the time incrementally beyond switching time  $\tau$ . Equations (9.4)-(9.5) imply that at time  $\tau$  a transition  $f_i \rightarrow f_j$  occurs in the governing dynamics, and  $h_{ij}$  forces an impulsive step in the state. (No impulse occurs if  $h_{ij}(x) = x$  though.) The model induces the system flow

$$x(t) = \phi(t, x_0) \quad (9.6)$$

This simple model provides clarity in the development and discussion of subsequent algorithms. However it is generally inadequate for representing power systems. A more elaborate differential-algebraic model, which incorporates switching and impulse effects, is described in [9].

A compact development of optimization and shooting method algorithms results from incorporating parameters  $\lambda \in \mathbb{R}^\ell$  into the dynamic states  $x$ . (Numerical implementation is also simplified.) This is achieved by introducing trivial differential equations  $\dot{\lambda} = 0$  into (9.1), and results in the natural partitioning

$$x = \begin{bmatrix} \underline{x} \\ \lambda \end{bmatrix}, \quad f = \begin{bmatrix} f \\ 0 \end{bmatrix}, \quad h_j = \begin{bmatrix} h_j \\ \lambda \end{bmatrix} \quad (9.7)$$

where  $\underline{x}$  are the true dynamic states, and  $\lambda$  are parameters.

<sup>1</sup>Tangential encounters are associated with grazing bifurcations, discussed later.

<sup>2</sup>Chattering is indicative of sliding mode behavior, with Filippov [7] concepts required to define solutions.

## 2.2 Trajectory sensitivities

Optimization and shooting method algorithms require the sensitivity of a trajectory to perturbations in parameters and/or initial conditions [10]. To obtain the sensitivity of the flow  $\phi$  to initial conditions  $x_0$ , the Taylor series expansion of (9.6) is formed. Neglecting higher order terms gives

$$\delta x(t) = \frac{\partial x(t)}{\partial x_0} \delta x_0 \equiv \Phi(t, x_0) \delta x_0 \quad (9.8)$$

where  $\Phi$  is the *sensitivity transition matrix*, or *trajectory sensitivities*, associated with the flow of  $x$  [11]. Equation (9.8) describes the change  $\delta x(t)$  in a trajectory, at time  $t$  along the trajectory, for a given (small) change in initial conditions  $\delta x_0 = [\underline{\delta x}_0^T \ \delta \lambda^T]^T$ .

Along smooth sections of the trajectory (between events), the variational equations describing the evolution of the trajectory sensitivities are given by the linear time-varying system

$$\dot{\Phi} = Df_\rho(t)\Phi, \quad \Phi(0) = I \quad (9.9)$$

where  $Df \equiv \frac{\partial f}{\partial x}$  and  $I$  is the identity matrix. For large systems, these equations have high dimension. However the computational burden is minimal when an implicit numerical integration technique such as trapezoidal integration is used to generate the trajectory. Further details can be found in [12, 13, 14].

It is shown in [12] that at an event  $i \rightarrow j$ , occurring at time  $\tau$ , the trajectory sensitivities  $\Phi$  generically jump according to

$$\Phi(\tau^+, x_0) = Dh_{ij}\Phi(\tau^-, x_0) + (f_j - Dh_{ij}f_i) \frac{\nabla s_{ij}^T \Phi(\tau^-, x_0)}{\nabla s_{ij}^T f_i} \quad (9.10)$$

$$= \left( Dh_{ij} + (f_j - Dh_{ij}f_i) \frac{\nabla s_{ij}^T}{\nabla s_{ij}^T f_i} \right) \Phi(\tau^-, x_0). \quad (9.11)$$

Notice that the transversality condition (9.3) ensures that the denominator of (9.10) is non-zero.

Equation (9.10) can be rewritten

$$\Phi^+ = Dh_{ij}\Phi^- - (f_j - Dh_{ij}f_i) \frac{\partial \tau}{\partial x_0} \quad (9.12)$$

where

$$\frac{\partial \tau}{\partial x_0} = - \frac{\nabla s_{ij}^T \Phi^-}{\nabla s_{ij}^T f_i}$$

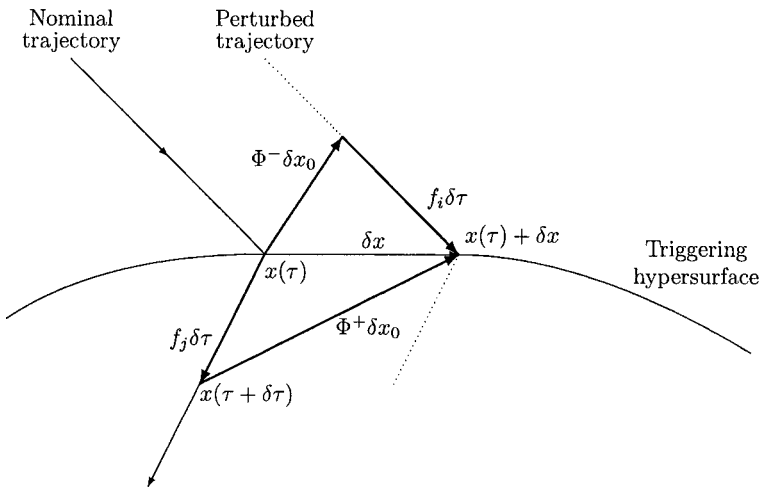


Figure 9.1. Jump conditions.

gives the sensitivity of the event triggering time to initial conditions. Visualizing this result is easiest when  $h_{ij}(x) = x$ , which gives  $Dh_{ij} = I$ . Then for a perturbation  $\delta x_0$ , (9.12) gives

$$\delta x = \Phi^- \delta x_0 + f_i \delta \tau = \Phi^+ \delta x_0 + f_j \delta \tau$$

which is illustrated in Figure 9.1.

### 3. Dynamic Embedded Optimization

Optimization problems arise frequently in the analysis of power system dynamics. Examples range from tuning generator AVR/PSSs [15] to determining the optimal location, amount and switching times for load shedding [16]. Many problems can be formulated using a Bolza form of objective function

$$\min_{\theta, t_f} \mathcal{J}(x, \theta, t_f) \quad (9.13)$$

$$\text{subject to } x(t) = \phi(t, x_0) \quad (9.14)$$

$$x \in \mathcal{S} \quad (\text{constraint set}) \quad (9.15)$$

where

$$\mathcal{J}(x, \theta, t_f) = \varphi(x(t_f), \theta, t_f) + \int_0^{t_f} \psi(x(t), \theta, t) dt \quad (9.16)$$

$\theta$  and  $\theta$  are the design parameters, i.e., the parameters adjusted to achieve the objective. Adjustability of the final time  $t_f$  is problem specific. This

problem is closely related to optimal control [17], but solves for finite dimensional  $\theta$ , rather than an infinite dimensional control input  $u(t)$ .

The solution of (9.13) for hybrid systems is complicated by discontinuous behavior at events. However those complications largely disappear under the assumption that the order of events does not change as  $\theta$  and  $t_f$  vary, i.e., no grazing situations occur. This assumption is common throughout the literature, though it is expressed in various ways: transversal crossings of triggering hypersurfaces are assumed in [18], existence of trajectory sensitivities is assumed in [19], and [20] assumes all flows have the same *history*. All statements are equivalent.

Under that assumption, and other mild assumptions, it is concluded in [20] that if  $\mathcal{J}$  is continuous in its arguments then a solution to (9.13) exists. Furthermore, [19] shows that if  $\mathcal{J}$  is a smooth function of its arguments, then it is continuously differentiable with respect to  $\theta$  and  $t_f$ . The minimization can therefore be solved using gradient-based methods. Trajectory sensitivities underlie the gradient information.

It is still an open question as to which gradient-based methods are most appropriate for solving (9.13)-(9.16). Steepest descent is simple to implement, but may require many iterations. This situation is to be avoided, as each evaluation of  $\mathcal{J}$  requires simulation of the embedded dynamical system. Encouraging results have been obtained with conjugate-gradient and quasi-Newton methods [21]. A further advantage of these latter methods is that they provide an estimate of the Hessian  $\partial^2 \mathcal{J} / \partial \theta^2$ . (Building the true Hessian is infeasible, as it involves second order trajectory sensitivities which are computationally expensive.) The (approximate) Hessian may provide an indication of coupling between design parameters  $\theta$ , and hence allow physical insights that assist in the design process.

If the event ordering assumption given above is not satisfied,  $\mathcal{J}$  may be discontinuous. The optimization problem then takes on a combinatorial nature, as each continuous section of  $\mathcal{J}$  must be searched for a local minimum [19].

**Example** Non-traditional design capabilities arise from embedding a hybrid system model within the optimization framework (9.13)-(9.16). To illustrate, consider the generator AVR/PSS shown in Figure 9.2. The clipping limits on the PSS output  $V_{PSS}$  and the anti-windup limits on the field voltage  $E_{fd}$  introduce events that result in non-smooth behavior. Typically PSS output limits are assigned on an *ad hoc* basis. However [15] determines optimal limit values by establishing a cost function (9.16) that maximizes damping whilst penalizing deviations in the generator terminal voltage. Figure 9.3 compares optimal performance with that

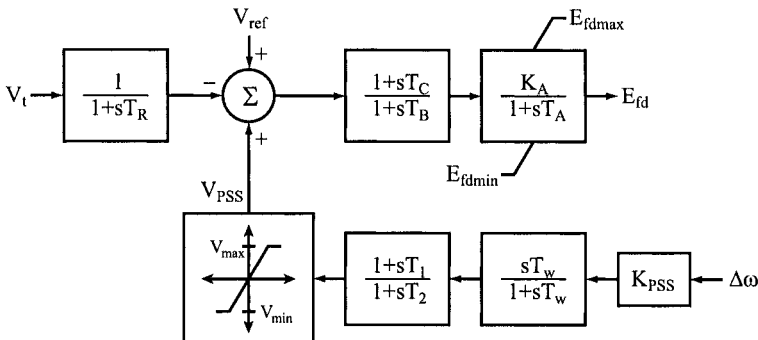


Figure 9.2. AVR/PSS block representation.

obtained using standard limit values. (Note that only the limit values differ between these two cases. All other parameters are fixed.) The underlying non-smoothness of this example is apparent from the field voltage behavior.

□

Other optimization problems do not naturally fit the Bolza form of objective function (9.16). Cascaded tap-changing transformers provide an interesting example [22]. Minimizing the number of tap change operations is equivalent to minimizing the number of crossings of triggering hypersurfaces. Such a problem, by definition, does not satisfy the earlier assumption requiring constant ordering of events.

## 4. Shooting Methods

Boundary value problems have the form

$$r(x_0, x(t_f)) = 0 \quad (9.17)$$

where  $t_f$  is the final time, and  $x(t)$  is the trajectory that starts from  $x_0$  and is generated by the hybrid system model (9.1). The initial values  $x_0$  are variables that must be adjusted to satisfy  $r$ . (Though  $r$  may directly constrain some elements of  $x_0$ .) To establish the solution process, (9.17) may be rewritten

$$r(x_0, \phi(t_f, x_0)) = 0 \quad (9.18)$$

which has the form  $\tilde{r}(x_0) = 0$ . Boundary value problems are solved by shooting methods [10, 23], which are a combination of Newton's method for solving (9.18) along with numerical integration for obtaining the flow  $\phi$ . Newton's method requires the Jacobian

$$J = \frac{\partial r}{\partial x_0} + \frac{\partial r}{\partial x} \Phi(t_f) \quad (9.19)$$

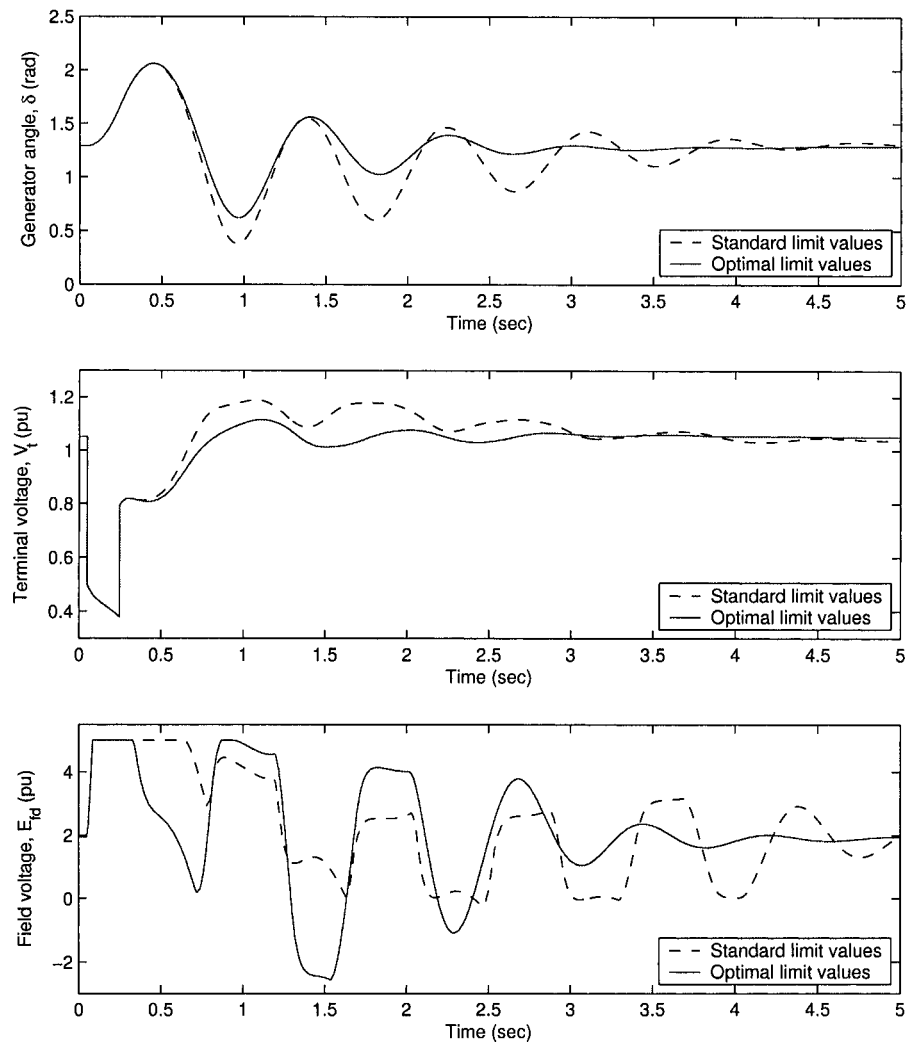


Figure 9.3. Damping improvement from optimally tuning PSS limits.

which is dependent upon the trajectory sensitivities evaluated at  $t_f$ .

Boundary value problems *per se* are uncommon in power systems. However, two applications are of increasing importance: limit cycles (sustained oscillations) and grazing phenomena. They are discussed in the following subsections.

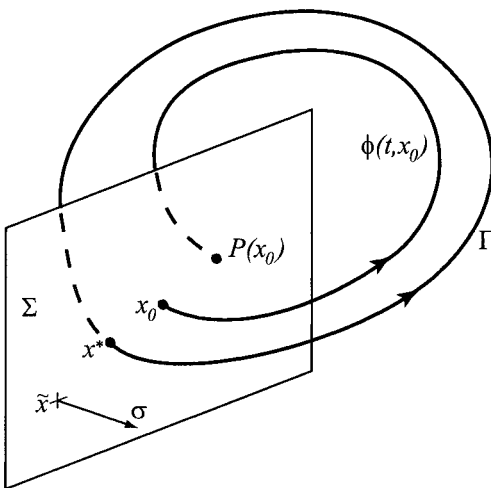


Figure 9.4. Poincaré map.

## 4.1 Limit cycles

Oscillations have been observed in a variety of power systems, from generation [2] to distribution [24]. In this latter case, oscillations were driven by interactions between transformer tapping and capacitor switching. A hybrid system representation is necessary for capturing such phenomena.

Periodic behavior of limit cycles implies that the system state returns to its initial value every cycle. This can be expressed in terms of the flow as

$$x^* = \phi(T, x^*) \quad (9.20)$$

where  $T$  is the limit cycle period. For non-autonomous systems, the period  $T$  is a known quantity. However, it is not known *a priori* for autonomous systems. The unknown period, or *return time*, can be found using Poincaré map concepts [25, 23]. These concepts are well known; the following summary is provided for completeness.

Referring to Figure 9.4, let  $\Sigma$  be a hyperplane that is transversal to the flow  $\phi(t, x_0)$ , and defined by

$$\Sigma = \{x : \sigma^T(x - \tilde{x}) = 0\} \quad (9.21)$$

where  $\tilde{x}$  is a point anchoring  $\Sigma$  and  $\sigma$  is a vector normal to  $\Sigma$ . The return time  $\tau_r$  for a trajectory emanating from  $x_0 \in \Sigma$  is therefore given by

$$\sigma^T(\phi(\tau_r, x_0) - \tilde{x}) = 0 \quad (9.22)$$

The flow  $\phi$  and hyperplane  $\Sigma$  together describe a Poincaré map  $P : \Sigma \rightarrow \Sigma$ , defined by

$$P(x_0) = \phi(\tau_r(x_0), x_0) \quad (9.23)$$

where  $\tau_r(\cdot)$  is given (implicitly) by (9.22). Therefore from (9.20), a limit cycle of an autonomous system must satisfy

$$x^* = P(x^*) = \phi(\tau_r(x^*), x^*) \quad (9.24)$$

The corresponding limit cycle is labelled  $\Gamma$  in Figure 9.4.

Limit cycles can be located by solving (9.20) for non-autonomous systems or (9.24) for autonomous systems. For autonomous systems, rewriting (9.24) gives

$$F_l(x^*) = \phi(\tau_r(x^*), x^*) - x^* = 0 \quad (9.25)$$

The solution  $x^*$  can be obtained using a shooting method<sup>3</sup>, which solves the iterative scheme

$$x^{k+1} = x^k - \left( DF_l(x^k) \right)^{-1} F_l(x^k) \quad (9.26)$$

where

$$DF_l(x^k) = \Phi(\tau_r(x^k), x^k) - f|_{\tau_r(x^k)} \frac{\sigma^T \Phi(\tau_r(x^k), x^k)}{\sigma^T f|_{\tau_r(x^k)}} - I \quad (9.27)$$

$$= \left( I - \frac{f|_{\tau_r(x^k)} \sigma^T}{\sigma^T f|_{\tau_r(x^k)}} \right) \Phi(\tau_r(x^k), x^k) - I \quad (9.28)$$

Derivation of  $DF_l$  is given in [25, 26].

As shown in Section 2.2, the sensitivity transition matrix  $\Phi$  in (9.28) is well defined for hybrid systems. Therefore the proposed shooting method is suitable for non-smooth limit cycles. This will be illustrated in the later example.

Stability of limit cycles can be determined using Poincaré maps. The Poincaré map (9.23) effectively samples the flow of a periodic system once every period. If the limit cycle is stable, oscillations approach the limit cycle over time. The samples provided by the corresponding Poincaré map approach a fixed point. A non-stable limit cycle results in divergent oscillations. For such a case the samples of the Poincaré map diverge.

<sup>3</sup>Reformulation as a multiple shooting method [10] is straightforward.

Stability of the Poincaré map is determined by linearizing  $P$  at the fixed point  $x^*$ ,

$$\Delta x_{k+1} = DP(x^*)\Delta x_k \quad (9.29)$$

For autonomous systems, it follows from (9.28) that

$$DP(x^*) = \left( I - \frac{f(x^*)\sigma^T}{\sigma^T f(x^*)} \right) \Phi(\tau_r(x^*), x^*) \quad (9.30)$$

The eigenvalues of  $DP(x^*)$  are known as the *characteristic multipliers*  $m_i$  of the periodic solution. The matrix  $\Phi(\tau_r(x^*), x^*)$  in (9.30) is exactly the sensitivity transition matrix after one period of the limit cycle, i.e., starting from  $x^*$  and returning to  $x^*$ . This matrix is called the *Monodromy matrix*.

It is shown in [25] that for an autonomous system, one eigenvalue of  $\Phi(\tau_r(x^*), x^*)$  is always unity, and the corresponding eigenvector lies along  $f(x^*)$ . The remaining eigenvalues of  $\Phi(\tau_r(x^*), x^*)$  coincide with the eigenvalues of  $DP(x^*)$ , i.e., the characteristic multipliers. These characteristic multipliers are independent of the choice of hyperplane  $\Sigma$ . Therefore, for hybrid systems, it is often convenient to choose  $\Sigma$  as a triggering hypersurface corresponding to an event that occurs along the periodic solution.

Because the characteristic multipliers  $m_i$  are the eigenvalues of the linear map  $DP(x^*)$ , they determine the local stability of the Poincaré map  $P(.)$ , and hence the local stability of the periodic solution. If all  $m_i$  lie within the unit circle, the map is locally stable, so the periodic solution is locally stable. Alternatively, if any of the  $m_i$  lie outside the unit circle, then the periodic solution is unstable.

**Example** A simple single machine infinite bus system can be used to illustrate power system limit cycles. The machine is represented by a sixth order model [27], and has an AVR of the form shown in Figure 9.2, but with the PSS disabled. The system has an asymptotically stable operating point for values of AVR gain  $K_A < 278$ . A supercritical Hopf bifurcation [23] occurs near  $K_A = 278$ . For  $K_A > 278$ , the equilibrium point becomes unstable and a stable limit cycle appears. The amplitude of that limit cycle grows as  $K_A$  increases, with the maximum field voltage limiter becoming active for  $K_A > 294$ .

The limit cycle corresponding to  $K_A = 300$  is shown in Figure 9.5, as a plot of field voltage  $E_{fd}$  versus terminal voltage  $V_t$ . Notice that the limit cycle is non-smooth due to the field voltage limit  $E_{fd,max} = 5$  p.u.

For this case the eigenvalues of the Monodromy matrix are 1, 0.84,  $0.21 \pm j0.25$ , 0.08 and four at 0. The unity eigenvalue is always present for

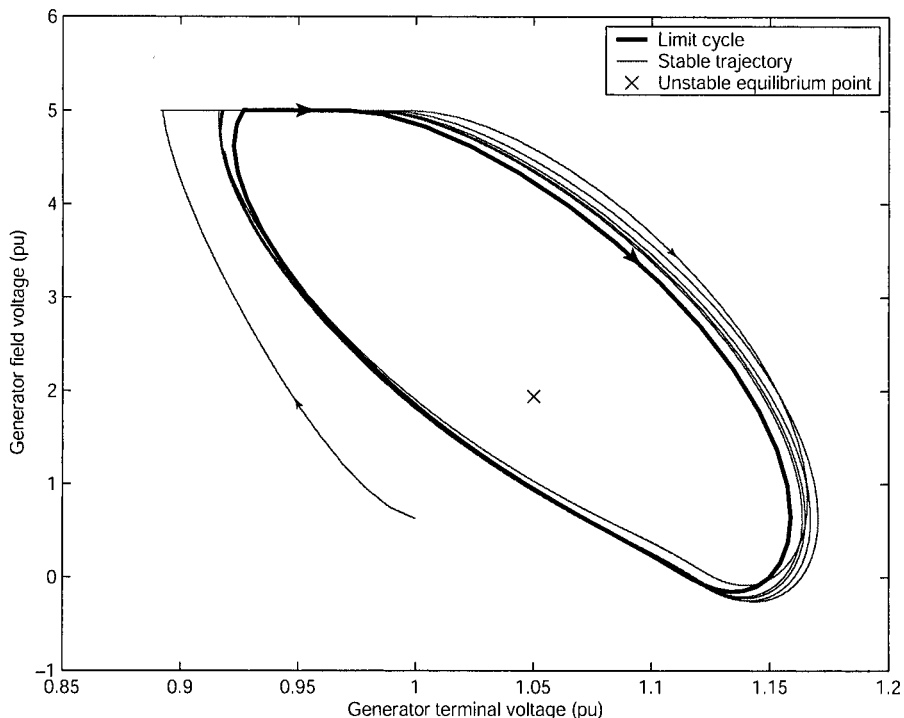


Figure 9.5. Non-smooth limit cycle.

autonomous systems, as suggested by the theory. The other eigenvalues are the characteristic multipliers for this limit cycle. Notice that one of the characteristic multipliers is relatively close to unity, indicating that the limit cycle is quite poorly damped. Indeed the non-equilibrium trajectory in Figure 9.5 converges slowly to the limit cycle.

Even though it is theoretically possible to obtain this limit cycle by simulation, slow convergence makes the process impractical. On the other hand, shooting method convergence properties follow from the underlying Newton solution process, rather than from the behavior of the dynamical system. For this example, the shooting method was initialized at the unstable equilibrium point corresponding to  $K_A = 300$ , except that the angle state was perturbed slightly. Convergence was obtained in eight iterations from this onerous initialization.

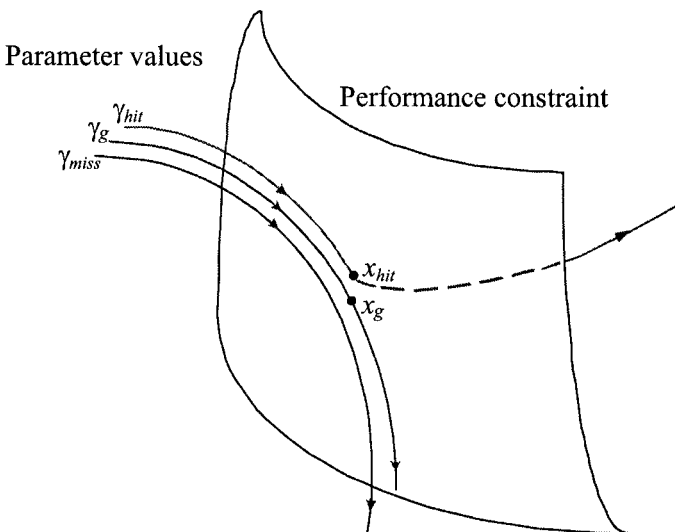


Figure 9.6. Grazing phenomenon.

## 4.2 Grazing phenomena

As suggested in Section 1, if a system trajectory encounters the operating characteristic of a protection device, a trip signal is sent to circuit breakers. If the trajectory almost touches the operating characteristic but just misses, no trip signal is issued. The bounding (separating) case corresponds to the trajectory grazing, i.e., just touching, the operating characteristic, but not crossing it. Under certain circumstances, this is referred to as a *grazing bifurcation* [28, 29]; it separates two cases that have significantly different forms of behavior.

Figure 9.6 provides a more general picture. For a certain value of parameter  $\gamma_{hit}$ , the system trajectory encounters a performance constraint<sup>4</sup> at a point  $x_{hit}$ . An event occurs, and the trajectory continues accordingly. However, for a small change in parameter value, to  $\gamma_{miss}$ , the trajectory misses (at least locally) the constraint and subsequently exhibits a completely different form of response. At a critical parameter value  $\gamma_g$ , lying between  $\gamma_{hit}$  and  $\gamma_{miss}$ , the trajectory tangentially encounters (*grazes*) the constraint. Behavior beyond the grazing point  $x_g$  is generally unpredictable, in the sense that without further knowledge of the system, it is impossible to determine whether or not the event triggers.

<sup>4</sup>This may be a protection operating characteristic, or some other constraint established to ensure adequate system performance.

Grazing is characterised by a trajectory (flow) of the system touching a triggering hypersurface tangentially. Let the target hypersurface be described by

$$b(x) = 0 \quad (9.31)$$

where  $b : \mathbb{R}^n \rightarrow \mathbb{R}$ . Vectors that are normal to  $b$  are therefore given by  $\nabla b = (\partial b / \partial x)^T$ , and the tangent hyperplane is spanned by vectors  $u$  that satisfy  $\nabla b^T u = 0$ . The vector  $\dot{x} = f(x)$  is directed tangentially along the flow, so at a grazing point

$$\nabla b^T f(x) = 0 \quad (9.32)$$

A single degree of freedom is available for varying parameters to find a grazing point. Recall from (9.7) that parameters  $\lambda$  are incorporated into the initial conditions  $x_0$ . Therefore the single degree of freedom can be achieved by parameterization  $x_0(\theta)$ , where  $\theta$  is a scalar.

Grazing points are therefore described by combining together the flow definition (9.6) (appropriately parameterized by  $\theta$ ), target hypersurface (9.31), and tangency condition (9.32), to give

$$F_{g1}(x_g, \theta, t_g) := \phi(t_g, x_0(\theta)) - x_g = 0 \quad (9.33)$$

$$F_{g2}(x_g) := b(x_g) = 0 \quad (9.34)$$

$$F_{g3}(x_g) := \nabla b(x_g)^T f(x_g) = 0 \quad (9.35)$$

Grazing occurs at time  $t_g$  along the trajectory, and its state-space location is given by  $x_g$ . This set of equations may be written compactly as

$$F_g(x_g, \theta, t_g) = F_g(z) = 0 \quad (9.36)$$

where  $F_g : \mathbb{R}^{n+2} \rightarrow \mathbb{R}^{n+2}$  and  $z = [x_g^T \ \theta \ t_g]^T$ .

Numerical solution of (9.36) using Newton's method amounts to iterating on the standard update formula

$$z^{k+1} = z^k - \left( DF_g(z^k) \right)^{-1} F_g(z^k) \quad (9.37)$$

where  $DF_g$  is the Jacobian matrix

$$DF_g = \begin{bmatrix} -I & \Phi \frac{dx_0}{d\theta} & f \\ \nabla b^T & 0 & 0 \\ f^T \nabla^2 b + \nabla b^T Df & 0 & 0 \end{bmatrix} \quad (9.38)$$

More complete details of this algorithm are given in [26].

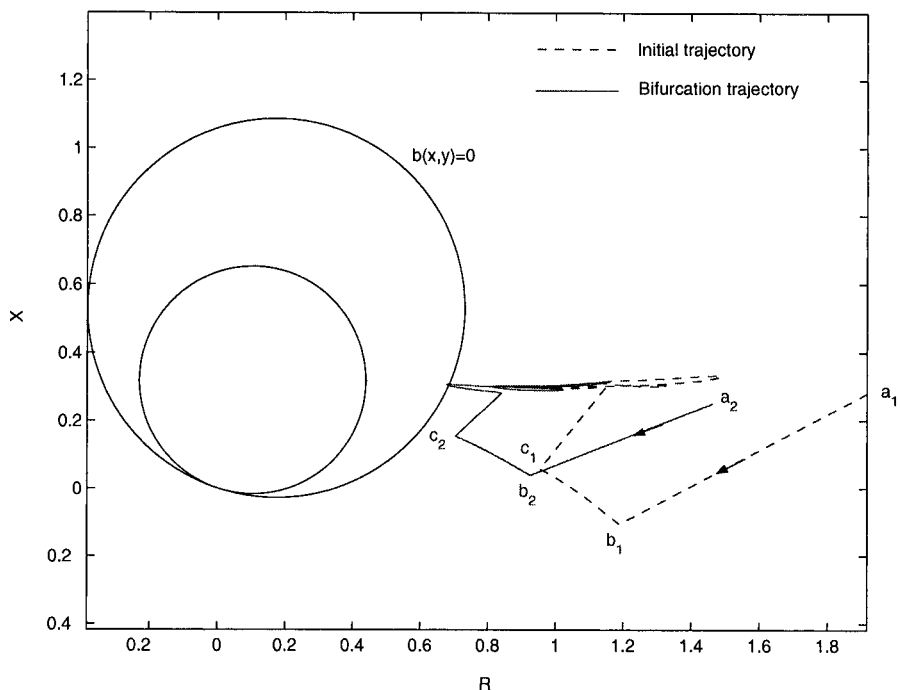


Figure 9.7. Impedance plane trajectories.

**Example** An example of grazing is presented in Figure 9.7, where zone 1 and 2 operating characteristics for a distance protection relay appear as circles in the impedance plane. The dashed line, which begins at the pre-fault operating point  $a_1$ , shows the system response to a disturbance for nominal system conditions. At the onset of the fault, the apparent impedance jumps from  $a_1$  to  $b_1$ . It then evolves to  $c_1$  during the fault-on period. At fault clearing, the apparent impedance jumps, approaches the zone 2 characteristic, then turns away. Under these nominal conditions the relay characteristic is not encountered.

As load increases, the impedance trajectory moves closer to the relay characteristic. The example considered the load increase required for the relay characteristic to be encountered. This established the maximum secure loading level. The problem was formulated according to (9.33)-(9.35), with  $b$  describing the zone 2 operating characteristic, and  $\theta$  giving the load deviation. Convergence of (9.37) was obtained in four iterations, with the grazing trajectory shown as the solid curve in Figure 9.7. The load change moved the pre-fault operating point from  $a_1$  to  $a_2$ . As required, this trajectory just touches the relay characteristic.

## 5. Challenges in Dynamic Performance Enhancement

Power systems are becoming increasingly complex. Trends include greater utilization of special protection schemes, FACTS devices, and distributed resources. (Market dynamics may also become influential as the associated time-constants diminish.) These newer influences, together with operation closer to limits, is resulting in a greater level of switching (non-smooth) activity. The techniques proposed in this paper are suited to such hybrid behavior. However more work is required. Hybrid dynamics introduce new challenges for control design. For example, minimization of switching events does not fit a normal optimization framework [30]. Also, assessment of stability limits is technically difficult [31].

Distributed resources, such as small generation sources, newer FACTS technology [32], and load control [33, 34], individually exert negligible influence on dynamic behavior. However collectively their effect may be significant. Modelling of each device is impossible, so techniques for aggregating behavior and handling the associated model uncertainty will become vital for meaningful assessment of dynamics. Monte Carlo techniques are impractical, due to the computational burden of repeated simulations. Emerging practical techniques build on probabilistic collocation [35] and trajectory approximation [36]. Further work is required though.

## 6. Conclusions

The response of power systems to large disturbances often involves interactions between continuous dynamics and discrete events. Power systems therefore provide an important application area for hybrid systems. Systematic modelling of hybrid systems facilitates efficient computation of trajectory sensitivities. The variational equations describing the evolution of trajectory sensitivities through events are well defined, even though the underlying behavior may be non-smooth.

Many design questions associated with enhancement of power system dynamic performance can be formulated as dynamic embedded optimization problems. Such problems are constrained to satisfy system dynamics, and so are closely related to optimal control. If the ordering of events remains fixed as parameters vary, the cost function is smooth, even though underlying dynamic behavior may be non-smooth. Gradient-based algorithms are appropriate, with trajectory sensitivities providing the gradient information. Changes in event ordering may how-

ever result in non-smoothness or even discontinuities in the cost function. In that case, a combinatorial optimization process may be required.

In contrast to design, analysis questions often take the form of boundary value problems, which can be solved using shooting methods. Limit cycles provide an example. Smooth and non-smooth limit cycles have been observed in power systems. Furthermore, unstable limit cycles often partially bound the region of stable operation. All limit cycles, whether stable or unstable, smooth or non-smooth, can be obtained reliably using shooting methods.

Power system performance constraints seek to achieve appropriate post-fault response by bounding behavior away from undesirable regions of state space. An indication of system vulnerability can therefore be obtained by determining trajectories that tangentially encounter (graze) those constraints, i.e., by pushing the system to the limit. The conditions governing such grazing trajectories take the form of a boundary value problem, which can be solved via a shooting method.

### Acknowledgements

The assistance of Bhageerath Reddy in establishing the limit cycle example is gratefully acknowledged. This research was supported by the National Science Foundation through grant ECS-0332777.

## References

- [1] U.S.-Canada Power System Outage Task Force. *Final Report on the August 14, 2003 Blackout in the United States and Canada: Causes and Recommendations*. April 2004.
- [2] K. Kim, H. Schättler, V. Venkatasubramanian, J. Zaborszky, and P. Hirsch. Methods for Calculating Oscillations in Large Power Systems. *IEEE Transactions on Power Systems*, 12:1639–1648, 1997.
- [3] G. Rogers. *Power System Oscillations*. Kluwer Academic Publishers, Norwell, MA, 2000.
- [4] L.G. Perez, A.J. Flechsig, and V. Venkatasubramanian. Modeling the Protective System for Power System Dynamic Analysis. *IEEE Transactions on Power Systems*, 9:1963–1973, 1994.
- [5] M.S. Ćalović. Modeling and Analysis of Under-Load Tap-Changing Transformer Control Systems. *IEEE Transactions on Power Apparatus and Systems*, PAS-103:1909–1915, 1984.
- [6] M.D. Lemmon, K.X. He, and I. Markovsky. Supervisory Hybrid Systems. *IEEE Control Systems Magazine*, 19:4:42–55, August 1999.
- [7] A.F. Filippov. *Differential Equations with Discontinuous Righthand Sides*. Kluwer Academic Publishers, The Netherlands, 1988.

- [8] D. Liberzon. *Switching in Systems and Control*. Birkhäuser, Boston, MA, 2003.
- [9] I.A. Hiskens. Power System Modeling for Inverse Problems. *IEEE Transactions on Circuits and Systems I*, 51:539–551, 2004.
- [10] J. Stoer and R. Bulirsch. *Introduction to Numerical Analysis*, 2nd edition. Springer, New York, 1993.
- [11] P.M. Frank. *Introduction to System Sensitivity Theory*. Academic Press, New York, 1978.
- [12] I.A. Hiskens and M.A. Pai. Trajectory Sensitivity Analysis of Hybrid Systems. *IEEE Transactions on Circuits and Systems I*, 47:204–220, 2000.
- [13] W.F. Feehery, J.E. Tolsma, and P.I. Barton. Efficient Sensitivity Analysis of Large-Scale Differential-Algebraic Systems. *Applied Numerical Mathematics*, 25:41–54, 1997.
- [14] S. Li, L. Petzold, and W. Zhu. Sensitivity Analysis of Differential-Algebraic Equations: A Comparison of Methods on a Special Problem. *Applied Numerical Mathematics*, 32:161–174, 2000.
- [15] I.A. Hiskens. Systematic Tuning of Nonlinear Power System Controllers. *Proceedings of the 2002 IEEE International Conference on Control Applications*, 19–24, Glasgow, Scotland, September 2002.
- [16] C. Moors and T. Van Cutsem. Determination of Optimal Load Shedding Against Voltage Instability. *Proceedings of the 13th Power Systems Computation Conference*, 2:993–1000, Trondheim, Norway, June 1999,
- [17] F.L. Lewis and V.L. Syrmos. *Optimal Control*, 2nd edition. Wiley, New York, 1995.
- [18] M.S. Branicky, V.S. Borkar, and S.K. Mitter. A Unified Framework for Hybrid Control: Model and Optimal Control theory. *IEEE Transactions on Automatic Control*, 43:31–45, 1998.
- [19] S. Galán and P.I. Barton. Dynamic Optimization of Hybrid Systems. *Computers Chemical Engineering*, 22:S183–S190, 1998.
- [20] B. Piccoli. Hybrid Systems and Optimal Control. *Proceedings of the 37<sup>th</sup> IEEE Conference on Decision and Control*, Tampa, FL, December 1998.
- [21] J. Nocedal and S.J. Wright. *Numerical Optimization*. Springer-Verlag, New York, 1999.
- [22] M. Larsson. *Coordinated Voltage Control in Electric Power Systems*. PhD Thesis, Department of Industrial Electrical Engineering and Automation, Lund Institute of Technology, Lund, Sweden, 2000.

- [23] R. Seydel. *Practical Bifurcation and Stability Analysis*. Springer-Verlag, New York, 1994.
- [24] P. Gavey. Voltage Stability in the Mid North Coast: Investigation of Voltage Oscillation Occurrence on 26<sup>th</sup> March 1993. Final Year Project Report, Department of Electrical and Computer Engineering, The University of Newcastle, Australia, 1995.
- [25] T.S. Parker and L.O. Chua. *Practical Numerical Algorithms for Chaotic Systems*. Springer-Verlag, New York, NY, 1989.
- [26] V. Donde and I.A. Hiskens. Shooting Methods for Locating Grazing Phenomena in Hybrid Systems. *International Journal of Bifurcation and Chaos*, 2004, Submitted.
- [27] P.W. Sauer and M.A. Pai. *Power System Dynamics and Stability*. Prentice Hall, Upper Saddle River, NJ, 1998.
- [28] M.H. Fredriksson and A.B. Nordmark. Bifurcations Caused by Grazing Incidence in Many Degrees of Freedom Impact Oscillators. *Proceedings of Royal Society London A*, 453:1961:1261–1276, 1997.
- [29] M. di Bernardo, C.J. Budd, and A.R. Champneys. Grazing and Border-Collision in Piecewise-Smooth Systems: A Unified Analytical Framework. *Physical Review Letters*, 86:2553–2556, 2001.
- [30] R.W. Brockett. Minimum attention control. *Proceedings of the 36<sup>th</sup> IEEE Conference on Decision and Control*, 2628–2632, 1997.
- [31] V. Venkatasubramanian, H. Schättler, and J. Zaborszky. Dynamics of Large Constrained Nonlinear Systems—a Taxonomy Theory. *Proceedings of the IEEE*, 83:1530–1561, 1995.
- [32] D. Divan. Smart Wires: Demonstration of a Distributed Static Series Compensator (DSSC) Module. SoftSwitching Technologies Presentation, Middleton, WI, March 2004.
- [33] B. Ramanathan and V. Vittal. A Structured Singular Value Based Small Signal Stability Performance Boundary for Direct Load Control. *Proceedings of IEEE Power Systems Conference and Exposition (PSCE)*, New York, October 2004 (to appear).
- [34] I.A. Hiskens and B. Gong. Voltage Stability Enhancement via Model Predictive Control of Load. *Proceedings of the Symposium on Bulk Power System Dynamics and Control VI*, Cortina d'Ampezzo, Italy, August 2004 (to appear).
- [35] J.R. Hockenberry and B.C. Lesieutre. Evaluation of Uncertainty in Dynamic Simulations of Power System Models I: the Probabilistic Collocation Method. *IEEE Transactions on Power Systems*, 19:1483–1491, 2004.

- [36] I.A. Hiskens, M.A. Pai, and T.B. Nguyen. Bounding Uncertainty in Power System Dynamic Simulations. *Proceedings of IEEE PES Winter Meeting*, Singapore, January 2000.

## Chapter 10

# COMPUTATIONAL INTELLIGENCE TECHNIQUES FOR CONTROL OF FACTS DEVICES

Ganesh K. Venayagamoorthy

*University of Missouri-Rolla*

[gkumar@ieee.org](mailto:gkumar@ieee.org)

Ronald G. Harley

*Georgia Institute of Technology*

[ron.harley@ece.gatech.edu](mailto:ron.harley@ece.gatech.edu)

**Abstract** The increasing complexity of the modern power grid highlights the need for advanced modeling and control techniques for effective control of Flexible AC Transmission Systems (FACTS). The crucial factor affecting the modern power systems today is load flow control. Simulation studies carried out in the PSCAD/EMTDC environment is described and results show the successful control of the FACTS devices and the power system with adaptive and optimal neurocontrol. Performances of the neurocontrollers are compared with the conventional PI controllers for system oscillation damping under different operating conditions for large disturbances.

**Keywords:** Computational Intelligence, FACTS, neurocontrol, power system oscillation, damping control, adaptive control, adaptive critic design.

### 1. Introduction

With the ever increasing complexities in power systems across the globe and the growing need to provide stable, secure, controlled, economic, and high-quality electric power—especially in today's deregulated environment—it is envisaged that Flexible AC Transmission System

(FACTS) controllers are going to play a critical role in power transmission systems [1]. Transmission congestion results when there is insufficient capacity to transmit power over existing lines and maintain the required safety margins for reliability. FACTS enhance the stability of the power system both with their fast control characteristics and continuous compensating capability. The two main objectives of FACTS technology are to control power flow and increase the transmission capacity over an existing transmission corridor [2].

The static synchronous compensator (STATCOM) [1] is a controlled voltage source inverter and its output voltage is connected in shunt with the transmission line (across the phases) through a coupling transformer. Regulating reactive power injected into the network and the active power drawn from it by this device, provides control over the line voltage at the point of coupling and over the DC bus voltage inside the device respectively. The amount of active power exchanged between the STATCOM and power line is used to charge or discharge a capacitor across the dc link inside the inverter, and is therefore a relatively small amount, compared with the amount of reactive power exchanged.

The static synchronous series compensator (SSSC) [1] is also a controlled voltage source inverter, but in this case its output voltage is connected in series with the transmission line through a series insertion transformer. The injected series voltage can lead the line current by 90 degrees, resulting in a capacitive effect or can lag the current by 90 degrees, resulting in an inductive effect. While originally developed to behave as an electronically controlled capacitor in long series compensated transmission lines, it can also be used in any other lines, long or short, to re-route active power flow in the case of overloaded lines, and even damp any active power swings when disturbances occur.

Gyugyi then proposed the Unified Power Flow Controller (UPFC), a new generation of FACTS devices in 1991 [3] as a combination of the STATCOM and the SSSC. The two are coupled via a common dc link, to allow bidirectional flow of real power between series output terminals of the SSSC and the shunt terminals of the STATCOM, and are controlled to provide concurrent real and reactive series line compensation without an external electric energy source. The UPFC by means of angularly unconstrained series voltage injection is able to control, concurrently or selectively, the transmission line voltage, impedance, and angle or, alternatively, the real and reactive power flow in the line. The UPFC may also provide independently controllable shunt-reactive compensation.

Rapid control of these FACTS devices is obtained by varying their switching patterns. This rapid control can be used to provide voltage support and control power flow, thereby improving stability and

allowing the transmission system to be operated more efficiently with a smaller stability margin. However, while FACTS devices offer increased network power flow controllability, the decentralized nature of their actions may cause deleterious interactions between one FACTS device and another, as well as FACTS devices and neighboring generators. In addition, FACTS devices are nonlinear and when connected to a nonlinear power system with a changing configuration, the performance of the conventionally designed FACTS controllers therefore also degrade as the operating points move away from the point where the controllers were designed. One possible solution to all these problems is the use of nonlinear adaptive intelligent neurocontrollers based on advanced identification and control schemes.

Computational intelligence techniques including neural networks, genetic algorithms, fuzzy logic and adaptive critic designs, are useful tools for complex nonlinear system dynamics' identification and intelligent control. Neural networks are suitable for multi-variable applications because they can easily identify the interactions between the system's inputs and outputs. Their ability to learn and store information about system nonlinearities allows neural networks to be used for modeling and designing intelligent controllers for power systems [4], [5], and thus, offering alternatives for traditional linear and nonlinear control. A radial basis function (RBF) neural network controller for a UPFC based on the direct adaptive control scheme has been reported to improve the transient stability performance of a power system [6]. It is known that indirect adaptive control is able to improve the control of a nonlinear system with fast changing dynamics, like a power system, because the dynamics are continually identified by a model. Advantages of the neurocontrollers over the conventional controllers are that they are able to adapt to changes in the system operating conditions automatically unlike the conventional controllers whose performances degrade for such changes.

This chapter explains how computational intelligence techniques such as neural networks and adaptive critic designs can be applied to a STATCOM, SSSC, and UPFC in order to mainly improve their dynamic performance.

## **2. FACTS Devices and Conventional Control**

Currently, the control of FACTS devices are carried out using linear PI controllers with fixed parameters. The PI controller parameters are selected to give some desirable performance for a particular region of operation and conditions; outside of which the performance of

the controllers degrade. Thus, the need for the design of nonlinear robust/adaptive controllers for FACTS devices arise in order to cater to a wide range of operating conditions, and to handle small as well as large disturbances.

The following subsections describe the different types of FACTS devices considered in this chapter, namely: STATCOM, SSSC, and UPFC and their conventional control.

## 2.1 Static Compensators (STATCOM)

Figure 10.1 shows a STATCOM connected to a single-machine infinite-bus system. The generator is modeled together with its automatic voltage regulator (AVR), exciter, and turbine dynamics all taken into account [7]. The generator is a 37.5 MVA, 11.85 kV (line voltage) machine. System parameters used in the simulations appear in [13].

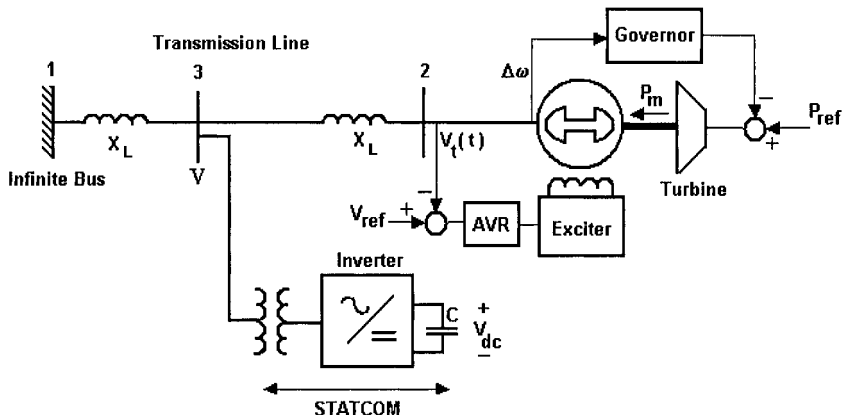


Figure 10.1. STATCOM connected to SMIB system (plant).

The STATCOM is first controlled using a conventional PI controller as described in [8] and shown in Figure 10.2, where switches S1 and S2 would both be in position 1. The  $d$ -axis and  $q$ -axis voltage deviations are derived from the difference between actual and reference values of the power network line voltage  $V$  and the DC bus voltage  $V_{dc}$  (inside the STATCOM), respectively, and are then passed through two PI controllers, whose output values and in turn determine the modulation index and inverter output phase shift  $\alpha$  applied to the PWM module as

$$m_\alpha = \frac{\sqrt{\Delta e_d^2 + \Delta e_q^2}}{V_{dc}}, \quad \alpha = \cos^{-1} \left( \frac{\Delta e_d}{\sqrt{\Delta e_d^2 + \Delta e_q^2}} \right) \quad (10.1)$$

Controlling the voltage  $V$  at the point of connection to the network is the main objective of the STATCOM considered in this paper.

Parameters of the STATCOM PI controller are tuned so that the controller provides satisfactory and stable performance when the system is exposed to small changes in reference values as well as large disturbances such as a three phase short circuit on the power network. These PI controllers are tuned at a single operating point (active and reactive power at the generator terminals are 0.6 p.u. and 0.2 p.u., respectively, in this study).

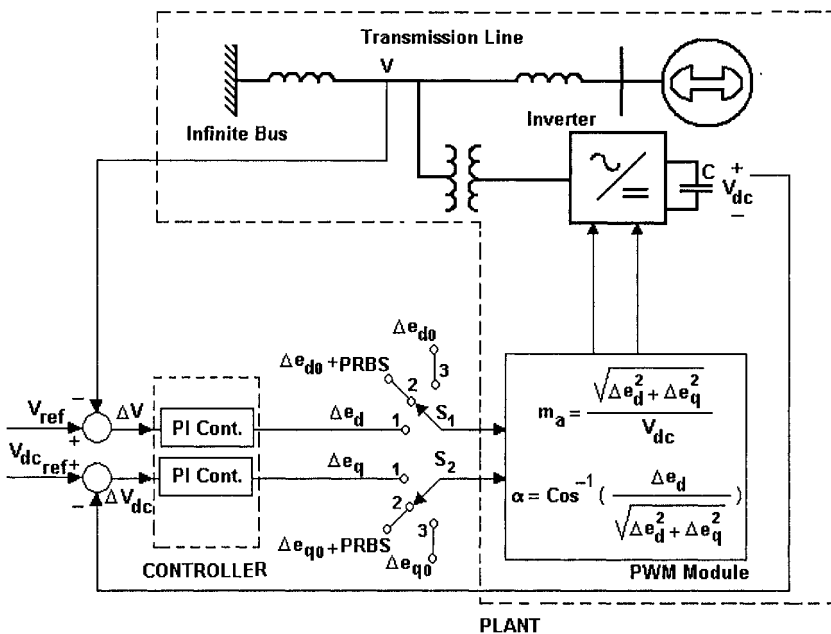


Figure 10.2. STATCOM controller.

The “Plant” indicates the generator, its controllers, the transmission line, the STATCOM, and the PWM module with  $\Delta e_d$  and  $\Delta e_q$  as inputs, and  $\Delta V$  (line voltage deviation) and  $\Delta V_{dc}$  (DC bus voltage deviation) as outputs, whereas “Controller” represents the line voltage and DC bus voltage control loops.

## 2.2 Static Synchronous Series Compensator (SSSC)

The static synchronous series compensator (SSSC) converter can control the reactive and/or active power on an ac system by changing both

the phasor angle and magnitude of the converter's output voltage with a fast control action. Especially, the exchange of active power, which is the particular characteristic of the SSSC, is accomplished by controlling the dc voltage inside the SSSC [3].

**2.2.1 Modeling of SSSC.** The single machine infinite bus (SMIB) system shown in Figure 10.3 is used to compare the damping control capabilities of the Dual Heuristic Programming based neurocontroller (DHPNC) and the conventional PI controller (CONVC) for the SSSC. The plant consists of the synchronous generator (160 MVA, 15 kV (L-L)), turbine-governor system, automatic voltage regulator (AVR)-exciter system, transmission line connected to an infinite bus, and SSSC connected in series with transmission line. The parameters of the synchronous generator and transmission line are given in [9].

The EXAC1A (IEEE alternator supplied rectifier excitation system) and H\_TUR1/GOV1 (IEEE type hydro turbine-governor) models in the PSCAD/EMTDC software package are used as the AVR/exciter system and turbine/governor, respectively.

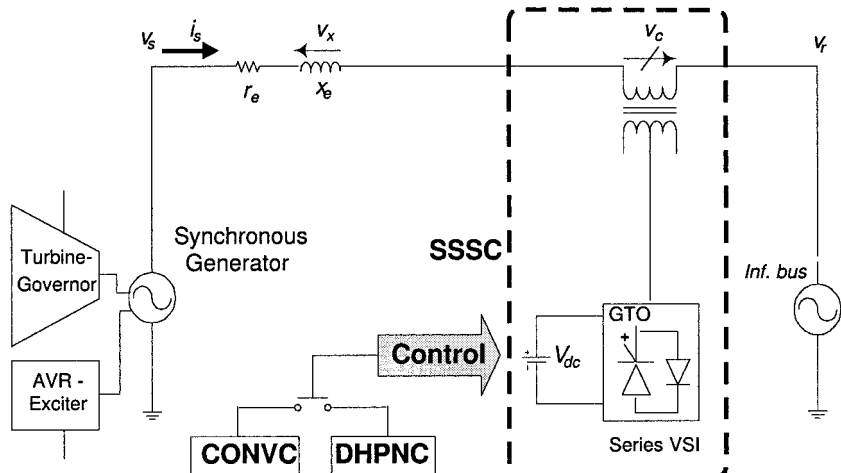


Figure 10.3. Plant: 160 MVA, 15 kV (L-L) SMIB test system.

For the mathematical model of the SSSC, the associated equation can be represented with the lumped series transmission line reactance  $x'_e$  (transmission line  $x_e$  plus the equivalent reactance of the series-connected transformer) and the transmission series resistance  $r_e$  (the

inverter is regarded simply to have no conduction losses) in per unit as

$$\frac{d}{dt} \begin{bmatrix} i_{sa} \\ i_{sb} \\ i_{sc} \end{bmatrix} = -\frac{r_e \omega_s}{x'_e} \begin{bmatrix} 1 & 0 & 0 \\ 0 & 1 & 0 \\ 0 & 0 & 1 \end{bmatrix} \begin{bmatrix} i_{sa} \\ i_{sb} \\ i_{sc} \end{bmatrix} + \frac{\omega_s}{x'_e} \begin{bmatrix} v_{sa} + v_{ca} - v_{ra} \\ v_{sb} + v_{cb} - v_{rb} \\ v_{sc} + v_{cc} - v_{rc} \end{bmatrix} \quad (10.2)$$

where  $\omega_s$  is the synchronous speed of the power system,  $v_s$  is the sending-end voltage (terminal voltage in practice),  $v_{sa}$ ,  $v_{sb}$ , and  $v_{sc}$  are the sending-end voltages of phase  $a$ ,  $b$ , and  $c$  respectively,  $i_s$  is the current in transmission line,  $i_{sa}$ ,  $i_{sb}$ , and  $i_{sc}$  are the currents in transmission line phase  $a$ ,  $b$ , and  $c$  respectively,  $v_r$  is the receiving-end voltage in the infinite bus,  $v_{ra}$ ,  $v_{rb}$ , and  $v_{rc}$  are the receiving-end voltages of phase  $a$ ,  $b$ , and  $c$  respectively,  $v_c$  is the injected series compensation voltage and  $v_{ca}$ ,  $v_{cb}$ , and  $v_{cc}$  are the injected series compensation voltages of phase  $a$ ,  $b$ , and  $c$ .

Using the synchronously rotating reference frame based transformation [10] in which the  $d$ -axis is always coincident with the instantaneous voltage vector  $v_s$  and the  $q$ -axis leads the  $d$ -axis by  $90^\circ$ , the three-phase circuit equations in (10.2) can be transformed to the  $d$ - $q$  axis vector representation

$$\frac{d}{dt} \begin{bmatrix} i_d \\ i_q \end{bmatrix} = \begin{bmatrix} -\frac{r_e \omega_s}{x'_e} & \omega \\ -\omega & -\frac{r_e \omega_s}{x'_e} \end{bmatrix} \begin{bmatrix} i_d \\ i_q \end{bmatrix} + \begin{bmatrix} \frac{\omega_s}{x'_e} (|v_s| + v_{cd} - v_{rd}) \\ \frac{\omega_s}{x'_e} (v_{cq} - v_{rq}) \end{bmatrix} \quad (10.3)$$

Neglecting the series inverter harmonics, the ac side injected voltage  $v_c$  in Figure 10.3 can be expressed with relation to the capacitor voltage  $V_{dc}$  on the dc link as follows.

$$v_{cd} = mV_{dc} \cos(\alpha), \quad v_{cq} = mV_{dc} \sin(\alpha) \quad (10.4)$$

where  $\alpha$  is the phase angle difference between the voltages  $v_c$  and  $v_s$  ( $v_c$  leading  $v_s$ ), and  $m$  is the modulation index of the series inverter. The dynamics of the dc capacitor voltage are described by

$$\frac{dV_{dc}}{dt} = \frac{1}{C} \frac{P_{dc}}{V_{dc}} = \frac{1}{C} \frac{V_{dc} i_{dc}}{V_{dc}} = \frac{1}{C} \frac{v_{cd} i_d + v_{cq} i_q}{V_{dc}} = \frac{m [\cos(\alpha) i_d + \sin(\alpha) i_q]}{C} \quad (10.5)$$

**2.2.2 Conventional control strategy.** The main goal of the SSSC is to inject the series voltage in quadrature with the line current and to maintain the dc voltage  $V_{dc}$ . For this purpose, the  $P$ - $Q$  (real and reactive power) automatic power flow control mode [3] in Figure 10.4 is used.

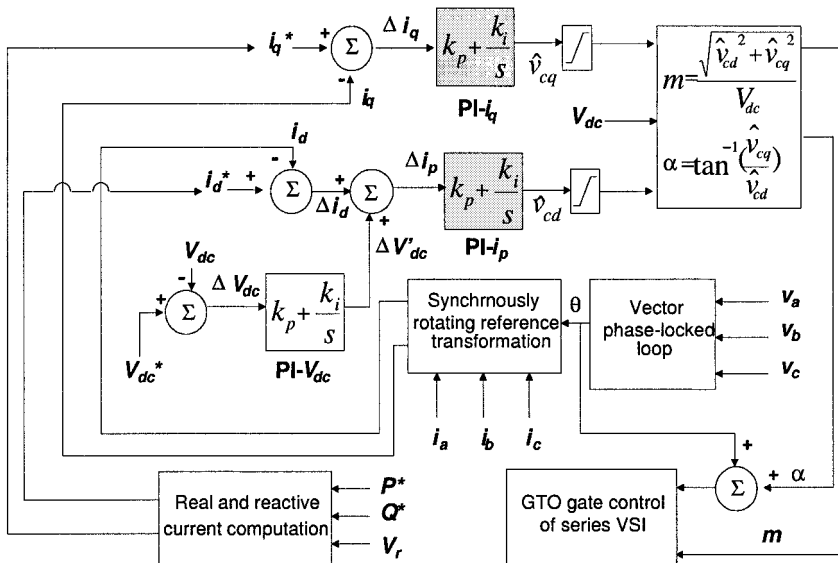


Figure 10.4.  $P$ - $Q$  automatic power flow control diagram for the internal control of the SSSC.

In Figure 10.4, an instantaneous three-phase set of line voltages,  $v_a$ ,  $v_b$ , and  $v_c$  is used to calculate the transformation angle, provided by the vector phase-locked loop for synchronous operation of the series voltage source inverter (VSI) shown in Figure 10.3. As shown in (10.3), the three-phase set of measured line currents at the ac terminal of the SSSC is decomposed into its real/direct component,  $i_d$ , and reactive/quadrature component,  $i_q$ . These actual signals ( $i_d$  and  $i_q$ ) and the reference  $d$ - $q$  current signals ( $i_d^*$  and  $i_q^*$ ) are compared, respectively.

The error signal  $\Delta i_q$  for the reactive power exchange is passed through the PI regulator  $PI-i_q$ . The signal  $\Delta i_p$  for the real power exchange and maintenance of a constant  $V_{dc}$ , is passed through the  $PI-i_p$ . The  $\Delta i_p$  consists of the  $\Delta i_d$  and error signal  $\Delta V'_{dc}$  (which passes through the  $PI-V_{dc}$ ). The  $V_{dc}^*$  is the desired value for  $V_{dc}$ . The value of  $V_{dc}^*$  is determined by selecting a suitable value of the modulation index within its range of 0 to 1.

## 2.3 Unified Power Flow Controller (UPFC)

The UPFC is the most versatile FACTS device. It is a combination of the STATCOM and the SSSC. For identifying and controlling the dynamics of a UPFC and a power system, the single machine infinite-bus

(SMIB) power system in Figure 10.5 is studied in the PSCAD/EMTDC environment. This power system comprises of a synchronous generator with exciter-automatic voltage regulator (AVR) and turbine-governor combinations connected to an infinite bus through two sections of transmission lines. The UPFC is placed between the two sections of the transmission lines, between Bus 2 and 3 as shown in Figure 10.5. This simple system is chosen in order to evaluate the performance of the UPFC with two different control strategies.

The series inverter provides the main function of the UPFC by injecting a voltage with magnitude  $V_{inj}$ , which is controllable and at a phase angle  $\theta_{inj}$  in series with the line via an insertion transformer. This injected voltage acts essentially as a synchronous ac voltage source. The transmission line current flows through this voltage source resulting in a reactive and active power exchange between itself and the ac system. The inverter generates the reactive power exchanged at the ac terminal internally. The active power exchanged at the ac terminal is converted into dc power, which appears at the dc link as a positive or negative real power.

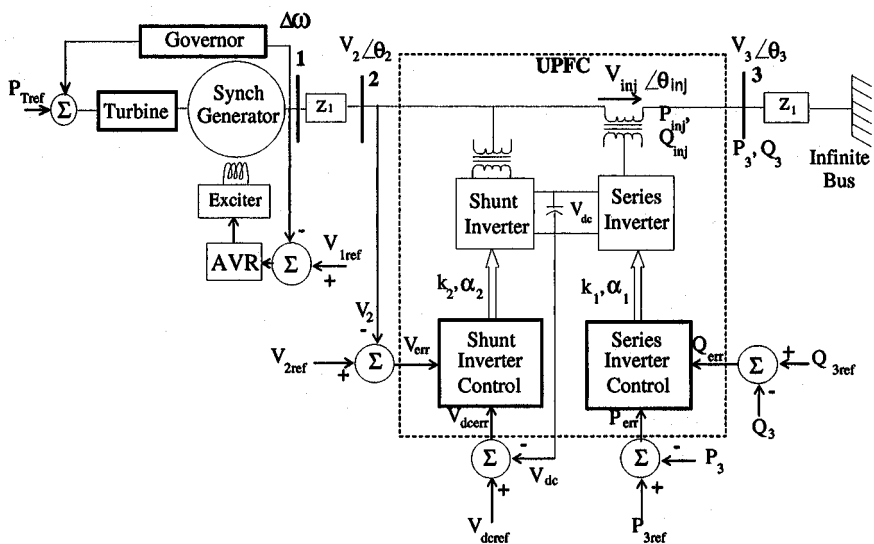


Figure 10.5. Single machine infinite bus power system with a UPFC (dashed lines show the “plant”).

The basic function of the shunt inverter is to generate or absorb the real power demanded by the series inverter at the common dc link. The power demanded by the series inverter at the dc link is converted back to ac by the shunt inverter and fed to the transmission line bus via a

shunt-connected transformer. In addition to this, the shunt inverter can also generate or absorb controllable reactive power if desired and thereby provides independent shunt reactive compensation for the line [3].

The three main control parameters of the UPFC are the magnitude and the angle of the injected voltage  $V_{inj}$ , and the shunt reactive current at  $V_2$ . The control of real and reactive power can be achieved by injecting  $V_{inj}$ , with an appropriate magnitude and angle. The transient stability model for the shunt and series branch of a UPFC in the  $dq$  reference frame is given in [8]. The conventional shunt and series branch control of the UPFC is briefly described below.

**2.3.1 Series branch control.** The block diagram of the conventional PI controllers for the series branch of the UPFC is shown in Figure 10.6. The control of the series inverter can be achieved using  $PQ$ -decoupled control. The outputs of the control system are the modulation index  $k_1$  for the series inverter with a phase shift  $\alpha_1$  between inverter output voltage and the synchronous voltage reference frame (in this case  $\theta_2$ ). Neglecting the inverter losses, the injected active power  $P_{inj}$ , reactive power  $Q_{inj}$ , output active power  $P_3$ , and reactive power  $Q_3$  are given by the equations below.

$$P_{inj} = \frac{V(E_{1q} - E_{1q} \cos(\delta) + E_{1d} \sin(\delta))}{X} \quad (10.6)$$

$$Q_{inj} = \frac{VE_{1d} \cos(\delta) + VE_{1q} \sin(\delta) - VE_{1d} + E_{1d}^2 + E_{1q}^2}{X} \quad (10.7)$$

$$P_3 = \frac{V^2 \sin(\delta) + VE_{1q}}{X} \quad (10.8)$$

$$Q_3 = \frac{2VE_{1d} \cos(\delta) + 2VE_{1q} \sin(\delta) + E_{1d}^2 + E_{1q}^2}{2X} \quad (10.9)$$

where

$$\begin{aligned} V_{inj} &= \sqrt{E_{1d}^2 + E_{1q}^2}, \quad E_{1q} = V_{inj} \sin(\theta_{inj}), \quad E_{1d} = V_{inj} \cos(\theta_{inj}) \\ V_2 &= V_3 = V, \quad \delta = \theta_2 - \theta_3 \end{aligned} \quad (10.10)$$

In (10.8),  $P_3$  is mainly affected by  $E_{1q}$  whereas (10.9) shows that is affected by both  $E_{1q}$  and  $E_{1d}$ . In incremental form, the line active and reactive power can be expressed in terms of  $\Delta E_{1q}$  and  $\Delta E_{1d}$  as given

$$\Delta P_3 = \frac{V}{X} \Delta E_{1q} \quad (10.11)$$

$$\Delta Q_3 = \frac{1}{X} (\Delta E_{1d} V \cos(\delta) + \Delta E_{1q} V \sin(\delta) + \Delta E_{1d} E_{1d0} + \Delta E_{1q} E_{1q0}) \quad (10.12)$$

However, it can be assumed in practice that  $\cos(\delta)$  is close to unity and  $\sin(\delta)$  is close to zero since the phase angle between the two buses (receiving and sending ends) on a transmission line is less than  $30^\circ$ , which leads to

$$\Delta Q_3 = \frac{1}{X} (V \Delta E_{1d} + E_{1d0} \Delta E_{1d} + E_{1q0} \Delta E_{1q}) \quad (10.13)$$

The conventional PI control for the series branch of the UPFC (with the switches  $S_1$  and  $S_2$  at position 1) is shown in Figure 10.6.

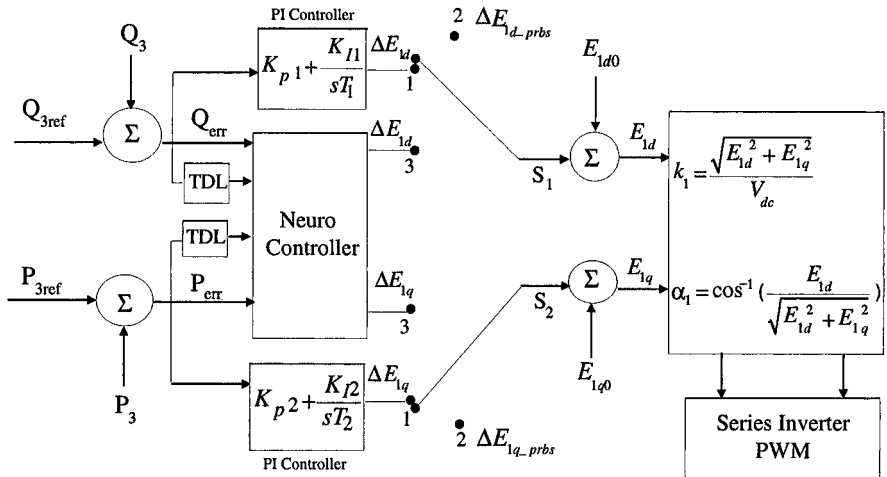


Figure 10.6. Series inverter control with conventional PI controllers, with neuro-controller and the inputs to the neurocontroller including two previous time delayed values of the signals (TDL means tapped delayed lines).

**2.3.2 Shunt branch control.** Control of the shunt active and reactive current is achieved by varying the shunt inverter voltage active  $E_{2d}$  and reactive components  $E_{2q}$ , respectively. The reactive power flow and shunt input voltage can be regulated by the active voltage component  $E_{2d}$  and the dc-link capacitor voltage  $V_{dc}$  support can be achieved by regulating  $E_{2q}$ . Figure 10.7 shows a typical block diagram of the conventional PI controllers for the UPFC's shunt branch control. The outputs of the control system are the modulation index  $k_2$  for the shunt inverter with a phase shift  $\alpha_2$  between the inverter output voltage and the synchronous voltage reference frame (in this case  $\theta_2$ ). The conven-

tional PI control for the shunt branch of the UPFC (with the switches  $S_1$  and  $S_2$  at position 1) is shown in Figure 10.7.

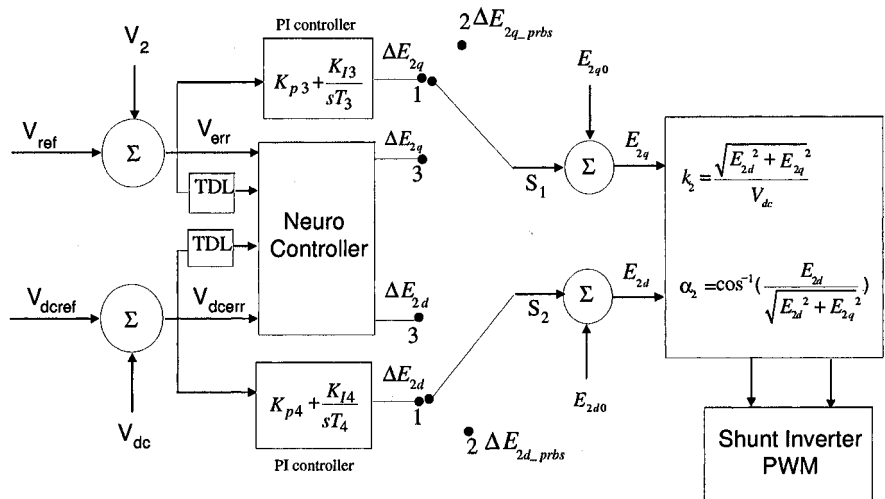


Figure 10.7. Shunt inverter control with conventional PI controllers and neurocontroller (TDL means tapped delayed lines).

### 3. Adaptive Neurocontrol of FACTS Devices

Neural networks can be used to adaptively control a nonlinear system and will continue to have some desired dynamic response even when system conditions change. Two distinct approaches for the design of adaptive controllers using neural networks are *Direct Adaptive Neurocontrol* and *Indirect Adaptive Neurocontrol* schemes. In direct control, the parameters of the controller are adjusted to minimize the observed output error, while in the indirect control scheme, parameters of the plant to be controlled are estimated using a neural network, called the *identifier* or the *model* and the controller parameters are adjusted based on these estimates [11]. The latter technique is presented in this chapter due to the ever changing nature of the power system.

A schematic diagram of an indirect adaptive neurocontroller connected to a plant is shown in Figure 10.8. It basically consists of one neural network used as a neurocontroller, along with a second neural network used for identifying the plant called the neuroidentifier [5]. It also contains a desired response predictor. All these components are described below.

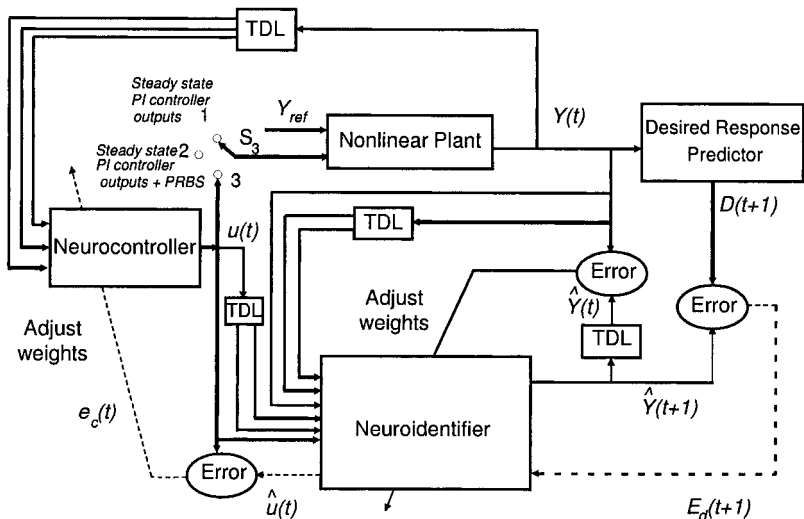


Figure 10.8. Indirect adaptive neurocontroller design structure for a nonlinear plant consisting of a neuroidentifier and a desired response predictor.

### 3.1 Neuroidentifier

The neuroidentifier is developed using the series-parallel Nonlinear Auto Regressive Moving Average (NARMA) model [11]. This model output  $\hat{Y}$  at time  $t + 1$  depends on both  $n$  past values of output and  $m$  past values of input. The neuroidentifier output equation takes the form

$$\hat{Y}(k+1) = f \begin{bmatrix} Y(t), Y(t-1), \dots, Y(t-n+1) \\ u(t), u(t-1), \dots, Y(t-m+1) \end{bmatrix} \quad (10.14)$$

where  $Y(t)$  and  $u(t)$  represent the output and input of the plant to be controlled at time  $t$ , respectively. The NARMA model has been chosen in preference to all other system identification models [11] because online training is desired to correctly identify the dynamics of the FACTS device and therefore avoiding a feedback loop in the model, which allows static backpropagation to be used to adjust the neural network weights. This reduces the computational overhead substantially for online training.

### 3.2 Neurocontroller

The neurocontroller in Figure 10.8 replaces the conventional linear controller and its weights are adapted if necessary at every time step based on the neuroidentifier's prediction of the system outputs at the next time step. The difference between the outputs of the desired re-

sponse predictor (described below) and the neuroidentifier forms the error signal which is then backpropagated through the neuroidentifier for the neurocontroller weight update.

### 3.3 Desired response predictor

The desired response predictor (DRP) in Figure 10.8 is designed [21] to have the following characteristics:

- 1 It must be flexible enough to modify the dynamic performance of the neurocontroller such as the rise time and damping.
- 2 The desired response signal  $D(t + 1)$  must ensure that the FACTS device is inherently stable at all times. In other words, the predictor must be stable.
- 3 The desired response signal must incorporate the effects of a damping controller for the plant.

The DRP is designed on the basis of guiding the disturbed output variables  $Y(t)$ , in this case the deviations in terminal voltage and speed, to a desired steady-state operating point or set point, in a step-by-step fashion. In other words, a desired trace of outputs from  $t$  to  $t + 1$  can be predicted, based on the present and past-time values of the outputs  $Y$ . The equation of the DRP is

$$D(t + 1) = A_0 Y(t) + A_1 Y(t - 1) + \dots + A_N Y(t - N) \quad (10.15)$$

where  $A_i$  ( $i = 0, 1, \dots, N$ ) are chosen so that any disturbed output variable always transfers towards the desired steady-state operating point, that is, the DRP is always globally asymptotically stable.  $D(t + 1)$  is the value predicted for the next immediate time step, and  $Y$ , for example, in the case of a STATCOM, can be the voltage deviations  $\Delta V$  at the bus where the STATCOM is connected or its dc capacitor voltage deviations  $\Delta V_{dc}$ .

In (10.15), it is assumed that each output variable  $D$  of the DRP is a linear combination of the independently predicted output variables of the dynamic system. The magnitude of the coefficients,  $A_i$ , determines the magnitude of the error signal between the neuroidentifier output  $\hat{Y}(t + 1)$  and the desired response signal  $D(t + 1)$ , and therefore, the magnitude of the error to be backpropagated to the neurocontroller to adapt its weights.

If the output  $Y(t)$  is bounded for  $0 < t < \infty$  and

$$\lim_{t \rightarrow \infty} (Y(t) - D(t)) = 0 \quad (10.16)$$

then a predictor can be designed which forces the FACTS device to respond, by means of the neurocontroller, to return the system to its desired setpoints [21]. The magnitude of the forcing signal depends on the coefficients  $A_i$ .

If (10.16) does not hold then the control variables will not return the system to its setpoints after a disturbance. The fundamental assumption made in this design is that it is possible for a controller to return the system variables to their setpoints after a disturbance as explained in [4], [21].

### 3.4 Adaptive neurocontrol of a STATCOM based power system

The indirect adaptive neurocontrol architecture of Figure 10.8 is used to replace the conventional PI controllers of the STATCOM. The design and simulation results are described in the following subsections. First of all, such a neurocontroller needs an identifier which replaces the need for any conventional mathematical description of the system.

**3.4.1 Neuroidentifier.** The artificial neural network identifier (ANNI) in Figure 10.8 is a neural network which is trained to identify/model the dynamics of the plant in Figure 10.2 to be controlled. The inputs of the ANNI are the plant inputs  $u = (\Delta e_d, \Delta e_q)$  and the plant outputs  $Y = (\Delta V, \Delta V_{dc})$  at times  $t$ ,  $(t - 1)$ , and  $(t - 2)$  along with a constant bias input, and the neural network training sampling time step is  $375 \mu s$ . This sampling time step is chosen since the simulation is carried out in the PSCAD/EMTDC software where small time steps are required for numerical integration to be stable. The PSCAD simulation is carried out at  $75 \mu s$  time steps and every fifth samples ( $375 \mu s$ ), information is sent from PSCAD/EMTDC to the neuroidentifier. For the combination of inputs mentioned above, the ANNI estimates the plant outputs  $\hat{Y} = (\Delta \hat{V}, \Delta \hat{V}_{dc})$  at time  $(t + 1)$  (Figure 10.9).

The ANNI is trained in a way that it learns the dynamics of the plant during small disturbances as well as during large natural disturbances or faults in the network. In order to do this, two sets of training are applied to the neuroidentifier. The first set which is called *forced-training*, with switches  $S_1$  and  $S_2$  in Figure 10.2 in position 2, trains the identifier to track the plant dynamics when it is perturbed using small Pseudorandom Binary Signals (PRBS). The second set, called *natural training*, trains the identifier to learn the dynamics of the plant when the PRBS is stopped and the system is exposed to a large disturbance such as a three-phase short circuit. In each case the estimated output of the identifier

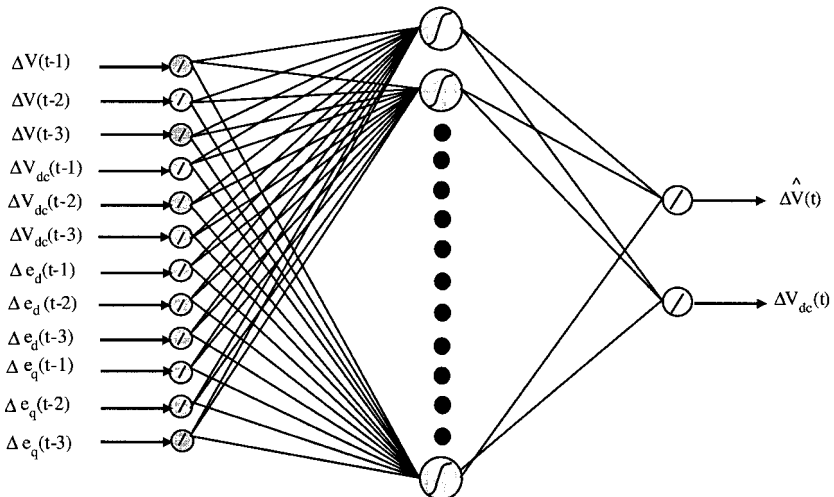


Figure 10.9. Neuroidentifier structure for a STATCOM neurocontroller design.

is compared with the actual output of the plant and the resultant error vector is formed which is backpropagated through the neural network to adjust its weights (Figure 10.10).

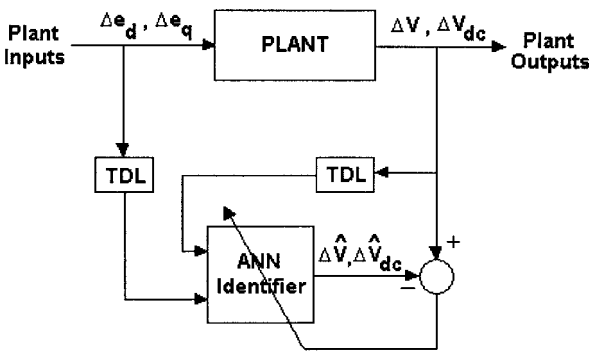


Figure 10.10. Neuroidentifier training for a STATCOM neurocontroller design.

Details of training the neuroidentifier appear in the authors' previous work in [5].

**3.4.2 Neurocontroller.** The neurocontroller is a neural network trained to adaptively control the plant outputs. The seven inputs to the neurocontroller are the plant outputs  $Y = (\Delta V, \Delta V_{dc})$  at times  $(t - 1)$ ,  $(t - 2)$ , and  $(t - 3)$  along with a constant bias input. In turn the neurocontroller generates the optimal control signals  $u = (\Delta e_d, \Delta e_q)$  as

the plant inputs in order to reduce the error between the reference and actual values of  $V$  and  $V_{dc}$  in the plant.

Here, the neurocontroller consists of two separate neural networks, one for the line voltage control and the other for the dc link voltage control (Figure 10.11).

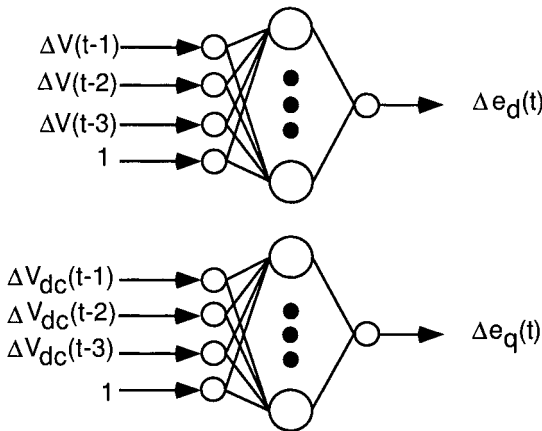


Figure 10.11. Neurocontroller structure for a STATCOM.

The neurocontroller undergoes two training stages, namely, a *pre-training stage* and a *post-training stage* [5].

In the pre-training stage, the system is simulated in the normal mode (with conventional PI controllers controlling the plant), until it reaches a steady state, where the controller outputs are at their constant values  $\Delta e_{d0}$  and  $\Delta e_{q0}$ . Now the PI controllers are deactivated by moving switches  $S_1$  and  $S_2$  from position 1 to position 2 (Figure 10.2), and the plant inputs  $\Delta e_d$  and  $\Delta e_q$  are held constant at  $\Delta e_{d0}$  and  $\Delta e_{q0}$ , respectively, while PRBS signals (called forced training) are added to each one from an external source and the neurocontroller is trained using the error signal  $e_c$  shown in Figure 10.8. The magnitudes of the PRBS signals for  $\Delta e_d$  and  $\Delta e_q$  are selected in a way that result in  $\pm 5\%$  change in their corresponding controlled variables, i.e., the line voltage and DC link voltage, respectively. It should be noted that at this stage, the neurocontroller is not controlling the plant (i.e., switch  $S_3$  in Figure 10.8 is in position 2).

During the post-training stage, the neurocontroller controls the plant (i.e., switch  $S_3$  in Figure 10.8 is now in position 3), while the PRBS is set to zero and the system is exposed to some natural faults/disturbances such as short circuit tests. Training of the neurocontroller still continues using the same scheme shown in Figure 10.8.

**3.4.3 Simulation results.** A 100 ms three-phase short circuit is applied to the middle of the transmission line, where the STATCOM is connected to the network. Simulation results appear in the Figures 10.12 and 10.13, which show that the proposed neurocontroller provides more effective damping compared to that of the PI controller. Detailed results are given in [13].

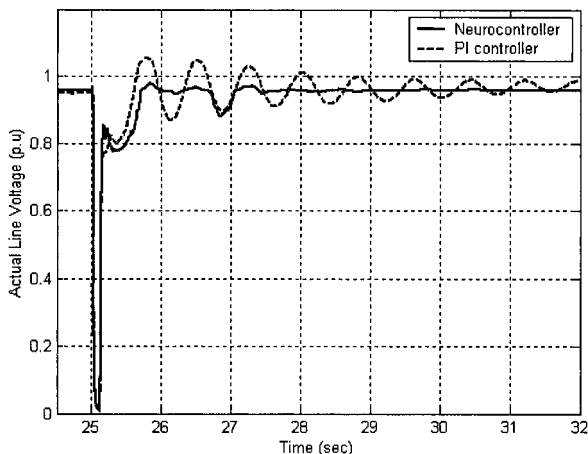


Figure 10.12. Line voltage during a 100 ms three-phase short circuit at the midline.

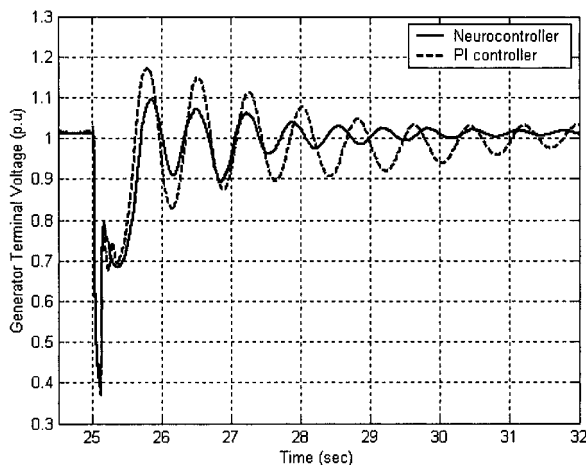


Figure 10.13. Generator terminal voltage during a 100 ms short circuit at the midline.

### 3.5 Adaptive neurocontrol of a UPFC based power system

In the series and shunt UPFC branch neurocontroller (NC) design, each neurocontroller consists of two separate neural networks, one for the identifier/model (described in Section 3.1) and the other for the controller (described in Section 3.2). The neurocontroller is used to replace the conventional PI controllers in each branch (Figures 10.6 and 10.7). The training of neurocontrollers like the neuroidentifiers also takes place in two phases, namely a *pre-control phase* and a *post-control phase* [5]. Both neurocontrollers are trained simultaneously.

**3.5.1 Pre-control training phase.** During the pre-control phase, the inputs to the neurocontrollers in Figures 10.14 and 10.15 are the perturbed outputs from the plant. The PRBS signals (with switches  $S_1$  and  $S_2$  at position 1 in Figures 10.14 and 10.15, respectively) are applied as inputs to the neuroidentifiers and to the plant to cause the necessary perturbations. During this phase the weights of the neuroidentifiers are held fixed.

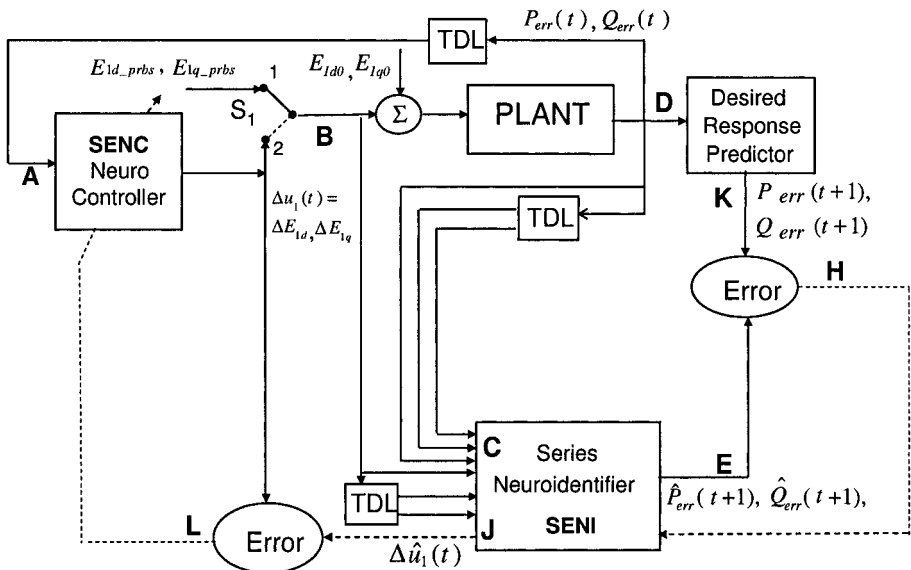


Figure 10.14. Training of SENC to update its weights by backpropagating the error signals at L.

**Series Neurocontroller:** The series UPFC branch neurocontroller (SENC) in Figure 10.14 is a three-layer feedforward neural network with six inputs, a single hidden layer with eighteen sigmoidal neurons and two

outputs. There are two types of inputs to the SENC, namely,  $P_{err}$  and  $Q_{err}$ . These signals at time  $t - 1$ ,  $t - 2$ , and  $t - 3$  form the six inputs. The two outputs of the SENC ( $\Delta E_{d1}$  and  $\Delta E_{q1}$ ) are the control signals  $\Delta u_1(t)$ . The outputs  $(P_{err}(t), Q_{err}(t))$  of the plant at D are fed into the desired response predictor [4], which predicts  $P_{err}(t + 1)$  and  $Q_{err}(t + 1)$  at K. The output  $(\hat{P}_{err}(t + 1), \hat{Q}_{err}(t + 1))$  of the series neuroidentifier (SENI) at E is subtracted from the outputs of the desired response predictor at K to produce the error signal at H which is backpropagated through the SENI to obtain the desired control signal  $\Delta \hat{u}_1(t)$ . The difference between  $\Delta \hat{u}_1(t)$  and the output  $\Delta u_1(t)$  of SENC generates the error signal at L which is used to update the weights of the SENC using backpropagation. Pre-control training is terminated when the weights of the SENC have converged for the PRBS signal applied over a number of operating points of the plant. The next phase of the training (post-control) for the SENC is carried out while the SENC is allowed to control the plant.

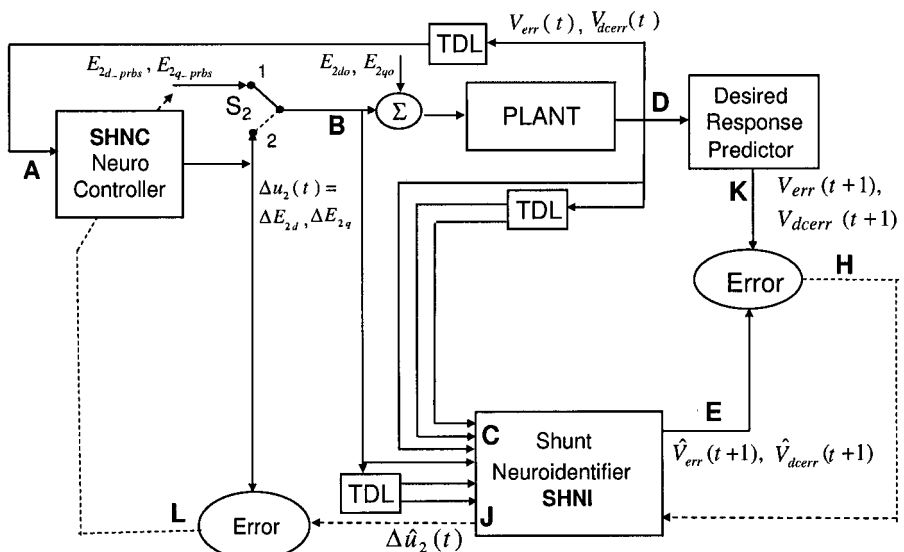


Figure 10.15. Training of SHNC to update its weights by backpropagating the error signals at L.

**Shunt Neurocontroller:** The shunt UPFC branch neurocontroller (SHNC) in Figure 10.15, is a three-layer feedforward neural network with six inputs, a single hidden layer with eighteen sigmoidal neurons and two outputs. Figure 10.15 shows the SHNC development architecture and the respective inputs and outputs for the pretraining phase. The PRBS signals are applied to the input of the shunt UPFC branch and the shunt

neuroidentifier (SHNI) by placing the switch  $S_2$  at position 1. The outputs of the plant at D are fed into the desired response predictor, which predicts  $V_{err}(t + 1)$  and  $V_{dcerr}(t + 1)$  at K. The output of SHNI at E is subtracted from the output of the desired response predictor at K to produce the error signal at H which is backpropagated through the SHNI to obtain the desired control signal  $\Delta\hat{u}_2(t)$ . The difference between  $\Delta\hat{u}_2(t)$  and the outputs  $\Delta u_2(t)$  of SHNC, generates the error signal at L which is used to update the weights of the SHNC using backpropagation. Pre-control training is terminated when the weights of the SHNI and SHNC have converged over a number of operating points. The next phase of the training (post-control) for the SHNC is carried out while the SHNC is allowed to control the plant.

**3.5.2 Post-control training phase.** During this phase, online training of the neurocontrollers continues while they are controlling their respective branches of the UPFC. The PRBS signals used in the pre-control phase are now set to zero and outputs from the neurocontrollers are applied to the plant (with switches  $S_1$  and  $S_2$  in Figures 10.14 and 10.15 respectively at position 2). The following steps are carried out during the post-control phase.

- 1 In the post-training of the neurocontrollers, the output of the neuroidentifiers at E ( $\hat{P}_{err}(t + 1)$ ,  $\hat{Q}_{err}(t + 1)$  of the SENI, and  $\hat{V}_{err}(t + 1)$ ,  $\hat{V}_{dcerr}(t + 1)$  of the SHNI), and the desired response at K ( $P_{err}(t + 1)$ ,  $Q_{err}(t + 1)$  of the series branch and  $V_{err}(t + 1)$ ,  $V_{dcerr}(t + 1)$  of shunt branch), are subtracted respectively to produce error signals at H. The error signals at H are backpropagated through the neuroidentifiers and their derivatives are obtained at J (with the weights of the neuroidentifiers fixed). The backpropagated signals at J are subtracted from the output signals of the neurocontrollers to produce other error signals at L.
- 2 These error signals at L are then used to update the weights of the neurocontrollers using the backpropagation algorithm. This causes the neurocontrollers to change their outputs in a way which drives the error signals at L, and therefore at H, to zero.
- 3 New control signals are calculated  $\Delta E_{1d}$ ,  $\Delta E_{1q}$ , for the series branch, and  $\Delta E_{2d}$ ,  $\Delta E_{2q}$  for the shunt branch, using the updated weights in step (2) and are then applied at the next time step ( $t + 1$ ) to the plant at B.

These steps are repeated for the subsequent time periods [4].

**3.5.3 Simulation results.** The system model in Figure 10.16 comprises of a synchronous generator (590 MVA, 38 kV line to line) [9] operating at real power output,  $P = 0.5$  p.u. and reactive power output,  $Q = 0.1$  p.u., with a total transmission line impedance of  $Z = 0.02 + j0.4$  p.u. ( $= 2Z_1 + Z_2$ ). The governor and turbine models are the IEEE standard models of PSCAD/EMTDC [14]. The parameters of the PI controllers are fine tuned for this operating point using a time response analysis method [15]. A sampling frequency of 10 kHz is used to sample the outputs of the plant.

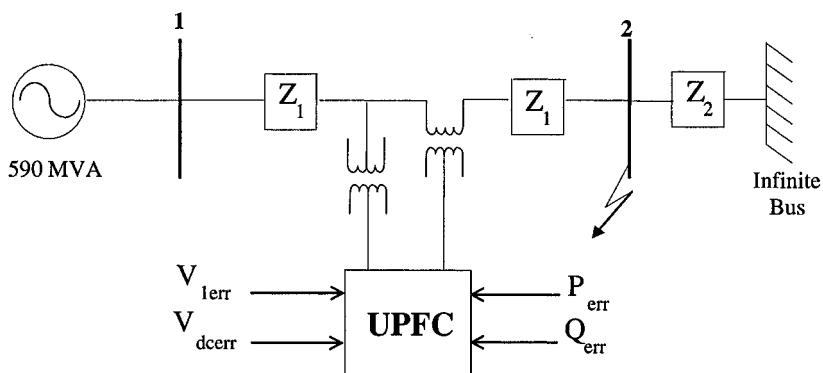


Figure 10.16. Single machine infinite bus power system with a single transmission line and a UPFC.

*Neuroidentification of Plant Dynamics:* Identification of the error signals  $P_{err}(t)$ ,  $Q_{err}(t)$  by SENI and  $V_{err}(t)$ ,  $V_{dcerr}(t)$  by SHNI are carried out at different plant operating points and their weights are continually updated. Figures 10.17 and 10.18 show typical outputs of SENI ( $\hat{P}_{err}(t)$ ,  $\hat{Q}_{err}(t)$ ), and Figures 10.19 and 10.20 show typical outputs of SHNI ( $\hat{V}_{err}(t)$ ,  $\hat{V}_{dcerr}(t)$ ).

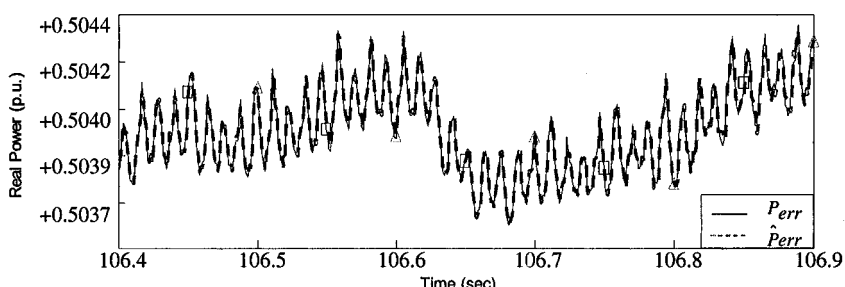


Figure 10.17. Actual signal  $P_{err}(t)$  of the plant and estimated signal  $\hat{P}_{err}(t)$  by the SENI.

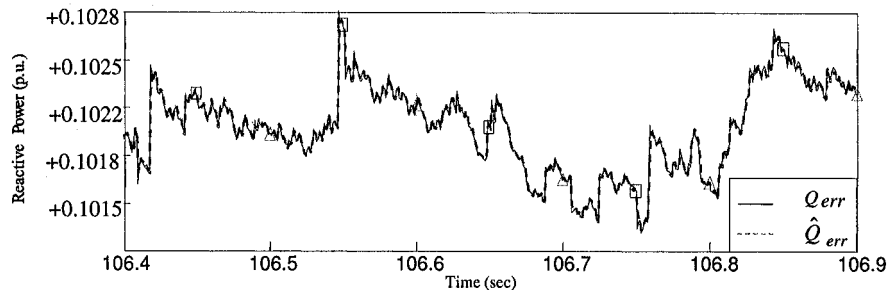


Figure 10.18. Actual signal  $Q_{err}(t)$  of the plant and estimated signal  $\hat{Q}_{err}(t)$  by the SENI.

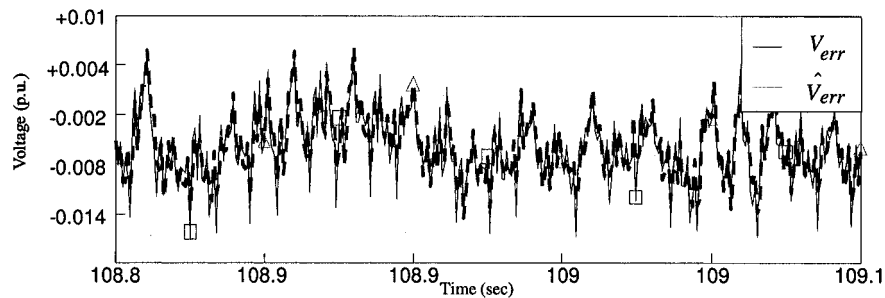


Figure 10.19. Actual signal  $V_{dcerr}(t)$  of the plant and estimated signal  $\hat{V}_{dcerr}(t)$  by the SHNI.

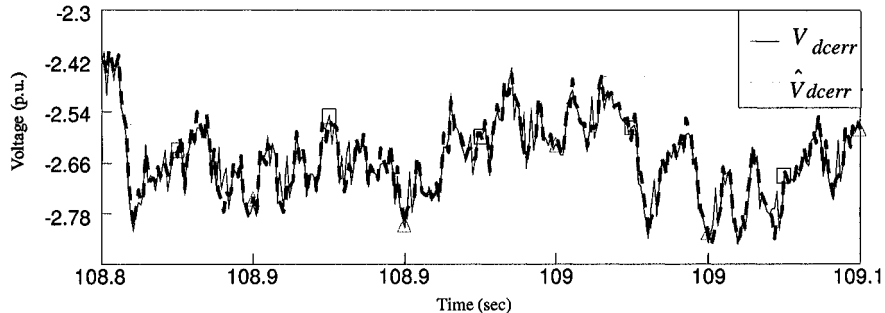


Figure 10.20. Actual signal  $V_{err}(t)$  of the plant and estimated signal  $\hat{V}_{err}(t)$  by the SHNI.

*Neurocontrol of Plant:* The NCs and the PI controllers' performances are evaluated by applying a 180 ms three phase short circuit fault at bus

2 in Figure 10.16 at two different operating points given below. Figures 10.21 to 10.23 show the response of the plant with the NCs (SENC and SHNC) in solid lines and with the PI controllers in dashed lines.

- First operating point –  $P = 0.65$  p.u. and  $Q = 0.12$  p.u.: Figures 10.21 and 10.22 show the terminal voltage and load angle responses respectively. For this operating point, it can be seen that the responses of NCs are found to perform better than that of the PI controllers in damping the system oscillations. The maximum overshoot and the settling time are less when compared to that with the PI controllers. In addition, it can be observed especially from Figure 10.19 that the PI controllers' performances have degraded because they were not fine tuned at this operating point.
- Second operating point –  $P = 0.8$  p.u. and  $Q = 0.15$  p.u.: Figure 10.23 shows the load angle response for this operating point which is even further away from the one at which the PI controllers were fine tuned. For the plant with the PI controllers, the load angle increases drastically after the fault, and eventually loses stability. The plant with NCs on the other hand damps out the oscillations and restores the system to stability. The NCs give performances similar to those at previous operating points and maintain plant stability. This is because the NCs are trained online and hence they are able to adapt to changes in operating conditions with the use of the neuroidentifiers. Detailed results and explanations are given in [16].

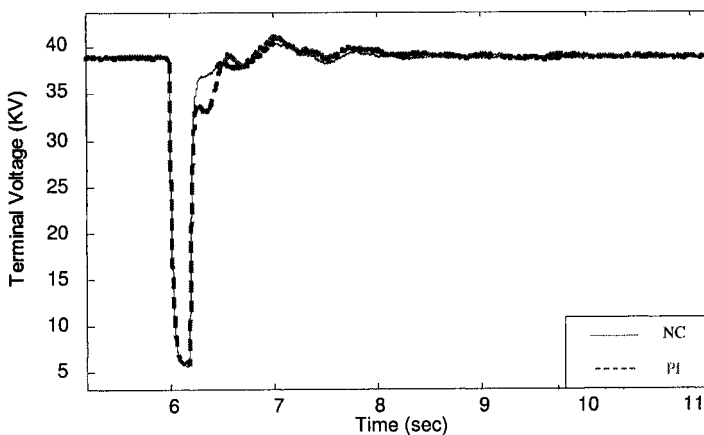


Figure 10.21. Terminal voltage response of the synchronous generator operating ( $P = 0.65$  p.u. and  $Q = 0.12$  p.u.) for a 180 ms three phase short circuit at Bus 2.

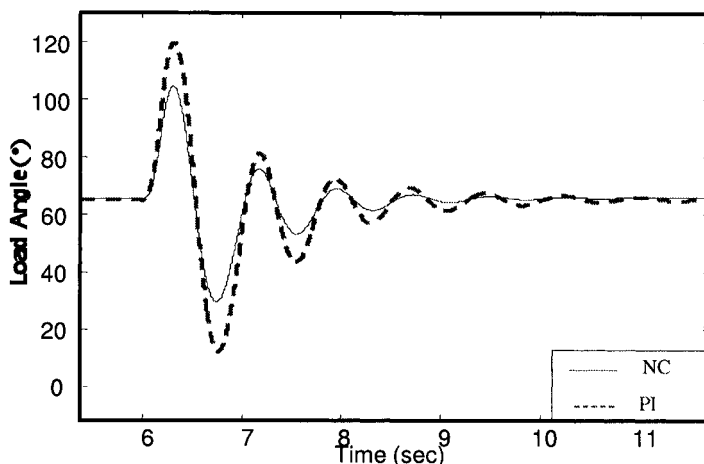


Figure 10.22. Load angle response of the synchronous generator operating ( $P = 0.65$  p.u. and  $Q = 0.12$  p.u.) for a 180 ms three phase short circuit at Bus 2.

The next section describes how optimal neurocontrollers can be designed based on adaptive critic designs which uses an approximate cost-to-go function of the Bellman's equation to update the weights of the neurocontroller unlike adaptive neurocontrol which uses the error predicted for next time step.

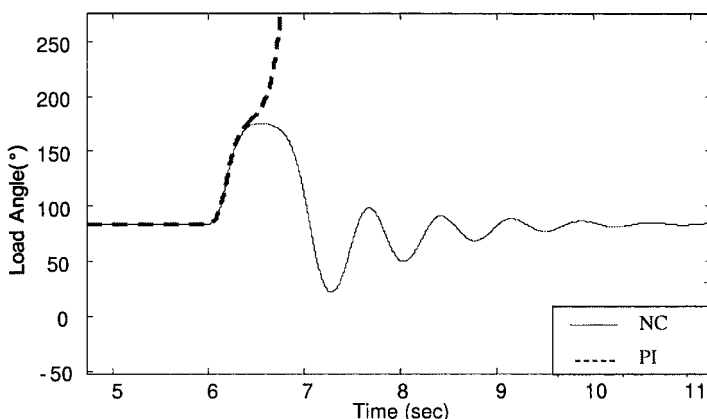


Figure 10.23. Load angle response of the synchronous generator operating ( $P = 0.8$  p.u. and  $Q = 0.15$  p.u.) for a 180 ms three phase short circuit at Bus 2.

#### 4. Optimal Neurocontrol with Adaptive Critic Designs

Adaptive Critic Designs (ACDs) are neural network designs capable of optimization over time under conditions of noise and uncertainty. A family of ACDs was proposed by Werbos [17] as a new optimization technique combining concepts of reinforcement learning and approximate dynamic programming. For a given series of control actions that must be taken in sequence, and not knowing the quality of these actions until the end of the sequence, it is impossible to design an optimal nonlinear controller using traditional supervised ANN learning.

Dynamic programming prescribes a search which tracks backward from the final step, rejecting all suboptimal paths from any given point to the finish, but retains all other possible trajectories in memory until the starting point is reached. However, many paths which may be unimportant are nevertheless also retained until the search is complete. The result is that the procedure is too computationally demanding for most real problems. In supervised learning, an ANN training algorithm utilizes a desired output and, comparing it to the actual output, generates an error term to allow learning. For a multilayer perceptron (MLP) type ANN the backpropagation algorithm is typically used to get the necessary derivatives of the error term with respect to the training parameters and/or the inputs of the network. However, backpropagation can be linked to reinforcement learning via a neural network called the ***Critic*** network, which has certain desirable attributes.

Critic based methods remove the learning process one step from the control neural network (traditionally called the “**Action** network” or “**actor**” in ACD literature), so the desired trajectory or control action information is not necessary. The Critic network learns to approximate the cost-to-go or strategic utility function, and uses the output of an Action network as one of its inputs directly or indirectly. When the Critic network learns, backpropagation of error signals is possible along its input pathway from the Action network. To the backpropagation algorithm, this input pathway looks like just another synaptic connection that needs weight adjustment. Thus, no desired signal is needed. All that is required is a desired cost function

$$J(t) = \sum_{k=0}^{\infty} \gamma^k U(t+k) \quad (10.17)$$

where  $\gamma$  is a discount factor for finite horizon problems ( $0 < \gamma < 1$ ), and  $U(\cdot)$  is the utility function or local cost. The utility function here

is similar to the desired response predictor output described in Section 3.3.

The Critic and Action neural networks can be connected together directly (Action-dependent designs) or through an identification model of a plant provided by a neuroidentifier (Model-dependent designs). There are three classes of implementations of ACDs called Heuristic Dynamic Programming (HDP), Dual Heuristic Programming (DHP), and Globalized Dual Heuristic Dynamic Programming (GDHP), listed in order of increasing complexity and power [18]. In the work described below, the DHP based neurocontroller design technique is illustrated for the SSSC.

## 4.1 Optimal DHP neurocontrol of a Static Synchronous Series Compensator (SSSC)

The DHP algorithm described below therefore uses three different multilayer (three-layer) perceptron neural networks (MLPNNs), one for each of the critic, model, and action networks. The weight vector  $V$  of the MLPNN is adjusted/trained using the gradient descent based backpropagation algorithm. By trial-and-error, fourteen neurons are used in the hidden layer of the MLPNN for the model network, and ten neurons for each of the critic and action networks.

**4.1.1 Critic network.** As mentioned before, the DHPNC is designed to replace the PI regulators  $\text{PI}-i_q$  and  $\text{PI}-i_p$  in Figure 10.4. The input reference vector  $Y_{ref}$  into the SSSC and output vector  $\Delta Y$  from the SSSC are:

- $Y_{ref}(t)$ , input reference vector to the SSSC =  $[i_p^*(t), i_d^*(t), V_{dc}^*(t)]$ .
- $\Delta Y(t)$ , output vector from the SSSC =  $[\Delta i_p(t), \Delta i_q(t)]$ .

The configuration for the critic network adaptation in the DHP is shown in Figure 10.24<sup>1</sup>. The inputs and outputs of the action and model networks used in the critic network adaptation are shown in Figures 10.25 and 10.26.

<sup>1</sup>The same critic network is shown for two consecutive times,  $t$  and  $t+1$ . The discount factor  $\gamma$  is chosen to be 0.5. Backpropagation paths are shown by dotted and dash-dot lines. The output of the critic network  $\hat{\lambda}(t+1)$  is backpropagated through the model network from its outputs to its inputs, yielding the first term of (10.20) and  $\partial J(t+1)/\partial A(t)$ . The latter is backpropagated through the action network from its outputs to its inputs forming the second term of (10.20). Backpropagation of the vector  $\partial U(t)/\partial A(t)$  through the action network results in a vector with components computed as the last term of (10.21). The summation of all these signals produces the error vector  $e_c(t)$  used for training the critic network.  $A(t)$  is the action network output signal shown in Figure 10.26.  $U(t)$  is the utility function given by (10.25).

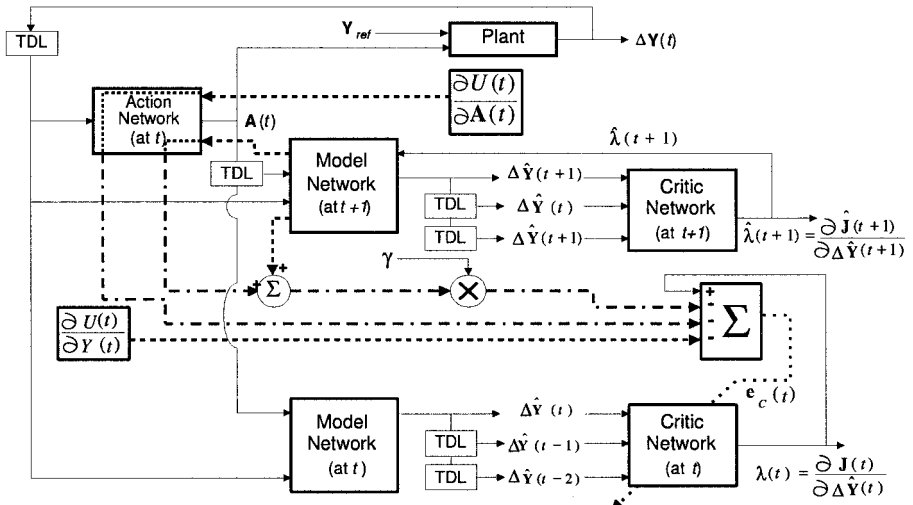


Figure 10.24. Critic network adaptation in DHP showing the implementation of (10.21).

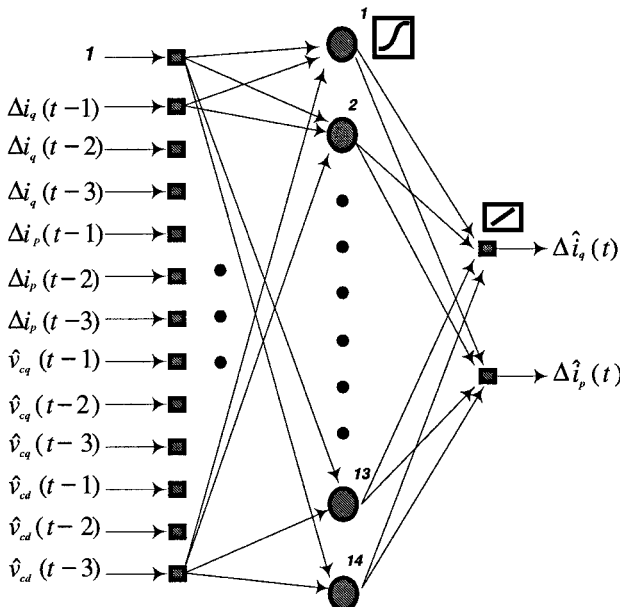


Figure 10.25. Input-output mapping of the model network at  $t$  used in the critic network adaptation in Figure 10.24.

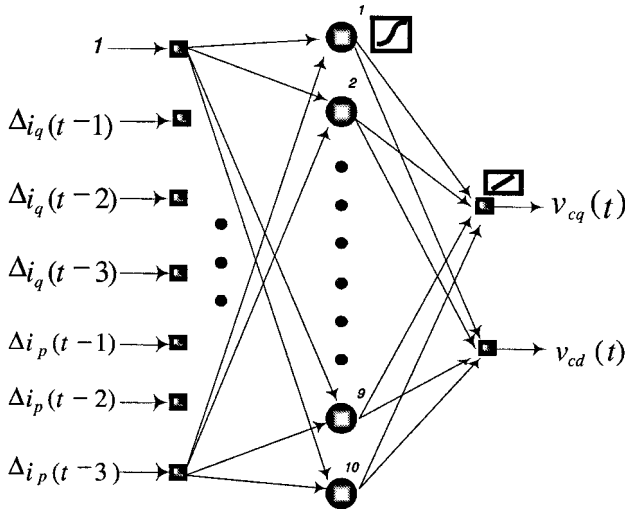


Figure 10.26. Input-output mapping of the action network at  $t$  used in the critic network adaptation in Figure 10.24.  $A(t)$  in Figure 10.24 is  $v_{cq}(t)$  and  $v_{cd}(t)$ .

The critic network estimates the derivatives of function  $J$  with respect to the vector of observables of the plant (identified by the model network), which is  $\Delta \hat{Y}(t) = [\Delta \hat{i}_p(t), \Delta \hat{i}_q(t)]$  (input vector of the critic network), and it learns to minimize the error measure over time

$$\|E_C\| = \sum_t e_C^T(t) e_C(t) \quad (10.18)$$

where

$$e_C(t) = \frac{\partial J[\Delta \hat{Y}(t)]}{\partial \Delta \hat{Y}(t)} - \gamma \frac{\partial \hat{J}[\Delta \hat{Y}(t+1)]}{\partial \Delta \hat{Y}(t)} - \frac{\partial U[\Delta Y(t)]}{\partial \Delta Y(t)} \quad (10.19)$$

and  $\hat{J}$  denotes estimated value of  $J$ .

After exploiting all relevant pathways of backpropagation as shown in Figure 10.24, where the paths of derivatives and adaptation of the critic network are depicted by dotted and dash-dot lines, the error signal  $e_C(t)$  is used for training to update the weights of the critic network.

The  $j^{th}$  component of the second term in (10.19) can be expressed by the output of the critic network at time  $t+1$ ,

$$\hat{\lambda}_i(t+1) = \partial \hat{J}[\Delta \hat{Y}(t+1)] / \partial \Delta \hat{Y}_i(t+1)$$

as

$$\begin{aligned} \frac{\partial \hat{J} [\Delta \hat{Y}(t+1)]}{\partial \Delta Y_j(t)} &= \sum_{i=1}^n \hat{\lambda}_i(t+1) \frac{\partial \hat{Y}_i(t+1)}{\partial \Delta Y_j(t)} \\ &\quad + \sum_{k=1}^m \sum_{i=1}^n \hat{\lambda}_i(t+1) \frac{\partial \Delta \hat{Y}_i(t+1)}{\partial A_k(t)} \frac{\partial A_k(t)}{\partial \Delta Y_j(t)} \end{aligned} \quad (10.20)$$

where  $n$  and  $m$  are the number of outputs of the model and the action networks, respectively.

By using (10.20), each component of the vector  $e_C(t)$  from (10.19) is determined by

$$\begin{aligned} e_{Cj}(t) &= \frac{\partial J [\Delta \hat{Y}(t)]}{\partial \Delta \hat{Y}_j(t)} - \gamma \frac{\partial \hat{J} [\Delta \hat{Y}(t+1)]}{\partial \Delta Y_j(t)} - \frac{\partial U [\Delta Y(t)]}{\partial \Delta Y_j(t)} \\ &\quad - \sum_{k=1}^m \frac{\partial U [\Delta Y(t)]}{\partial A_k(t)} \frac{\partial A_k(t)}{\partial \Delta Y_j(t)} \end{aligned} \quad (10.21)$$

Using (10.21), the expression for the weights' update for the critic network is

$$\Delta V_C(t) = -\eta_C e_C^T(t) \frac{\partial e_C(t)}{\partial V_C(t)} \quad (10.22)$$

where  $\eta_C$  is a positive learning rate and  $V_C$  contains the weights of the DHP critic network.

**4.1.2 Action network.** The adaptation of the action network in Figure 10.24 is illustrated in Figure 10.27<sup>2</sup>, which propagates  $\hat{y}(t+1)$  back through the model network to the action network to give the correct control signal(s),  $A(t)$  in Figures 10.24, 10.26 and 10.27. The goal of this adaptation is expressed as

$$\frac{\partial U [\Delta Y(t)]}{\partial A(t)} + \gamma \frac{\partial \hat{J} [\Delta \hat{Y}(t+1)]}{\partial A(t)} = 0, \quad \forall t \quad (10.23)$$

<sup>2</sup>The discount factor  $\gamma$  is chosen to be 0.5. Backpropagation paths are shown by dotted lines. The output of the critic network  $\hat{y}(t+1)$  at time  $(t+1)$  is backpropagated through the model network from its outputs to its inputs (output of the action network,  $A(t)$ ), and the resulting vector multiplied by the discount factor ( $\gamma = 0.5$ ) and added to  $\partial U(t)/\partial A(t)$ . Then, an incremental adaptation of the action network is carried out by (10.24).

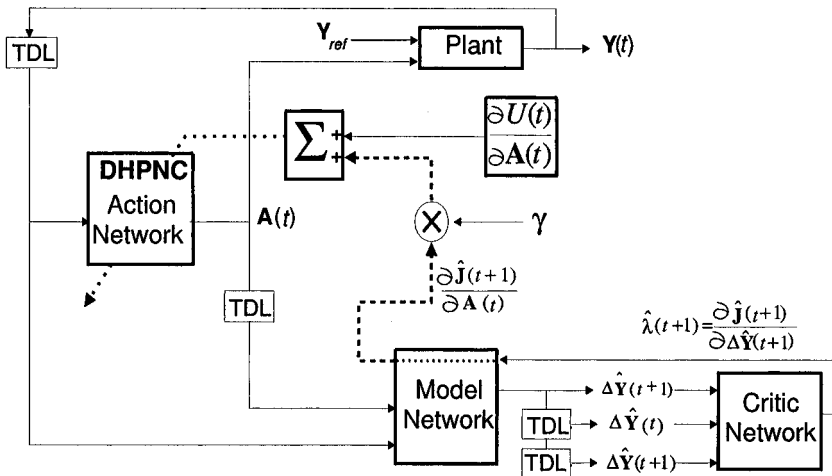


Figure 10.27. Action network adaptation in DHP.

and the weights of the action network are updated by

$$\Delta V_A(t) = -\eta_A \left[ \frac{\partial U[\Delta Y(t)]}{\partial A(t)} + \gamma \frac{\partial \hat{J}[\Delta \hat{Y}(t+1)]}{\partial A(t)} \right]^T \frac{\partial A(t)}{\partial V_A(t)} \quad (10.24)$$

where  $\eta_A$  is a positive learning rate and  $V_A$  contains the weights of the DHP action network.

The discount factor  $\gamma$  is 0.5 and the user-defined utility function  $U(t)$

$$\begin{aligned} U(t) &= [\Delta i_q(t) + \Delta i_q(t-1) + \Delta i_q(t-2)]^2 \\ &+ [\Delta i_p(t) + \Delta i_p(t-1) + \Delta i_p(t-2)]^2 \end{aligned} \quad (10.25)$$

are used in (10.21) and (10.23) during the adaptation of the critic and action networks. The design of the utility function is explained in detail in [21].

**4.1.3 Model network.** Figure 10.28 illustrates how the model network (neuroidentifier) is trained to identify the dynamics of the plant in Figure 10.3. The nonlinear autoregressive moving average with exogenous inputs (NARMAX) model is used as the structure for the on-line identification. The components of vectors  $Y_{ref}(t)$ ,  $\Delta Y(t)$ ,  $A(t)$ , and  $\Delta \hat{Y}(t)$  are already noted above (see Figures 10.25 and 10.26).

The residual vector,  $e_M(t)$  in Figure 10.28 given by (10.26), is used for updating the model network's weights  $V_M$  in (10.14) during training

by the backpropagation algorithm:

$$e_M(t) = \Delta Y(t) - \Delta \hat{Y}(t) = [\Delta i_q(t) - \Delta \hat{i}_q(t), \Delta i_p(t) - \Delta \hat{i}_p(t)] \quad (10.26)$$

$$\Delta V_M(t) = -\eta_M e_M^T(t) \frac{\partial e_M(t)}{\partial V_M(t)} \quad (10.27)$$

where  $\eta_M$  is a positive learning rate and  $V_M$  is the weights of the DHP model network.

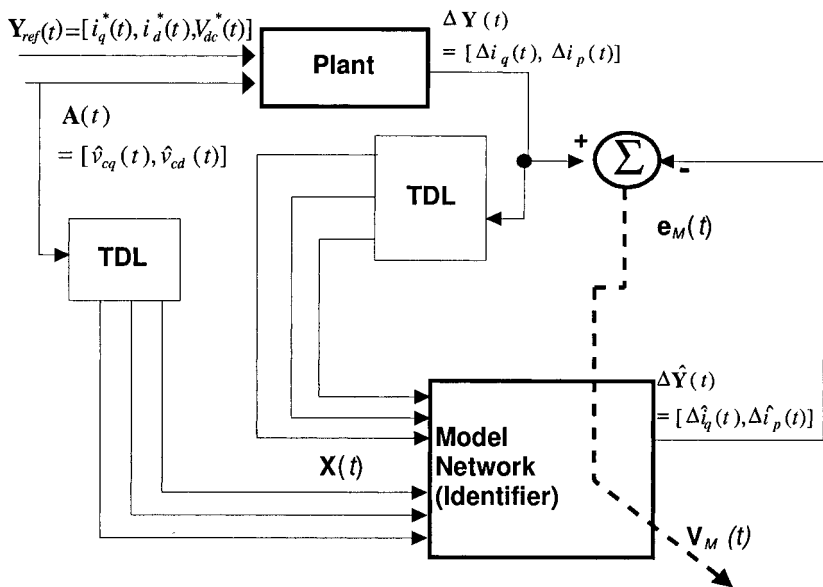


Figure 10.28. NARMAX model for on-line training of the model network.

The training of the critic, action, and model networks in the DHP scheme is carried out in an online mode using different small pseudo-random binary (PRBSs) signals [21] and the training procedures are explained in [21], [17].

Note that the model network is trained before the training of the action and critic networks, and the DHPNC with the fixed (converged) weights for the critic and action networks is used to control the plant for real-time operation. In other words, they have been successfully trained to their optimization purposes, which are the value iteration for the critic network and the policy iteration for the action network [19]. The beauty of the DHP scheme is that it is able to perform well with model uncertainties.

**4.1.4 Simulation results.** This subsection uses simulated results to compare the plant damping when it has a DHP type neuro-controlled SSSC. Results are presented first for a 100 ms and then for a 120 ms three phase short circuit, applied to the infinite bus (receiving end in Figure 10.3) at  $t = 1$  s. The generator operates with a pre-fault steady-state rotor angle of  $53.6^\circ$  ( $P_t=1.0$  p.u.,  $Q_t=0.59$  p.u.). In Figures 10.29 to 10.32, “Uncompensated”, “CONVC”, and “DHPNC” denote the responses of the generator controlled without a SSSC, with a PI controlled SSSC, and with a DHP neuro-controlled SSSC, respectively.

From Figures 10.29 to 10.30, the DHPNC damping control is more effective compared to the CONVC. Also, it is clear from Figures 10.31 and 10.32 that the generator without the SSSC control goes unstable and loses synchronism when the fault duration is 120 ms. In contrast, the DHPNC and CONVC restore the generator to a stable mode, and the DHPNC damping control is more effective compared to the CONVC, which means that the DHPNC allows the generator to be operated closer to its stability limit. Detailed results and explanations are given in [20].

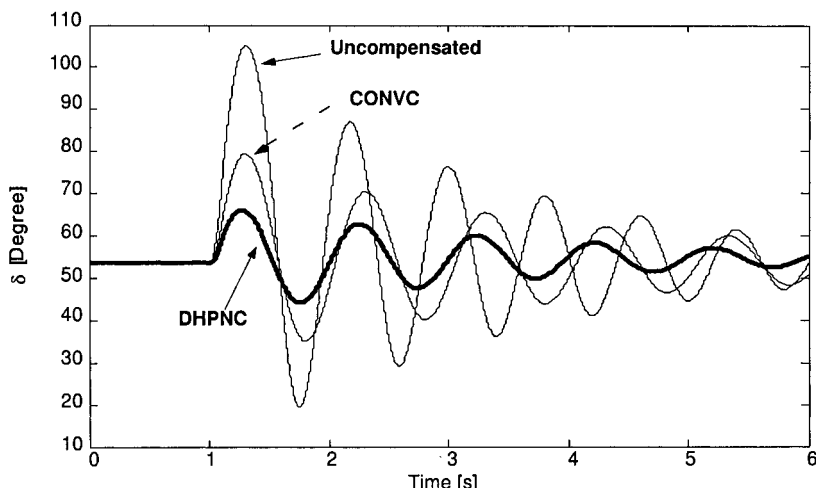


Figure 10.29. A 100 ms three phase short circuit test:  $\delta$ .

## 5. Conclusions

Closed loop feedback controllers which use computational intelligence techniques can be designed to be nonlinear while at the same time able to optimize certain system variables. This chapter has presented adaptive and optimal neurocontrol of several FACTS devices includ-

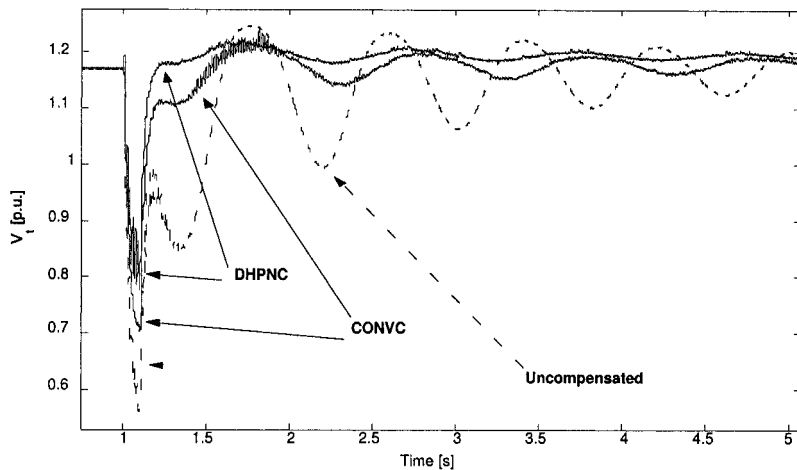


Figure 10.30. A 100 ms three phase short circuit test:  $V_t$ .

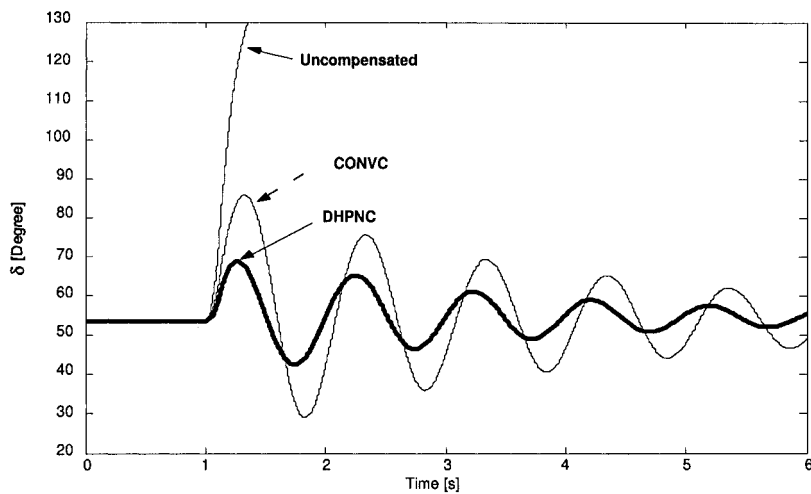


Figure 10.31. A 120 ms three phase short circuit test:  $\delta$ .

ing a STATCOM, an SSSC, and a UPFC on the electric power grid. The PSCAD/EMTDC simulation results show that the selected FACTS devices equipped with such a neurocontroller provide better dynamic performances than when using conventional PI based controllers, with

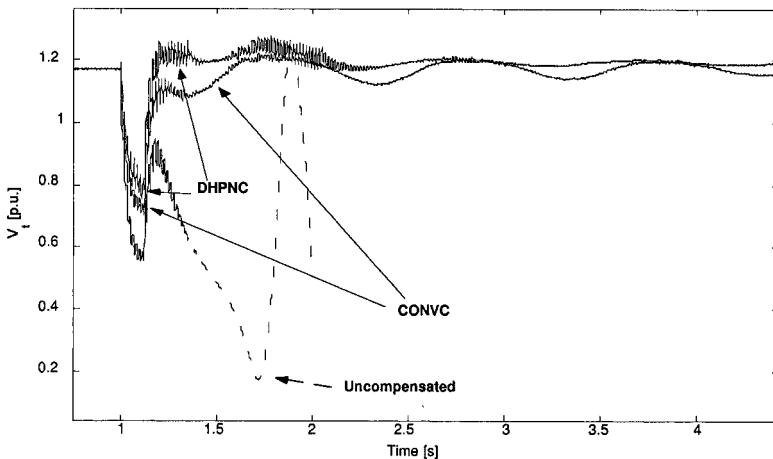


Figure 10.32. A 120 ms three phase short circuit test:  $V_t$ .

respect to damping low-frequency power oscillations and minimizing terminal voltage variations.

The use of fixed parameters in the adaptive critic design based neurocontroller for real-time control not only has an important significance in terms of reducing the number of computations in dealing with the infinite optimal control problem by using the artificial neural networks, but also proves robustness of the adaptive critic designs (ACDs) based controllers. This removes any criticism of not being able to guarantee closed-loop stability when using neural network based controllers. The use of computational intelligence techniques in controlling FACTS devices promises maximum benefit of the usage of FACTS technology.

## 6. Future Research

The authors have applied neurocontrollers to the excitation and turbine control in a single generator [4], [5] as well as multi-generator power systems [21], [21], both by simulation as well as on actual hardware. They then extended this to single-generator systems containing neurocontrollers on a STATCOM [13], or a SSSC [20], or a UPFC [16], and lately to a neurocontrolled series capacitive reactance compensator (SCRC) and a generator in a three-machine ten-bus system [22]. All this work confirms the superior damping abilities of neurocontrolled devices, without the need to have any mathematical knowledge of the system to be controlled. Future work will extend these concepts to larger networks

such as the IEEE 39-bus and 118-bus systems, with particular emphasis on the interaction of multiple neurocontrolled FACTS devices of different types such as STATCOM, SSSC, SCRC and UPFC, and neurocontrolled generators.

## References

- [1] R.M. Mathur and R.K. Varma. *Thyristor-based FACTS Controllers for Electrical Transmission Systems*. IEEE Press and John Wiley & Sons, New York, 2002.
- [2] L. Chunlei, S. Hongbo, and D.C. Yu. A Novel Method of Power Flow Analysis with Unified Power Flow Controller (UPFC). *Proceedings of IEEE PES Winter Meeting*, 4:1114–1120, 2000.
- [3] N.G. Hingorani and L. Gyugyi. *Understanding FACTS: Concepts and Technology of Flexible AC Transmission Systems*. IEEE Press, New York, 1999.
- [4] G.K. Venayagamoorthy and R.G. Harley. Two Separate Continually Online-Trained Neurocontrollers for Excitation and Turbine Control of a Turbo Generator. *IEEE Transactions on Industry Applications*, 38:887–893, 2002.
- [5] G.K. Venayagamoorthy and R.G. Harley. A Continually Online Trained Neurocontroller for Excitation and Turbine Control of a Turbogenerator. *IEEE Transactions on Energy Conversion*, 16:261–269, 2001.
- [6] P.K. Dash, S. Mishra, and G. Panda. Radial Basis Function Neural Network Controller for UPFC. *IEEE Transactions on Power Systems*, 15:1293–1299, 2000.
- [7] P. Kundur. *Power System Stability and Control*. McGraw-Hill, New York, 1994.
- [8] L.Y. Dong, L. Zhang, and M.L. Crow. A New Control Strategy for the Unified Power Flow Controller. *Proceedings of IEEE PES Winter Meeting*, 1:562–566, 2002.
- [9] P.M. Anderson and A.A. Fouad. *Power System Control and Stability*. IEEE Press, New York, 1994.
- [10] T. Makombe and N. Jenkins. Investigation of a Unified Power Flow Controller. *IEE Proceedings on Generation, Transmission and Distribution*, 146:400–408, 1999.
- [11] K.S. Narendra and K. Parthasarathy. Identification and Control of Dynamical Systems using Neural Networks. *IEEE Transactions on Neural Networks*, 1:4–27, 1990.

- [12] G.K. Venayagamoorthy, R.G. Harley, and D.C. Wunsch. Dual Heuristic Programming Excitation Neurocontrol for Generators in a Multimachine Power System. *IEEE Transactions on Industry Applications*, 39:382–394, 2003.
- [13] S. Mohagheghi, R.G. Harley, and G.K. Venayagamoorthy. Intelligent Control Schemes for a Static Compensator Connected to a Power Network. *Proceedings of the 2<sup>nd</sup> IEE International Conference on Power Electronics, Machines and Drives*, 594–599, University of Edinburgh, UK, 2004.
- [14] Manitoba HVDC Research Centre Inc. PSCAD/EMTDC manual Version 3.0, Winnipeg, Canada.
- [15] K. Ogata. *Modern Control Engineering*, 3rd ed.. Prentice-Hall, Upper Saddle River, NJ, 1996.
- [16] R.P. Kalyani and G.K. Venayagamoorthy. Two Separate Continually Online Trained Neurocontroller for a Unified Power Flow Controller. *Proceedings of IEEE-IAS 38<sup>th</sup> Annual Meeting*, 308–315, Salt Lake City, Utah, October 2003.
- [17] P.J. Werbos. Approximate Dynamic Programming for Real-Time Control and Neural Modeling. In D. White and D. Sofge (eds.), *Handbook of Intelligent Control*. 493–526, Van Nostrand Reinhold, New York, 1992.
- [18] D. Prokhorov and D.C. Wunsch. Adaptive Critic Designs. *Transactions on Neural Networks*, 8:997–1007, 1997.
- [19] D.M. Bertsekas. *Dynamic Programming and Optimal Control*. Athena Scientific, Belmont, Massachusetts, 2001.
- [20] J.W. Park, R.G. Harley, and G.K. Venayagamoorthy. New Internal Optimal Neurocontrol for a Series FACTS Device in a Power Transmission Line. *Neural Networks*, 16:881–890, 2003.
- [21] G.K. Venayagamoorthy, R.G. Harley, and D.C. Wunsch. Implementation of Adaptive Critic Based Neurocontrollers for Turbogenerators in a Multimachine Power System. *IEEE Transactions on Neural Networks*, 14:1047–1064, 2003.
- [22] J.W. Park, R.G. Harley, and G.K. Venayagamoorthy. Decentralized Optimal Neuro-Controllers for Generation and Transmission Devices in an Electric Power Network. *IFAC Journal Engineering Applications of Artificial Intelligence*, to appear.

## Chapter 11

# PLACEMENT AND COORDINATED TUNING OF CONTROL DEVICES FOR CAPACITY AND SECURITY ENHANCE- MENT USING METAHEURISTICS

Djalma M. Falcão

*Federal University of Rio de Janeiro, Brazil*

falcao@nacad.ufrj.br

Glauco N. Taranto

*Federal University of Rio de Janeiro, Brazil*

tarang@coep.ufrj.br

**Abstract** This chapter introduces a general framework for the use of Metaheuristics to the problem of placement and tuning of power system controllers. Metaheuristics are top-level general strategies that guide other heuristics to search for feasible solutions in domains where the task is hard. Examples of Metaheuristics are Genetic Algorithms, Simulated Annealing, Tabu Search, Particle Swarm Optimizations, etc. Two applications of Genetic Algorithms to problems in this category are also described. The first application deals with the placement of protection devices in distribution networks in such a way that the benefit produced by these devices, measured in terms of the reduction in the expected outage cost to customers, exceeds the investment, installation, and maintenance costs of the devices. The results obtained in the computational experiments indicate that the proposed methodology produces automatically results comparable to the ones obtained by an expert in the field. The second application deals with the coordinated tuning of power oscillation dampers (POD) in FACTS devices. The tuning procedure is based on simultaneous closure of decentralized control loops. Control robustness is assessed on multiple system scenarios. Results are shown for a test system presenting two lightly damped interarea modes of oscillation. The design objective is to tune a SVC and a TCSC POD to

enhance the damping of the interarea modes to a minimum acceptable value in five operating scenarios.

**Keywords:** Power system control, placement, tuning, metaheuristics.

## 1. Introduction

The deregulation process of the power industry, under way in many countries, has been pushing power system operation towards new and extreme practices. Operating conditions close to physical limits, unusual power flow configurations, lack of adequate reactive support, etc. became common practice in many systems. Combined with the aging of generation and transmission components, these new ways of operating the power system have increased the probability of unpredictable outages which, in many cases, have caused partial or total catastrophic failures leaving large numbers of customers not served [1]-[3].

Power systems, like many other engineering systems, must operate reliably and efficiently under a variety of conditions. This means that control apparatus and systems must be designed in such way as to deal with many operating conditions, including unpredictable situations caused by multiple contingencies, hidden failures, misoperation, etc [4].

This chapter introduces a general framework for the use of Metaheuristics to the problem of placement and tuning of power system controllers. Two applications of Genetic Algorithms to problems in this category are described. The first application deals with the placement of protection devices in distribution networks in such a way that the benefit produced by these devices, measured in terms of the reduction in the expected outage cost to customers, exceeds the investment, installation, and maintenance costs of the devices. The results obtained in the computational experiments indicate that the proposed methodology produces automatically results comparable to the ones obtained by an expert in the field.

The second application deals with the coordinated tuning of power oscillation dampers (POD) in FACTS devices. The tuning procedure is based on simultaneous closure of decentralized control loops. Control robustness is assessed on multiple system scenarios. Results are shown for a test system presenting two lightly damped interarea modes of oscillation. The design objective is to tune a SVC and a TCSC POD to enhance the damping of the interarea modes to a minimum acceptable value in five operating scenarios.

## 2. Problem Formulation

Modern power system economic and secure operation relies heavily on several layers of controls acting on different time-scales and with a variety of objectives and constraints. Examples of such controls are: (a) the ones associated with generating units such as governors, automatic voltage regulators (AVRs), power system stabilizers (PSSs), etc.; (b) transmission and distribution network controls like under-load-tap-changing (ULTC) transformers, voltage regulators, flexible AC transmission system (FACTS) devices, HVDC links, etc; (c) protection devices including relays and circuit breakers, reclosers, etc.; and (d) automatic generation control (AGC).

Most of the controls referred to above, probably with the only exception of AGC, follow local or task oriented control strategies. These controls do not take into consideration a system-wide perspective in their locations, control strategies, and adaptations to operating conditions. Conflicts among local control actions and poor performance in abnormal operating conditions have been identified. The placement and tuning of these controllers are usually decided on an ad hoc basis instead of using procedures based on system performance.

The present complexity of power system operation and economic constraints requires a better use of the available controllers as well as an optimal design of the new ones. In order to achieve that, the system-wide performance of the different control devices must be taken into consideration as well as a guaranty of robust operation in the presence of component losses and contingencies. Hence, control design methods aiming to achieve these goals are of the most relevant importance. These methods should take into consideration both the problems of placement and tuning of the controllers.

### 2.1 The placement problem

A first step in defining a robust and efficient control system is to decide the location (network branch or bus, generator, etc) and type (different FACTS device, PSSs, reclosers, protection device, etc.) of the controllers. Second, the control structure and the allowed parameter range of the devices should be chosen. Extensive simulation studies are required to assess the performance of the available options, which should be guided by the experience of operating personnel and economic and technical constraints. The usual problem is of expanding a control system already in operation rather than to design a brand new one, for instance, to locate new PSSs to improve the oscillation damping in a transmission corridor, considering that the system already have several

PSSs in operation. Another example could be the installation of new switching and protection devices in a distribution network to improve reliability indices related to the frequency and duration of interruptions. The problem can be formulated as an integer/binary programming problem, which may lead to a practically unsolvable formulation if realistic modeling is used. No systematic and automatic approach to solve this problem is available at present. Trial-and-error is the usual procedure followed in the power industry.

## 2.2 The coordinated tuning problem

Given a set of controllers available to perform a control task, either already installed in the system or chosen by solving the placement problem described in the previous section, the next step in the control design is to tune or adjust the parameters of the control devices in order to achieve an overall adequate performance of the control system. Adequate performance in a wide range of operating condition is necessary as on-line adaptive adjustment of parameters is not a practice commonly accepted in the power industry. Robust control techniques have been proposed to solve this problem [5], [6] but present difficulties to deal with large scale power system models. The problem can be formulated as a large-scale nonlinear programming problem with the controller's parameters as optimization variables.

## 2.3 The combined placement and tuning problem

The consideration of the placement and tuning problems as independent problems is justified only for reducing the complexity of the solution approach. If a global optimization of the control system performance is sought, then both problems must be considered together simultaneously, as an optimal tuning may reduce the number and size of the control devices and, conversely, a good choice of the place and type of device may facilitate better tuning.

In practical applications, the combined placement and tuning problem is a mixed-integer nonlinear optimization problem with some *unfriendly* characteristics: high dimensionality, non-convex functions, some function not available explicitly, design bounds not easily determined, etc. Practical application problems usually require the optimization of multiple objectives. Possible approaches to this problem are:

- Some form of decomposition approach that allows the solution in a two-stage iterative fashion: first, propose a potential solution for the placement problem; then, establish the tuning for this potential

solution. Bender's decomposition is a possible technique to be used in such an iterative solution. An illustration of this approach is shown in Figure 11.1, in which different techniques are suggested for the sub-problems solutions.

- A simultaneous solution approach using some form of Metaheuristics. This approach will be further discussed in the next section.

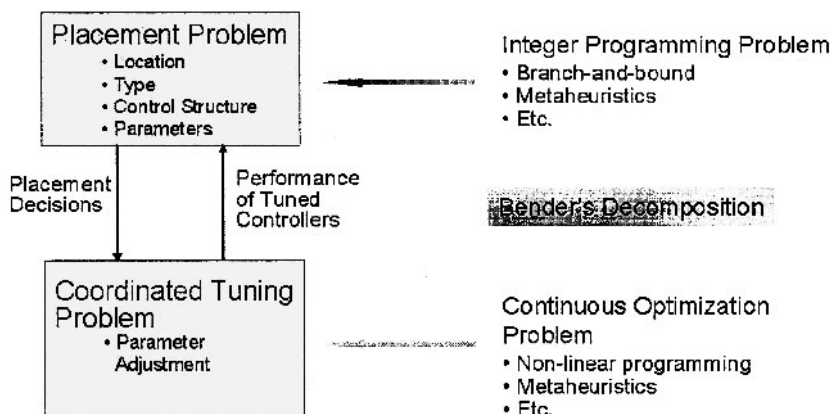


Figure 11.1. Decomposed approach for the simultaneous placement and tuning problem.

### 3. The Metaheuristics Approach

Metaheuristics are top-level general strategies that guide other heuristics to search for feasible solutions in domains where the task is hard [7]. Metaheuristics have been most generally applied to problems classified as NP-hard or NP-complete by the theory of computational complexity. Metaheuristics have also been applied to other combinatorial optimization problems for which it is known that a polynomial-time solution exists but is not practical. Examples of Metaheuristics are Tabu Search, Simulated Annealing, Genetic Algorithms, Particle Swarm Optimization, etc [8].

The application of the Metaheuristics approach to the combined placement and tuning problem, or to each one of these problems separately, follows some general guidelines regardless of the specific technique used. In general, a potential candidate to the problem solution is coded in a string using different alphabets (binary, integer, real, etc.). A typical form of this string, for the placement and tuning problem, is shown in Figure 11.2. Then, an initial *population* (set) of potential candidates of the solution, with the same structure, is generated randomly. This popu-

lation is, then, *evolved* according to the particularly used metaheuristics rules.

Location	Type	Control Structure	Parameters
----------	------	-------------------	------------

Figure 11.2. Representation of a potential solution for the combined placement and tuning problem for the Metaheuristics approach.

An advantage of the metaheuristics approach is its ability to deal with mathematical models with the characteristics referred to in the previous section. Moreover, this approach also adequately handles multi-objective problems. Disadvantages of the approach are the impossibility to assure that an optimal solution is reached and large computational requirements. However, although not guaranteed to be optimal, solutions found by the Metaheuristics approach are usually *good engineering* solutions. On the other hand, most of the Metaheuristics approaches are nicely suited for parallel implementation, which can be used to reduce computing time requirements.

Figure 11.3 illustrate a general procedure for the solution of the placement and tuning problem using the Metaheuristics approach. In particular, a Genetic Algorithm (GA) is used in the illustrative figure. Initially, a population of potential solutions, with the individual structures, as shown in Figure 11.2, is randomly generated. Next, these individual performances are analyzed using any chosen techniques, for instance, time domain simulation, eigenanalysis, etc. From the result of this analysis, a performance index or fitness function is calculated for each individual. This index indicates the relative quality of each potential solution regarding to the chosen objective or objectives. Finally, genetic operators, known as selection, mutation, and crossover (see the Appendix for more details), are applied to the population of potential solutions in order to generate a new population and start the cycle again. It can be shown [11] that the average performance of the population improves from one generation to the other converging, eventually, to the optimal solution.

In the next section, two examples of the Metaheuristics approach application to a placement and to a tuning problem are presented. The Metaheuristics used in both applications are Genetic Algorithms.

#### 4. Optimal Protection Devices Placement in Distribution Networks

Most of the electricity customer interruptions occur due to failures in the distribution network. One way of reducing the number and duration of these interruptions is by installing protection devices in certain loca-

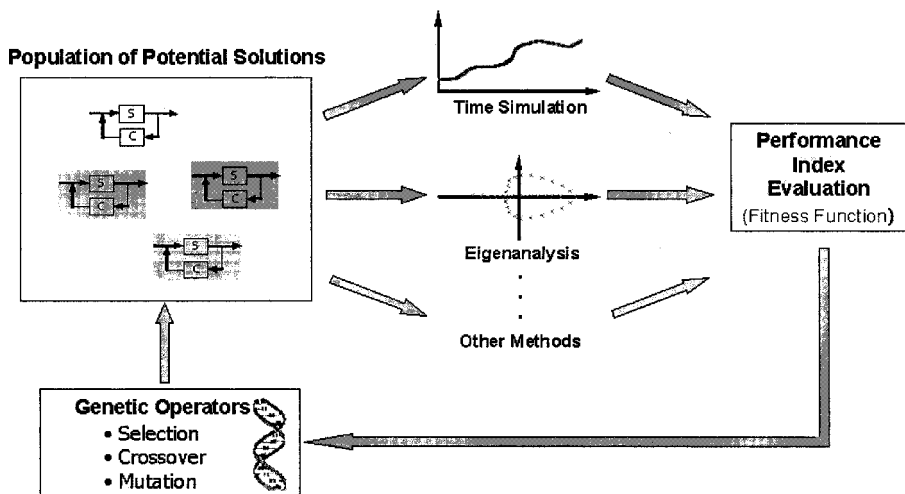


Figure 11.3. Illustrative solution of a control design problem using Genetic Algorithms.

tions of the network in order to reduce the amount of customers affected by a fault. Device type and placement should be determined taking into consideration investment and operational costs and the improvement in the network reliability measured by several indices.

The problem of selecting places for installation of protection devices in a large radial distribution network is a very complex combinatorial optimization problem. Conventional techniques, like linear and nonlinear integer programming, require large computational effort and impose severe modeling simplifications.

#### 4.1 Proposed approach

The traditional criteria used to decide which type and place to install these devices are based on the protection philosophy adopted in the company, including selectivity and coordination analysis. More recently, criteria based on the benefits of these devices to system reliability have been increasingly used in this type of analysis. In this section, the approach introduced in [9], [10] is described. The method is composed of two parts:

- A procedure to compute the impact of new switching and protection devices installation on the system reliability indices based

on analytical techniques<sup>1</sup>. This procedure can be used to evaluate the solutions proposed by an expert or as a component of the methodology described below.

- An automatic methodology that uses a GA as an optimization tool and the analytical procedure described above for the assessment of the potential solutions. The GA replaces the expert in the task of generating potential solutions to the problem. Considerations regarding the protection system selectivity and coordination are included in the methodology as weights in the fitness function used in the GA, as will be explained later.

The solution found by the methodology using a GA is a compromise between the costs incurred by the installation and operation of the switching and protection devices and the reliability indices, while avoiding configurations that violates practical experience rules of distribution protection engineering. Distribution networks are often either radial or operated in radial form. This fact makes easier the reliability evaluation of this type of network. The usual technique for reliability evaluation is the analytical approach. This method is based on a failure mode and effect analysis and some basic equations for calculating the reliability indices in series connected systems [9].

## 4.2 Genetic algorithm formulation

The fitness function used to drive the GA to the solution is the ratio between the benefit achieved by the installation of switching and protection devices, measured by the improvements in the ECOST (Expected Outage Cost to Customers)<sup>2</sup>, and the investment and operational costs incurred by these devices installations. Formally, this function is defined as

$$F = K \frac{B}{C} \quad (11.1)$$

where

$$B(\text{Benefit}) = ECOST(\text{before}) - ECOST(\text{after})$$

$$C(\text{Total Cost}) = C_{inv} + C_{inst} + C_{man}$$

in which  $C_{inv}$  is the investment cost,  $C_{inst}$  is the installation cost,  $C_{man}$  is the maintenance cost, and  $K < 1$  is a constant enforcing the penalties on potential solutions that do not fully satisfy practical constraints.

<sup>1</sup>See [9] for a complete description of the analytical techniques to compute the system reliability indices.

<sup>2</sup>See [9] for the definition and procedures on how to calculate the ECOST and other reliability indices (SAIDI, SAIFI, and ENS) used in this chapter.

Experts on distribution network protection impose restrictions on some switching and protection device configurations. The information from practical experience is introduced in the GA formulation through the constant  $K$  as defined in (11.1). In this work, the potential solutions violating the following constraints are penalized:

- more than three fuse devices in series owing to coordination difficulties;
- fuse devices on main feeders;
- fuse devices located upstream of sectionalizing switches;
- SAIDI (System Average Interruption Duration Index) and SAIFI (System Average Interruption Frequency Index) indices below predefined thresholds.

Besides the technical constraints introduced above, potential solutions with the total cost exceeding predefined values are also penalized.

The GA used in this work is based on the simple or canonical GA described in [11] with a few changes to improve its performance. The main characteristics of the GA are:

- *Solution encoding*: the possible solution to the problem is encoding using 2 bits for each gene as follows:

00: no device  
01: sectionalizing switch  
10: fuse  
11: recloser

- *Genetic operators*: the GA uses a proportional selection scheme based on the roulette wheel method and uniform crossover; the mutation ratio decreases exponentially with the number of generations.
- *Stopping Rule*: the rule adopted is a fixed number of generations.

### 4.3 Computational results

The methodology proposed in this section was tested using several networks, including data from actual distribution networks. For the sake of comparison and to avoid the need to include long lists of network parameters, only the results obtained in the tests performed with two distribution networks reported in the literature, and already used to test other methodologies, are described here.

**4.3.1 Example 1.** The test system used in this example is shown in Figure 4 and was the same used in [12] where the load and feeder parameters are given. Only automatic sectionalizing switches are considered. The investment and maintenance cost considered for the sectionalizing switches are US\$ 11,250 and US\$ 200, respectively, and the switching time considered is 0.03 h.

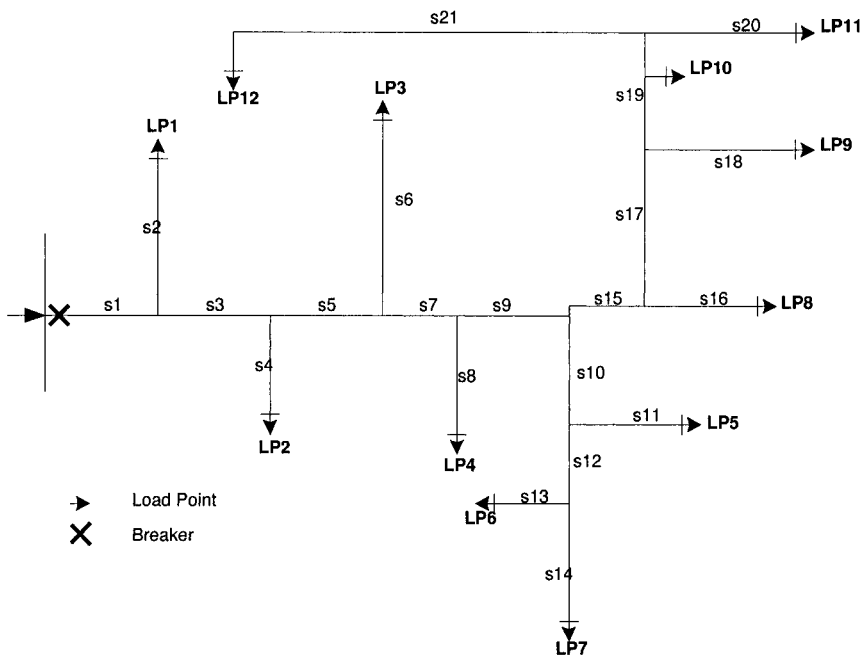


Figure 11.4. System used in Example 1.

Solution alternatives extracted from [12] are considered as solutions given by an expert. These solutions were assessed using the analytical method described in [9] and the results found are shown in Table 11.1.

Two runs of the GA are selected for comparison with the solutions given in Table 11.1. In the first one (GA1), no constraints related to reliability indices were included; in the second one (GA2), a minimum level of  $SAIDI = 2.704$  was chosen because that was the best one among the solutions shown in Table 11.1. In both runs, a limited budget of US\$ 50,000 was adopted. In both runs, a population of 500 individuals is used

Table 11.1. Reliability indices and benefit-cost ratio for the expert's solution in Example 1.

<i>Allocation</i>		<i>SAIFI</i>	<i>SAIDI</i>	<i>ENS</i>	<i>ECOST</i>	<i>B/C</i>
1	Base Case	1.952	5.856	20339	70003	
2	S(15)	1.952	4.738	17001	59191	0.9360
3	S(10)	1.952	4.415	15370	53906	1.3930
4	S(9+15)	1.952	4.262	15900	55623	0.6220
5	S(5+9+11+15+17+19)	1.952	2.704	10010	36540	0.4130

and the maximum number of generations was set to 250. Figure 11.5 shows the maximum and average fitness of the population in both runs. In the GA1 run, the best solution is for  $B/C = 1.4968$  which corresponds to the placement of a sectionalizing switch in section s17 while in the GA2 run, the solution is for  $B/C = 1.3509$  with the placement of two switches in sections s10 and s17, respectively. Table 11.2 shows these complete results. In these tables, besides the SAIDI and SAIFI, the index ENS (Energy Not Supplied) is also presented.

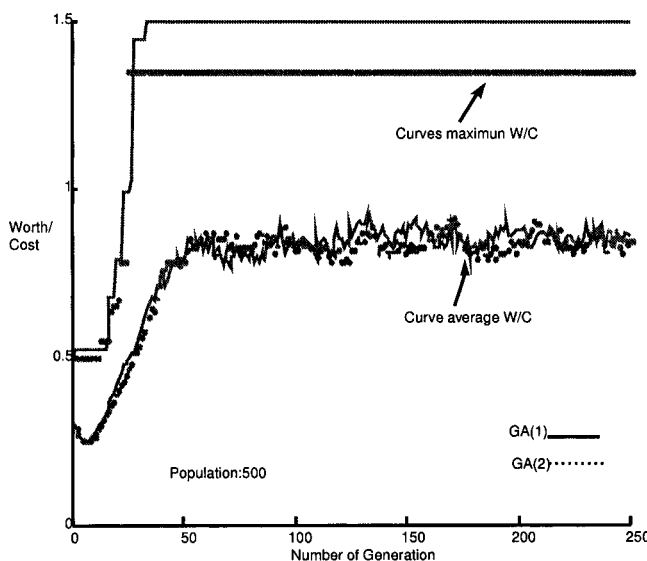


Figure 11.5. Maximum and average fitness in Example 1.

It can be observed that the GA1 run achieved a solution with a  $B/C$  greater than all the other solutions. On the other hand, the GA2 run

Table 11.2. Reliability indices and benefit-cost ratio for the GA solutions in Example 1.

Allocation	SAIFI	SAIDI	ENS	ECOST	B/C
GA1: S(17)	1.952	4.329	15002	52715	1.4968
GA2: S(10+17)	1.952	2.886	10034	36619	1.3509

reduced the  $B/C$  value but improved the SAIDI index owing to the constraint introduced in this index. The complete set of results is shown in Figures 11.6 and 11.7.

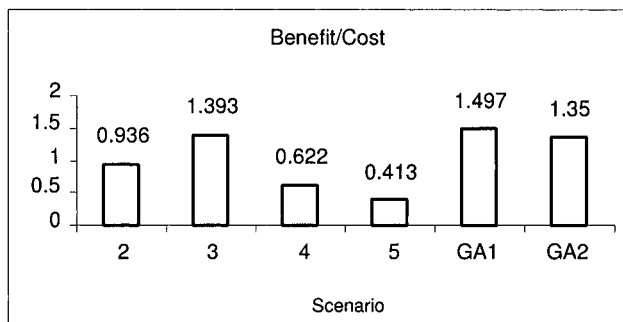


Figure 11.6. Comparison of  $B/C$  for the expert's and GA solutions.

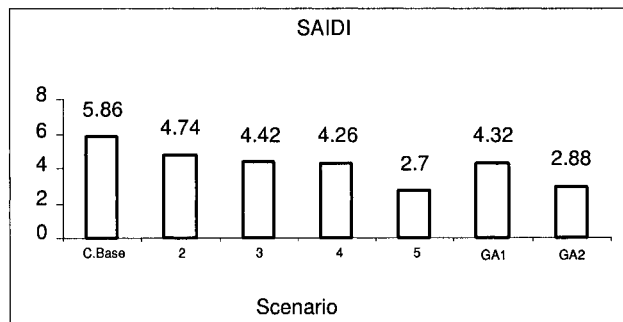


Figure 11.7. Comparison of the SAIDI index for the expert's and GA solutions.

**4.3.2 Example 2.** The test system used in this example is part of the RBTS system given in [13]. Two feeders (F1 and F4), connected to Bus 2 are used in the example. In this example the installations of

both sectionalizing switches and fuses were considered. The test system is shown in Figure 11.8.

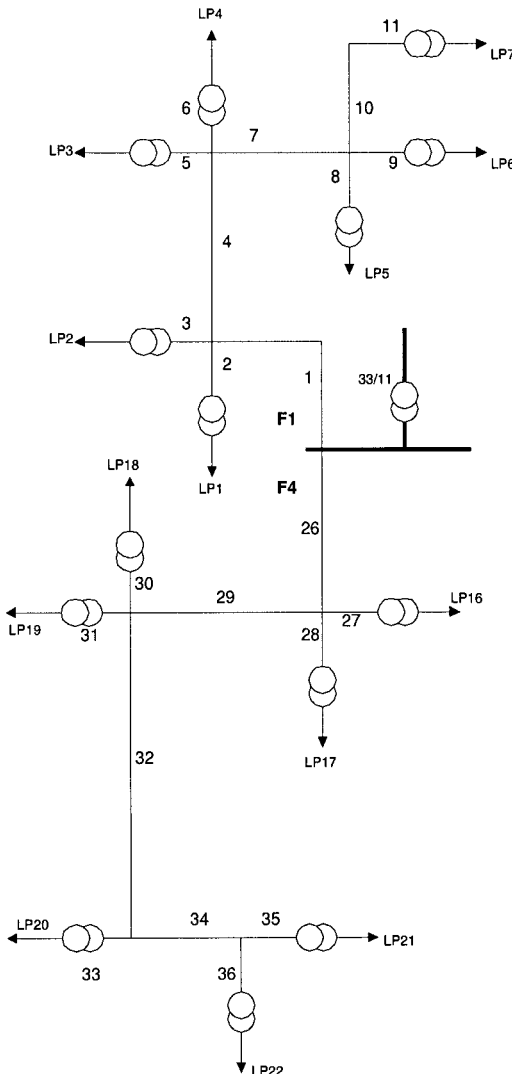


Figure 11.8. System used in Example 2.

- a. **Expert's solutions for feeder F4:** They are assumed to be the scenarios considered in [13], i.e.,

- no devices installed (base case),
- fuses on sections 27, 28, 30, 31, 33, 35, and 36 and no sectionalizing switches,
- sectionalizing switches without any fuses on sections 29, 32, and 34,
- fuses in sections 28, 33, and 35, and sectionalizing switches in sections 29 and 32.

The results obtained for the four scenarios described above are shown in Table 11.3.

*Table 11.3.* Reliability indices and benefit-cost ratio for the expert's solutions in Example 2 (F4) (F: fuse, S: sectionalizing switch).

<i>Allocation</i>		<i>SAIFI</i>	<i>SAIDI</i>	<i>ENS</i>	<i>ECOST</i>	<i>B/C</i>
1	Base Case	1.32	7.28	74299	105133	
2	F(27+28+30+31+33+35+36)	0.49	3.16	34460	52467	2.239
3	S(29+32+34)	1.32	6.21	50441	78662	0.763
4	S(28+33+35), F(29+32)	0.99	5.04	44642	70031	1.057

**b. GA solutions for feeder F4:** The results of two runs of the GA are shown for this case. In the first one (GA1), it is allowed only the allocation of one sectionalizing switch as it is assumed a budget limit of US\$ 20,000 and the cost of the sectionalizing switches is the same as in Example 1. The solution found by the GA is to install the sectionalizing switch in section 32. In the second run (GA2), the solution of GA1 is kept unchanged and only the installation of fuses is considered. In this case, the GA allocated three fuses in sections 27, 28, and 31. The overall results of two runs are shown in Table 11.4.

*Table 11.4.* Reliability indices and benefit-cost ratio for the GA solutions in Example 2 (F4).

<i>Allocation</i>	<i>SAIFI</i>	<i>SAIDI</i>	<i>ENS</i>	<i>ECOST</i>	<i>B/C</i>
GA1: S(32)	1.32	6.20	57914	86475	1.610
GA2: S(32)+F(27+28+31)	0.95	4.44	40667	63235	1.937

**c. GA solutions for feeder F1:** In this case only the solutions found by the GA are reported. The results are summarized in Table 11.5. In

the first run (GA1), no financial or reliability constraint is considered. In the second run (GA2), constraints on the SAIDI (2.0) and SAIFI (0.5) are taken into consideration. The objective of the GA is to improve these indices what leads naturally to a better  $B/C$  ratio.

*Table 11.5.* Reliability indices and benefit-cost ratio for the GA solutions in Example 2 (F1).

<i>Allocation</i>	<i>SAIFI</i>	<i>SAIDI</i>	<i>ENS</i>	<i>ECOST</i>	<i>B/C</i>
GA1: F(7+9)	0.73	4.31	56757	80956	4.25
GA2: F(2+3+4+7)	0.36	2.48	42720	661815	2.85

## 5. Coordinated Tuning of Power System Controls

The damping enhancement in power system oscillatory problems has been a subject of interest for more than 50 years, when isolated systems became interconnected forming bulk power systems, and power electronic technologies started to be widespread and employed by the power industry. Besides the utilization of the cost-effective power system stabilizers (PSS) for damping enhancement, power oscillation dampers (POD) at FACTS devices, may also be used for the same purpose. The addition of these new damping sources [14], [15] together with more stressed operation in present deregulated interconnected power grids, trigger the importance for methods that can handle an overall coordination for the damping controllers.

Conventional design approaches, like the decoupled and sequential loop-closure utilized in [16], cannot properly handle a truly coordinated design. Here we present a methodology based on Genetic Algorithms (GAs) [11] for the coordinated tuning of PODs. The basic operation of a GA is conceptually simple: maintain a population of solutions to a problem, select the better solutions for recombination with each other, and use their offsprings to replace poorer solutions. Recently, GAs have been gaining attention in the power engineering community as an increasing number of related work [17]-[20] is being published. Similar in principles to the works presented in [6], [21], [22], we present a highly flexible linear control design methodology, which takes advantage of the simplicity of GAs. Usual concerns in optimization problems such as non-differentiability, non-linearity and non-convexity do not limit the use of this search method. The method is based on the optimization of a min-max problem of a nonexplicit objective function, related to

the closed-loop spectrum damping ratio, over the controller parameter space [19]. The damping controllers are assumed to be of a fixed conventional structure, consisting basically of lead-lag filters. The robustness of the controllers is taken into account on a scenario-based approach. In addition to the constraints on the parameter bounds, the GA-based optimization problem can readily accommodate for control performance constraints, such as minimum damping requirements. A truly decentralized coordinated design is performed as the controller channels are closed simultaneously. The methodology is applied in the design of two PODs available in a static var compensator (SVC) and in a thyristor-controlled series compensator (TCSC) to enhance the damping of the interarea modes in the six-machine system first presented in [16]. The robustness of the GA-designed PODs is assessed in five scenarios.

## 5.1 Problem formulation

Power system damping controllers are designed to operate on a decentralized way. Input signals from remote sites are considered not reliable enough and avoided. Robustness of the controllers is ensured by considering the performance of the control system for various scenarios. The choice of these scenarios is based on experience and simulation studies.

Tuning of power system damping controllers typically uses a small-signal model represented by the well-known state-space equations

$$\begin{aligned}\dot{x}(t) &= Ax(t) + Bu(t) \\ y(t) &= Cx(t) + Du(t)\end{aligned}\tag{11.2}$$

where  $x$  is the vector of the state variables, such as the machine speeds, angles, and fluxes,  $u$  is the vector of the input variables, such as control signals,  $y$  is the vector of the measured variables, such as bus voltages and machine speeds,  $A$  is the power system state matrix,  $B$  is the input matrix,  $C$  is the output matrix, and  $D$  is the feedforward matrix.

Let  $P_i(s)$ ,  $i = 1, 2, \dots, m$ , in Figure 11.9, represent the set  $\Omega$  of selected scenarios and  $K_d(s)$  be a diagonal transfer function matrix with  $p$  individual controllers.

Defining the error signal as  $e = y_{ref} - y$ , where  $y_{ref}$  is the constant reference level for  $y$ , the decentralized control design requires a control law  $u = K_d(s)e$ , such that the closed-loop system is stable.

For each one of the  $p$  controllers, it is assumed a classical control structure with the dynamic model consisting of a constant gain, a washout filter, and a double lead-lag filter as

$$K_i(s) = k_i \times \frac{T_w s}{1 + T_w s} \times \frac{(1 + \alpha_i T_i s)^2}{(1 + T_i s)^2}\tag{11.3}$$

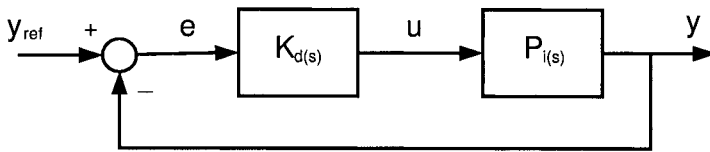


Figure 11.9. Closed-loop setup.

for  $i = 1, 2, \dots, p$ .

From the viewpoint of a washout function, the precise value of the associated time constant  $T_w$  is not critical. The main consideration is that it should be small enough such that stabilizing signals at the frequencies of interest will be relatively unaffected. For this reason,  $T_w$  is considered to be a known parameter. Therefore,  $k_i$ ,  $\alpha_i$  and  $T_i$ ,  $i = 1, \dots, p$ , are the parameters that should be determined by the tuning procedure.

## 5.2 Robust tuning using GAs

**5.2.1 Formulation as an optimization problem.** The problem is formulated as a max-min optimization problem, where the objective function maximizes the minimum damping ratio in all  $p$  scenarios in  $\Omega$ . The constraint set comprises the parameter bounds. Therefore, the design problem can be formulated as the optimization problem

$$F = \max_p \min_n \zeta \quad (11.4)$$

subject to

$$\begin{aligned} k_{i_{\min}} &\leq k_i \leq k_{i_{\max}} \\ \alpha_{i_{\min}} &\leq \alpha_i \leq \alpha_{i_{\max}} \\ T_{i_{\min}} &\leq T_i \leq T_{i_{\max}} \end{aligned} \quad (11.5)$$

where  $n$  is the system order and  $\zeta$  is the closed-loop damping ratio.

This problem is a complex optimization problem with an implicit objective function, which depends on the evaluation of the eigenvalues of a large matrix. This problem is very difficult to solve using conventional methods.

**5.2.2 Modified GA elements.** The solution of the optimization problem defined in (11.4) and (11.5) can be obtained using a modified version of the simple GA described in [11]. The main elements of the GA are defined as follows:

## Parameter encoding and limits

The controller parameters are encoded as fixed-length binary strings or as real number strings, using a concatenated multiparameter representation. The upper and lower limits on the design parameters are established based on either engineering judgment or previous controller setups [19]. During the optimization process the parameter limits are modified. Experiments have shown that the use of variable parameter limits is computationally more efficient than the use of a larger search parameter space from the beginning of the optimization problem. Another advantage of using adaptive limits is that a wrong choice made by the designer, can eventually be corrected during the optimization problem.

## Genetic operators

Selection is performed using the tournament scheme. An elitist strategy is also used: the best individual of the population is guaranteed to be present in the next population with the replacement of the worst individual of the next generation by the best individual of the previous one. The uniform crossover operator is utilized both in the binary and in the real coding. Mutation is implemented using an exponentially decreasing mutation rate, which starts at a specified maximum value and decreases exponentially until it reaches a given minimum value. In the case of real encoding the uniform mutation method is used, in which a randomly selected gene is replaced by another real number randomly selected within its bounds.

## Initialization procedure

The initial population is chosen at random. However, computational experiments have indicated that better results are obtained if some individuals of the initial population correspond to solutions with damping higher than a specified negative threshold  $\zeta < 0$ . The strategy of allowing unstable solutions for the selected individuals in the initial population proved to be better than the one where the selected threshold was set equal to zero (stable solutions). This is achieved by simply continuing the random generation process until a certain number of individuals satisfy the threshold criterion. The computation time spent in this initialization process is compensated by a greater chance of finding a better final solution.

## Stopping rule

The GA is stopped whenever a maximum number of generations is reached.

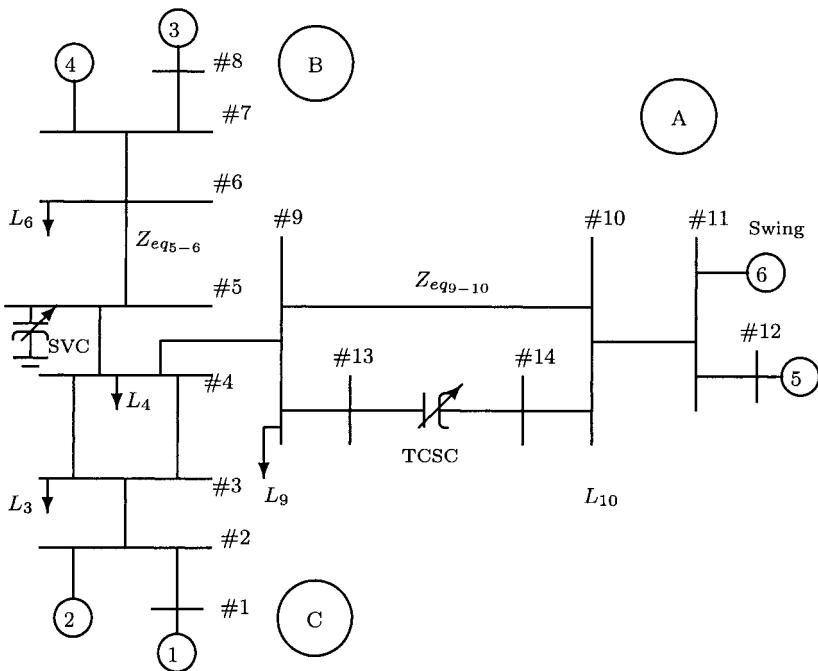


Figure 11.10. Three-area six-machine power system

### 5.3 Test results

This section presents the results after applying the proposed methodology to the simultaneous tuning of an SVC and a TCSC POD for the test system shown in Figure 11.10.

All generators are modeled with 6 state variables [23] and identical parameters. All exciters (model ST3 in [24]) are represented by 2-state variables with identical parameters. The system is analyzed under two nominal power flow conditions. In the first condition, denoted as the Nominal Direct-Flow System (NDFS), Machines 3 and 4 are exporting 640 MW and Machines 5 and 6 are exporting 610 MW. Most of the exported active power is consumed by Load L3. In the second condition, the power flow on the TCSC path reverses due to a decrease in Load L3, and an increase in Load L10. Now Machines 1 and 2 are exporting 710 MW and Machines 3 and 4 are exporting 650 MW. The latter power flow condition is denoted as the Nominal Reversed-Flow System (NRFS).

At both nominal flow conditions the system presents approximately the same mode shapes. There are two low-frequency inter-area elec-

tromechanical modes in the system. The first inter-area mode (Mode 1) consists of the machines of Area B oscillating against the machines of Areas A and C, and the second inter-area mode (Mode 2) consists of the machines of Area A oscillating against the machines of Area C, with minimal participation from machines of Area B. The other three electromechanical modes are local modes of machine oscillations within the areas. An SVC POD on Bus 5 is tuned to enhance the damping of Mode 1, and a TCSC POD in one of the tie lines between Buses 13 and 14 is tuned to enhance the damping of Mode 2.

To achieve robustness, the PODs must be able to provide additional damping to all credible system conditions. Besides the two nominal conditions NDFS and NRFS, three weaker operating conditions are considered as described in Table 11.6. The Weak 1 system represents a weaker tie in the SVC transmission path, and the Weak 2 system represents a weaker tie in the TCSC transmission path with both scenarios in the NDFS condition. The Weak 3 system represents a weaker tie in the TCSC transmission path with the scenario in the NRFS condition. The frequencies  $f(\text{Hz})$  and the damping ratios  $\zeta(\%)$  of the inter-area modes are also given in Table 11.6.

Table 11.6. Open-loop Operating Conditions.

System	$Z_{eq5-6}$	$Z_{eq9-10}$	$L_3$	$L_{10}$	Mode 1		Mode 2	
	p.u.	p.u.	MW	MW	$f(\text{Hz})$	$\zeta(\%)$	$f(\text{Hz})$	$\zeta(\%)$
NDFS	0.08+j0.8	0.04+j0.4	3000	400	0.60	1.94	1.21	4.24
NRFS	0.08+j0.8	0.04+j0.4	400	3000	0.62	3.70	1.12	3.67
Weak 1	0.095+j0.95	0.04+j0.4	3000	400	0.39	-8.83	1.19	4.10
Weak 2	0.08+j0.8	0.28+j2.8	3000	400	0.44	-6.33	1.03	3.99
Weak 3	0.08+j0.8	0.28+j2.8	400	3000	0.74	13.44	0.77	-4.93

## 5.4 Feedback signal selection

The best feedback signals to observe the inter-area modes would be the synchronous-machine speed signals. However, these signals are, in general, remote from the sites most suitable for locating FACTS. Instead, we consider feedback signals derived from local voltage and current measurements in order to synthesize the aggregate machine angles of the coherent areas as in [15], [16].

## 5.5 Robust decentralized control

The following decentralized structure is imposed on the design:

$$u = \begin{bmatrix} u_1 \\ u_2 \end{bmatrix} = \begin{bmatrix} K_1(s) & 0 \\ 0 & K_2(s) \end{bmatrix} \times \begin{bmatrix} e_1 \\ e_2 \end{bmatrix} = K_d(s)e \quad (11.6)$$

In (11.6)  $K_1(s)$  represents the SVC POD and  $K_2(s)$  represents the TCSC POD, both having the structure given by (11.3).

To gain insight into the parameter magnitude order, we performed a decoupled design in the NDFS operating condition, such that a minimum of 9% damping ratio for each inter-area mode was achieved. Using the root-locus technique the following nominal PODs were obtained:

$$K_1(s) = K_{nSVC} = 0.3 \times \frac{10s}{1+10s} \times \frac{(1+0.59s)^2}{(1+0.12s)^2} \quad (11.7)$$

$$K_2(s) = K_{nTCSC} = 0.8 \times \frac{10s}{1+10s} \times \frac{(1+0.29s)^2}{(1+0.06s)^2} \quad (11.8)$$

The parameters  $\alpha$  are easily defined due to the phase-compensation limitation using the fixed structure of two lead-lag stages. Setting the limits at  $0.1 < \alpha_i < 10$  yields a minimum lag compensation of  $-109.8^\circ$  and a maximum lead compensation of  $109.8^\circ$ . On the other hand, the controller gain bounds could theoretically be set to  $-\infty < k_i < +\infty$ . However, based on the designed controllers (11.7) and (11.8) the bounds were set to  $-5 < k_i < 5$ . These narrower bounds greatly improve the GA performance. The time constants  $T_i$  in (11.3), were set such that the lead-lag filter has maximum/minimum phase at the frequency of the interarea modes at the NDFS scenario. So  $T_i$  is calculated as a function of  $\alpha_i$ .

An additional constraint, reflecting design performance, was included in the optimization problem to guarantee that a minimum of 9% damping ratio would be achieved in all five scenarios. The incorporation of such constraint is readily made in the GA optimization framework.

The initial population consisted of the parameter set ( $k_1 = 0.3, k_2 = 0.8, \alpha_1 = 5, \alpha_2 = 5$ ) obtained in the nominal control design (11.7) and (11.8) plus 4 parameter sets that at least stabilize the system, plus 95 randomly selected set of parameters ( $k_1, k_2, \alpha_1, \alpha_2$ ) within the bounds defined previously. With the GA parameters set to  $p_c = 0.6$  (crossover probability) and  $p_m = 0.001$  (mutation probability), the GA solution obtained after 40 generations was

$$K_{SVC} = 0.91 \times \frac{10s}{1+10s} \times \frac{(1+0.40s)^2}{(1+0.18s)^2} \quad (11.9)$$

$$K_{nTCSC} = 1.78 \times \frac{10s}{1+10s} \times \frac{(1+0.30s)^2}{(1+0.06s)^2} \quad (11.10)$$

Figure 11.11 shows the GA convergence performance corresponding to the mean value of the fitness function for each generation. One can notice the fast convergence rate at the initial iterations and a flat convergence rate at final stages. This curve shape is very common in GA applications.

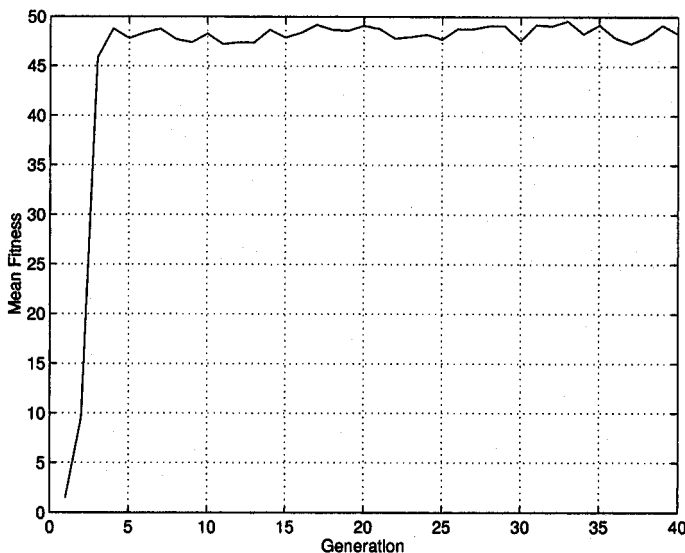


Figure 11.11. GA convergence performance.

Table 11.7 shows the damping ratios of Mode 1 and Mode 2 for the five scenarios when controlled by the nominal PODs (11.7), (11.8) and when controlled by the GA-designed PODs (11.9), (11.10).

Table 11.7. Damping ratio (in %) for closed-loop eigenvalues.

Control	NDFS		NRFS		Weak 1		Weak 2		Weak 3	
	Mode	1	2	1	2	1	2	1	2	1
Nominal	12.1	10.9	14.0	3.2	1.0	11.1	12.9	31.0	18.7	8.1
GA	12.9	14.3	15.8	9.3	12.7	16.0	32.4	38.5	18.0	9.2

Note that although the nominal PODs satisfy the performance requirement in the operating condition (NDFS) in which they were designed, they do not satisfy the performance requirement in the oper-

ating conditions NRFS, Weak 1, and Weak 3. On the other hand, the GA-designed PODs satisfy the performance requirement in all scenarios.

Figure 11.12 shows the frequency response of the nominal (11.7) and the GA-designed SVC PODs (11.9). Figure 11.13 shows the frequency response of the nominal (11.8) and the GA-designed TCSC PODs (11.10).

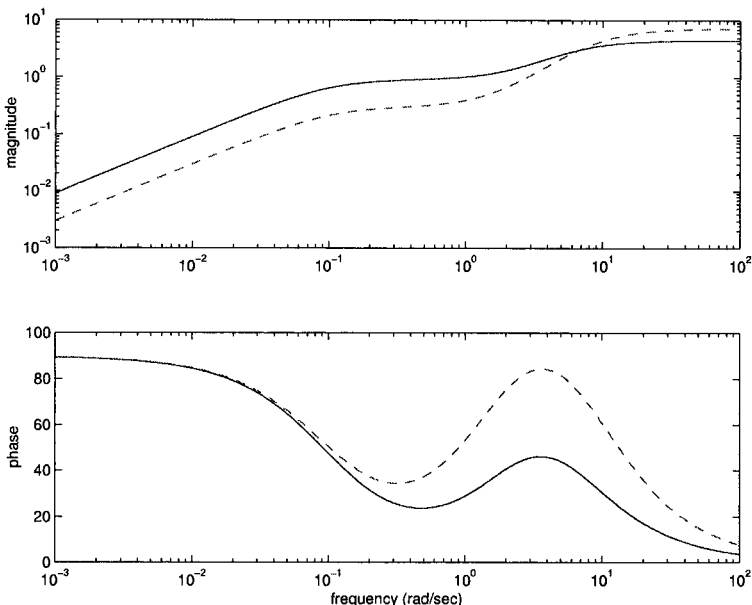


Figure 11.12. Frequency response of the nominal SVC POD controller (dashed line) and the GA-designed SVC POD controller (solid line).

## 5.6 Time simulation results

To evaluate the small-signal stability performance of the designed controllers, a time simulation was performed on the test system using nonlinear power system models. The system is in the Weak 1 operating condition. At 0.1 sec., a 0.01 p.u. active power load is added to Bus 5 and a 0.01 p.u. active power load is removed from Bus 6. After 0.005 sec., the loads are restored. For this load-switching disturbance, the nonlinear system effects are not significant. Figure 11.14 shows the machine speeds using the nominal PODs (11.7) and (11.8), and Figure 11.15 shows the machine speeds using the GA-designed PODs (11.9) and (11.10).

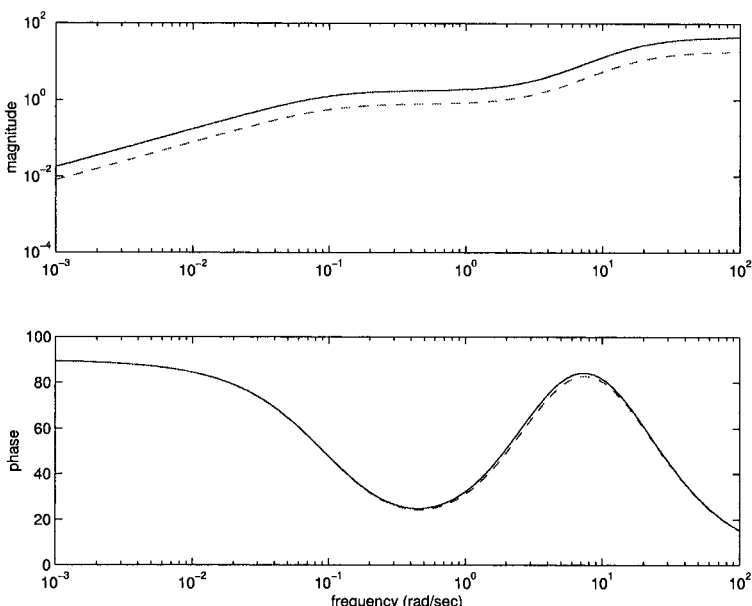


Figure 11.13. Frequency response of the nominal TCSC POD controller (dashed line) and the GA-designed TCSC POD controller (solid line).

## 6. Conclusions and Further Developments

The use of Metaheuristics in the solution of the placement and tuning of power system controllers is a promising field of research with almost immediate application to practical problems. Techniques like Genetic Algorithms, Simulated Annealing, Tabu Search, Particle Swarm Optimizations, etc., are mature enough to practical application and have already been successfully applied to other areas of engineering design. Used on its own, or combined with other design techniques, Metaheuristics can be made very powerful by the incorporation of heuristic knowledge available in the field.

In this chapter, a general framework for the use of Metaheuristics to the problem of placement and tuning of power system controllers has been introduced. Also, two applications of Genetic Algorithms to problems in this category have been described. The first application dealt with the placement of protection devices in distribution networks in such a way that the benefit produced by these devices, measured in terms of the reduction in the expected outage cost to customers, exceeds the investment, installation, and maintenance costs of the devices. The results obtained in the computational experiments indicate that the proposed methodology produces automatically results comparable to the ones ob-

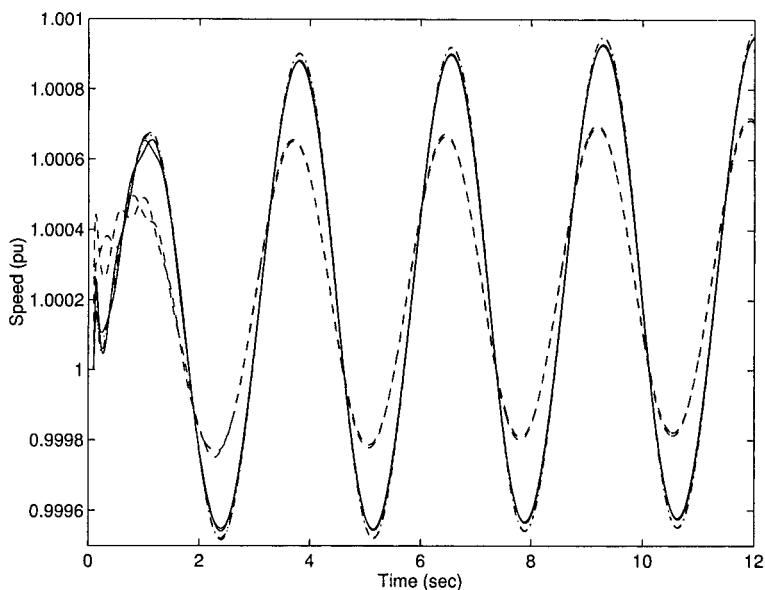


Figure 11.14. Rotor speeds for the load-switching simulation using the nominal SVC and TCSD POD controllers.

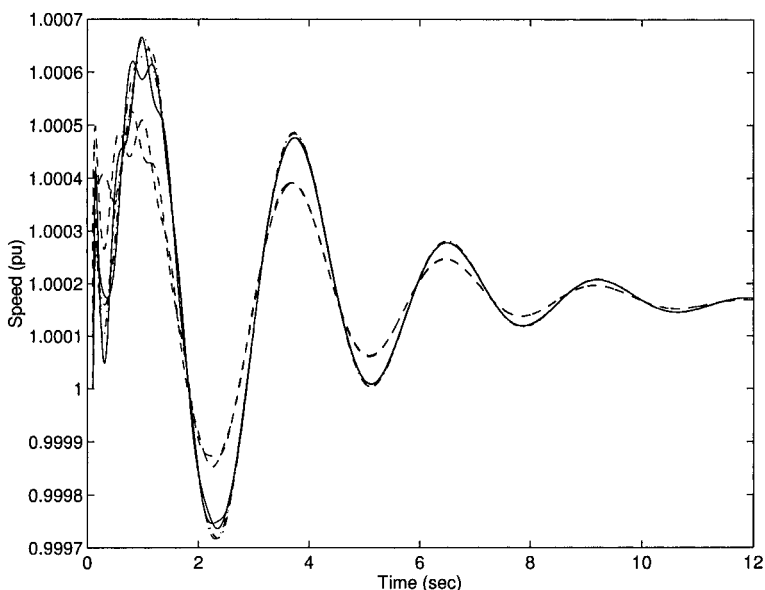


Figure 11.15. Rotor speeds for the load-switching simulation using the GA-designed SVC and TCSD POD controllers.

tained by an expert in the field. The second application dealt with the coordinated tuning of PODs for FACTS devices. The tuning procedure is based on simultaneous closure of decentralized control loops. Results were shown for a test system having two lightly damped interarea modes of oscillation. The objective was the tuning of a SVC and a TCSC POD to enhance the damping of the interarea modes in five operating scenarios.

Further research work being developed in this area includes the combined tuning of power system stabilizers and automatic voltage regulators in order to guarantee, simultaneously, adequate oscillation damping and voltage regulation response. Another area being investigated is the combined optimal placement and tuning of FACTS devices. A more challenging and utterly important problem is the wide-area coordination of control and protection schemes. An optimal placement and tuning of control and protection devices may prevent cascading events eventually leading to blackouts.

### Acknowledgements

The authors acknowledge the work done by their former graduate students A.L.B. do Bomfim and R.M.G. Velasquez.

## Appendix: Genetic Algorithms

Genetic algorithms are search procedures inspired by the mechanisms of evolution and natural genetics. They combine the *survival of the fittest* principle with information exchange among individuals to produce computationally simple yet powerful tools for system optimization and other applications. GA differs from traditionally optimization methods on the following points:

- They usually work with a coding of the variables instead of the variables themselves.
- The search process iterates on a population of solution alternatives, not a single one.
- The only problem-dependent information required are evaluations of the objective function, not derivatives or other auxiliary information.
- The transition rules, from a set of solution alternatives to the next one, are probabilistic.

The first step in the solution of an optimization problem using GA is the encoding of the optimization problem's variables. The most usual approach is to represent these variables as strings of 0's and 1's. These strings are often referred to as *chromosomes* by analogy to the natural genetic process. First, the relationship between these strings and the actual value of the variables may be established in different ways and the best way may differ from one problem to another. Second, the objective function is converted to a *fitness function* that normalizes the objective function to a convenient range and then is used to evaluate each string.

An initial population of solution alternatives is usually chosen at random. Potentially good candidate solutions known beforehand can be included in the initial

population to speed up computation and increase the chances of finding the global optimum.

After this start, successive populations are generated using the following *genetic operators*:

- *Selection*—This is a process in which strings are copied to a *mating pool* according to their fitness value, i.e., the ones with a higher value have a higher probability of contributing one or more offspring in the next generation.
- *Crossover*—This operator proceeds in three steps: first, pairs of strings are picked at random from the mating pool; second, if a randomly generated number in the range 0 to 1 is greater than  $p_c$  (the crossover rate), this pair is selected for crossover, otherwise they remain unaltered; third, the crossover process itself consists of interchanging the portions of strings beyond a position  $l$  ( $1 \leq l \leq$  number of bits in the string) which is randomly selected.
- *Mutation*—This is the random flipping of bits in the population of strings according to the mutation rate  $p_m$ .

Selection is responsible for the implementation of the survival of the fittest principle. Crossover implements information exchange among individuals of a population, in an attempt to generate better fitted new individuals. Mutation has the role of restoring good genetic material that may have been lost by selection and crossover. There are different ways of performing selection, crossover, and mutation. A detailed description of these operators together with other forms of variables encoding, can be found in [11].

The values of  $p_c$  and  $p_m$ , and the population size are referred to as the control parameters of the GA. Their choice determines the speed of convergence and the probability of finding the optimum solution. Typical values for these parameters are:

- population: 30 – 200,
- crossover rates: 0.5 – 1.0,
- mutation rates: 0.001 – 0.05.

## References

- [1] M. Amin. Toward Self-Healing Energy Infrastructure Systems. *IEEE Computer Applications in Power*, 14(1):20–28, January 2001.
- [2] G. Reed, J. Paserba, and P. Salavantis. The FACTS on Resolving Transmission Gridlock. *IEEE Power and Energy Magazine*, 1(5):41–46, Sep./Oct. 2003.
- [3] S.H. Horowitz and A.G. Phadke. Boosting Immunity to Blackouts. *IEEE Power and Energy Magazine*, 1(5):47–53, Sep./Oct. 2003.
- [4] R.M. Murray, K.J. Aström, S.P. Boyd, R.W. Brockett, and G. Stein. Future Directions in Control in an Information-Rich World. *IEEE Control Systems Magazine*, 23(2):20–33, April 2003.
- [5] G.N. Taranto and J.H. Chow. A Robust Frequency Domain Optimization Technique for Tuning Series Compensation Damping Controllers. *IEEE Transactions on Power Systems*, 10:1219–1225, 1995.

- [6] P. Pourbeik and M.J. Gibbard. Simultaneous Coordination of Power System Stabilizers and FACTS Device Stabilizers in a Multimachine Power System for Enhancing Dynamic Performance. *IEEE Transactions on Power Systems*, 13:473–479, 1998.
- [7] F. Glover and G.A. Kochenberger. *Handbook of Metaheuristics*. Kluwer Academic Publishers, New York, 2003.
- [8] K.Y. Lee and M.A. El-Sharkawi, eds. *Modern Heuristic Optimization Techniques with Applications to Power Systems*. IEEE PES Publication 02TP160, 2002.
- [9] R.M.G. Velasquez and D.M. Falcão. Optimal Switching and Protection Devices Placement in Distribution Networks for Reliability Improvement Using Genetic Algorithms. *Proceedings of the International Conference on Intelligent System Application to Power Systems (ISAP)*, Budapest, Hungary, June 2001.
- [10] D.M. Falcão. Genetic Algorithms Applications in Electrical Distribution Systems. *Proceedings of the 2002 World Congress on Computational Intelligence*, Honolulu, Hawaii, May 2002.
- [11] D. Goldberg. *Genetic Algorithms in Search, Optimization and Machine Learning*. Addison-Wesley, Reading, MA, 1989.
- [12] Y. He, G. Andersson, and R.N. Allan. Determining Optimum Location and Number of Automatic Switching Devices in Distribution Systems. *Proceedings of the IEEE Power Tech'99 Conference*, Budapest, Hungary, August 29-September 2, 1999.
- [13] R.N. Allan, R. Billinton, I. Sjafreif, L. Goel, and K.S. So. A Reliability Test System for Educational Purposes—Basic Distribution System Data and Results. *IEEE Transactions on Power Systems*, 6:813–819, 1991.
- [14] N.G. Hingorani. Power Electronics in Electric Utilities: Role of Power Electronics in Future Power Systems. *Proceedings of the IEEE*, 76:481–482, 1988.
- [15] E.V. Larsen, J.J. Sanchez-Gasca, and J.H. Chow. Concepts for Design of FACTS Controllers to Damp Power Swings. *IEEE Transactions on Power Systems*, 10:948–956, 1995.
- [16] G.N. Taranto, J.H. Chow, and H.A. Othman. Robust Decentralized Control Design for Damping Power System Oscillations. *Proceedings of the 33<sup>rd</sup> IEEE Conference on Decision and Control*, 4080–4085, Orlando, FL, December 1994.
- [17] P. Ju, E. Handschin, and F. Reyer. Genetic Algorithm Aided Controller Design with Application to SVC. *IEE Proceedings on Generation, Transmission and Distribution*, 143:258–262, 1996.

- [18] V. Miranda, D. Srinivasan, and L.M. Proena. Evolutionary Computation in Power Systems. *Proceedings of the 12<sup>th</sup> Power System Computation Conference*, Dresden, Germany, August 1996.
- [19] G.N. Taranto and D.M. Falcão. Robust Decentralised Control Design using Genetic Algorithms in Power System Damping Control. *IEE Proceedings on Generation, Transmission and Distribution*, 145:1–6, 1998.
- [20] A.L.B. Do Bomfim, G.N. Taranto, and D.M. Falcão. Simultaneous Tuning of Power System Damping Controllers using Genetic Algorithms. *IEEE Transactions on Power Systems*, 15:163–169, 2000.
- [21] G.N. Taranto, J.K. Shiao, J.H. Chow, and H.A. Othman. A Robust Decentralized Design for Multiple FACTS Damping Controllers. *IEE Proceedings on Generation, Transmission and Distribution*, 144:61–1997.
- [22] A.J.A. Simões Costa, F.D. Freitas, and A.S. Silva. Design of Decentralized Controllers for Large Power Systems Considering Sparsity. *IEEE Transactions on Power Systems*, 12:144–152, 1997.
- [23] R.P. Schulz. Synchronous Machine Modeling. In IEEE Publication Adequacy and Philosophy of Modeling System Dynamic Performance, 75 CH 0970-PWR, 1975.
- [24] IEEE Committee Report. System Models for Power Systems Stability Studies. *IEEE Transactions on Power Apparatus and Systems*, 100:494–509, 1981.

## Chapter 12

# LOAD FORECASTING

Eugene A. Feinberg

*State University of New York, Stony Brook*

[Eugene.Feinberg@sunysb.edu](mailto:Eugene.Feinberg@sunysb.edu)

Dora Genethliou

*State University of New York, Stony Brook*

[dgenethl@ams.sunysb.edu](mailto:dgenethl@ams.sunysb.edu)

**Abstract** Load forecasting is vitally important for the electric industry in the deregulated economy. It has many applications including energy purchasing and generation, load switching, contract evaluation, and infrastructure development. A large variety of mathematical methods have been developed for load forecasting. In this chapter we discuss various approaches to load forecasting.

**Keywords:** Load, forecasting, statistics, regression, artificial intelligence.

### 1. Introduction

Accurate models for electric power load forecasting are essential to the operation and planning of a utility company. Load forecasting helps an electric utility to make important decisions including decisions on purchasing and generating electric power, load switching, and infrastructure development. Load forecasts are extremely important for energy suppliers, ISOs, financial institutions, and other participants in electric energy generation, transmission, distribution, and markets.

Load forecasts can be divided into three categories: short-term forecasts which are usually from one hour to one week, medium forecasts which are usually from a week to a year, and long-term forecasts which are longer than a year. The forecasts for different time horizons are important for different operations within a utility company. The natures

of these forecasts are different as well. For example, for a particular region, it is possible to predict the next day load with an accuracy of approximately 1-3%. However, it is impossible to predict the next year peak load with the similar accuracy since accurate long-term weather forecasts are not available. For the next year peak forecast, it is possible to provide the probability distribution of the load based on historical weather observations. It is also possible, according to the industry practice, to predict the so-called weather normalized load, which would take place for average annual peak weather conditions or worse than average peak weather conditions for a given area. Weather normalized load is the load calculated for the so-called normal weather conditions which are the average of the weather characteristics for the peak historical loads over a certain period of time. The duration of this period varies from one utility to another. Most companies take the last 25-30 years of data.

Load forecasting has always been important for planning and operational decision conducted by utility companies. However, with the deregulation of the energy industries, load forecasting is even more important. With supply and demand fluctuating and the changes of weather conditions and energy prices increasing by a factor of ten or more during peak situations, load forecasting is vitally important for utilities. Short-term load forecasting can help to estimate load flows and to make decisions that can prevent overloading. Timely implementations of such decisions lead to the improvement of network reliability and to the reduced occurrences of equipment failures and blackouts. Load forecasting is also important for contract evaluations and evaluations of various sophisticated financial products on energy pricing offered by the market. In the deregulated economy, decisions on capital expenditures based on long-term forecasting are also more important than in a non-deregulated economy when rate increases could be justified by capital expenditure projects.

Most forecasting methods use statistical techniques or artificial intelligence algorithms such as regression, neural networks, fuzzy logic, and expert systems. Two of the methods, so-called end-use and econometric approach are broadly used for medium- and long-term forecasting. A variety of methods, which include the so-called similar day approach, various regression models, time series, neural networks, statistical learning algorithms, fuzzy logic, and expert systems, have been developed for short-term forecasting.

As we see, a large variety of mathematical methods and ideas have been used for load forecasting. The development and improvements of appropriate mathematical tools will lead to the development of more accurate load forecasting techniques. The accuracy of load forecasting

depends not only on the load forecasting techniques, but also on the accuracy of forecasted weather scenarios. Weather forecasting is an important topic which is outside of the scope of this chapter. We simply mention significant progress in the development of computerized weather forecasting systems, including the Mesoscale Model MM5 developed and supported by a consortium of universities (see e.g. [8]).

## 2. Important Factors for Forecasts

For short-term load forecasting several factors should be considered, such as time factors, weather data, and possible customers' classes. The medium- and long-term forecasts take into account the historical load and weather data, the number of customers in different categories, the appliances in the area and their characteristics including age, the economic and demographic data and their forecasts, the appliance sales data, and other factors.

The time factors include the time of the year, the day of the week, and the hour of the day. There are important differences in load between weekdays and weekends. The load on different weekdays also can behave differently. For example, Mondays and Fridays being adjacent to weekends, may have structurally different loads than Tuesday through Thursday. This is particularly true during the summer time. Holidays are more difficult to forecast than non-holidays because of their relative infrequent occurrence.

Weather conditions influence the load. In fact, forecasted weather parameters are the most important factors in short-term load forecasts. Various weather variables could be considered for load forecasting. Temperature and humidity are the most commonly used load predictors. An electric load prediction survey published in [17] indicated that of the 22 research reports considered, 13 made use of temperature only, 3 made use of temperature and humidity, 3 utilized additional weather parameters, and 3 used only load parameters.

Among the weather variables listed above, two composite weather variable functions, the THI (temperature-humidity index) and WCI (wind chill index), are broadly used by utility companies. THI is a measure of summer heat discomfort and similarly WCI is cold stress in winter.

Most electric utilities serve customers of different types such as residential, commercial, and industrial. The electric usage pattern is different for customers that belong to different classes but is somewhat alike for customers within each class. Therefore, most utilities distinguish load behavior on a class-by-class basis [36].

### 3. Forecasting Methods

Over the last few decades a number of forecasting methods have been developed. Two of the methods, so-called end-use and econometric approach are broadly used for medium- and long-term forecasting. A variety of methods, which include the so-called similar day approach, various regression models, time series, neural networks, expert systems, fuzzy logic, and statistical learning algorithms, are used for short-term forecasting. The development, improvements, and investigation of the appropriate mathematical tools will lead to the development of more accurate load forecasting techniques.

Statistical approaches usually require a mathematical model that represents load as function of different factors such as time, weather, and customer class. The two important categories of such mathematical models are: additive models and multiplicative models. They differ in whether the forecast load is the sum (additive) of a number of components or the product (multiplicative) of a number of factors.

For example, Chen *et al.* [4] presented an additive model that takes the form of predicting load as the function of four components:

$$L = L_n + L_w + L_s + L_r,$$

where  $L$  is the total load,  $L_n$  represents the “normal” part of the load, which is a set of standardized load shapes for each “type” of day that has been identified as occurring throughout the year,  $L_w$  represents the weather sensitive part of the load,  $L_s$  is a special event component that creates a substantial deviation from the usual load pattern, and  $L_r$  is a completely random term, the noise.

Chen *et al.* [4] also suggested electricity pricing as an additional term that can be included in the model. Naturally, price decreases/increases affect electricity consumption. Large cost sensitive industrial and institutional loads can have a significant effect on loads. The study in [4] used Pennsylvania-New Jersey-Maryland (PJM) spot price data (as it related to Ontario Hydro load) as a neural network input. The authors report that accurate estimates were achieved more quickly with the inclusion of price data.

A multiplicative model may be of the form

$$L = L_n \cdot F_w \cdot F_s \cdot F_r,$$

where  $L_n$  is the normal (base) load and the correction factors  $F_w$ ,  $F_s$ , and  $F_r$  are positive numbers that can increase or decrease the overall load. These corrections are based on current weather ( $F_w$ ), special events ( $F_s$ ), and random fluctuation ( $F_r$ ). Factors such as electricity pricing ( $F_p$ ) and

load growth ( $F_g$ ) can also be included. Rahman [29] presented a rule-based forecast using a multiplicative model. Weather variables and the base load associated with the weather measures were included in the model.

### 3.1 Medium- and long-term load forecasting methods

The end-use modeling, econometric modeling, and their combinations are the most often used methods for medium- and long-term load forecasting. Descriptions of appliances used by customers, the sizes of the houses, the age of equipment, technology changes, customer behavior, and population dynamics are usually included in the statistical and simulation models based on the so-called end-use approach. In addition, economic factors such as per capita incomes, employment levels, and electricity prices are included in econometric models. These models are often used in combination with the end-use approach. Long-term forecasts include the forecasts on the population changes, economic development, industrial construction, and technology development.

**End-use models.** The end-use approach directly estimates energy consumption by using extensive information on end use and end users, such as appliances, the customer use, their age, sizes of houses, and so on. Statistical information about customers along with dynamics of change is the basis for the forecast.

End-use models focus on the various uses of electricity in the residential, commercial, and industrial sector. These models are based on the principle that electricity demand is derived from customer's demand for light, cooling, heating, refrigeration, etc. Thus end-use models explain energy demand as a function of the number of appliances in the market [15].

Ideally this approach is very accurate. However, it is sensitive to the amount and quality of end-use data. For example, in this method the distribution of equipment age is important for particular types of appliances. End-use forecast requires less historical data but more information about customers and their equipment.

**Econometric models.** The econometric approach combines economic theory and statistical techniques for forecasting electricity demand. The approach estimates the relationships between energy consumption (dependent variables) and factors influencing consumption. The relationships are estimated by the least-squares method or time series methods.

One of the options in this framework is to aggregate the econometric approach, when consumption in different sectors (residential, commer-

cial, industrial, etc.) is calculated as a function of weather, economic and other variables, and then estimates are assembled using recent historical data. Integration of the econometric approach into the end-use approach introduces behavioral components into the end-use equations.

**Statistical model-based learning.** The end-use and econometric methods require a large amount of information relevant to appliances, customers, economics, etc. Their application is complicated and requires human participation. In addition such information is often not available regarding particular customers and a utility keeps and supports a profile of an “average” customer or average customers for different type of customers. The problem arises if the utility wants to conduct next-year forecasts for sub-areas, which are often called load pockets. In this case, the amount of the work that should be performed increases proportionally with the number of load pockets. In addition, end-use profiles and econometric data for different load pockets are typically different. The characteristics for particular areas may be different from the average characteristics for the utility and may not be available.

In order to simplify the medium-term forecasts, make them more accurate, and avoid the use of the unavailable information, Feinberg *et al.* ([11], [12]) developed a statistical model that learns the load model parameters from the historical data. Feinberg *et al.* ([11], [12]) studied load data sets provided by a utility company in Northeastern US. The focus of the study was the summer data. We compared several load models and came to the conclusion that the following multiplicative model is the most accurate

$$L(t) = F(d(t), h(t)) \cdot f(w(t)) + R(t),$$

where  $L(t)$  is the actual load at time  $t$ ,  $d(t)$  is the day of the week,  $h(t)$  is the hour of the day,  $F(d, h)$  is the daily and hourly component,  $w(t)$  is the weather data that include the temperature and humidity,  $f(w)$  is the weather factor, and  $R(t)$  is a random error.

In fact,  $w(t)$  is a vector that consists of the current and lagged weather variables. This reflects the fact that electric load depends not only on the current weather conditions but also on the weather during the previous hours and days. In particular, the well-known effect of the so-called heat waves is that the use of air conditioners increases when the hot weather continues for several days.

To estimate the weather factor  $f(w)$ , we used the regression model

$$f(w) = \beta_0 + \sum \beta_j X_j,$$

where  $X_j$  are explanatory variables which are nonlinear functions of current and past weather parameters and  $\beta_0, \beta_j$  are the regression coefficients.

The parameters of the model can be calculated iteratively. We start with  $F = 1$ . Then we use the above regression model to estimate  $f$ . Then we estimate  $F$ , and so on.

The described algorithm demonstrated rapid convergence on historical hourly load and weather data. We have applied it to many areas with population between 50,000 and 250,000 customers. Figure 12.1 presents an example of a scatter plot that compares the model and real parameters. Figure 12.2 demonstrates the convergence of the correlation between the actual load and the model for the iteration process. Figure 12.3 demonstrates the convergence of the linear regression procedures in the algorithm.

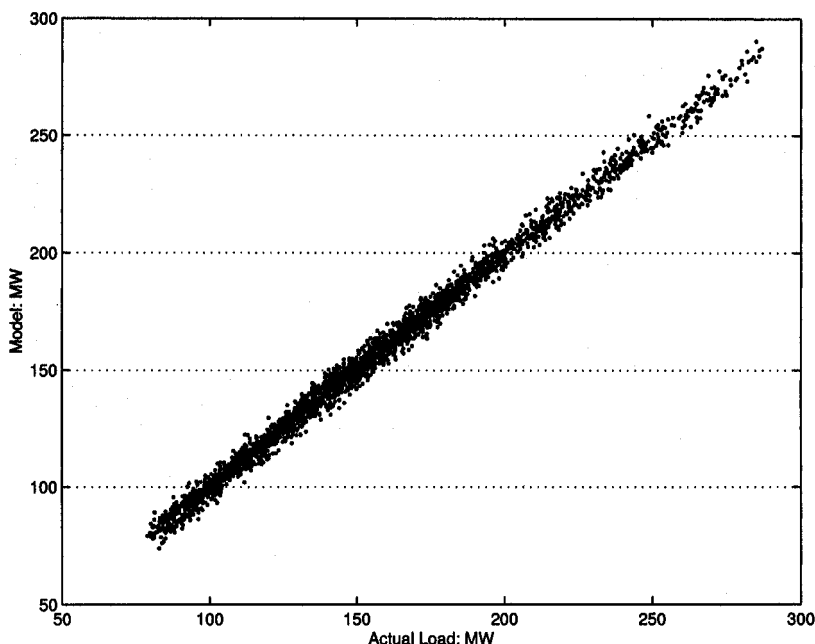


Figure 12.1. Scatter plot of the actual load vs the model.

The software [13], that uses the described method, learns the model parameters and makes next-year predictions based on the model loads for the last 25-30 years of data. Though historical loads may not available, the software applies the last year models to the historical weather data to estimate the next year's peak distribution.

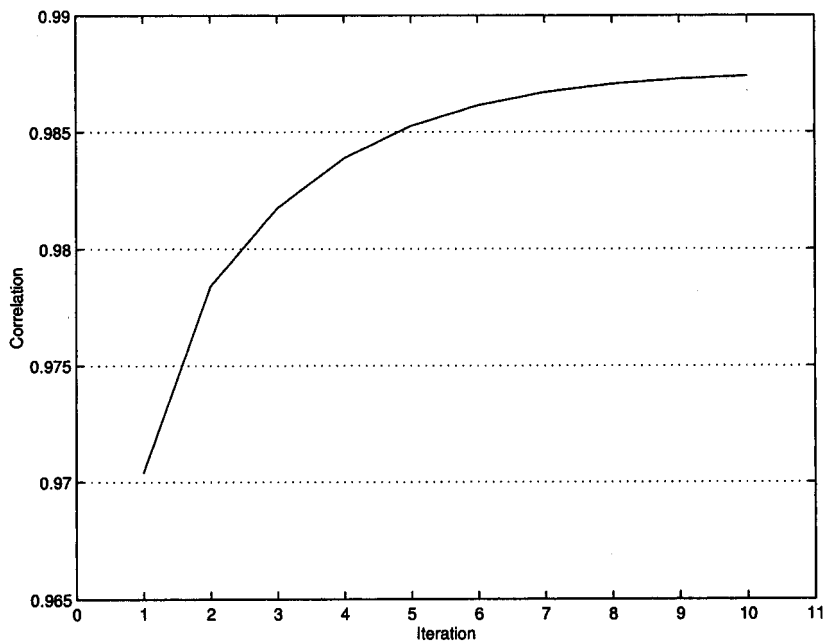


Figure 12.2. Correlation between the actual load and the model.

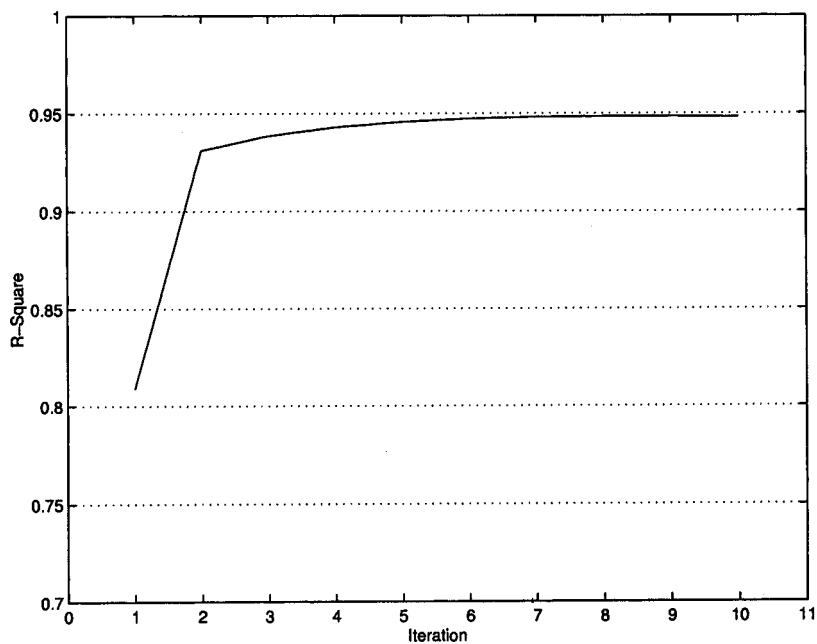


Figure 12.3. Convergence of the  $R^2$  for the actual load vs the model.

The software generates several important characteristics. For example, for each load pocket and for the system, it calculates a weather normalization factor that is a ratio of the peak load to the load that would be observed under average peak conditions. It also produces probability distributions for the next year peaks.

The described methods can be applied to both medium- and long-term forecasting. However, the long-term forecasts should incorporate economic and population dynamic forecasts as input parameters.

### 3.2 Short-term load forecasting methods

A large variety of statistical and artificial intelligence techniques have been developed for short-term load forecasting.

**Similar-day approach.** This approach is based on searching historical data for days within one, two, or three years with similar characteristics to the forecast day. Similar characteristics include weather, day of the week, and the date. The load of a similar day is considered as a forecast. Instead of a single similar day load, the forecast can be a linear combination or regression procedure that can include several similar days. The trend coefficients can be used for similar days in the previous years.

**Regression methods.** Regression is the one of most widely used statistical techniques. For electric load forecasting regression methods are usually used to model the relationship of load consumption and other factors such as weather, day type, and customer class.

Engle *et al.* [9] presented several regression models for the next day peak forecasting. Their models incorporate deterministic influences such as holidays, stochastic influences such as average loads, and exogenous influences such as weather. References [19], [31], [16], [3] describe other applications of regression models to loads forecasting.

**Time series.** Time series methods are based on the assumption that the data have an internal structure, such as autocorrelation, trend, or seasonal variation. Time series forecasting methods detect and explore such a structure. Time series have been used for decades in such fields as economics, digital signal processing, as well as electric load forecasting. In particular, ARMA (autoregressive moving average), ARIMA (autoregressive integrated moving average), ARMAX (autoregressive moving average with exogenous variables), and ARIMAX (autoregressive integrated moving average with exogenous variables) are the most often used classical time series methods. ARMA models are usually used for stationary processes while ARIMA is an extension of ARMA to non-stationary processes. ARMA and ARIMA use the time and load as the only input parameters. Since load generally depends on the weather and

time of the day, ARIMAX is the most natural tool for load forecasting among the classical time series models.

Fan and McDonald [10] and Cho *et al.* [5] describe implementations of ARIMAX models for load forecasting. Yang *et al.* [37] used evolutionary programming (EP) approach to identify the ARMAX model parameters for one day to one week ahead hourly load demand forecast. Evolutionary programming [14] is a method for simulating evolution and constitutes a stochastic optimization algorithm. Yang and Huang [38] proposed a fuzzy autoregressive moving average with exogenous input variables (FARMAX) for one day ahead hourly load forecasts.

**Neural networks.** The use of artificial neural networks (ANN or simply NN) has been a widely studied electric load forecasting technique since 1990 (see [28]). Neural networks are essentially non-linear circuits that have the demonstrated capability to do non-linear curve fitting.

The outputs of an artificial neural network are some linear or non-linear mathematical function of its inputs. The inputs may be the outputs of other network elements as well as actual network inputs. In practice network elements are arranged in a relatively small number of connected layers of elements between network inputs and outputs. Feed-back paths are sometimes used.

In applying a neural network to electric load forecasting, one must select one of a number of architectures (e.g. Hopfield, back propagation, Boltzmann machine), the number and connectivity of layers and elements, use of bi-directional or uni-directional links, and the number format (e.g. binary or continuous) to be used by inputs and outputs, and internally.

The most popular artificial neural network architecture for electric load forecasting is back propagation. Back propagation neural networks use continuously valued functions and supervised learning. That is, under supervised learning, the actual numerical weights assigned to element inputs are determined by matching historical data (such as time and weather) to desired outputs (such as historical electric loads) in a pre-operational “training session”. Artificial neural networks with unsupervised learning do not require pre-operational training.

Bakirtzis *et al.* [1] developed an ANN based short-term load forecasting model for the Energy Control Center of the Greek Public Power Corporation. In the development they used a fully connected three-layer feedforward ANN and back propagation algorithm was used for training. Input variables include historical hourly load data, temperature, and the day of the week. The model can forecast load profiles from one to seven days. Also Papalexopoulos *et al.* [27] developed and implemented a multi-layered feedforward ANN for short-term system load

forecasting. In the model three types of variables are used as inputs to the neural network: season related inputs, weather related inputs, and historical loads. Khotanzad *et al.* [20] described a load forecasting system known as ANNSTLF. ANNSTLF is based on multiple ANN strategies that capture various trends in the data. In the development they used a multilayer perceptron trained with the error back propagation algorithm. ANNSTLF can consider the effect of temperature and relative humidity on the load. It also contains forecasters that can generate the hourly temperature and relative humidity forecasts needed by the system. An improvement of the above system was described in [21]. In the new generation, ANNSTLF includes two ANN forecasters, one predicts the base load and the other forecasts the change in load. The final forecast is computed by an adaptive combination of these forecasts. The effects of humidity and wind speed are considered through a linear transformation of temperature. As reported in [21], ANNSTLF was being used by 35 utilities across the USA and Canada. Chen *et al.* [4] developed a three layer fully connected feedforward neural network and the back propagation algorithm was used as the training method. Their ANN though considers the electricity price as one of the main characteristics of the system load. Many published studies use artificial neural networks in conjunction with other forecasting techniques (such as with regression trees [26], time series [7] or fuzzy logic [32]).

**Expert systems.** Rule based forecasting makes use of rules, which are often heuristic in nature, to do accurate forecasting. Expert systems, incorporates rules and procedures used by human experts in the field of interest into software that is then able to automatically make forecasts without human assistance.

Expert system use began in the 1960's for such applications as geological prospecting and computer design. Expert systems work best when a human expert is available to work with software developers for a considerable amount of time in imparting the expert's knowledge to the expert system software. Also, an expert's knowledge must be appropriate for codification into software rules (i.e. the expert must be able to explain his/her decision process to programmers). An expert system may codify up to hundreds or thousands of production rules.

Ho *et al.* [18] proposed a knowledge-based expert system for the short-term load forecasting of the Taiwan power system. Operator's knowledge and the hourly observations of system load over the past five years were employed to establish eleven day types. Weather parameters were also considered. The developed algorithm performed better compared to the conventional Box-Jenkins method. Rahman and Hazim [30] developed a site-independent technique for short-term load forecasting. Knowledge

about the load and the factors affecting it are extracted and represented in a parameterized rule base. This rule base is complemented by a parameter database that varies from site to site. The technique was tested in several sites in the United States with low forecasting errors. The load model, the rules, and the parameters presented in the paper have been designed using no specific knowledge about any particular site. The results can be improved if operators at a particular site are consulted.

**Fuzzy logic.** Fuzzy logic is a generalization of the usual Boolean logic used for digital circuit design. An input under Boolean logic takes on a truth value of “0” or “1”. Under fuzzy logic an input has associated with it a certain qualitative ranges. For instance a transformer load may be “low”, “medium” and “high”. Fuzzy logic allows one to (logically) deduce outputs from fuzzy inputs. In this sense fuzzy logic is one of a number of techniques for mapping inputs to outputs (i.e. curve fitting).

Among the advantages of fuzzy logic are the absence of a need for a mathematical model mapping inputs to outputs and the absence of a need for precise (or even noise free) inputs. With such generic conditioning rules, properly designed fuzzy logic systems can be very robust when used for forecasting. Of course in many situations an exact output (e.g. the precise 12PM load) is needed. After the logical processing of fuzzy inputs, a “defuzzification” process can be used to produce such precise outputs. References [22], [24], [32] describe applications of fuzzy logic to electric load forecasting.

**Support vector machines.** Support Vector Machines (SVMs) are a more recent powerful technique for solving classification and regression problems. This approach was originated from Vapnik’s [35] statistical learning theory. Unlike neural networks, which try to define complex functions of the input feature space, support vector machines perform a nonlinear mapping (by using so-called kernel functions) of the data into a high dimensional (feature) space. Then support vector machines use simple linear functions to create linear decision boundaries in the new space. The problem of choosing an architecture for a neural network is replaced here by the problem of choosing a suitable kernel for the support vector machine [6].

Mohandes [25] applied the method of support vector machines for short-term electrical load forecasting. The author compares its performance with the autoregressive method. The results indicate that SVMs compare favorably against the autoregressive method. Chen *et al.* [2] proposed a SVM model to predict daily load demand of a month. Their program was the winning entry of the competition organized by the EU-

NITE network. Li and Fang [23] also used a SVM model for short-term load forecasting.

## 4. Future Research Directions

In this chapter we have discussed several statistical and artificial intelligence techniques that have been developed for short-, medium-, and long-term electric load forecasting. Several statistical models and algorithms that have been developed though, are operating ad hoc. The accuracy of the forecasts could be improved, if one would study these statistical models and develop mathematical theory that explains the convergence of these algorithms.

Researchers should also investigate the boundaries of applicability of the developed models and algorithms. So far, there is no single model or algorithm that is superior for all utilities. The reason is that utility service areas vary in differing mixtures of industrial, commercial, and residential customers. They also vary in geographic, climatologic, economic, and social characteristics. Selecting the most suitable algorithm by a utility can be done by testing the algorithms on real data. In fact, some utility companies use several load forecasting methods in parallel. As far as we know, nothing is known on a priori conditions that could detect which forecasting method is more suitable for a given load area. An important question is to investigate the sensitivity of the load forecasting algorithms and models to the number of customers, characteristics of the area, energy prices, and other factors.

As mentioned above, weather is an important factor that influences the load. The usual approach to short-term load forecasting uses the forecasted weather scenario as an input. However, one of the most important recent developments in weather forecasting is the so-called ensemble approach which consists of computing multiple forecasts. Then probability weights can be assigned to these ensembles.

Instead of using the single weather forecast, weather ensemble predictions can be used as multiple inputs for load forecasts. These inputs generate multiple load forecasts. In recent papers [33, 34], the authors describe ensemble load predictions based on 51 weather ensembles and various statistical forecasting methods. There are two advantages of having load forecasts in the probabilistic form: (i) they can lead to a more accurate hourly forecast obtained by using multiple ensembles, for example, by averaging them; (ii) the probabilistic description of the future load can be used as an input to decision support systems to make important generation, purchasing, and switching decisions. In general, it is known from the appropriate mathematical models that the knowledge

of the demand distribution leads to more cost efficient decisions than the knowledge of the expected demand. On a broader scale, we think that the important research and development directions are: (i) combining weather and load forecasting and (ii) incorporating load forecasting into various decision support systems.

## 5. Conclusions

Accurate load forecasting is very important for electric utilities in a competitive environment created by the electric industry deregulation. In this paper we review some statistical and artificial intelligence techniques that are used for electric load forecasting. We also discussed factors that affect the accuracy of the forecasts such as weather data, time factors, customer classes, as well as economic and end use factors. Load forecasting methods use advanced mathematical modeling. Additional progress in load forecasting and its use in industrial applications can be achieved by providing short-term load forecasts in the form of probability distributions rather than the forecasted numbers; for example the so-called ensemble approach can be used. We believe that the progress in load forecasting will be achieved in two directions: (i) basic research in statistics and artificial intelligence and (ii) better understanding of the load dynamics and its statistical properties to implement appropriate models.

## References

- [1] A.G. Bakirtzis, V. Petridis, S.J. Kiartzis, M.C. Alexiadis, and A.H. Maissis. A Neural Network Short-Term Load Forecasting Model for the Greek Power System. *IEEE Transactions on Power Systems*, 11:858–863, 1996.
- [2] B.J. Chen, M.W. Chang, and C.J. Lin. Load Forecasting using Support Vector Machines: A Study on EUNITE Competition 2001. Technical report, Department of Computer Science and Information Engineering, National Taiwan University, 2002.
- [3] W. Charytoniuk, M.S. Chen, and P. Van Olinda. Nonparametric Regression Based Short-Term Load Forecasting. *IEEE Transactions on Power Systems*, 13:725–730, 1998.
- [4] H. Chen, C.A. Canizares, and A. Singh. ANN-Based Short-Term Load Forecasting in Electricity Markets. *Proceedings of the IEEE Power Engineering Society Transmission and Distribution Conference*, 2:411–415, 2001.

- [5] M.Y. Cho, J.C. Hwang, and C.S. Chen. Customer Short-Term Load Forecasting by using ARIMA Transfer Function Model. *Proceedings of the International Conference on Energy Management and Power Delivery*, 1:317–322, 1995.
- [6] N. Christiani and J.S. Taylor. *An Itroduction to Support Vector Machines and Other Kernel-Based Learning Methods*. Cambridge University Press, Cambridge, 2000.
- [7] T.W.S. Chow and C.T. Leung. Nonlinear Autoregressive Integrated Neural Network Model for Short-Term Load Forecasting. *IEE Proceedings on Generation, Transmission and Distribution*, 143:500–506, 1996.
- [8] J. Dudhia and J.F. Bresch. A Global Version of the PSU-NCAR Mesoscale Model. *Monthly Weather Review*, 130:2989–3007, 2002.
- [9] R.F. Engle, C. Mustafa, and J. Rice. Modeling Peak Electricity Demand. *Journal of Forecasting*, 11:241–251, 1992.
- [10] J.Y. Fan and J.D. McDonald. A Real-Time Implementation of Short-Term Load Forecasting for Distribution Power Systems. *IEEE Transactions on Power Systems*, 9:988–994, 1994.
- [11] E.A. Feinberg, J.T. Hajagos, and D. Genethliou. Load Pocket Modeling. *Proceedings of the 2<sup>nd</sup> IASTED International Conference: Power and Energy Systems*, 50–54, Crete, 2002.
- [12] E.A. Feinberg, J.T. Hajagos, and D. Genethliou. Statistical Load Modeling. *Proceedings of the 7<sup>th</sup> IASTED International Multi-Conference: Power and Energy Systems*, 88–91, Palm Springs, CA, 2003.
- [13] E.A. Feinberg, J.T. Hajagos, B.G. Irrgang, R.J. Rossin, D. Genethliou and D.E. Feinberg. Load pocket forecasting software. Submitted to *IASTED Journal on Energy and Power Systems*.
- [14] D.B. Fogel. An Introduction to Simulated Evolutionary Optimization. *IEEE Transactions on Neural Networks*, 5:3–14, 1994.
- [15] C.W. Gellings. *Demand Forecasting for Electric Utilities*. The Fairmont Press, Lilburn, GA, 1996.
- [16] T. Haida and S. Muto. Regression Based Peak Load Forecasting using a Transformation Technique. *IEEE Transactions on Power Systems*, 9:1788–1794, 1994.
- [17] H.S. Hippert, C.E. Pedreira, and R.C. Souza. Neural Networks for Short-Term Load Forecasting: A Review and Evaluation. *IEEE Transactions on Power Systems*, 16:44–55, 2001.
- [18] K.L. Ho, Y.Y. Hsu, F.F. Chen, T.E. Lee, C.C. Liang, T.S. Lai, and K.K. Chen. Short-Term Load Forecasting of Taiwan Power System

- using a Knowledge Based Expert System. *IEEE Transactions on Power Systems*, 5:1214–1221, 1990.
- [19] O. Hyde and P.F. Hodnett. An Adaptable Automated Procedure for Short-Term Electricity Load Forecasting. *IEEE Transactions on Power Systems*, 12:84–93, 1997.
  - [20] A. Khotanzad, R.A. Rohani, T.L. Lu, A. Abaye, M. Davis, and D.J. Maratukulam. ANNSTLF-A Neural-Network-Based Electric Load Forecasting System. *IEEE Transactions on Neural Networks*, 8:835–846, 1997.
  - [21] A. Khotanzad, R.A. Rohani, and D. Maratukulam. ANNSTLF—Artificial Neural Network Short-Term Load Forecaster—Generation Three. *IEEE Transactions on Neural Networks*, 13:1413–1422, 1998.
  - [22] S.J. Kiartzis and A.G. Bakirtzis. A Fuzzy Expert System for Peak Load Forecasting: Application to the Greek Power System. *Proceedings of the 10<sup>th</sup> Mediterranean Electrotechnical Conference*, 3:1097–1100, 2000.
  - [23] Y. Li and T. Fang. Wavelet and Support Vector Machines for Short-Term Electrical Load Forecasting. *Proceedings of International Conference on Wavelet Analysis and its Applications*, 1:399–404, 2003.
  - [24] V. Miranda and C. Monteiro. Fuzzy Inference in Spatial Load Forecasting. *Proceedings of IEEE Power Engineering Winter Meeting*, 2:1063–1068, 2000.
  - [25] M. Mohandes. Support Vector Machines for Short-Term Electrical Load Forecasting. *International Journal of Energy Research*, 26:335–345, 2002.
  - [26] H. Mori and N. Kosemura. Optimal Regression Tree Based Rule Discovery for Short-Term Load Forecasting. *Proceedings of IEEE Power Engineering Society Transmission and Distribution Conference*, 2:421–426, 2001.
  - [27] A.D. Papalexopoulos, S. Hao, and T.M. Peng. An Implementation of a Neural Network Based Load Forecasting Model for the EMS. *IEEE Transactions on Power Systems*, 9:1956–1962, 1994.
  - [28] M. Peng, N.F. Hubele, and G.G. Karady. Advancement in the Application of Neural Networks for Short-Term Load Forecasting. *IEEE Transactions on Power Systems*, 7:250–257, 1992.
  - [29] S. Rahman. Formulation and Analysis of a Rule-Based Short-Term Load Forecasting Algorithm. *Proceedings of the IEEE*, 78:805–816, 1990.

- [30] S. Rahman and O. Hazim. Load Forecasting for Multiple Sites: Development of an Expert System-Based Technique. *Electric Power Systems Research*, 39:161–169, 1996.
- [31] S. Ruzic, A. Vuckovic, and N. Nikolic. Weather Sensitive Method for Short-Term Load Forecasting in Electric Power Utility of Serbia. *IEEE Transactions on Power Systems*, 18:1581–1586, 2003.
- [32] S.E. Skarman and M. Georgiopoulos. Short-Term Electrical Load Forecasting using a Fuzzy ARTMAP Neural Network. *Proceedings of SPIE*, 181–191, 1998.
- [33] J.W. Taylor and R. Buizza. Using Weather Ensemble Predictions in Electricity Demand Forecasting. *International Journal of Forecasting*, 19:57–70, 2003.
- [34] J.W. Taylor and R. Buizza. Neural Network Load Forecasting With Weather Ensemble Predictions. *IEEE Transactions on Power Systems*, 17:626–632, 2002.
- [35] V.N. Vapnik. *The Nature of Statistical Learning Theory*. New York, Springer Verlag, 1995.
- [36] H.L. Willis. *Spatial Electric Load Forecasting*. Marcel Dekker, New York, 1996.
- [37] H.T. Yang, C.M. Huang, and C.L. Huang. Identification of AR-MAX Model for Short-Term Load Forecasting: An Evolutionary Programming Approach. *IEEE Transactions on Power Systems*, 11:403–408, 1996.
- [38] H.T. Yang and C.M. Huang. A New Short-Term Load Forecasting Approach using Self-Organizing Fuzzy ARMAX Models. *IEEE Transactions on Power Systems*, 13:217–225, 1998.

## Chapter 13

# INDEPENDENT COMPONENT ANALYSIS TECHNIQUES FOR POWER SYSTEM LOAD ESTIMATION

*A Signal-Processing Approach*

Dagmar Niebur

*Drexel University*

[niebur@drexel.edu](mailto:niebur@drexel.edu)

Ekrem Gursoy

*Drexel University*

[eg54@drexel.edu](mailto:eg54@drexel.edu)

Huawei Liao

*Carnegie Mellon University*

[hliao@andrew.cmu.edu](mailto:hliao@andrew.cmu.edu)

**Abstract** This contribution presents the application of independent component analysis for active, reactive and harmonic load profile estimation. Assuming that the individual bus loads are statistically independent and not Gaussian distributed, independent component analysis uses the higher order statistics of the loads to estimate individual loads from a limited number of voltage, current or power measurements that present linear combinations of the unknown loads. In contrast to traditional load estimation techniques, ICA does not require any knowledge of the power system parameters or the power system topology. Future applications to general state estimation problems are proposed at the end of this chapter.

**Keywords:** Independent component analysis, load profile, load estimation, state estimation, harmonics, power systems, blind source separation.

## 1. Introduction

The goal of traditional power system steady state estimation is to estimate the power system voltage magnitudes and phase angles based on voltage magnitude measurements, current magnitude measurements and active and reactive power measurements taken at a specific point in time or within a very small time interval. The network topology and the network parameters, including the line and transformer impedances, as well as the load models are assumed to be known [1]. Pseudo-measurements replace missing network data by the corresponding model data but nevertheless the amount of data necessary to obtain a real-time quasi-steady state power system model is quite extensive. A separate process is used to estimate the network topology in order to ensure that the topology used by the state estimator is indeed the topology present in the actual power network. During the events leading to the August 14, 2004 blackout, such a topology mismatch went undetected by the Midwest Independent System Operator (MISO). Subsequently the state estimator of the MISO system failed to converge and thus no adequate real-time model was available to the MISO (see [2]).

The large amount of necessary measurements becomes a major concern for harmonic state estimation. The main challenges in harmonic power system analysis are to ensure system observability based on a very limited number of available measurements. The number of harmonic measurements is limited by the installation cost and the instrumentation maintenance concerns. Harmonic measurements, which require synchronization of phase measurements, are more sophisticated and costly than ordinary measurements. Harmonic levels of the system and harmonic sources can be identified by harmonic state estimation (HSE) techniques [3]-[5]. However, these techniques require knowledge of network parameters and topology in addition to the large number of measurements.

For a large class of problems in power system state estimation it is of interest to estimate only a subset of the complete system data set. For example in load estimation, usually only the consumed complex power, current or voltage at the load is of interest, [6, 7]. On the other hand for load profile estimation the static variation of the load in time can only be estimated by performing several iterations of the state or load estimator. For harmonic source profile estimation, the profile of the harmonic source [4] has to be determined using only a limited number of harmonic measurements. The statistical distribution of the time series of the measurements and the loads are usually not taken into account.

It is to be expected that deregulation of power systems will severely limit the access to measurements because of ownership, privacy and security issues.

None of these traditional state and load estimation techniques is able to estimate loads using a partial set of measurements without any knowledge of the electrical network parameters and topology.

In this chapter, we demonstrate that Independent Component Analysis is well suited to estimate active, reactive and harmonic load profile provided that a limited number of voltage magnitude, current magnitude, and active or reactive power measurements are available as a time sequence of snapshots of measurements at buses or branches in the system. These measurements need not necessarily be located at the loads.

ICA is also a very useful tool to complement and cross-check the results obtained by state-estimation techniques. Results will be altered in state estimation with parameter and topology changes. Especially in the harmonic domain, the true system impedance matrix can be very different from the calculated value using the predefined models. Estimations from ICA will provide us approximate checks of results and online calibration of system parameters including the system topology. Furthermore, by providing information about the individual loads which are not directly measurable, ICA will increase redundancy of measurements. ICA will also provide information about the correlation among the loads. Further analysis of these correlations can be used for system planning.

## 2. Independent Component Analysis

Blind source separation [8] (BSS) techniques are based on recovering the source signals from the observed signals. In BSS, only the observations or measurements are available; source signals and the way the sources are mixed or the mixing environment are unknown. If there is no information available about the properties of the sources, then it is not easy to estimate the source signals from the observed mixtures. However, some knowledge concerning the statistical properties of the sources, such as statistical independence between source signals, allows the estimation of source signals in unknown mixing environments.

(ICA) is a BSS technique, which transforms the observed signals into mutually statistically independent signals [9]. ICA has received great attention in signal processing applications. Some of these applications are in audio separation, biomedical signals like brain imaging, telecommunication and financial data separation [10]. The outline of the theory



## 2.3 Objective functions for the maximization of source independence

There are different approaches for estimating the ICA model using the statistical properties of signals. These methods include ICA by maximization of non-gaussianity, minimization of mutual information, and maximum likelihood estimation [10, 11].

In this study the ICA model maximizes statistical independence by maximization of non-gaussianity of the source signal estimates. The differential entropy  $H(y)$  of a random vector  $y$  with density  $p_y(\eta)$  is defined as

$$H(y) = - \int p_y(\eta) \log p_y(\eta) d\eta \quad (13.6)$$

Let  $y$  be a random variable with mean  $\mu$  and standard variation  $\sigma$ . Let  $y_{gauss}$  denote a Gaussian (normally distributed) random variable having the same mean  $\mu$  and standard variation  $\sigma$  as  $y$ . Then we always have

$$H(y_{gauss}) \geq H(y) \quad (13.7)$$

A measure of non-gaussianity is the negentropy  $J(y)$  which is defined as the normalized differential entropy

$$J(y) = H(y_{gauss}) - H(y) \quad (13.8)$$

The negentropy is zero for gaussian variables and always nonnegative. By maximizing the negentropy, the mutual information  $H$  of the sources is minimized which is a measure of the independence of random variables.

The estimation of negentropy based on the definitions in (13.6) and (13.8) is difficult because this estimation requires an estimate of the probability functions of source signals, which are assumed to be unknown. The estimation problem can be simplified by using an approximation of the negentropy by a non-quadratic so-called contrast function  $G$ .

$$J(y_i) = J(E(w_i^T x)) = [E\{G(w_i^T x)\} - E\{G(y_{gauss})\}]^2 \quad (13.9)$$

where  $E$  represents the statistical expectation. The choice of  $G$  depends on the assumptions of super- or sub-gaussianity of the underlying probability distribution of the independent components. A detailed discussion concerning the appropriate choice of  $G$  can be found in [12].

In order to find the independent components we have to maximize the  $J(y_i)$  in (13.9). The optimization problem which maximizes the sum of  $N$  one unit contrast function with the constraint of decorrelation can be

expressed as

$$\begin{aligned} \text{Maximize} \quad & \sum_{i=1}^N J(y_i) = \sum_{i=1}^N J(w_i^T x) \\ \text{subject to constraint} \quad & E\left\{\left(w_k^T x\right)\left(w_j^T x\right)\right\} = \delta_{jk} \end{aligned} \quad (13.10)$$

where  $w_i, i = 1, \dots, N$  are the rows of the matrix  $W$ , i.e., the estimate of  $A^{-1}$ . The rows of the demixing matrix and the corresponding independent components can be estimated one by one using a fixed point algorithm for the optimization problem and a Gram-Schmidt-type procedure for the decorrelation constraint. The so-called FastICA algorithm [12] used for the estimation of load profiles is presented in the next section.

In general, signals are preprocessed by centering and whitening to simplify the ICA algorithm. Centering transforms the observed signals to zero-mean variables and whitening linearly transforms the observed signals, so that its elements are uncorrelated and their variances equal to unity.

## 2.4 FastICA source estimation algorithm

The *FastICA* estimation algorithm of the demixing matrix  $W = A^{-1}$  is given as follows [12]:

- 1 Center and whiten observed mixtures to obtain  $x$ .
- 2 Choose  $N$ , the number of independent components. Set counter  $p \leftarrow 1$ .
- 3 Initialize  $w_p$  randomly.
- 4 Let  $w_p \leftarrow E\{xg(w_p^T x)\} - E\{g'(w_p^T x)\} w_p$
- 5 Orthogonalize  $w_p$  by

$$w_p \leftarrow w_p - \sum_{j=1}^{p-1} (w_p^T w_j) w_j$$

- 6 Let  $w_p \leftarrow w_p / \|w_p\|$
- 7 If not converged, go back to Step 4.
- 8 Let  $p \leftarrow p + 1$ . If  $p \leq N$ , go back to Step 3.

We use a modified version of the public domain MATLAB-based Fast Independent Component Analysis Toolbox (FastICA) [10, 12] which is available from the authors' web site.

### 3. Application of ICA for Load Profile Estimation

Intelligent techniques such as neural networks, fuzzy logic, and genetic algorithms have been applied to power system applications; however ICA algorithms have very few applications [13]. In this chapter, we will present the application of ICA to active, reactive and harmonic load profile estimation in power systems.

In traditional state estimation, power system states are estimated at each single time of measurements. If the power system is observable, the estimation error depends on the redundancy of measurements, accurate knowledge of network parameters and topology, and minimal presence of measurement outliers. However this knowledge may not be available in a restructured network as explained in the Introduction. Also network parameters cannot be easily or accurately obtained as for example in the harmonic domain. In Section 3.1 the load profile models of general electric active, reactive, and harmonic producing loads are presented. In these applications, the Independent Component Analysis (ICA) method does not require any information about the network topology and parameters. Only the time series data of measurements including some statistical and properties of the original sources or loads are used.

#### 3.1 Linear mixing models for load profile estimation

In this section the linear mixing models for ICA-based electric load profile estimation will be developed. Traditional state estimation techniques use one complete set of measurements at time  $t$  to estimate the state of the system at this particular time  $t$ . Instead, we use a time sequence of available measurements to estimate the state of the system in a certain time window. In Section 4 the estimation results will be represented for active or reactive power profiles of electric loads.

**3.1.1 Power flow equations.** The complex power flow equations can be represented as

$$S_i = V_i \sum_{k=1}^n Y_{ik}^* V_k^* \quad (13.11)$$

Resolving into real and imaginary parts, we obtain

$$P_i = \sum_{k=1}^n |V_i| |V_k| |Y_{ik}| \cos(\theta_{ik} + \delta_k - \delta_i) \quad (13.12)$$

$$Q_i = \sum_{k=1}^n |V_i| |V_k| |Y_{ik}| \sin(\theta_{ik} + \delta_k - \delta_i) \quad (13.13)$$

In the equations above

$$\begin{aligned} V_i &= |V_i| (\cos \delta_i + j \sin \delta_i) \\ Y_{ij} &= |Y_{ij}| (\cos \theta_{ij} + j \sin \theta_{ij}) \end{aligned} \quad (13.14)$$

where  $S_i$  is complex power injection at Bus  $i$ ,  $P_i$  is active power injection at Bus  $i$ ,  $Q_i$  is reactive power injection at Bus  $i$ ,  $Y_{ij}$  is admittance between Buses  $i$  and  $j$ , and  $n$  is the number of buses.

The states of the system to be calculated are the voltage angles  $\delta_i$  and the voltage magnitudes  $|V_i|$ . We can represent (13.12) and (13.13) in a more compact form as

$$\begin{aligned} P &= f_P(|V|, \delta) \\ Q &= f_Q(|V|, \delta) \end{aligned} \quad (13.15)$$

where  $P$  and  $Q$  are the active and reactive power injection vectors at load buses, and  $|V|$  and  $\delta$  are the voltage magnitude vector and voltage phase angle vector at load buses respectively. Taylor expansion of (13.15) around the operating point ( $|V_0|, \delta_0$ ) gives

$$\begin{aligned} P &\approx f_P(|V_0|, \delta_0) + \frac{\partial f_P}{\partial |V|} (|V| - |V_0|) + \frac{\partial f_P}{\partial \delta} (\delta - \delta_0) \\ Q &\approx f_Q(|V_0|, \delta_0) + \frac{\partial f_Q}{\partial |V|} (|V| - |V_0|) + \frac{\partial f_Q}{\partial \delta} (\delta - \delta_0) \end{aligned} \quad (13.16)$$

Because active power injections are only weakly coupled with the voltage magnitude, we can neglect the voltage sensitivities in the first equation and approximate the phase angle deviations and the reactive power deviations in (13.16) by

$$\left( \frac{\partial f_P}{\partial \delta} \right)^{-1} (P - P_0) \approx (\delta - \delta_0) \quad (13.17)$$

$$Q - Q_0 \approx \frac{\partial f_Q}{\partial |V|} (|V| - V_0) + \frac{\partial f_Q}{\partial \delta} (\delta - \delta_0) \quad (13.18)$$

### 3.1.2 Active power load profile model.[14]

The nonlinear power flow model given in (13.17) and (13.18) can be linearized by assuming a lossless system and neglecting the voltage deviations, resulting in the so called linear DC power flow model for the active power flow deviations. Under these assumptions (13.17) can be

written as

$$\begin{aligned}\Delta P &= B\Delta\delta \\ B &= \left( \frac{\partial f_P}{\partial \delta} \right) \Big|_{r_{ij}=0}\end{aligned}\quad (13.19)$$

Branch flows can be represented as bus injections by simple manipulation of (13.19). The deviation of the active power on branch  $k$  which connects the Buses  $i$  and  $j$ , can be represented as

$$\Delta P_{ij}^k = B_{ij}\Delta\delta_i - B_{ij}\Delta\delta_j \quad (13.20)$$

where the index is  $k = 1 \dots M$  and  $M$  is the number of branches. In matrix form

$$\Delta P_{Branch} = T\Delta\delta = TB^{-1}\Delta P \quad (13.21)$$

In (13.21)  $\Delta P_{Branch}$  is an  $M$  dimensional vector and  $T$  is a rectangular matrix reflecting the imaginary part of the branch admittance and the network topology. Equation (13.21) expresses the active power line flows as a superposition of the bus injections. In this model, the active power varies only at load buses, whereas the active power injected from the generator buses remain constant except for the slack bus.

The DC power flow model given in (13.21) is similar to the ICA model given in (13.4). If we measure the line flows, then we can apply ICA to these measurements and estimate the bus injections. Combining both DC power flow model and ICA, source signals  $\ell(t)$  are the active power injections at buses, observations  $x(t)$  are the measured active power flows on lines and the mixing matrix is  $A := TB^{-1}$  in the DC power flow model

$$\begin{aligned}\ell(t) &= [\Delta P_{n_g+1}(t), \dots, \Delta P_n(t)] \\ x(t) &= \text{subvector } ([\Delta P_{1_{ij}}(t), \dots, \Delta P_{M_{ik}}(t)]) \\ A &= \text{reduced } (TB^{-1})\end{aligned}\quad (13.22)$$

where  $n_g$  is the number of generator nodes including the slack bus and  $k = 1, \dots, m$ . The submatrix and subvectors are computed using the matrix inversion lemma such that the system of linear equations is quadratic with  $A$  being nonsingular.

### 3.1.3 Reactive power load profile model.[15]

Using the decoupled model equations, we substitute in (13.17) and (13.18) obtain

$$Q - Q_0 \approx \frac{\partial f_Q}{\partial |V|} (|V| - V_0) + \frac{\partial f_Q}{\partial \delta} \left( \frac{\partial f_P}{\partial \delta} \right)^{-1} (P - P_0) \quad (13.23)$$

Assuming a constant power factor, the active power deviation is approximated as

$$P - P_0 \approx \alpha (Q - Q_0) \quad (13.24)$$

Then (13.23) can be expressed as

$$(V - V_0) \approx \left( \frac{\partial f_Q}{\partial |V|} \right)^{-1} \left( 1 - \frac{\partial f_Q}{\partial \delta} \left( \frac{\partial f_P}{\partial \delta} \right)^{-1} \alpha \right) (Q - Q_0) \quad (13.25)$$

Equation (13.25) represents the observations of voltage magnitudes as approximate linear mixtures of reactive power injections. Assuming constant output of reactive sources except for the slack bus, the ICA model for the reactive load profile estimation yields

$$\begin{aligned} \ell(t) &= Q_\ell(t) - Q_0 \\ x(t) &= V_m(t) - V_0 \\ A = \text{reduced } &\left( \left( \frac{\partial f_Q}{\partial |V|} \right)^{-1} \left( 1 - \frac{\partial f_Q}{\partial \delta} \left( \frac{\partial f_P}{\partial \delta} \right)^{-1} \alpha \right) \right) \end{aligned} \quad (13.26)$$

In (13.26), the sources are the unknown active or reactive power drawn at load buses, the measurements are the voltage magnitudes at selected buses and the mixing matrix is a constant real matrix.

### 3.1.4 Harmonic load profile model.[16]

The system equations under non-sinusoidal condition can be expressed by the linear equation

$$I_h = Y_h V_h \quad (13.27)$$

where  $h$  is the harmonic order,  $I_h$  is the bus current injection vector,  $V_h$  is the bus voltage vector, and  $Y_h$  is the system admittance matrix at each frequency  $h$ . The linear equation (13.27) is solved for each frequency of interest.

The linear measurement model for the harmonic load flow equations given in (13.27) can be defined as

$$V_h(t) = Z_h I_h(t) + \eta(t) \quad (13.28)$$

where  $V_h$  is the known harmonic voltage measurement vector,  $I_h$  is the unknown harmonic current source vector,  $Z_h$  is the impedance matrix, and  $\eta(t)$  denotes the measurement noise. The ICA model for the harmonic load estimation is given as

$$\begin{aligned} \ell(t) &= I_h(t) \\ x(t) &= V_h(t) \\ A = \text{reduced } &Z_h \end{aligned} \quad (13.29)$$

Comparing (13.29) with the ICA model, the sources are the harmonic current injections, the measurements are the harmonic voltage measurements, and the mixing matrix will be the reduced impedance matrix. Equation (13.29) is solved for each harmonic order  $h$  by ICA. In this model, the sources, the measurements and the mixing matrix are complex vectors and matrices. Thus a complex ICA algorithm is required. However, if we assume a constant power factor for the harmonic loads, we can apply a real-valued ICA algorithm to real and imaginary parts of the measurement vector.

The linear ICA model given for the active, reactive and harmonic load profile estimation can be extended to include the noise term  $\eta(t)$  as given in (13.3). In general, the measurement noise is modeled as a Gaussian distributed random variable. This will not be a problem for the ICA estimation because ICA is capable of estimating sources if at most one of the source signals is Gaussian distributed.

### 3.2 Preprocessing of load profile data

The main assumptions in estimation by ICA are the independency and non-gaussianity of sources. In general electric loads are not completely independent. A statistical correlation between load profiles may exist because of weather, temperature, time of day, day of week, seasonal variations etc. In order to apply ICA in our estimation process we have to remove this dependency among the loads.

In general, the load variations can be represented by two parts: A slow varying component representing a trend due to the external factors such as temperature, weather, day of week, etc., and a stochastic process representing fast fluctuations. In [17] temporal load variations are considered to consist of fast fluctuations in terms of second or minutes and slower fluctuations, hour to hour associated to common external causes. A linear filter can be used to separate these two components from the time-series data of loads.

Because ICA is a linear transformation, linear filtering of the signals does not change the ICA model [9]. The application of an appropriate moving-average filter, represented by the matrix  $M$ , to the ICA model in (13.4) separates the fast fluctuations  $L_{fast}$  and slower changing trends  $L_{slow}$  in the load time series matrix  $L$ . Thus

$$X_{slow} = XM = ALM = AL_{slow} \quad (13.30)$$

Because  $M$  is a component-wise filter, we obtain

$$X_{fast} = X - X_{slow} = AL - AL_{slow} = AL_{fast} \quad (13.31)$$

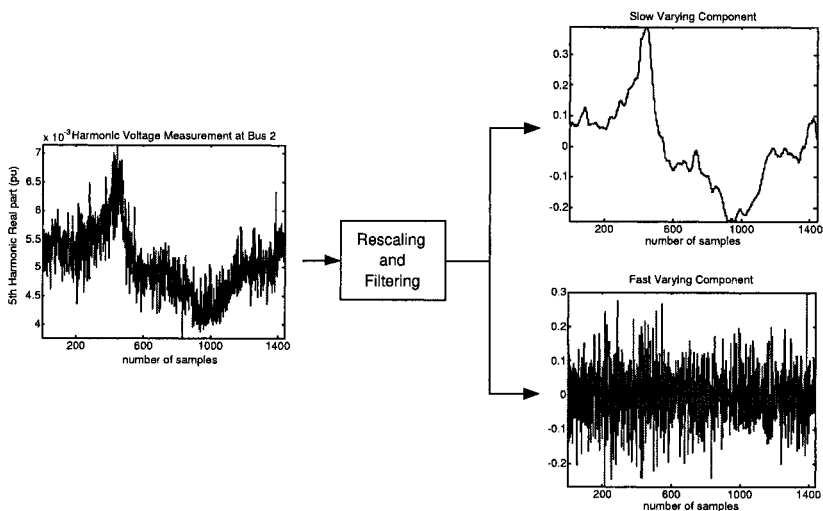


Figure 13.1. Rescaling and filtering of harmonic voltage measurements.

Using (13.31), the dependence on  $L_{slow}$  among the load time series can be removed from the observations and the mixing matrix  $A$  remains unchanged after linear filtering.

Consider a rescaling and filtering example using a harmonic voltage measurement. Figure 13.1 shows how an unscaled voltage measurement is split up into a slow varying component and a fast varying component. Both components are subsequently normalized and thus have zero mean and variance at unity.

In a previous paper [13], the assumptions on the independence and non-gaussianity of loads were verified for a particular load data obtained from New York ISO. The correlation coefficient matrix of fast intra-hour fluctuations of actual 15-minute data was calculated. The intra-hour fluctuations and inter-hour load trends were separated by a 4-point moving average filter. Correlation results yield that almost all of the correlation coefficients are close to zero. The sample skewness and sample kurtosis were calculated for the fast fluctuations. Results showed small values of skewness and positive average kurtosis which indicate a non-gaussian distribution of the fast fluctuations. We assume in this chapter that for all loads the fast fluctuations at different buses are mutually statistically independent.

### 3.3 Eliminating indeterminacy of ICs

Independent components can be estimated up to a scaling and a permutation factor. This is due to the fact that both the source matrix  $L$  and the mixing matrix  $A$  are unknown. A source can be multiplied by a factor  $k$  and the corresponding column of the mixing matrix can be divided by  $k$ , without changing the probability distribution and the measurement vector. Similarly, permuting two columns of  $A$  and the two corresponding rows of the source matrix  $L$  will not affect the measurement vector.

This indeterminacy can be eliminated if there is some prior knowledge about the loads. In fact, in electric power systems, it is reasonable to assume that historical load data is available, which can be used to match the estimated loads to original loads. Furthermore it is assumed that forecasted peak loads are available which then can be used to scale the load profiles.

For simplicity, only daily or monthly customer billing data and recorded or forecasted peak loads are used to restore the magnitude of load shapes assuming constant power factor. We approximate the load to be estimated using previous energy consumption and previous peak load as

$$\begin{aligned} \int_{T_0}^{T_1} [c_i \ell_{est\ i}(t) + b_i] dt &= W_i \\ c_i \ell_{est\ i,peak} + b_i &= \ell_{i,peak} \quad i = 1, 2, \dots, N \end{aligned} \quad (13.32)$$

where  $\ell_{est\ i}(t)$  is the estimated  $i^{\text{th}}$  load shape corresponding to the  $i^{\text{th}}$  actual load,  $c_i \ell_{est\ i}(t) + b_i$  is the scaled  $i^{\text{th}}$  estimated load approximation to the  $i^{\text{th}}$  actual load,  $W_i$  is the energy consumption of  $i^{\text{th}}$  load from  $T_0$  to  $T_1$ ,  $\alpha_i$  is the power factor for the  $i^{\text{th}}$  load,  $\ell_{est\ i,peak}$  is the peak of  $\ell_{est\ i}(t)$ ,  $\ell_{i,peak}$  is the peak of the  $i^{\text{th}}$  actual load, obtained from historic data or load forecasting, and  $N$  is the number of actual loads. Solving (13.31) yields the magnitude of the estimated  $i^{\text{th}}$  load shape (see [13]).

### 3.4 FastICA based load profile estimation algorithm

The FastICA Based Load Profile Estimation Algorithm can be summarized as follows:

- 1 If the number of observations  $M$  is larger than that of the loads,  $N$ , apply PCA to reduce the dimension of observations as well as the measurements errors to  $N$ .
- 2 Preprocess the observations with a linear filter to obtain mixtures of the fast varying components of the loads,  $X_{fast}$ .

- 3 Obtain the load estimates by applying the *FastICA* algorithm given in Section 2.4 to the fast varying components of the loads,  $X_{fast}$ , to estimate the mixing matrix  $A$ .
- 4 For harmonic estimation, perform Steps 2 and 3 for each harmonic component of interest.
- 5 Re-order the estimated loads by matching with the historical load shapes.
- 6 Scale the estimated load shapes using the techniques from Section 3.2 based on customer billing data and forecasted or historical peak loads.

The loads estimates present the active power, reactive power, or the real and imaginary parts of the harmonic current sources at harmonic frequency  $h$ .

## 4. Case Studies

### 4.1 Data generation

The proposed active, reactive and harmonic load profile estimation algorithm is tested on a standard IEEE 14-bus system presented in Figure 13.2. Due to the lack of real measurement data, the following steps generate observation vectors from a standard base case using public-domain load profiles from ERCOT [18], the Electric Reliability Council of Texas, for the active, reactive, and the harmonic load profile estimation. The IEEE 14-bus system operates at a complex power base of 100 MVA.

The data for the load profile estimation algorithm was generated as follows:

- 1 Normalize the load profiles to zero mean and the maximum load at unity.
- 2 Add zero mean Laplace distributed random fluctuations with 0.02 variances to the normalized load profiles obtained from Step 1 in order to mimic the effect of the super-gaussian distributed fast-varying temporary component of a realistic load profile.
- 3 Multiply the base case power injection at each load bus with one of load profiles.

To obtain the measurement vector, the active branch flows or voltage magnitudes for the placed meters were calculated at each sampling step using a public domain power flow solver, MATPOWER 2.0 [19], or the

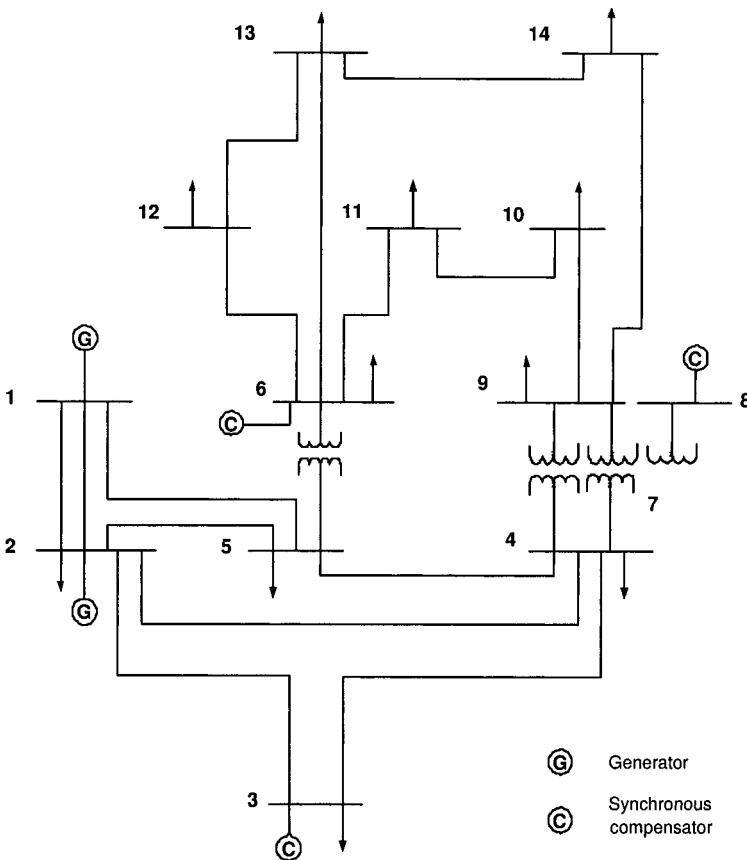


Figure 13.2. The one-line diagram of the IEEE 14-bus system.

harmonic power flow program developed at Drexel University based on MATPOWER.

## 4.2 Error measures

To quantify the estimation quality we used the following error measures for the slow varying component of the load profiles. Let the source signal  $\ell_{slow}(t)$  stand for either one of the active power, the reactive power, or the harmonic current profile to be estimated. Let  $\ell_{slow\_est}(t)$  be the corresponding estimated variable. Let  $res(t)$  denote the residual error between these 2 variables, and  $res_{max}$  its maximum:

$$res(t) = \ell_{slow}(t) - \ell_{slow\_est}(t), \quad t = 1, \dots, T \quad (13.33)$$

The error measures used are the following:

1 The maximum absolute error

$$e_{\max} = \max_{t=1,\dots,T} |res(t)| \quad (13.34)$$

2 The mean absolute error

$$e_{\text{mean}} = \frac{1}{T} \sum_{t=1}^T |res(t)| \quad (13.35)$$

3 The maximum absolute percentage error

$$e_{\max_{\text{perc}}} = \max_{t=1,\dots,T} \left| \frac{res(t)}{\ell_{\text{slow}}(t)} \right| \quad (13.36)$$

4 The mean absolute percentage error

$$e_{\text{mean-perc}} = \frac{1}{T} \sum_{t=1}^T \left| \frac{res(t)}{\ell_{\text{slow}}(t)} \right| \quad (13.37)$$

5 The largest correlation coefficient

$$\text{corr}(\ell_{\text{slow\_est}}^m, \ell_{\text{slow}}^k) = \max_{\substack{k=1,\dots,M \\ k \neq m}} \left( \ell_{\text{slow\_est}}^m \cdot (\ell_{\text{slow}}^k)^T \right) \quad (13.38)$$

where  $L_{\text{est}}$  and  $L_{\text{slow\_est}}$  denote the  $M \times T$  slow-varying source signal matrices, and  $\ell_{\text{slow}}^m$  and  $\ell_{\text{slow\_est}}^m$  denote the  $m^{\text{th}}$  row vectors containing the  $m^{\text{th}}$  source signals  $\ell_{\text{slow}}(t)$  and  $\ell_{\text{slow\_est}}(t)$  at the time steps  $t = 1, \dots, T$ .

## 4.3 Results for active load profile estimation

The active power load profiles of 8 loads in IEEE 14 bus data are shown in Figure 13.3. These load profiles are obtained by multiplying the active power injections from these buses with the corresponding load profiles. The horizontal axis denotes time in hours and the vertical axis denotes the active power drawn by the load buses in MW.

The mixed signals are the measurements of active power flow through the branches. To simulate these measurements, the active power flow through branches of 1-5, 4-5, 4-9, 6-12, 6-13, 9-14, 10-11, and 13-14 are obtained by MATPOWER. Suppose the output of all generator buses

and the power factor for the loads remain constant during the interval of consideration, with the slack bus (Bus 1) compensating for all load variations. The number of meters, 8, is equal to the number of load buses. This assures a square mixing matrix. For the selected branch flows, the mixed signals are shown in Figure 13.4. The power flow injects into the “From” end of the branch. The horizontal axis denotes time in hours and the vertical axis denotes the active power drawn by the load buses in MW.

The ICA algorithm in Section 3.4 is used to estimate the active power injections from the 8 load buses. The results are shown in Figure 13.5 for the smoothed load profiles. The estimated profiles (dotted lines) are practically indistinguishable from the original profiles (solid lines).

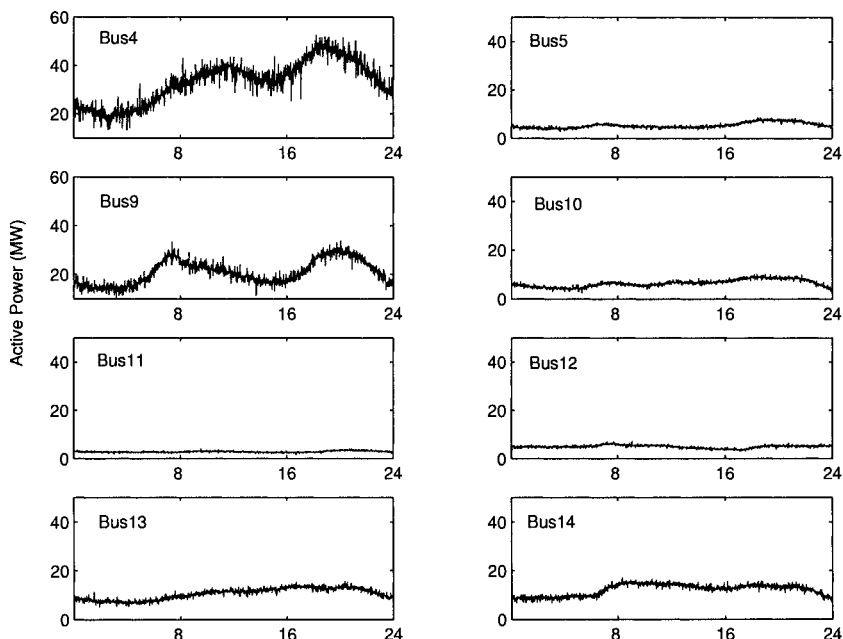


*Figure 13.3.* Original source signals: Active power drawn by load buses.

The errors and correlation coefficients are given in Table 13.1 . As we can see from these figures, the proposed approach can separate active load profiles with a mean percentage error less than 4%. We also note that the largest maximum and mean percentage errors occur at Bus 10, which shows a rather flat load profile. The largest absolute error occurs at Bus 4; its profile shows the largest deviation. Its percentage error,

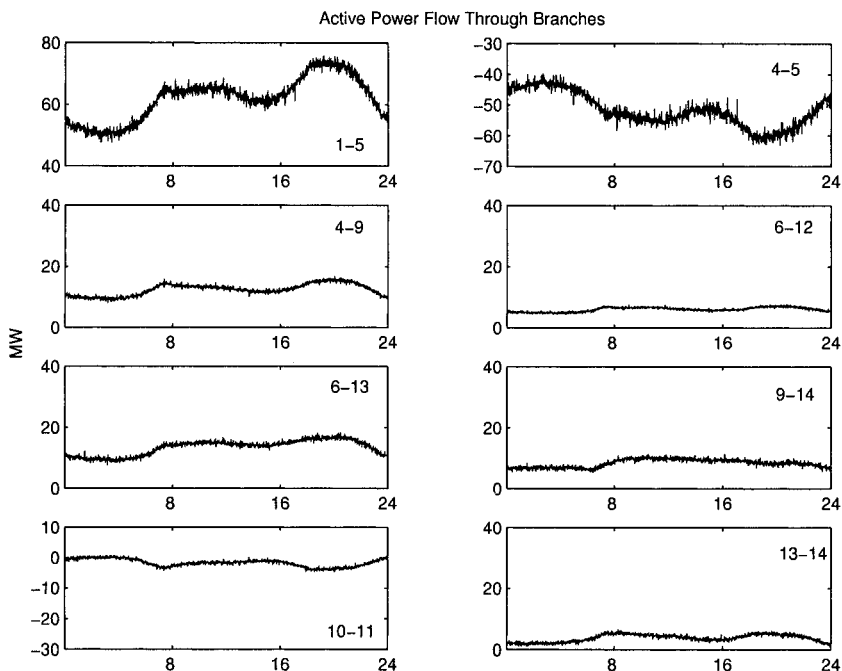


Figure 13.4. Mixed signals: Active power flow through branches.

however, is small. We note that in all cases the estimated profile follows the actual profile closely without any significant outliers.

Table 13.1. Errors between estimated and actual smoothed reactive load profiles.

Load at Bus	Correlation Coefficient	Maximum absolute error (MW)	Mean absolute error (MW)	Maximum Percentage Error (%)	Mean Percentage Error (%)
4	0.9992	0.7452	0.2303	2.15	0.74
5	0.9886	0.3704	0.1406	8.11	2.93
9	0.9980	0.6265	0.1960	2.50	0.95
10	0.9920	0.4297	0.1708	14.07	3.17
11	0.9877	0.0923	0.038	3.25	1.33
12	0.9980	0.0609	0.0264	1.24	0.53
13	0.9991	0.1359	0.0807	1.45	0.81
14	0.9976	0.3947	0.1486	5.35	1.38

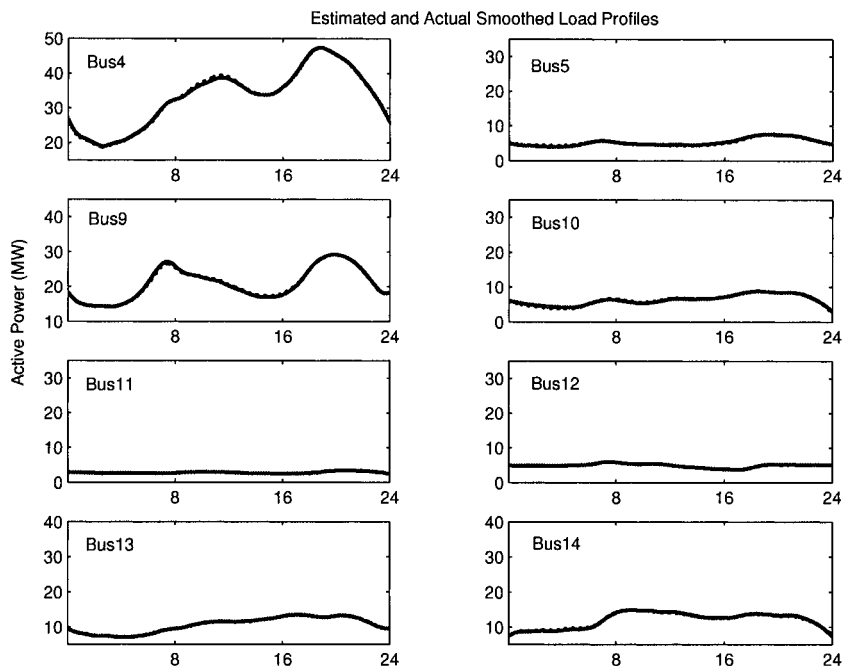


Figure 13.5. Comparison of smoothed original signals and estimated signals.

#### 4.4 Results for reactive load profile estimation

In the second example, the reactive load profiles at Buses 4, 5, 9, 10, 11, 12, 13, and 14 shown in Figure 13.6, need to be estimated from the measurements of the voltage magnitude (Figure 13.7) at Buses 4, 5, 9, 10, 11, 12, 13, and 14.

We apply ICA described in Section 3.4 to the measured signals to separate them into the unknown source signals, i.e., the reactive load profiles. The result is shown in Figure 13.8. The solid lines represent the original reactive profiles, and the dotted lines represent the estimated ones.

Table 13.2 shows that the proposed ICA has satisfactory precision with mean percentage errors below 4.5% and all but one maximum percentage error below 5%. The largest percentage error is encountered at Bus 5, which again shows a very flat profile. The largest absolute error occurs at Bus 9 whose reactive profile shows the largest deviation. Again, its percentage error is small. As in the case of the active profile estimation, none of the estimated profiles show any significant outliers. This indicates that the estimation of reactive load profiles from volt-

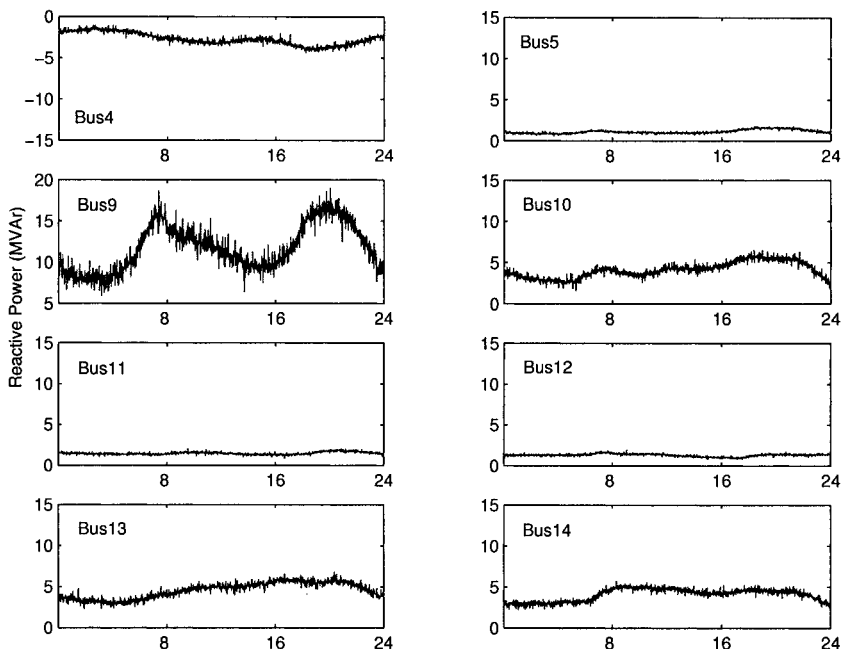


Figure 13.6. Original source signals: Reactive load profiles.

age magnitude measurements is feasible if all assumptions noted in this chapter hold.

Table 13.2. Errors between estimated and actual smoothed reactive load profiles.

Load at Bus	Correlation Coefficient	Maximum absolute error (MVAr)	Mean absolute error (MVAr)	Maximum Percentage Error (%)	Mean Percentage Error (%)
4	0.9991	0.0588	0.0190	2.28	0.71
5	0.9835	0.0887	0.0343	10.53	3.41
9	0.9975	0.2968	0.1369	2.43	1.26
10	0.9985	0.0953	0.0334	4.23	0.84
11	0.9895	0.0428	0.0168	3.02	1.19
12	0.9980	0.0156	0.0070	1.21	0.53
13	0.9991	0.0529	0.0347	1.58	0.81
14	0.9979	0.1178	0.0490	4.76	1.35

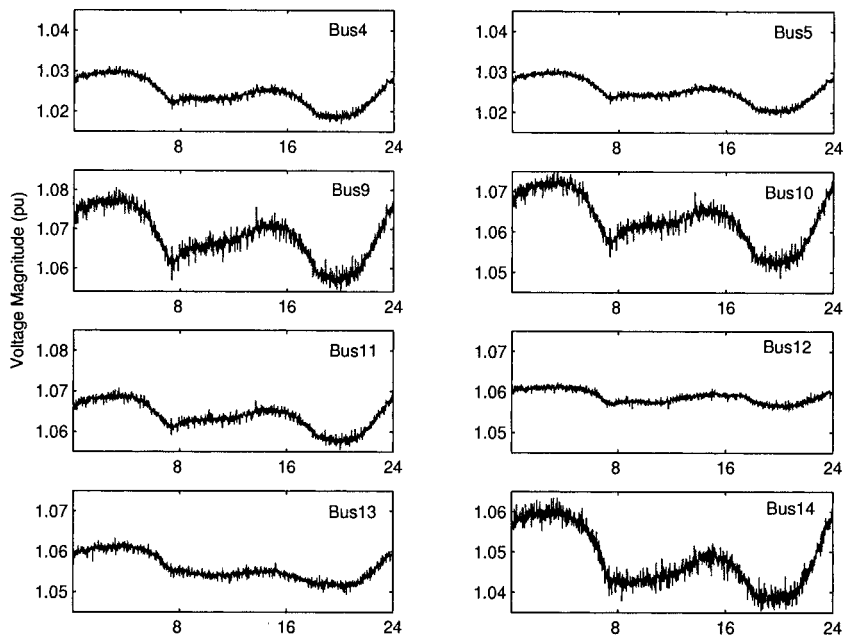


Figure 13.7. Mixed signals: Voltage magnitude measurements at load buses.

## 4.5 Results for harmonic load profile estimation

In this part, an example in the estimation of the load profiles of harmonic loads is given. Repeating the linear measurement model for the harmonic load flow given in (13.28)

$$V_h(t) = Z_h I_h(t) + \eta(t), \quad t = 1, \dots, T \quad (13.39)$$

where  $V_h(t)$  are the known harmonic voltage measurement vectors,  $I_h(t)$  are the unknown harmonic current source vectors,  $Z_h$  is the unknown mixing matrix relating measurements to the sources,  $\eta(t)$  is the Gaussian distributed measurement noise vector,  $h$  is the harmonic order,  $t$  the sample index, and  $T$  is the number of samples. Because in this example, there are only harmonic voltage measurements,  $Z_h$  is the reduced system impedance matrix at harmonic order  $h$ . In order to simplify the algorithm, we neglect the measurement noise.

The proposed load identification algorithm using ICA is tested on a modified IEEE 14-bus test system (Figure 13.9). In this example, we assume a constant power factor and statistical independence of the loads. Also the system is assumed to be symmetric and balanced. There are 3 harmonic producing loads at Buses 5, 10 and 12. These harmonic sources

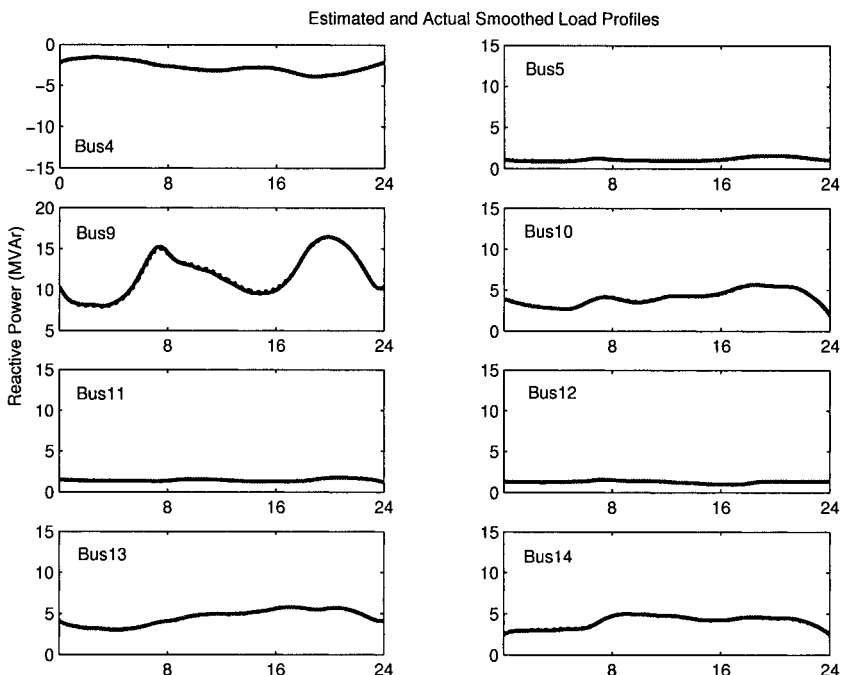


Figure 13.8. Comparisons between smoothed original and estimated reactive load profiles.

are modeled as harmonic current injections which have the harmonic orders of 5<sup>th</sup>, 7<sup>th</sup> and 11<sup>th</sup>. In addition to harmonic loads there are 5 linear loads at Buses 2, 9, 11, 13 and 14. These loads are modeled with impedance models [20]. However, impedance models of linear loads will be considered as current sources in the estimation process, which will increase the number of measurements [16]. The remaining buses are no-load buses.

The harmonic load profiles were generated using the data generation algorithm given in Section 4.1. Again, the Laplace distributed random variable represents the fast-varying component which is statistically independent and the load profiles represent the slow varying components. Harmonic current source models are obtained for harmonic sources using the harmonic power flow solution. Next we calculate the harmonic bus voltages by solving the linear system equations in (13.27) for each harmonic frequency of interest. There are 6 harmonic voltage measurements obtained from the Buses 2, 4, 6, 9, 11, and 13.

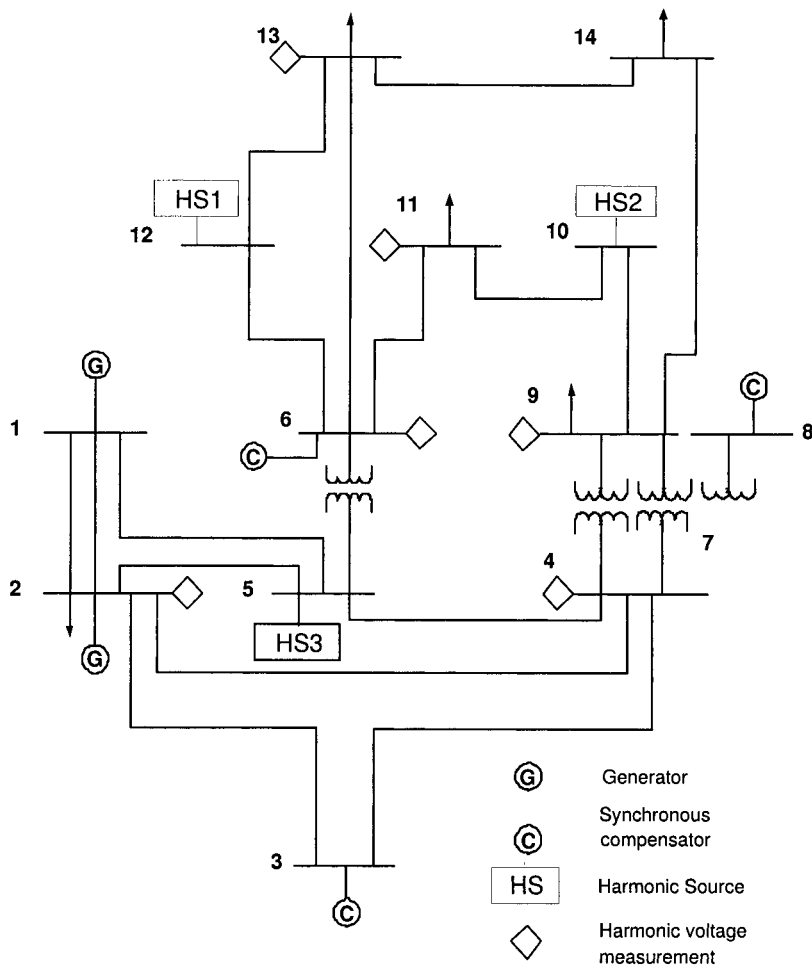


Figure 13.9. Modified IEEE 14-bus test system.

To remove the statistical dependence of the slow-varying component the harmonic voltage measurements are filtered as explained in Section 3.2 and shown in Figure 13.1. The FastICA based harmonic load identification algorithm described in Section 3.4 is applied to the voltage harmonic measurement data. Figures 13.10, 13.11, and 13.12 show the estimated (dashed line) and the actual (solid line) slow-varying components of the load profiles of harmonic current source at Buses 5, 10 and 12.

Correlation coefficients and errors for all three estimated harmonic sources are given in Table 13.3. As we can see from Table 13.3, corre-

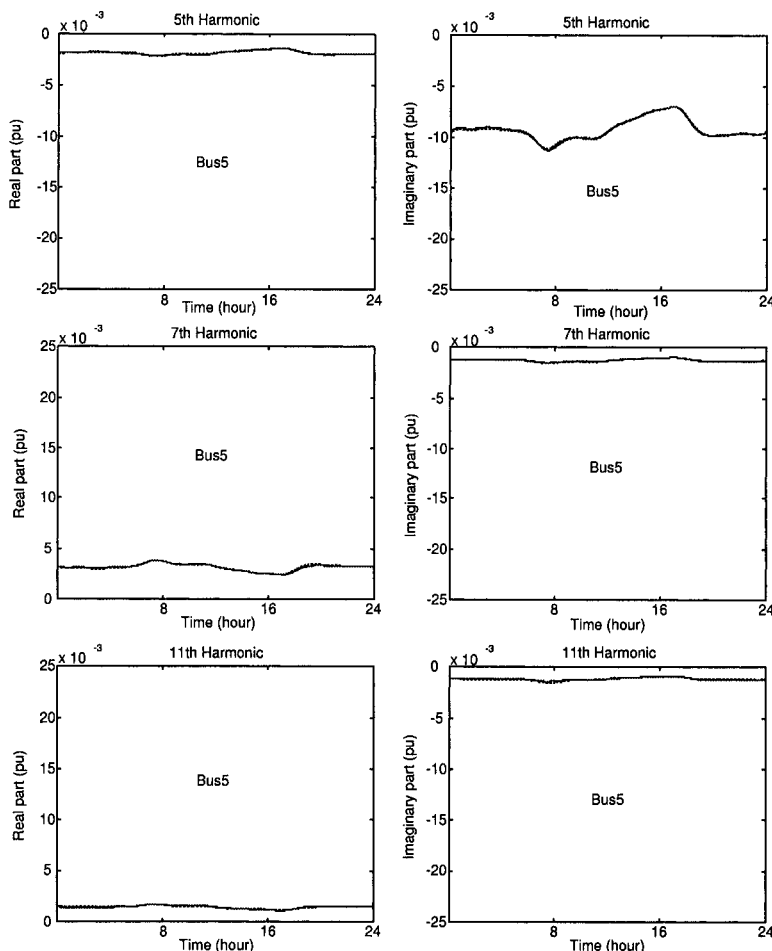


Figure 13.10. Comparison of smoothed harmonic components of current injection at Bus 5.

lation coefficients are close to 1 and the mean percentage error is quite small indicating a very good match between the estimated and actual values. The only exception is encountered at Bus 12, where the percentage errors for the imaginary part of the 11<sup>th</sup> harmonic component were quite high. Expanding the plot of the imaginary part of the 11<sup>th</sup> harmonic source current at Bus 12 at a scale of  $10^{-5}$  (Figure 13.13) reveals that the original source crosses the zero axis and shows numerically extremely small values. Computing the percentage error at these particular points does not provide meaningful results. The estimation results show that the dominant harmonic components with high ampli-

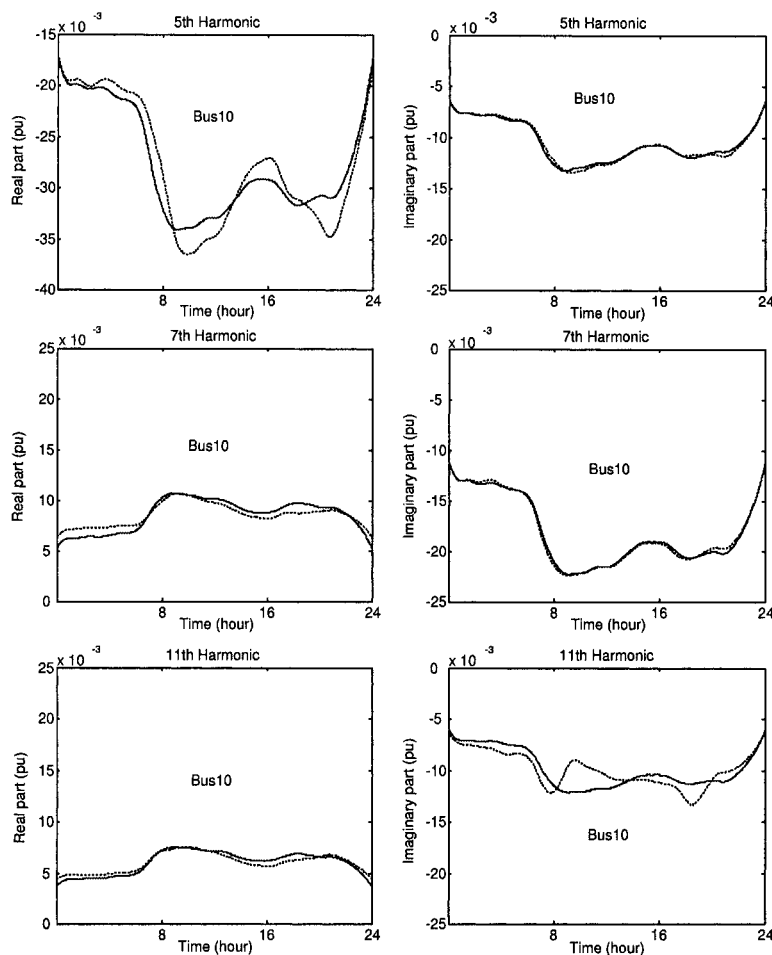


Figure 13.11. Comparison of smoothed harmonic components of current injection at Bus 10.

tude, which have a bigger impact on the harmonic distortions in the system, are estimated more accurately with a small error.

## 5. Conclusions

In this chapter we explored the use of higher order statistical information to obtain active, reactive, and harmonic load profiles estimates in electric power systems based on a limited number of measurements and without any knowledge of the power system branch impedances

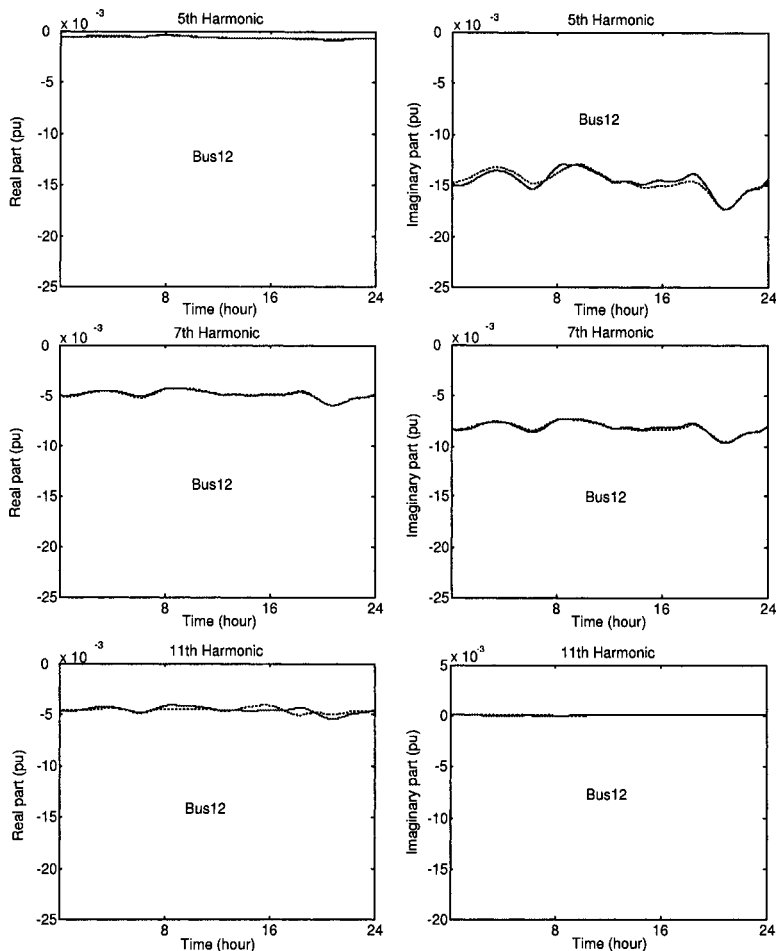


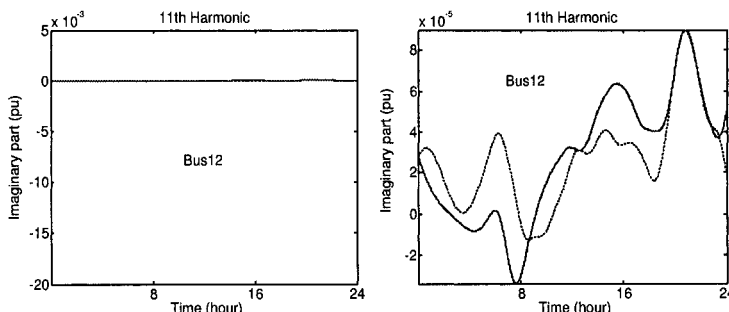
Figure 13.12. Comparison of smoothed harmonic components of current injection at Bus 12.

and topology. The proposed blind-source separation technique is purely signal-based and thus model independent.

Clearly, using only the assumptions of statistical independence and linear mixing does not yield results of the same accuracy as traditional state estimation techniques. However, the model independence presents a strong advantage in restructured power systems where network parameters might not be readily available or are subject to uncertainty.

Table 13.3. Errors between estimated and actual smoothed harmonic current profiles.

Bus	Harmonic Order	Correlation	Maximum absolute error (pu)	Mean absolute error (pu)	Maximum Percentage Error (%)	Mean Percentage Error (%)
		Coefficient				
5	5	Real	0.9689	0.00008	0.00004	4.66
		Imag	0.9948	0.00021	0.00008	1.94
5	7	Real	0.9744	0.00018	0.00005	5.86
		Imag	0.9852	0.00076	0.00002	5.08
5	11	Real	0.9299	0.00011	0.00005	7.00
		Imag	0.8776	0.00014	0.00006	11.08
10	5	Real	0.9367	0.00400	0.00150	13.58
		Imag	0.9916	0.00047	0.00015	4.01
10	7	Real	0.9421	0.00110	0.00052	21.31
		Imag	0.9954	0.00054	0.00017	2.87
10	11	Real	0.9377	0.00078	0.00031	21.41
		Imag	0.7076	0.00310	0.00093	25.77
12	5	Real	0.8135	0.00015	0.00004	23.07
		Imag	0.9350	0.00073	0.00029	5.27
12	7	Real	0.9809	0.00015	0.00007	3.25
		Imag	0.9830	0.00022	0.00009	2.71
12	11	Real	0.4068	0.00071	0.00023	16.19
		Imag	0.6044	0.00005	0.00002	—

Figure 13.13. Imaginary part of the 11<sup>th</sup> harmonic source current at Bus 12 at scale  $10^{-3}$  and scale  $10^{-5}$ .

## 6. Future Research

The research issues on the theory of ICA for load profile estimation include the following topics:

### 1 Non-linear ICA for power system load profile estimation

Independent Component Analysis is by design a linear technique which requires that power system measurements be modeled as lin-

ear combinations of the parameters to be estimated. Depending on the operating conditions this may present a rather coarse approximation of the underlying system model. Non-linear independent component analysis techniques [10, 16] need to be investigated to address the potential short-coming of ICA under heavy loading conditions.

## 2 *On-line load profile estimation*

While the presented work discusses off-line profile estimation, it is highly desirable to perform this type of estimation on-line. The computational limits depend on the availability of measurement data at sufficiently small time steps. Recursive estimation techniques and their potential application to ICA need to be studied.

## 3 *Piece-wise continuous mixing models*

ICA assumes that the underlying linear system model is continuous in time. Because switching operations in the power grid change the power system topology and thus the structure of underlying mixing matrix, it is necessary to discover the switchings and change the model automatically. Because the switching operation will only affect a small number of the mixing matrix elements, the continuity of the remaining elements can be used as a constraint for the estimation with piece-wise continuous mixing models.

## 4 *Power system measurement calibration*

Currently proposed measurement calibration techniques rely on complete knowledge of the power system impedances and the topology [21]-[24]. Under the assumption that individual instrument error offsets occur statistically independently and that additional measurement noise is Gaussian and can be filtered out, ICA can be used to provide a complementary approach to the determination of degrading instrument accuracy.

## 5 *Power system parameter and network topology estimation*

Power system parameter estimation is usually discussed as a subset of generalized state estimation techniques [1],[25]-[27]. In the traditional state estimation model these parameters are supposed to be known and fixed. But environmental conditions and aging materials may change branch parameter values. Furthermore, especially in the case of distribution systems, the network impedance data may not have been fully collected. Because the mixing matrix of ICA presents an equivalent impedance matrix of the system, it

can be used to obtain estimates of the equivalent impedances and the network topology.

### 6 Nodal load forecasting

Many regional transmission operators use locational marginal pricing strategies that penalize individual loads if these contribute to network congestion. Identification of nodal load profiles allows the forecast of the nodal load size and its impact on the available transfer capability. This type of information can be used for network security and reliability prediction. The availability and accuracy of nodal load forecasts also affect the development of real-time pricing and bidding strategies.

### Acknowledgments

The authors gratefully acknowledge the support of the project by the National Science Foundation under Grant # 9985119. Mr. H. Liao worked on this project as a graduate student during the academic year 2002-2003 at Drexel University's Center for Electric Power Engineering.

### References

- [1] A. Monticelli. Electric Power System State Estimation. *Proceedings of the IEEE*, 88:262–282, 2000.
- [2] Joint US-Canada Power System Outage Task Force. Final Report on the August 14th Blackout in the United States and Canada. US DoE, available at <http://reports.energy.gov/>, April 5, 2004.
- [3] G.T. Heydt. Identification of Harmonic Sources by a State Estimation Technique. *IEEE Transactions on Power Delivery*, 4:569–576, 1989.
- [4] Z.P. Du, J. Arrillaga, N.R. Watson, and S. Chen. Identification of Harmonic Sources of Power Systems using State Estimation. *IEE Proceedings on Generation, Transmission and Distribution*, 146:7–12, 1999.
- [5] A.P.S. Meliopoulos, F. Zhang, and S. Zelingher. Stability Regions of Nonlinear Autonomous Dynamical System. *IEEE Transactions on Power Delivery*, 9:1701–1709, 1994.
- [6] M.R. Irving and C.N. Macqueen. Robust Algorithm for Load Estimation in Distribution Networks. *IEE Proceedings on Generation, Transmission and Distribution*, 145:499–504, 1998.
- [7] J. Wan and K.N. Min. Weighted Least-Squares Methods for Load Estimation in Distribution Networks. *IEEE Transactions on Power Systems*, 18:1338–1345, 2003.

- [8] J.F. Cardoso. Blind Signal Separation: Statistical Principles. *Proceedings of the IEEE*, 86:2009–2025, 1998.
- [9] A. Hyvärinen and E. Oja. Independent Component Analysis: Algorithms and Applications. *Neural Networks*, 13:411–430, 2000.
- [10] A. Hyvärinen, J. Karhunen, and E. Oja. *Independent Component Analysis*. John Wiley, New York, 2001.
- [11] T.W. Lee, M. Girolami, A.J. Bell, and T.J. Sejnowski. A Unifying Information-Theoretic Framework for Independent Component Analysis. *Computers and Mathematics with Applications*, 39:1–21, 2000.
- [12] A. Hyvärinen. Fast and Robust Fixed-Point Algorithms for Independent Component Analysis. *IEEE Transactions on Neural Networks*, 10:626–634, 1999.
- [13] H. Liao and D. Niebur. Load Profile Estimation in Electric Transmission Networks using Independent Component Analysis. *IEEE Transactions on Power Systems*, 18:707–715, 2003.
- [14] H. Liao and D. Niebur. Exploring Independent Component Analysis for Electric Load Profiling. *Proceedings of the 2002 International Joint Conference on Neural Networks*, 2002.
- [15] H. Liao and D. Niebur. Estimating Reactive Load Profiles using Independent Component Analysis. *Proceedings of International Conference on Intelligent System Applications to Power Systems ISAP 2003*, Lemnos, Greece, 2003.
- [16] E. Gursoy and D. Niebur. Harmonic Load Identification using Independent Component Analysis. Submitted to *IEEE Transactions on Power Delivery*, 2004.
- [17] E. Hirst and B. Kirby. Defining Intra- and Inter-Hour Load Swings. *IEEE Transactions on Power Systems*, 13:1379–1385, 1998.
- [18] The Electric Reliability Council of Texas. Load Profiling. Available at <http://www.ercot.com/Participants/loadprofiling.htm>.
- [19] R.D. Zimmerman and D. Gan. MATPOWER: A MATLAB Power System Simulation Package. Available at <http://blackbird.pserc.cornell.edu/matpower/>, 1997.
- [20] R. Burch, G. Chang, C. Hatzidioniu, M. Grady, Y. Liu, M. Marz, T. Ortmeyer, S. Ranade, P. Ribeiro, and W. Xu. Impact of Aggregate Linear Load Modeling on Harmonic Analysis: A Comparison of Common Practice and Analytical Models. *IEEE Transactions on Power Delivery*, 18:625–630, 2003.
- [21] M.M. Adibi, K.A. Clements, R.J. Kafka, J.P. Stovall, J.N. Borkoski, L.E. Brittain, J.G. Dzwonczyk, W.A. Keagle, J.M. Kipp,

- K.R. Thomas, and B.F. Wollenberg. Integration of Remote Measurement Calibration with State Estimation—a Feasibility Study. *IEEE Transactions on Power Systems*, 7:1164–1172, 1992.
- [22] A. Fallaha, E. Cohen, A. Kayyali, and A. Ming. Calibration of Power Flow Measurements. *Electric Power Systems Research*, 38:1–10, 1996.
- [23] W. Hubbi. Computational Method for Remote Meter Calibration in Power Systems. *IEE Proceedings on Generation Transmission and Distribution*, 143:393–398, 1996.
- [24] F. Shoukri-Kourdi and E. Cohen. Two-Stage Calibration of Power Flow Measurements without Reliable Points. *Electric Power Systems Research*, 50:83–90, 1999.
- [25] O. Alsac, N. Vempati, B. Stott, and A. Monticelli. Generalized State Estimation. *IEEE Transactions on Power Systems*, 13:1069–1075, 1998.
- [26] A.S. Costa, E.M. Lourenco, and K.A. Clements. Power System Topological Observability Analysis Including Switching Branches. *IEEE Transactions on Power Systems*, 17:250–256, 2002.
- [27] E.M. Lourenco, A.S. Costa, and K.A. Clements. Bayesian-Based Hypothesis Testing for Topology Error Identification in Generalized State Estimation. *IEEE Transactions on Power Systems*, 19:1206–1215, 2004.

# Index

- Accumulation effect, 182
- Action network, 226, 230
- Adaptive critic design, 226
- Adaptive scheduling, 127
- AGC, 129
- Aggregating behavior, 195
- Aggregation, 111, 130
- Ancillary service, 63
- ANNI, 215
- Assessment
  - stability limit, 195
- ATC, 63, 71
  - corrective-mode, 68, 74, 96
  - preventive-mode, 68, 73, 92
- Available transfer capability, 63
- AVC, 129
- AVR, 185, 190
- Backpropagation algorithm, 226
- BBD structure, 154
- BCU
  - classifier, 89
  - limiter, 88
  - method, 89
- Bifurcation, 163
  - grazing, 192
  - Hopf, 40, 43, 45, 165
  - limit-induced, 81
  - saddle-node, 43, 81
  - stationary, 163
  - supercritical Hopf, 190
- Blackout
  - August 2003, 56, 107, 111, 180
  - Northeast US, 2
- Blind source separation, 289
- Bolza form, 184
- Boundary
  - corrector, 52
  - predictor, 51
  - tracing margin, 51
- Boundary value problem, 180, 186, 196
- Capacitor, 14
  - switching, 188
- Cascading system failure, 181
- Centering, 292
- Characteristic multiplier, 190–191
- Circuit breaker, 192
- Coherency analysis, 2
- Combinatorial optimization, 196
- Complex network, 108
- Computational intelligence, 5
- Constraint
  - information structure, 140
  - performance, 181
  - transient stability, 91
- Contingency
  - analysis, 23
  - topmost severe, 63
- Contingency screening
  - look-ahead, 79
- Continuation based approach, 40
- Continuous dynamics, 181
- Contrast function, 291
- Control
  - decentralized, 144
  - decentralized output, 147
  - robust exciter, 143
- Controller signal, 181
- Convergence properties
  - shooting method, 191
- Convex optimization, 140
- Coordinated tuning, 239
- Coordination
  - top-down, 111
- Correlation coefficient, 302
- CPFLOW, 64, 81, 84
- Critic network, 226–227
- Curve
  - $\lambda$ - $V$ , 81
  - $P$ - $V$ , 40, 53, 77
  - $Q$ - $V$ , 77
  - power-angle, 28
  - power-voltage ( $P$ - $V$ ), 28
  - voltage-angle, 28
- DAE model, 126
- Decomposition, 110, 242
  - Bender's, 243
- Desired response predictor, 214

- Differential algebraic equation, 116  
 Differential entropy, 291  
 Differential-algebraic model, 182  
 Direct adaptive control, 203  
 Direct method, 42  
 Discontinuity, 196  
 Discrete event, 181  
 Distributed resource, 195  
 Distribution network, 244  
 Dual heuristic programming, 206  
 Dynamic embedded optimization, 180, 184, 195  
 Dynamic programming, 226  
 Econometric model, 273  
 ECOST, 246  
 Eigenvalue, 47, 190  
     critical, 45  
     dominant, 41  
     real part, 47  
 EMTDC, 209  
 End-use model, 273  
 Energy function analysis, 2  
 Error  
     maximum absolute, 302  
     maximum absolute percentage, 302  
     mean absolute, 302  
     mean absolute percentage, 302  
     measures, 301  
 Estimation  
     load profile, 288  
     maximum likelihood, 291  
     network topology, 314  
     on-line load profile, 314  
     parameter, 314  
 Estimation algorithm  
     load profile, 299  
 Event, 182  
     discontinuous behavior, 185  
     switching, 195  
     triggering, 182  
 Excitation control, 22  
 Excitation system, 15  
 Expert system, 279  
 FACTS, 2, 44, 181, 195  
     controller, 202  
     device, 195, 240  
 Fast stability analysis, 2  
 FastICA, 292  
     algorithm, 292  
 FCITC, 67–68  
 Feedback signal selection, 258  
 FERC, 64  
 Fitness function, 244  
 Fuzzy logic, 280  
 GA, 243  
     optimization, 259  
 Generation source, 195  
 Genetic algorithm, 240, 243, 246  
 Genetic operator, 244, 247  
     crossover, 244, 265  
     mutation, 244, 265  
     selection, 244, 265  
 Gradient-based algorithm, 195  
 Gradient-based method, 185  
     conjugate-gradient, 185  
     steepest-descent, 185  
 Grazing phenomenon, 180–181, 185, 187, 192–193, 196  
 Harmonic current source, 296  
 Harmonic load flow, 296  
 Harmonic voltage measurement, 296  
 Hessian, 185  
 Hierarchical control, 129  
 High dimensionality, 242  
 Hybrid behavior, 195  
 Hybrid system, 125, 181–182, 195  
 ICA, 287  
     complex, 297  
     nonlinear, 313  
 IEEE 14-bus system, 300  
 Impedance  
     apparent, 194  
     plane, 194  
 Implicit numerical integration, 183  
 Impulse effect, 182  
 Impulsive step, 182  
 Independent component analysis, 287  
 Index  
     damping, 47  
     modulation, 204  
 Indirect method  
     manifold-based, 42  
 Infinite dimensional, 185  
 Information exchange, 153  
 Infrastructure, 107  
     IT, 107  
     multi-layered, 107  
     multi-rate, 107  
 Initial value, 186  
 Intelligent agent, 5  
 Inter-area mode, 258  
 Interior-point method, 2  
 Inverter output, 204  
 Jacobian matrix, 42, 186, 193  
 Kundur  
     Prabha, 16  
 Lachs  
     Walter, 16  
 Lagrangian-relaxation method, 2  
 Large-scale power system, 139

- Learning  
statistical model-based, 274
- Limit cycle, 180, 187–189, 196  
non-smooth, 189
- Limit  
anti-windup, 185  
bus voltage, 66, 74  
clipping, 185  
hard, 66  
soft, 66  
steady-state stability, 66, 74  
thermal, 15, 66, 74  
transient stability, 66, 74
- Linear approximation method, 64
- Linear feedback, 141
- Linear filtering, 297
- Linear matrix inequality, 140
- Load forecasting, 269  
long-term, 269, 273  
medium-term, 273, 269  
nodal, 315  
short-term, 277, 269
- Load margin  
nose-point, 75  
thermal-limit, 79  
transient-stability-limit, 87  
voltage-limit, 77
- Load  
control, 195  
forecasted, 114  
shedding, 184  
weather normalized, 270
- Look-ahead margin estimator, 97
- Margin, 181  
damping, 43, 47
- Market dynamics, 195
- Maximum power transfer, 15
- Max-min optimization problem, 255
- Measurement calibration, 314
- Metaheuristics, 243, 239–240
- Metzler-matrix, 110
- Mixing matrix, 290
- Model network, 231
- Model uncertainty, 195
- Monitoring, 160
- Monodromy matrix, 190
- Monotone response, 111, 115
- Monte Carlo  
simulation, 65  
techniques, 195
- Multilayer perceptron, 226
- Mutual information, 291
- NARMA model, 213
- Negentropy, 291
- Neural network, 203, 278
- Neurocontrol  
adaptive, 212
- Neurocontroller, 213, 216
- Neuroidentification, 222
- Neuroidentifier, 213, 215
- Newton's method, 186, 193
- Noise, 163
- Non-convex function, 242
- Non-gaussianity, 291
- Non-interacting control, 115
- Nose point, 77
- NP-complete, 243
- NP-hard, 243
- Numerical integration, 186
- OASIS, 64
- Objective function, 184
- Observability, 125
- OLTC, 127
- Open transmission access, 64
- Operating characteristic, 194
- Operating condition  
post-contingency, 68  
pre-contingency, 68
- Optimal control, 185, 195
- Oscillation, 188
- Parallel implementation, 244
- Participation factor, 160
- Particle swarm optimization, 243
- Periodic behavior, 188
- Perturbations, 183
- PI controller, 203, 206
- Piece-wise continuous mixing model, 314
- Placement, 239, 241  
sensor, 112
- POD, 240, 253
- Poincaré map, 188–189
- Point-to-point MW transaction, 71
- Population, 243
- Post-fault response, 181
- Power factor control, 14
- Power flow equation, 293
- Power flow solution, 81  
first, 82  
second, 82
- Power flow  
continuation, 64  
DC, 294  
optimal, 64
- Power spectral density, 163
- Power system stabilizer, 149, 180, 241
- Power system  
all DC, 126
- Power  
complex, 13  
instantaneous, 12  
reactive, 11–13  
real, 13
- Precursor, 163

- Probabilistic collocation, 195
- Probabilistic sensitivity, 114
- Probe signal, 160
- Protection, 181
- Protection device, 181, 192, 245
- Protection relay
  - distance, 194
  - zone 1, 194
  - zone 2, 194
- PSCAD, 209
- Pseudorandom binary signal, 215
- PSS, 180, 185
  - output limiter, 180
- Quality of service, 114, 120
- Quasi-Newton method, 185
- Radial basis function, 203
- Region
  - of attraction, 142, 181
  - of stable operation, 196
- Regression method, 277
- Relay characteristic, 194
- Return time, 188
- Reverse-time simulation, 181
- SAIDI, 247
- SAIFI, 247
- SCADA, 124
- Security assessment
  - dynamic, 89
  - static, 89
- Security constraint
  - dynamic, 63
  - static, 63, 68
- Security enhancement, 239
- Security
  - cost based, 54
- Sensitivity transition matrix, 183, 189–190
- Separation
  - spatial, 112
  - temporal, 112
- Series branch control, 210
- Series inverter, 209
- Series voltage source inverter, 208
- Shooting method, 180, 186, 189, 196
- Shunt branch control, 211
- Similar day approach, 277
- Simulated annealing, 243
- Slice-of-the-system, 71
- Solution encoding, 247
- Sparsity-preserving algorithm, 46
- Special protection scheme, 195
- SSSC, 202, 206
- Stability, 160, 189
  - local, 190
  - oscillatory, 40
  - small-signal, 2, 180, 261
  - transient, 65, 203
- voltage, 160
- Stabilization, 110
  - fast, 126
  - robust decentralized, 111
- STATCOM, 202, 204
- State estimation, 288, 293
  - harmonic, 288
- State estimator, 121
  - quasi-stationary, 123, 130
- Static Var compensator, 22, 56
- Statistical independence, 291
- Stopping rule, 256
- Supervisory control, 181
- Support vector machine, 280
- Surge impedance load, 15
- SVC, 254, 258
- Switching activity, 195
- Switching effect, 182
- System vulnerability, 196
- Tabu search, 243
- Tangency, 193
- Tangentially, 192–193, 196
- Target hypersurface, 193
- Taylor
  - Carson, 16
- TCSC, 73, 254, 258
- Time factor, 271
- Time scale
  - fast, 55
  - slow, 55
- Time series, 277
- Training stage
  - post-, 217
  - pre-, 217
- Trajectory, 183, 186
  - approximation, 195
  - grazing, 194
  - sensitivities, 183, 187, 195
- Transfer capability, 68
  - available, 63
- Transformer
  - insertion, 209
  - tap-changing, 181, 186
  - tapping, 188
- Transmission reliability margin, 99
- Transversal crossing, 185
- Transversality, 183
- Trapezoidal integration, 183
- Triggering hypersurface, 190,
- Trip signal, 192
- Unit commitment, 123
- UPFC, 202, 208
- Variational equation, 195
- Voltage collapse, 16, 35, 127, 160, 180
  - Dynamic, 16
  - Static, 16

- Voltage control, 11, 14, 119
- Voltage stability
  - margin index, 28
  - weak location, 33
- Voltage field, 186
- VSMI, 28
- Vulnerability, 181
- WAMS, 2
- Weather condition, 271
- Whitening, 292
- Zeno effect, 182